CLIMATE CHANGE IMPACT ON RAINFALL-INDUCED LANDSLIDES IN OTTAWA SENSITIVE MARINE CLAYS

by

Nattawadee Panikom

Thesis submitted to the University of Ottawa

Under the supervision of Prof. Mamadou Fall

In partial Fulfillment of the requirements for the
M.A.Sc. degree in Environmental Engineering

Civil Engineering Department
Faculty of Engineering
University of Ottawa

CLIMATE CHANGE IMPACT ON RAINFALL-INDUCED LANDSLIDES IN OTTAWA SENSITIVE MARINE CLAYS

Abstract

The City of Ottawa is situated in an area known as the Champlain Sea, 17,000 years before present (BP) the entire area was covered with sea water. This area deposited marine clays which are known to be highly sensitive. The City of Ottawa needs to expand land use to allow for the expansion of infrastructure and housing to support its growth. This study is intended to assist the City of Ottawa's geotechnical engineers in their decision-making by identifying future sensitive areas prone to landslides due to rainfall based on future climate model data. The project incorporates rainfall intensities from downscaled climate model data in the Transient Rainfall Infiltration and Grid-based Regional Slope-Stability (TRIGRS) model to investigate areas sensitive to landslides, then within a GIS platform, the future landslide susceptibility maps were created based on Factor of Safety (FS) values showing the areas prone to landslides. The data input for the model includes climate model data, topography, hydrogeology, geology and geophysical data obtained from a previous study. These data were prepared using ArcGIS software and converted into ascii format for TRIGRS model. The model was calibrated using historical rainfall intensities and validated by comparing to historical landslide areas. Sensitivity analysis were performed to ranges of geotechnical properties found within sensitive marine clays in the area to find the values best to create the ideal scenario, normal scenario and worst-case model scenario for the prediction. Rainfall intensities from projected climate data Intensities Duration Frequency (IDF) of 10 years and 50 years returning period and rainfall intensities of 12 hr, 24 hr, and 48 hr were selected for the model. Results from simulations find the projected climate rainfall intensity do not have impact or has minimal impact to slope stability in sensitive marine clay areas in Ottawa directly. However, higher rainfall runoff is expected from projected rainfall RCP8.5 than the RCP4.5. The infiltration rate remains constant throughout each simulation, which is the same value as the hydraulic conductivity. The time when the slope becomes unstable varies depending on initial water levels. Results from the ideal and normal scenario show no areas prone to slope failure after 48 hours of rainfall duration. However, the factor of safety decreases as the rainfall duration increases and is expected to decrease with longer rainfall durations. The worst-case scenario shows some areas prone to slope failure (FS < 1) with 2% probability of slope failure at 48 hours of rainfall duration. The distribution of these unstable areas are located along the Ottawa River, Rideau River, Carp River, Mississippi River and valleys along their

tributaries, the majority of the area prone to slope instability from rainfall are in the east part of the City of Ottawa.

While there are many uncertainties and limitations which contribute to the model results, this study is useful to engineers and planners in initial implementation of mitigation strategies to mitigate the damages and cost from landslides events. The susceptibility maps can also assist in decision making for planners in developing into these areas.

Contents

List of Figures

List of Tables

1 General Introduction

1.1 Problem Statement

Sensitive marine clay, also known as Leda clay or Champlain Sea clay in Canada, covers large areas of the Earth's land surface. In Canada, sensitive marine clay is found mostly in eastern Canada along the St. Lawrence lowlands in Ontario and Quebec, including beneath major Canadian cities such as Ottawa, Montreal, and Quebec City. In Ottawa, sensitive marine clays are found under 35% of the city's area, in some cases underlying highly populated areas, such as Orleans and major highways throughout the City.

The City of Ottawa is the fourth largest city in Canada, with a population of just over one million as of 2019 (Statistics Canada, 2020), and it continues to expand as its population continues to grow. The City of Ottawa is one of the fastest growing cities in Canada and its rapid growth is expected to continue well into the current century (City of Ottawa, 2016). There is more demand for housing, city services, and infrastructure. The City's planers need to look into rezoning land for new developments. However, development around sensitive marine clays is unavoidable, and extra caution needs to be exercised when constructing in these areas. These clays are sensitive, and thus could liquefy and cause landslides when disturbed. The sensitive nature of these marine clays poses a challenge to geotechnical engineers in coming up with cost effective solutions to ensure the safety of engineered structures.

Landslides cause death and extensive damage to infrastructure, with far-reaching impacts on the economy. It is impossible to avoid expanding land use over areas with sensitive marine clays, but having information that will help geotechnical engineers and City planers to be cautious and devise suitable methods for constructing civil engineering projects in these sensitive area would be very useful.

Rainfall is the most common trigger mechanism for landslides in sensitive marine clays (Crosta and Frattini, 2008; Terlien, 1998;). Infiltration of rain through soil increases the soil's pore water pressure, and when the pressure limit is exceeded, a landslide occurs. The intensity and duration of a given rainfall event play an important role in the amount and rate of infiltration and thus influence the likelihood of a landslide occurring (Terlien, 1998).

Climate Change has adversely affected global temperatures and precipitation, including in Ottawa and the surrounding areas. The greater frequency of extreme events, such as flooding, has

caused tremendous damage to local property and infrastructure. It is therefore imperative that we investigate how future rainfall will affect landslide susceptibility in this area, especially in regions with sensitive marine clays.

Knowing the degree of landslide susceptibility that might be expected in the future will help city planners and engineers to take proactive measures to avoid structural damage and safety hazards that may occur in the worst possible scenario. Such information could also assist in the creation of regulations regarding development in the sensitive areas.

It is difficult to predict the time and location of a rainfall-induced landslide. However, this difficulty may be overcome by combining future climate model data with a rainfall infiltration model. Such an approach will facilitate in the assessment of the factor of safety of various slopes in the Ottawa area that contain sensitive marine clays. This information is vital in pinpointing the time and location of potential future landslides in the Ottawa area. However, there are many uncertainties associated with various factors, such as the degree of accuracy of the data for the geotechnical properties of the soil, and the uncertainty arising from downscaled projected climate model data.

1.2 Research Objectives

The purpose of this study is to assess the influence of projected rainfall intensity on landslide susceptibility in Ottawa's sensitive marine clay regions. The GIS-based geotechnical model was used to determine how the projected duration of rainfall intensity in future downscaled climate model data may impact landslide occurrences. A map of areas prone to rainfall-induced landslides based on rainfall intensity and location of rainfall in Ottawa's sensitive marine clay regions will then be generated. The map can serve as a guide in taking precautions when planning future geotechnical engineering projects and also assist city planners in their decision-making.

1.3 Research Methodology and Approach

This study was conducted in five stages as illustrated in Figure 1-1 below. The first stage involved a literature review of previous and similar studies on sensitive marine clays to gain an understanding of the background of sensitive marine clays in Ottawa and of concepts relating to rainfall-induced landslides as well as to understand the configuration of the TRIGRS model and to determine the methods that should be employed to achieve the study's objectives.

The second stage was gathering the data, including projected regional climate model data for Intensity Duration Frequency (IDF), topography, hydrology, geology, and geotechnical properties data. Interpolation analysis in ArcGIS was applied to the data to obtain continuous values for the

entire Ottawa area. The data were clipped to areas which contain sensitive marine clays for analysis in the TRIGRS model. The analysis focused on the frequency of rainfall occurrence for 10, and 50 recurring years and intensity durations of 6 hr, 12 hr, 24 hr, and 48 hr.

The City of Ottawa LiDAR Digital Elevation Model (DEM), published in 2012, was obtained through University of Ottawa geospatial data library. The DEM provided 1m resolution for the entire City of Ottawa area. The DEM was then re-sampled to generalize the resolution to 25m for the TRIGRS model and clipped to the sensitive marine clay areas. Slope analysis was performed on the DEM using the Spatial Analyst extension in ArcGIS version 10.7. Direction of flow and depth of failure, which is used as a lower boundary, were also analyzed using the spatial analyst extension in ArcGIS. The depth of failure was calculated using a raster calculation based on slope function using equations embedded in TRIGRS.

Water Level was obtained from the Provincial Groundwater Monitoring Network (PGMN) well data through Ministry of Environment access. The PGMN well data provides information on baseline groundwater levels. Additional groundwater level obtained from the Water Well Information System (WWIS) well through Ministry of Environment.

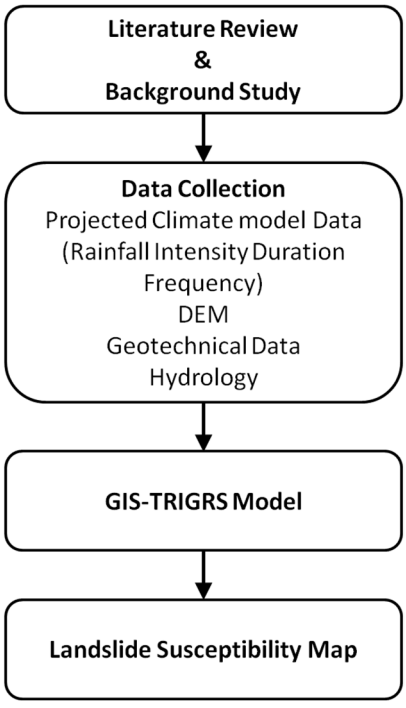

Figure 1-1 Flow chart of thesis organization

Another important set of data for the TRIGRS model is the geotechnical properties of the sensitive marine clays in the Ottawa area. These data were obtained from a previous study by Al-Umar, 2018.

The geotechnical properties include: effective cohesion, effective internal friction, volumetric water content at saturation, soil water diffusivity, residual water content, saturated hydraulic conductivity, and inverted capillary fringes. The inverted capillary fringes can be calculated by fitting parameters hydraulic pressure head, volumetric water content at saturation, and residual water content in the soil-water characteristic curve (SWCC).

The data were converted to raster format in ArcMap and clipped to the sensitive marine clays areas which were extracted from the surficial geology dataset. Then, the rasterized data were converted into ASCII format for use in TRIGRS model.

The third stage involved executing an analysis using the TRIGRS model. The TRIGRS model is a one-dimensional model that generates rainfall runoff and computes factor of safety from an infinite-slope model on a cell-by-cell analysis. It is written in FORTRAN and is executable software. The input text file contains the model specifications and directories of the data files. The results from the TRIGRS analysis were generated in ASCII format, which can be viewed in ArcGIS. More details on the infinite-slope stability model are provided in Chapter 7.

Lastly, the factor-of-safety results generated from the TRIGRS model for different rainfall intensities and durations were then plotted on a map, and landslide susceptibility maps were created.

1.4 Thesis Outline

This thesis contains six chapters, summarized below;

Chapter 2 provides background information on sensitive marine clays in Eastern Canada, including their origin, historical development, physical extent, physical geotechnical characteristics, as well as a review of GIS, the TRIGRS model, and climate model data used in this thesis.

Chapter 3 summarizes previous studies and literature on sensitive marine clays in eastern Canada.

Chapter 4 provides background on the study area including climate, population, geographical, geomorphological, and geological characteristics of the City of Ottawa and the geotechnical characteristic of sensitive marine clays in the Ottawa area.

Chapter 5 discusses the effect of climate change on rainfall intensity in the Ottawa area and provides background on downscaled global climate model data used in this study, including how the IDF curves were developed based on global climate models. This section also provides selections of times and durations from rainfall intensity data criteria for the model used in this study.

Chapter 6 presents results from the TRIGRS model analysis as well as a discussion on the sensitivity analysis derived from changing geotechnical parameters in the model, such as soil

cohesion and unit weight of the soil. A discussion and conclusions on the factor of safety results from the model, the limitation of the model, and geotechnical data are also provided in this chapter.

1.5 References

Al-Umar, M. (2018). GIS based assessment of climate-induced landslide susceptibility of sensitive marine clays in the Ottawa region, Canada. Unpublished doctoral thesis. The University of Ottawa, Ottawa, Canada. Available at: http://dx.doi.org/10.20381/ruor-21490.

City of Ottawa. (2016). *Growth Projections for Ottawa: Prospects for Population, Housing, Employment and Land, 2014-2036*. Available at: https://documents.ottawa.ca/sites/documents/files/growth_projections_2014to36_en.pdf.

Crosta, G. B. and Frattini, P. (2008). Rainfall-induced landslides and debris flows. *Hydrological Processes*, 22 (4), pp. 473–477. Available at: https://doi.org/10.1002/hyp.6885

and hazard assessments in a GIS framework. Eng. Geol., 102 (3), pp. 214–226.

Statistics Canada. (2020). Canada's population estimates: Subprovincial areas, July 1, 2019. *The Daily*, Thursday, February 13. Available at; https://www150.statcan.gc.ca/n1/en/daily-quotidien/200213/dq200213a-eng.pdf?st=xmUGS0Bw.

Terlien T. J. M. (1998). The determination of statistical and deterministic hydrological landslide-triggering thresholds. *Environmental Geology*, 35 (2-3), pp. 124–130.

2 Theoretical and Technical Backgrounds

2.1 Introduction

Sensitive Marine Clays are found in great abundance in the St. Lawrence Lowlands region, which was once the Champlain Sea. The clay was initially deposited in a marine environment, and later in an estuarine environment, when the land rose as a result of isostatic uplift and the area became a network of rivers. Sensitive marine clays have unique characteristics, which had been studied extensively in the past. These studies have been carried out using various computer applications, including the Geographic Information System (GIS). GIS is a tool that organizes, analyses, and displays sets of data on the basis of location—for example, data relating to geographical features such as topography, soil, hydrology, climate, etc. It is also a useful tool for reviewing, organizing, and processing data in engineering and other scientific fields. This chapter provides background information on sensitive marine clays, including their origin and characteristics. Background information about GIS and the TRIGRS model, as well as a summary of the climate model data that was used as input data for the model are presented in this chapter.

2.2 Background on Sensitive Marine Clays

In Canada, sensitive marine clays are also known as Leda Clays. The term Leda Clays was introduced before the 1980s. It was first used by the Canadian geologist, Dr. J. W. Dawson (Bechai, 1974). The name is derived from the fossil *Leda glacialis* found in great abundance in this type of clay. The clay is also called Champlain Sea clay, after the sedimentary basin in which it originated, the Champlain Sea. The name Quick clay is also widely used in Canada and Scandinavia, a reference to the clay's sensitivity.

2.2.1 Origin and Geological Setting

Sensitive marine clay is a sedimentation product of proglacial and postglacial water bodies that existed during the retreat of the Wisconsin Ice Sheet, between 18000 to 6000 years before present (BP). The Wisconsin Ice Sheet extended over most of Canada into the northern United States during the last Ice Age. The oldest deposits of sensitive marine clay are found in the south of Canada, along the St. Lawrence River Lowlands, and the youngest are in the north, around Hudson Bay, and to some extent in the Canadian arctic region. In the high Arctic, proglacial lakes still exist in contact with active glaciers, remnants of the continent-spanning Wisconsin glacier. The sedimentation covered large

areas where saline water from the Atlantic Ocean entered the depressed areas in coastal regions, and flocculated marine clays were deposited (Figure 2-1). The changing climate between 18000 and 6000 years BP controlled the melting and retreat of the Wisconsin Ice Sheet. This large-scale melting, combined with the glacio-isostatic rebound and eustatic rises in sea level, resulted in the development of this proglacial lacustrine system (Quigley, 1980).

As the extent of the Wisconsin Ice Sheet reached a maximum between 18000 and 20000 years BP, the ice reached a maximum thickness of up to 5000 m, centered over Hudson Bay. The weight of this massive ice sheet depressed the underlying land surface; the earth's crust in the Hudson Bay area may have been depressed by up to 1000 m (Quigley, 1980). At this time, due to the mass of water captured in the great ice sheets, ocean water levels were at least 120 m below present-day levels.

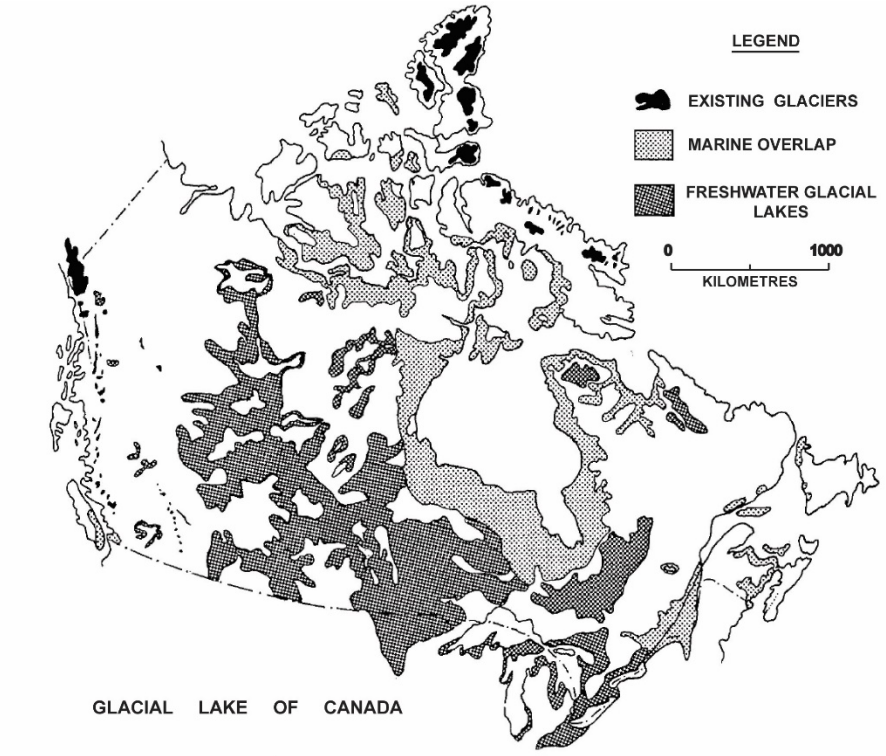

Figure 2-1 Distribution of marine and freshwater glacial and postglacial lakes of Canada (Quigley, 1980).

As the climate began to warm, beginning roughly 18000 years BP, the ice began to retreat. The retreat of the Wisconsin glacier happened in stages, created large or small proglacial lakes at the ice front depending on the rate of meltwater production, with major re-advances of ice at approximately 13500, 11800, and 8200 years BP.

As the ice sheet thinned and retreated northward, the earth's crust rebounded. The rebound was approximately 200 m in the Ottawa area, as shown in Figure 2-2 (Andrews and Retherford, 1978; Quigley, 1980).

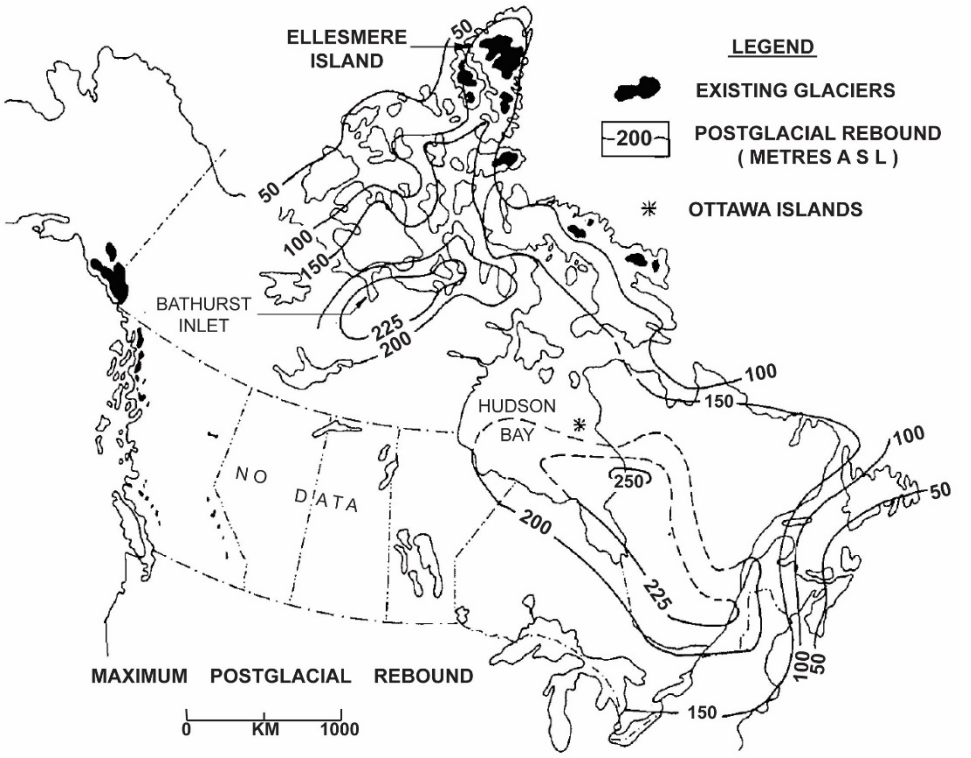

Figure 2-2 Maximum postglacial rebound of Eastern Canada (Quigley, 1980, after Andrews, 1972).

At 11800 years BP, the major proglacial water bodies were the Champlain Sea, Lake Algonquin, and Lake Agassiz (Quigley, 1980). Lake Algonquin covered the Georgian Bay, Lake Simcoe, and western Superior areas. Lake Agassiz covered the area that extended from Lake Nipigon and Hudson Bay into the United States (Figure 2-3) (Nader, 2014).

The Champlain Sea existed between 12500 and 10000 years BP, in the present-day location of the St. Lawrence Lowlands and the Ottawa area. It is believed to have invaded the lowlands from the Gulf of St. Lawrence when an ice dam melted in the Quebec City area. The seawater from the Champlain Sea flowed into freshwater lakes in the valley and marine clays were deposited over freshwater varved clays in many areas including the Ottawa area (Quigley, 1980). Marine clay deposits close to the centre of the Champlain Sea are thick, while deposits nearer to the edge of the sea are interlayered with fluvial sand and gravel or glacial till (Nader, 2014).

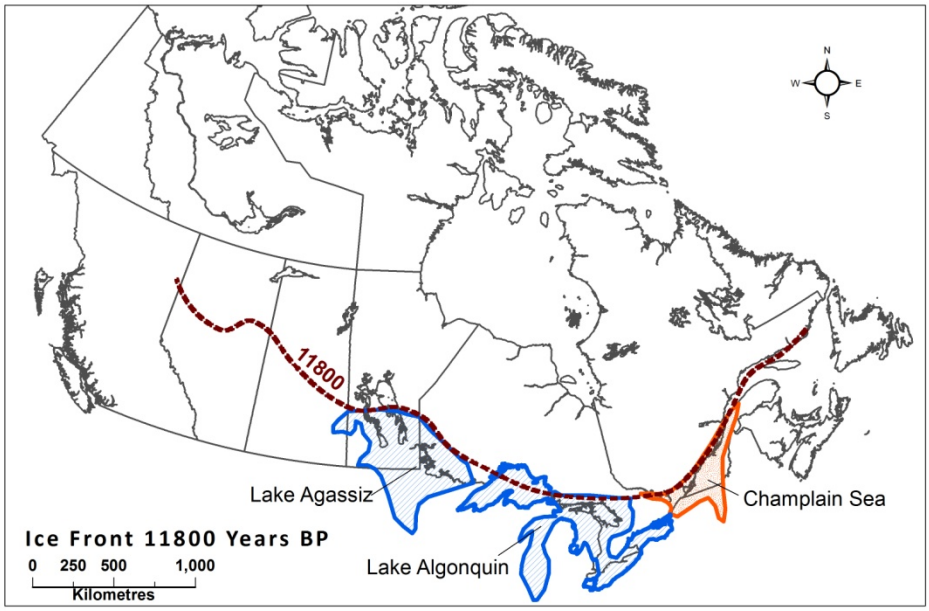

Figure 2-3 Evolution of the major glacial lakes of Canada 11 800 years BP (Quigley, 1980).

At 10000 years BP, the ice front was at the end of the Champlain Sea and the start of Mer LaFlamme in the St. Jean region of Quebec. At 8200 years BP the ice front was at the start of Lake Barlow-Ojibway south of James Bay and the shrinking of Lake Agassiz (Figure 2-3).

At the location of the ice front at 7000 years BP, the final phase of sensitive marine clay deposition occurred, in the present-day Tyrrell and Iberville Seas around Hudson Bay (see Figure 2-4). There was also extensive clay deposition in the region south of Fort Rupert, Quebec. Due to isostatic rebound after deglaciation, the land rose 200 m, resulting in the exposure of the marine deposits to weathering forces. The ice retreat in the Hudson Bay area was extremely rapid and invasion by seawater via Hudson Strait happened in a similar way to that of the Champlain Sea (Quigley, 1980)

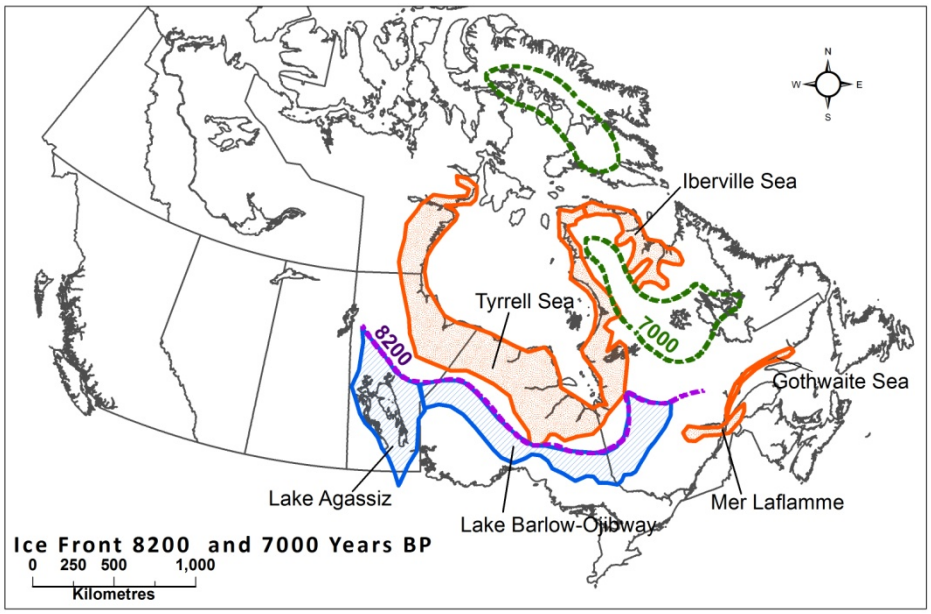

Figure 2-4 Evolution of the major glacial lakes of Canada 8200 and 7000 years BP

2.2.2 Sedimentology of Sensitive Marine Clays

The sedimentary environment in the proglacial lakes and marine estuaries is very important for interpreting the geology and geotechnical behaviour of the sensitive marine clay deposits. Table 2.1 lists the major types of deposits that may be encountered in geotechnical practice. The first three types—water-laid tills, lacustrotills, and mudflow deposits—consist of coarse-grained material within a fine clayey matrix. Varved clay and marine clay deposits occur at quite a distance from their sources, and they consist of more uniform, silty clays and fine textures.

Table 2.1 Types of soft clayey soil deposits (Quigley, 1980)

Type of deposit	Origin
1. Water-laid tills	Unsorted lacustrine sedimentation below floating ice
2. Lacustrotills	Subaqueous, proximal, flow deposits in proglacial lakes
3. Mudflow deposits	Subaerial and submarine flows
4. Turbidity current deposits	Heavy-density current deposits generated by mudflow dilution, floods, ice calving, slumping, etc.
5. Varved clays	Turbidity current summer deposits and winter clay deposition by settling
6. Marine clays	Salt-water flocculation and sedimentation

In geotechnical practice, varved clays are layered sediments deposited in glacial freshwater lakes. A single varve, representing 1 year of deposition, consists of a couplet of summer silt and winter clay. During the summer, the cold inlet streams have a relatively high density of about 1g/L, close to the maximum density of water. This dense water flows into the bottom of the proglacial lake, potentially travelling for a long distance as shown in Figure 2-5(b). This relatively fast-moving water deposits sand and silt. During the winter, the inlet streams, which carry less sediment, have a lower density than the sediment-laden lake water; thus overflow occurs, as shown in Figure 2-5(a) and the slow settling of clay particles from the winter layer is relatively undisturbed (Quigley, 1980).

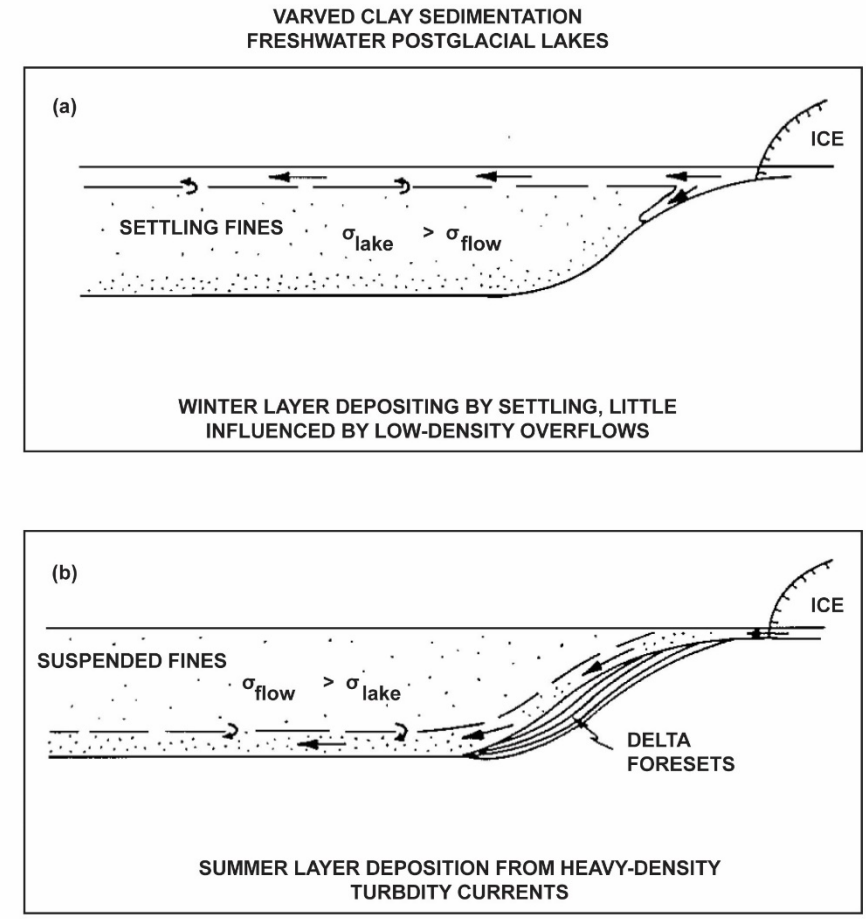

Figure 2-5 Deposition of varved clays by turbidity currents (summer layers) and settling (winter layers) in cold proglacial lakes (Quigley, 1980).

The summer layer of the varve, a silt-rich layer (80% of particles> 2 μm), is thicker (up to ~ 1 m) than the clay-rich (80% < 2 μm) winter layer, indicating high-velocity bottom flows near the sediment source. The transition zone and winter layer are more likely to contain silt laminae from the winter thaw period because they are close to the glacial meltwater source.

When the meltwater from the ice front enters the sea, it enters as an overflow because the density of the meltwater (< 4g/L) is less than the density of the seawater or salt water (~1020 g/L at a salinity of 35g/L). Mixing of freshwater and saltwater proceeds by diffusion and turbulence down to a depth of about 5 m, where flocculation of the clay particles begins. Below this zone, extensive pelletization occurs when aquatic organisms ingest the clay flocs and produce fecal pellets or floccules containing a significant amount of organic matter. These organic-rich floccules are a fertile ground for bacterial activity, which is partially responsible for the black mottling commonly observed in marine clay. The organic content in marine clay is between 0.4 and 1.0%.

Marine clays acquire an open, flocculated structure in the process of sedimentation. This open structure is maintained even when the deposits are subsequently buried under several metres of soil, if the rate of deposition is slow and deposition is accompanied by the development of electrostatic bonds. From a geotechnical standpoint, then, a major concern is that flocculation of the sediments under these conditions produces a soil with a high void ratio. (Quigley, 1980)

In its early phases, the Champlain Sea was very deep, as shown in Figure 2-6. The Champlain Sea probably remained saline until crustal rebound reduced its depth during later phases, about 10000 years BP. In these later phases, the area experienced sudden influxes of fresh water from lakes surrounding the region. The currents created by these influxes eroded the marine clays from the scarps and terraces and redeposited them downstream, creating two distinct layers consisting of two different types of clay. The older layer, deposited in a marine or brackish-water environment, consists of very soft, blue-grey, silty clay. The younger layer above it, deposited in a fresh-water, or fluvial, environment, consists of stiff, grey to brownish-grey, rust-mottled silty clay (Bechai, 1974). The silt and clay are composed predominantly of minerals such as quartz, feldspar, amphibole, mica, and chlorite, usually with small amounts of smectite, which represent glacial rock flour (Quigley, 1980).

The deep-water deposits represent a variably cemented accumulation of inorganic floccules, organic agglomerates, and fecal pellets, which retain their structure *in situ* until destroyed by consolidation. The flocculated structures in these marine sediments form a strongly bonded soil skeleton, which is 'glued' together by highly mobile sea-salt ions with high water content (Al-Umar, 2018). The positive charge of the sodium cations in the sea salt binds to the negative charge on the surface of the clay particles, balancing the charge in the diffuse double layer around each particle, thus conferring on the soil a liquidity index close to 1.0 (Locat, 1995).

In the absence of sodium and other electrolytes in the water, the negative charge on the surface of the clay particles binds to positively charged hydrogen ions in the water molecules. This

electrostatic bonding between the clay particles and water molecules produces a repulsive force between individual clay particles and causes the soil to swell and be unstable. As the concentration of electrolytes in the water increases and the hydrogen ions are replaced by salt ions, the diffuse double layer contracts and the repulsion between the clay particles decreases, resulting in greater soil stability and increased shear strength. Thus, as salinity decreases, soil sensitivity increases and remoulded shear strength decreases. A decrease in salinity occurs typically through leaching, as rainwater and snow melt wash away the salt layer that bonds the clay particles together leaving the soil extremely weak and highly sensitive (Nader, 2014).

A more detailed discussion on the geotechnical characteristics of sensitive marine clays will be presented in Section 2.2.4.

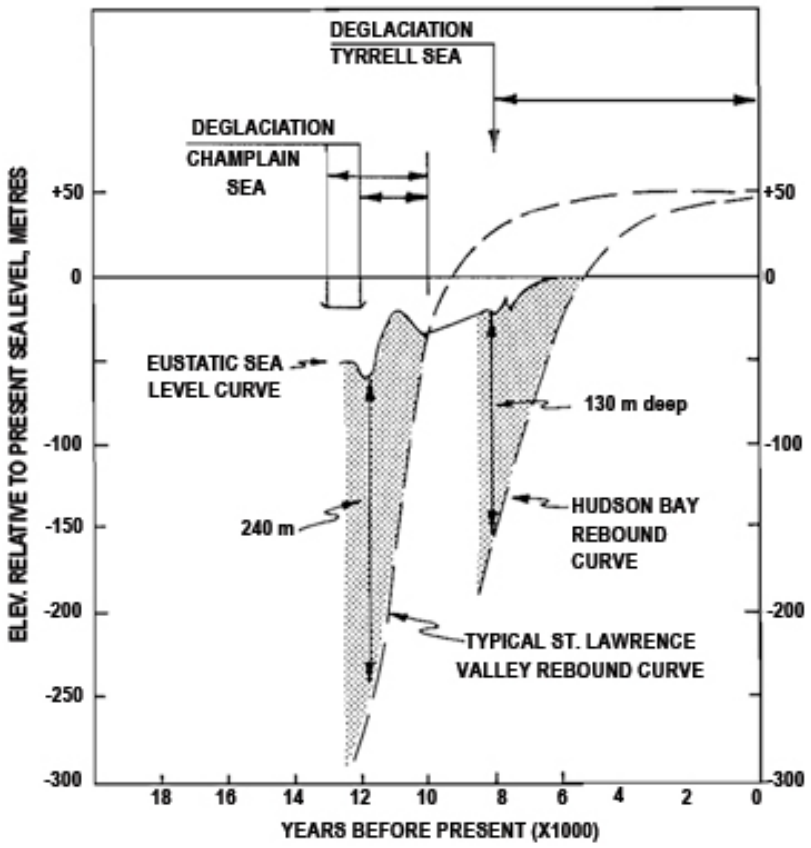

Figure 2-6 Marine transgression and expulsion by crustal rebound, Champlain and Tyrell Seas (Quigley, 1980).

2.2.3 Current Extent of Sensitive Marine Clays in Canada

The majority of the marine deposits in Canada were bound by the inland sea limit of the Champlain Sea, currently the St. Lawrence Lowlands; part of eastern Ontario and southern Quebec along the St. Lawrence River (Figure 2-7). A number of major cities are situated within this region, including Ottawa, Montreal, and Quebec City. Marine deposits are also found in the LaFlamme Sea, situated in the present-day towns of Saguenay and Dolbeau-Mistassini in the province of Quebec, the Goldwait Sea, situated on Quebec's northern shoreline and in valleys along the shore, and the Tyrell and Iberville Seas, surrounding present-day Hudson Bay and south of Fort Rupert in the province of Quebec.

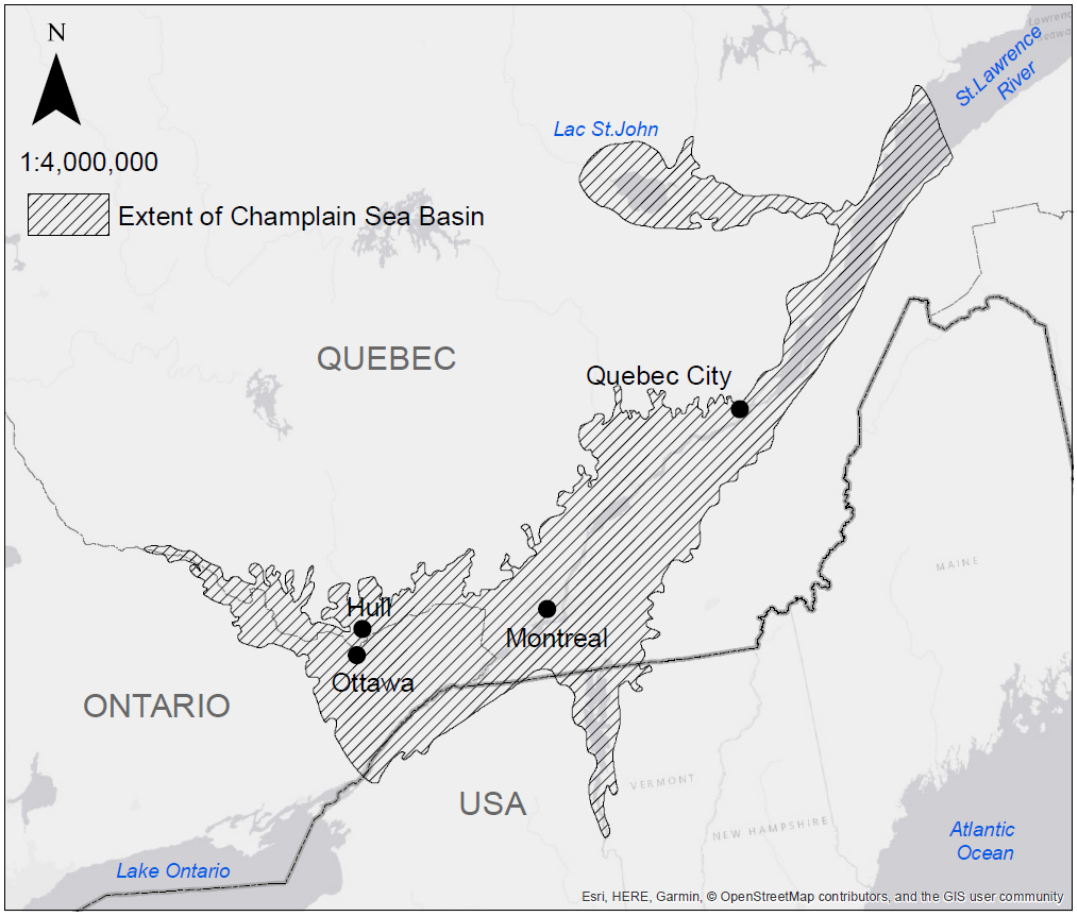

Figure 2-7 Extent of sensitive marine clays limit in Ottawa Valley and Quebec areas (modified from McEniry, 1978).

The sensitive marine clays deposits are of variable thickness. Figure 2-8 shows the variations in clay thickness in the Ottawa area as the map shows, the clay thickness ranges between 1 m and 88

m, the thickest deposits occurring along the Carp River and in the eastern part of the City. A study by Nastev et al. in 2016 found thick clay deposits, about 100 m deep, in the Ottawa suburb of Orleans.

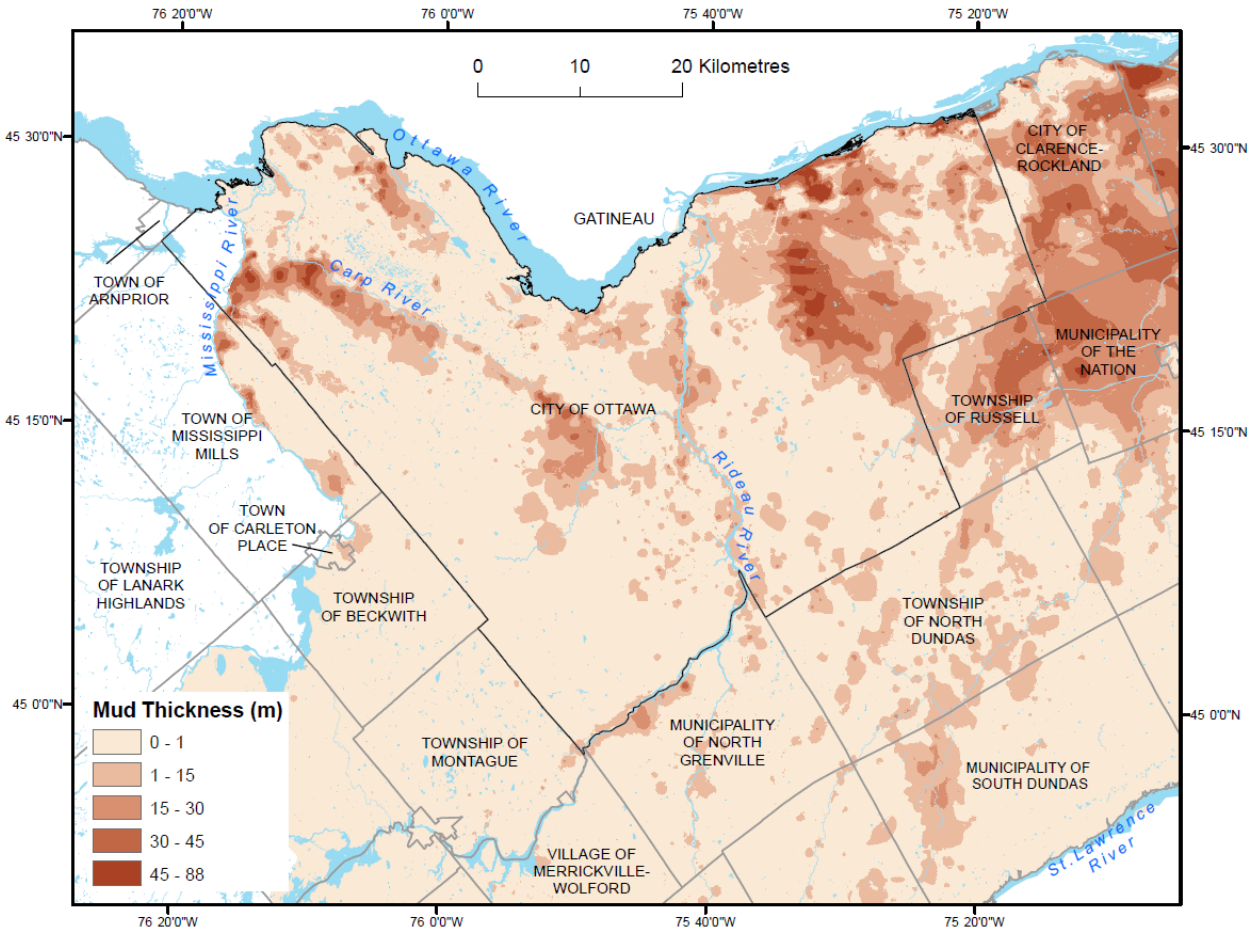

Figure 2-8 Mud thickness in Ottawa area (Logan et al., 2009)

2.2.4 Characteristics of Canadian Sensitive Marine Clays

The physical, mineralogical, geochemical, and geotechnical properties of sensitive marine clays are key factors to be considered in controlling the clays' sensitivity (Locat, 1984). In this section, these properties will be reviewed to gain an understanding of how they affect the clays' sensitivity.

2.2.4.1 Mineralogy

In the Champlain Sea, there were two major sources of sediment rock flour: igneous rocks of the Canadian Shield and metamorphic rocks of the Appalachians. The primary materials in the marine sediments in the Champlain Sea are: illite, quartz, feldspar, amphibole, mica, and chlorite, with small

amounts of smectite, glacially ground amorphous material, and carbonates, with trace amounts of kaolinite and vermiculite (Brydon and Patry, 1961; Nader, 2014; Quigley, 1980; Taha, 2010). Over time, chlorite is oxidized into smectite and vermiculite as a result of erosion, thus the surface layers of a given soil may contain higher amounts of smectite and/or vermiculite than the underlying layers (Barton and Karathanasis, 2006; Nader, 2014).

The LaFlamme sediments contain rock flour of ultramafic composition. The primary minerals are: feldspar, mica, quartz, hornblende, and chlorite, along with about 5-13% carbonate of local Paleozoic origin. For the Tyrell Sea, information about the composition of the sediments is limited; however, early work at Fort Rupert showed that the deposits contain abundant carbonate of Paleozoic origin from the Hudson Bay lowlands (Quigley, 1980).

The mineral content of marine clays varies from site to site, depending on their principal sediment sources. The dominant minerals tend to differ in their relative quantities from region to region and at different depths. It has been observed that when the amount of illite increases, the amounts of the other clay minerals decrease. Aluminum and iron oxides increase as the particle size decreases. The presence of these oxides, known as amorphous sesquioxides, is significant because they create a coating around clay minerals and contribute to the bonding mechanism and cementation (Nader, 2014). The amorphous sesquioxides consist of complex hydroxides of silica, alumina, and iron produced by glacial grinding. Previous studies have revealed an inverse relationship between the amount of amorphous material present in marine clays and the sensitivity of the soil. Amorphous sesquioxides are so reactive that, when present in abundance, they act as a clay mineral thickener, enhancing cementation in the soil and thus increasing the remoulded shear strength and reducing sensitivity (Quigley, 1980).

Another cementation agent present in marine clays is calcium carbonate of organic origin, predominantly from seashells. Typical marine clays contain 1-4% carbonate, but concentrations can go much higher. For example, in Saint-Jean-Vianney, Quebec (which was completely demolished in a catastrophic landslide in 1971), concentrations range from 6 to 13% (though the carbonates here possibly came from Paleozoic limestone in the vicinity rather than from organic sources); in the Arnprior region, northwest of Ottawa, the concentration is as high as 13%; and at Port Rupert, on James Bay, it reaches 30% (Ballivy et al, 1975; Quigley, 1980).

The lists in Table 2.2 reveal how the mineralogical and geotechnical properties of the clays control the soil's undisturbed and remoulded shear strength and sensitivity. The relationship between sensitivity, and the soil's undisturbed and remoulded shear strength is expressed in the following formula (Quigley, 1980).

$$S_t = \frac{S_u \text{ (undisturbed)}}{S_u \text{ (remoulded)}}$$

Where: S_t = sensitivity
S_u = shear strength

Table 2.2 Geochemical and mineralogical controls on sensitivity of clayey soils (adapted from Quigley, 1980)

Factors Producing High Undisturbed Strength and High Sensitivity	Factors Producing Low Remoulded Strength and High Sensitivity
1. Depositional flocculation High salinity (low zeta potential) High sediment concentration Divalent cation adsorption 2. Slow increase in sediment load 3. Cementation bonds Carbonates & sesquioxides (amorphous)	1. High water content ($w_n \geq w_l$) Little consolidation, or decrease in w_l > decrease in w_n 2. Low specific surface of soil grains High silt content or high rock flour in < 2 μm fraction High primary mineral ≡ low clay mineral content 3. High zeta potential (Expanded double layers → high inter-particle repulsion → dispersed or peptized state) Low salinity by leaching (< 2 g/L) Organic dispersants (anion adsorption) Inorganic dispersants (anion adsorption) High monovalent cation adsorption relative to divalent cations 4. Low amorphous content 5. Low smectite content

2.2.4.2 Grain-Size Distribution and Clay-Size Fraction

In the Ottawa area, the sensitive marine clay is topped by a sandy silt layer containing only 16.9% clay. This upper layer sits on top of a deep silty clay layer with a maximum thickness of 20 m and a clay content of about 80% (Nader, 2014).

By definition, a soil particle is identified as clay if it has a diameter of <2 μm. In the Ottawa area, the clay-size fraction of the sensitive marine clays is in the range of 56% to 97% (Nader, 2014; Rasmussen, 2012; Taha, 2010; Taha and Fall, 2010; Mitchell, 1970; Quigley and Thompson, 1966). The clay-size fraction of these soils exhibits seasonal variations, with silty summer deposits containing <80% clay and clayey winter deposits containing >80 % (Nader 2014).

2.2.4.3 Clay Particle Properties

According to Penner (1965), clay particles consist of a negatively charged surface, which attracts positively charged hydrogen ions in the water molecules. The bonding between the clay particles and water molecules causes repulsion between the soil particles, resulting in swelling of the soil. The bonding produces a diffuse double layer. There is a fixed negatively charged layer at the surface of the clay particles. The charge potentially drops exponentially in moving away from the centre of the clay particles. After the fixed negatively charged layer, there is a stern layer and then a positively charged diffusion layer. The diffusion layer attracts negative electrodes or cathodes, such as the hydrogen ions in water molecules. The negative particles in the absorbed water layer are called the immobile layer, it attracts positive electrodes or anodes (Figure 2-9).

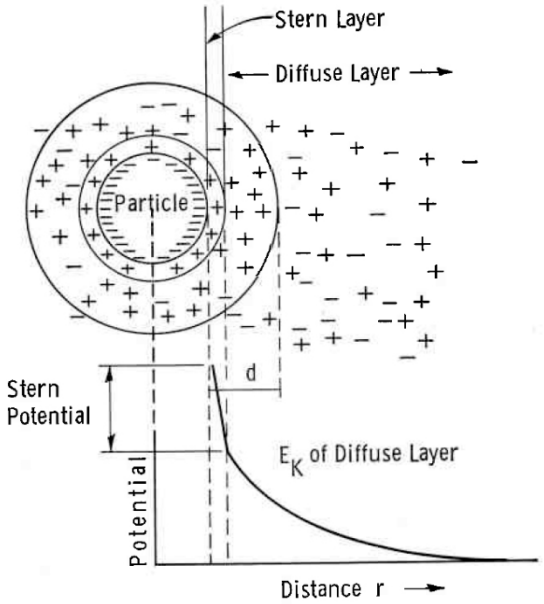

Figure 2-9 The electrokinetic potential E_K, and the electrical double layer (Penner, 1965).

The potential difference between the clay particles and the surrounding liquid is called the electrokinetic potential. In marine clays, ions of sodium (and other electrolytes) replace the hydrogen ions in the diffuse layer and thereby displace the water, decreasing the electrokinetic potential and causing the diffuse layer to contract. An increase in the electrolyte concentration in the water therefore reduces the repulsive force between the clay particles and consequently decreases the soils sensitivity. It is easy to achieve structural breakdown in sensitive marine clays, but difficult to recreate the original random open structure because of the difficulty in restoring the electrokinetic potential. Although, marine clays have open flocculation at the particle level, they have strong

cementation bonds at the interparticle level, and it is these fabric bonds between the soil particles that dominate the soil's behaviour. When high confining pressure is applied on the soil the fabric bonds collapse (Nader, 2014).

The open flocculated structure of marine clays is the result of the property of clay by which it flocculates rapidly in water containing electrolytes, that is water with some degree of salinity, the ideal concentration being 10 psu (Sutherland et al. 2015). The flocculated particles approximate the size of silt and sand particles and thus settle simultaneously with them, forming a loose, porous structure consisting of a mixture of clay, silt, and sand. By contrast, in fresh water, flocculation does not occur, and the clay particles, which remain dispersed, therefore settle more slowly than the sand and silt particles. Slower settling gives the clay particles time to assume a parallel orientation resulting from the repulsive forces between the particles. This produces a more tightly packed structure. Flocculation of clay particles takes place through electrostatic attraction between the particles' negatively charged faces and their positively charged edges. This creates an edge-to-edge, an edge-to-face, or a random arrangement, known as the "card-house" structure, which produces a flaky fabric (Bennett et al., 1978; Gillot, 1987). A comparison of the two types of structures is shown in Figure 2-10 and the flaky fabric of the marine clays is shown in Figure 2-11.

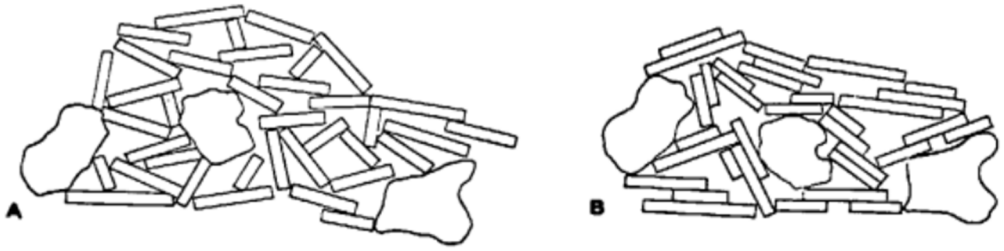

Figure 2-10 The "card-house" structure contrasted with the parallel structure.
A. Undisturbed saltwater deposit ("card-house" structure). B. undisturbed freshwater deposit (parallel structure). (Gillot, 1987).

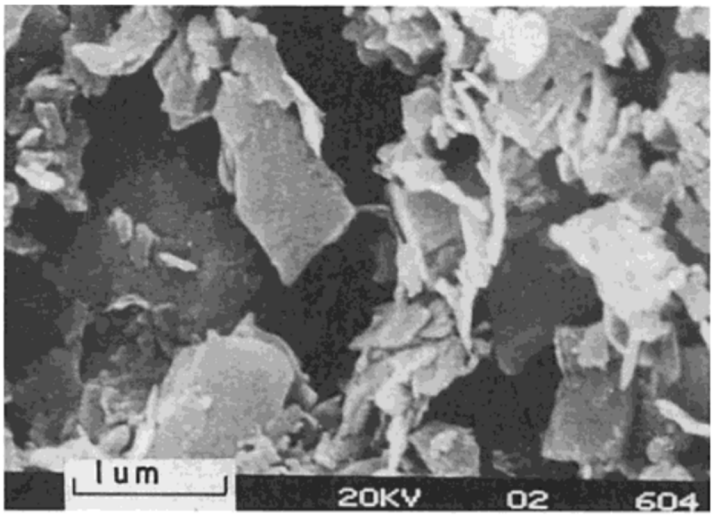

Figure 2-11 Scanning electron micrograph of the flaky open fabric of a sample of marine clay taken from Kars on the Rideau River in south Ottawa (Gillot, 1987).

2.2.4.4 Clay Microstructures and Macrostructures

Clay structure plays an important role in the mechanical behaviour of sensitive marine clays and thus influences the engineering response of the soil. Two types of structure are generally recognized: (1) microstructures, which are <1 mm in size; (2) macrostructures, which are >1 mm, that is, visible to the naked eye. A clay deposit's entire geologic and stress history is recorded in the clay's micro- and macro-structures. In the earliest stages, individual clay particles flocculate to form submicroscopic fabric units known as domains. Domains then aggregate together to form clusters, which are visible to an optical microscope. Finally, biogeochemical processes at work in the soil cause the clusters to adhere to each other in clumps, known as peds, which are visible to the naked eye. Peds frequently contain fecal pellets, consisting of waste products deposited by biological agents, such as plankton, in the soil (Figure 2-12) (Quigley, 1980; Taha, 2010).

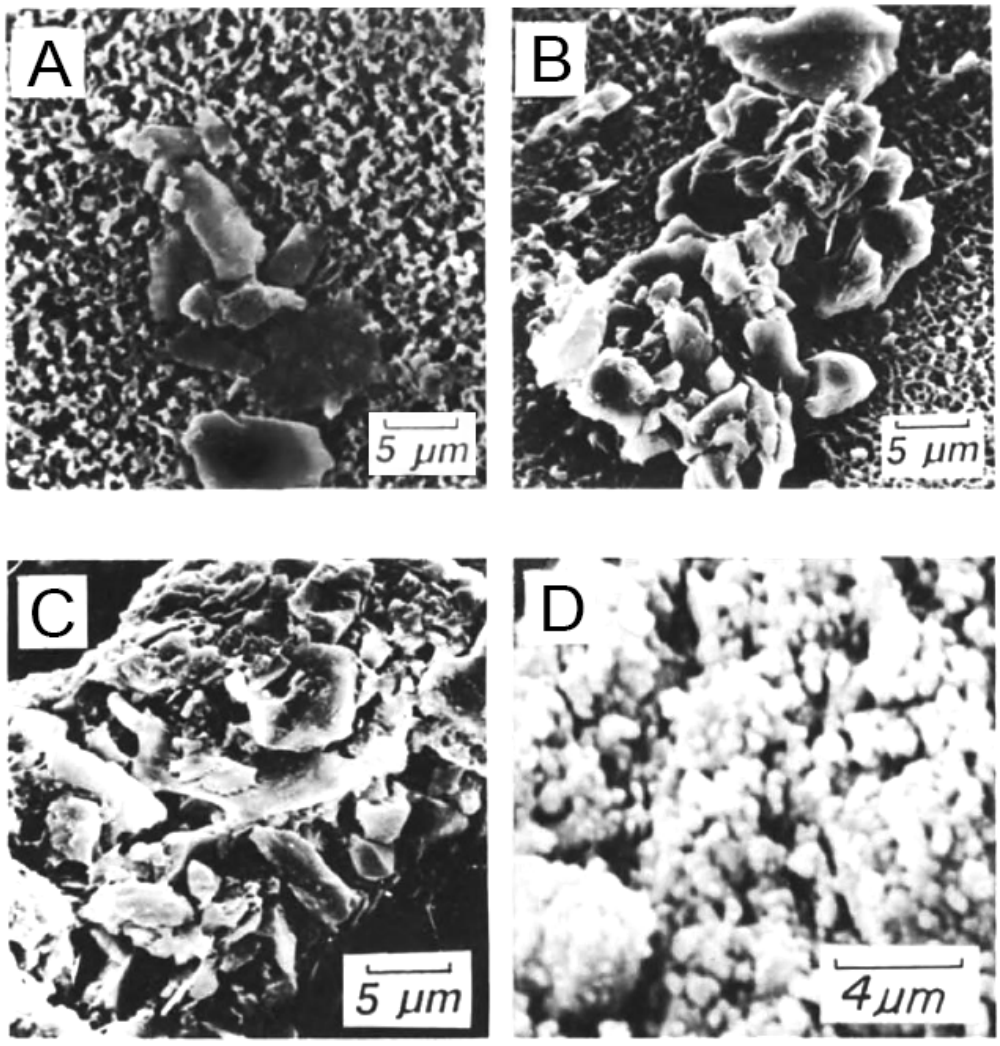

Figure 2-12 Scanning electron micrograph images of clay microstructures and macro-structures.
(A) A small edge-to-edge floccule (a domain); (B) A large face-to-face floccule (a cluster); (C) A ped, formed by a mineral-bearing fecal pellet; (D) microstructures and macrostructures in Leda clay (Adapted from Quigley, 1983).

2.2.4.5 Pore Structure and Properties

The pores (also known as "voids") of sensitive marine clays are complex spaces enclosed by solid particles held together by plastic and rigid ionic bonds. In general, pores change their shape as pressure from the overburden increases. In the Ottawa area, however, the original pore structure has remained intact, despite the stress exerted by pressure from the several meters of overburden that lie above it. This retention of original porosity was the result of the fact that in the Ottawa area the rate of deposition of sediments was slow and was accompanied by the creation of ionic bonds between the clay particles to form the "card-house" structure (Quigley, 1980).

In sensitive marine clays, pores are of two types and sizes: (1) *inter-aggregate pores*, i.e., the spaces between larger aggregates (such as clusters or peds), also known as *macropores*, which are large and open; and (2) *intra-aggregate pores*, i.e., the spaces between the constituent particles of the aggregates, also known as *micropores*, which are small. This type of distribution of pore type and size has significant implications for engineering. The shape, size, and volume of both types of pores are not affected by remoulding (Gillott, 1987; Taha, 2010).

The macropores (inter-aggregate pores) are typically wedge-shaped and may contain air, or water, or both. (Gillott, 1987). However, because the clay particles are deformable, if water is present in the pore spaces, the water alters the shape and structure of the pores, resulting in the shrinking and swelling of the soil as water content decreases or increases (Chertkov, 2000).

In soils in general, pore size is controlled by particle size: the smaller the particles the smaller the pore size. Since clay particles are smaller than 2 μm in diameter, the pores in marine clays are proportionately small. An inverse relation exists between pore size and capillary force; thus, in marine clays, capillary force is high. As a consequence, water retention in the pores is correspondingly high. Surface tension in pores that contain both air and water is similarly high, and it increases as pore diameter decreases (Gillott, 1987).

The flow of air and water through soil is determined by the pore structure; thus, the nature of the pore fabric controls the soil's permeability (Gillott, 1987). Pores are connected to one another through narrow openings, knows as "pore throats". The number, size, and distribution of pore throats determine the flow, capillary pressure, and resistivity of the soil. In marine clays, the pore-throat size is extremely small. Consequently, the narrow pore throats are susceptible to clogging as minerals get transported and deposited during the process of cementation by precipitation (Gillott, 1987). Clogging of the pore throats reduces the already low flow and permeability of marine clays.

Consolidation occurs when water is expelled from the pores over time and pore size diminishes as a result of pressure exerted by the overburden. As noted above, marine clays in the Ottawa area resisted consolidation. Consolidation resistance occurs when the stress from the overburden is absorbed by the "card-house" structure of the soil skeleton and by porewater. However, when a breaking point is reached, the "card-house" structure collapses and the pore structure abruptly falls apart, resulting in massive settlement (Nader 2014).

Pores are the site of considerable biological activity. Biological agents play an important role in determining the chemical composition of the pores' contents. They extract carbon dioxide and other gases from pore air, and their metabolic processes and decomposition products affect the partial pressure of pore gases such as carbon dioxide, hydrogen sulphide, and ammonia. They also

synthesize complex organic molecules that may affect soil pH; serve as protective colloids, deflocculants, or chelating agents; and have other properties that influence the behaviour of the soil (Gillott, 1987).

2.2.4.6 Void Ratio and Porosity

Marine clays have a high void ratio as a consequence of clay's susceptibility to flocculation in a saline environment, which produces an open fabric structure (Quigley, 1983). As a result of this high void ratio, marine clays have a high degree of compressibility and therefore experience high vertical displacement during shearing (Taha, 2010). In general terms, void ratio and porosity decrease with depth. Void ratio and porosity for sensitive marine clays in the Ottawa area range from 0.82 to 2.80 and 45% to73.7%, respectively (Nader, 2014).

2.2.4.7 Unit Weight

The unit weight of Ottawa's sensitive marine clay ranges between 14.4 and 21.0 kN/m^3 (Lo et al., 1976; Rasmussen, 2012; Nader, 2014). The unit weight increases as the elevation decreases (Nader, 2014).

2.2.4.8 Water Content and Atterberg Limits

The Atterberg limits include the liquid limit and the plastic limit. From an engineering point of view, these limits are useful in predicting the mechanical behaviour of the soil and estimating values for soil properties such as short term shear strength and oedometric compressibility. Ottawa's marine clays have a high moisture content in the range 17-85%. The high moisture content of the clays yields high liquid limits, in the range 19-83%, and high plastic limits, in the range 14-35%. The plasticity index of the clays is in the range 15-49% and the liquidity index is in the range 1.1-2.3 (Nader, 2014; Dejong et al., 2011; Rasmussen 20,12; Taha, 2010; Taha and Fall, 2010; Leroueil, 1999; Lo et al., 1976; Mitchell, 1970; Quigley and Thompson, 1966).

These values show that the water content of the clay is close to or exceeds its liquid limit. This exceeding of the liquid limit is made possible by the open fabric structure of marine clays, which allows them to hold and retain large amounts of water, but also causes them to undergo rapid collapse when remolded (Taha 2010). A high liquidity index, which is defined as an *in-situ* water content close to or greater than the liquid limit, is typical of sensitive marine clays. A high liquidity index implies one of two things: (1) cementation bonding has largely prevented soil compression from taking place, leaving the large open pores intact, or (2) chemical or biochemical activity has

lowered the liquid limit to a greater extent than consolidation has decreased the *in-situ* water content. While cementation bonding plays a key role, generally, in maintaining the soil's natural water content above its liquid limit, geochemical factors are particularly significant in the case of clayey soils (Quigley, 1980). With their high liquidity index, marine clays remain stable as long as they are left undisturbed; however, when disturbed, they typically transform into a liquid, posing several geotechnical problems, such as landslides (Taha 2010).

With regard to the plasticity index, according to the Unified Soil Classification System, the sensitive marine clays in the Ottawa area can be classified as clays of high plasticity (CH) (Taha and Fall, 2010).

2.2.4.9 Porewater Chemistry

The pore water in marine clays contains dissolved minerals that affect the soil's liquid limit, plastic limit, sensitivity, flocculation potential, and other geotechnical properties and processes, such as the rate of porewater flow and cementation. The liquid limit, the plastic limit, sensitivity, the compression index, and the swelling index are all in an inverse relationship to salinity: they decrease as porewater salinity increases, whereas the coefficient of consolidation and the shear strength increase with increased salinity (Ajalloeian, 2013, Nader, 2014; Torrance, 1975). Flocculation occurs typically in conditions of low salinity, usually between 1 and 2.5%, but depends on a complex relationship between salinity and clay concentration (Mhashhash et al., 2018; Nader, 2014; Sutherland et al., 2015). When salinity is high, the dissolved minerals may crystallize and be deposited between clay particles to form cementation bonds, but they may also be deposited on the surfaces of the clay particles, thus interfering with flocculation (Ajalloeian, 2013).

Generally, the pore water in sensitive marine clays contains a low concentration of salt. However, the salinity varies with depth and location. These variations may be the result of weathering, leaching, or redeposition, and are related to the season in which the original deposition occurred, with summer depositions being more saline than winter depositions (Nader, 2014). Decrease in salinity through leaching is ubiquitous in the Ottawa region, the primary cause being rainfall, which percolates through the soil, washing salinity downwards. Leaching also occurs through diffusion, with dissolved minerals diffusing from areas of high concentration to areas of low concentration until salinity is uniform throughout the soil. Since a decrease in salinity causes sensitivity to increase, leaching, which produces an overall lowering of salinity, is a major factor in the gradual increase in the sensitivity of the soil, which may behave like a liquid when a critical level of low salinity is reached and the soil is disturbed. (Nader 2014; Torrance 1974).

The chemical composition of pore water also varies, depending on the age of the deposit. The pore water in older clays has a higher sodium, iron, and manganese content, which suggests deposition in a marine environment. The pore water in younger clays contains more calcium and magnesium, which is indicative of deposition in a freshwater environment (Bechai, 1974; Sangrey and Paul, 1971). Fresh water contains a high concentration of Ca^{2+} ions compared to sea water. When fresh water comes into contact with salt water, as in an estuarine environment, rapid chemical reactions take place in which the Ca^{2+} ions are replaced by Mg^{2+} and K^{+} ions (Torrance, 1979). This is precisely what happened in the Champlain Sea at the end of the last Ice Age, when ice melt water from the retreating glaciers flowed into its saline waters.

As noted above, sensitivity and plasticity decrease as salinity increases, and salinity increases with depth; hence, sensitivity and plasticity decrease with depth. This relationship is shown in Figure 2-13 using data from five samples of marine clay taken from Hawkesbury, Ontario on the south bank of the Ottawa River. The figure also shows the corresponding concentrations of sodium, magnesium, calcium, and potassium ions in the pore water. The dominant cation here at all depths is that of sodium, a phenomenon also observed by Taha (2010). Field tests conducted by Nader (2014) at a site just southeast of Ottawa reflect the inverse relationship between the sensitivity and plasticity of the soil on one hand, and the concentration of chloride, sodium, potassium, and magnesium ions in the clay's pore water on the other (Figure 2-14). It should be noted that there is a large variation in the composition of pore water and in the relative concentrations of the various electrolyte ions from one site to another (Quigley, 1983).

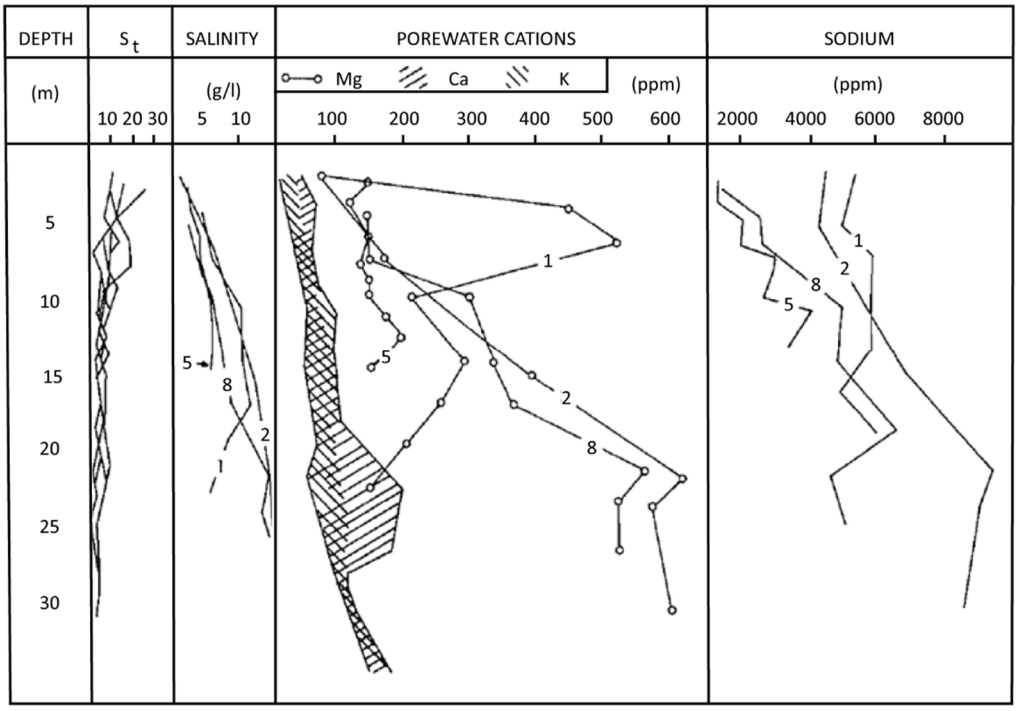

Figure 2-13 Sensitivity, salinity, and pore water cation chemistry vs. depth, for Hawkesbury Leda clay (Quigley, 1980).

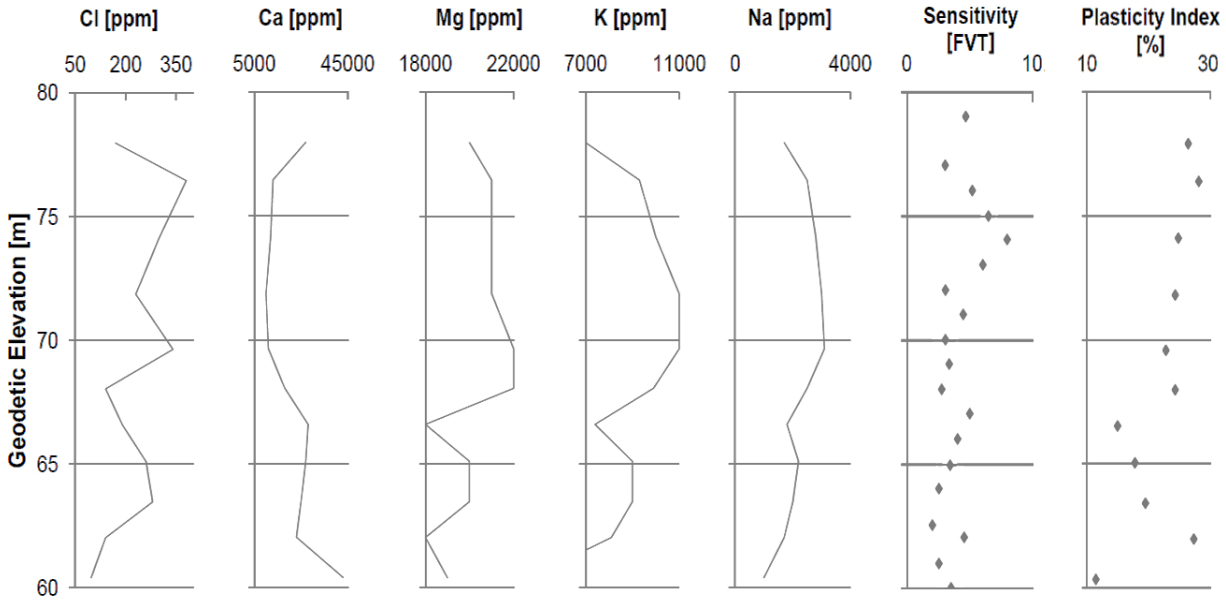

Figure 2-14 Concentration of chloride (Cl), calcium (Ca), magnesium (Mg), and sodium (Na) ions in Ottawa clay pore water vs. soil sensitivity and plasticity index with increasing depth (adapted from Nader, 2014).

2.2.4.10 Zeta or Electrokinetic Potential

Zeta potential, also known as electrokinetic potential, is the electrical charge that builds up at the interface between the surface of clay particles and the pore water, in the diffuse double layer, discussed above. Specifically, it is the difference in potential between the 'stern' layer on the clay particle's surface and the layer of opposite charge that builds up around it. The thicker the diffuse double layer, the higher the zeta potential. Variations in the zeta potential arise from variations in the pH of the pore water and the nature and concentration of electrolytes in it (Nader, 2014; Quigley, 1985).

The zeta potential of a given body of marine clay is related positively to that clay's sensitivity: the higher the zeta potential, the higher the sensitivity—and the lower the remoulded strength of the soil (Nader, 2014; Quigley, 1985). As the zeta potential increases, the clay particles de-flocculate and become dispersed, or peptized, thus making the soil more sensitive. Peptization occurs as a result of natural chemical and biochemical reactions in the soil. These include: (1) a decrease in porewater salinity; (2) adsorption of organic anions; (3) adsorption of inorganic anions; (4) adsorption of monovalent cations. (Quigley, 1985). Monovalent cations (Na^+ and K^+) promote peptization, whereas divalent (Ca^{2+} and Mg^{2+}) and trivalent (Al^{3+}) cations promote flocculation. This is because monovalent cations produce a thicker diffuse double layer than divalent and trivalent cations, and therefore a higher zeta potential and weaker electrostatic bonds (Ajalloeian et al. 2013).

With regard to low porewater salinity, in the Ottawa area, gradual leaching over time has caused a lowering of the clay's porewater salt content and a corresponding dispersal of the peptized soil, a process that is responsible for the frequent landslides in the region. With regard to organic anion adsorption, in pore water with low salinity, anaerobic bacterial digestion of organic matter produces humic peptizing agents, which disperse the clay particles and thus create high soil sensitivity and extremely low remoulded strength. With regard to inorganic anion adsorption, carbonate and sulphide anions are present in marine clay pore water, and when adsorbed, they expand the diffusion double layer, act as peptizing agents, and lower the remoulded shear strength of the soil (Quigley, 1985). With regard to monovalent cation adsorption, Penner (1965) demonstrated that high adsorption of the monovalent cations Na^+ and K^+ relative to the divalent ions Ca^{2+} and Mg^{2+} played a major role in creating a high zeta potential in Ottawa's marine clay, as shown in Figure 2-15 (Quigley, 1983).

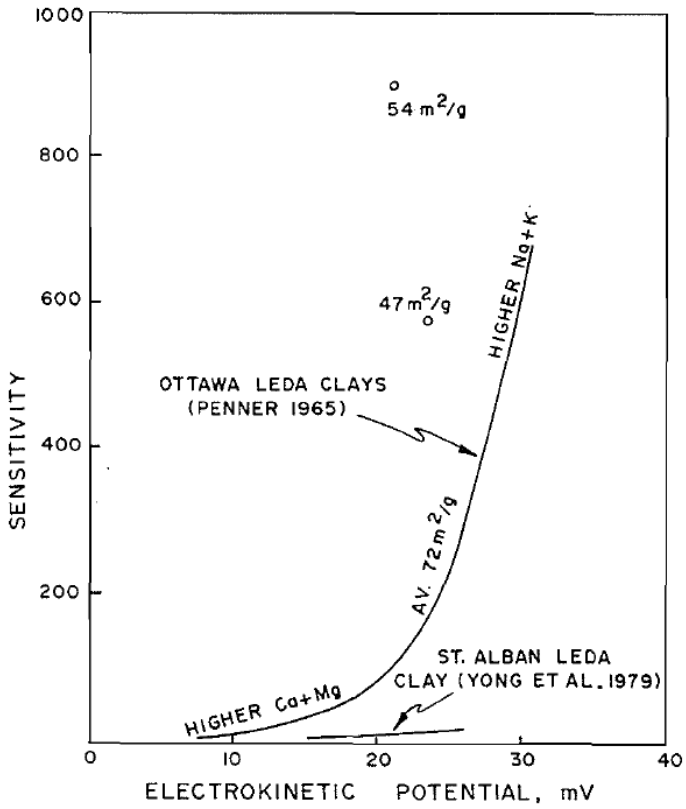

Figure 2-15 Sensitivity vs. electrokinetic (zeta) potential for Ottawa area clays and St. Lawrence lowlands clays (Quigley, 1980).

In all cases, a high zeta potential results in a highly peptized, highly sensitive soil with a moderately low undisturbed strength and an extremely low remoulded strength (Quigley, 1985).

2.2.5 Geotechnical Characteristics of Canadian Sensitive Marine Clays

The geotechnical properties of sensitive marine clays are very important to structural and geotechnical engineers in developing adequate practices to deliver safe and cost effective engineering projects. Sensitive marine clays do not behave like other soils or clays. Their high sensitivity poses an especially difficult challenge for engineers. Thus, their behaviour has been the subject of considerable investigation and analysis by researchers for over a century (Gillott, 1987). In this section, important geotechnical characteristics of sensitive marine clays will be reviewed, including consolidation, shear strength, sensitivity, activity, and hydraulic conductivity.

2.2.5.1 Compression and Consolidation

Consolidation is a phenomenon, unique to saturated or nearly saturated clay soils of low permeability, in which pore water is gradually expelled over time from the soil's pores as a result of long-term constant static compressive pressure exerted by the overburden. The net effect of consolidation is a shrinking in pore size and a consequent reduction in the void ratio and the porosity of the soil. Consolidation brings about significant structural, physical, and chemical changes in the soil and the soil's pore contents (Gillott, 1987).

As discussed above, the fabric of sensitive marine clays has a "card-house" structure, which absorbs the stress exerted by the overburden and resists the compressive force. As the pressure exerted by the overburden continues to increase with continuing deposition of sediments, it reaches a certain critical limit, known as the preconsolidation pressure, which is defined as the maximum effective past pressure. At this critical limit, the electrostatic and cementation bonds between clay particles that hold the "card-house" structure in place break apart and the structure abruptly collapses. The clay particles are free to move more easily, and under the vertical pressure of the overburden they experience marked reorientation, becoming increasingly parallel to each other and perpendicular to the vertical force. The net effect is that the stress from the overburden is transferred to the pore contents, and the soil consolidates to a lower void ratio (Nader 2014; Taha, 2010; Quigley and Thompson, 1966). The stages of the consolidation process are illustrated in Figure 2-16. Consolidation can also occur as a result of remoulding, and consolidated clay that is remoulded can undergo even further consolidation under the original pressure (Nader, 2014; Newland and Allely, 1957).

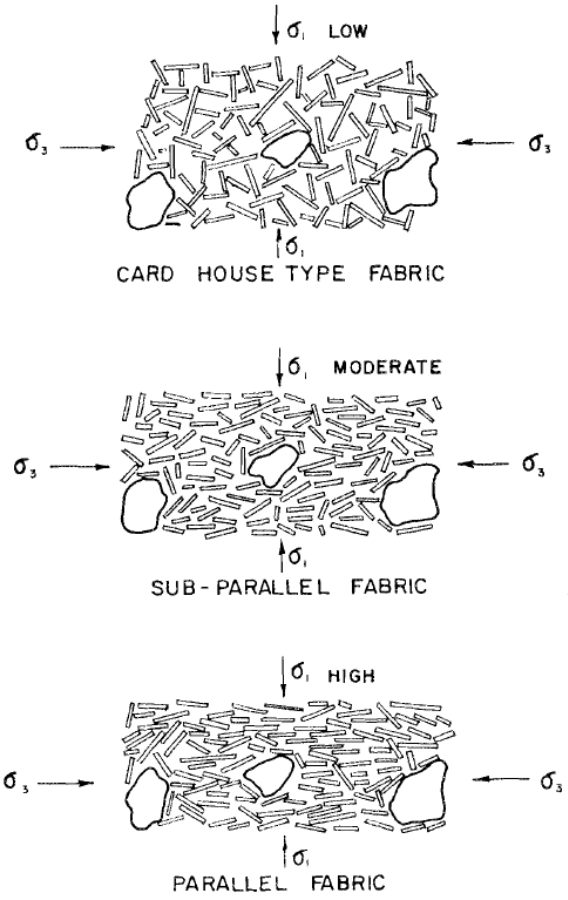

Figure 2-16 Fabric of marine clay at different stages of anisotropic consolidation (Quigley and Thompson, 1966).

The rate at which consolidation occurs is known as the *coefficient of consolidation* (C_v) and is measured in square centimeters (or inches) per second. It is inversely related to the liquid limit of the soil: it decreases as the liquid limit increase. The relationship to stress is slightly more complex. In general, the coefficient decreases with increasing stress, but it may increase at first, before decreasing. This is because the "card-house" structure initially resists the increasing stress, but yields a little, until the structure reaches breaking point and collapses, at which point the rate of consolidation begins to decrease (Nader, 2014). Determining the coefficient of consolidation is essential in predicting the time it will take for a given area of soil to settle. Such time predictions are fundamental in geotechnical engineering, especially when sensitive marine clays are involved.

Two states of consolidation are distinguished: (1) *normal consolidation*; and (2) *overconsolidation*. Normally consolidated soil is one that has never experienced a vertical effective stress greater than its present vertical effective stress; that is, its present effective overburden pressure is equal to the maximum overburden pressure that it had experienced in the past (the

preconsolidation pressure). An overconsolidated soil is one whose present vertical effective stress is less than the vertical stress that it experienced in the past; that is, its present overburden pressure is less than it was in the past (Das and Sobhan, 2014). The *overconsolidation ratio* (OCR) is the ratio of the preconsolidation pressure to the present effective vertical pressure at a given depth (Das and Sobhan, 2014; Nader, 2014). Overconsolidation results in a clay with a dense structure and minimal pore space that has little room for further compression (Taha, 2010). This greater density resulting from a higher OCR means that the shear strength of marine clay increases and its compressibility decreases as the OCR increases. The OCR decreases moderately with depth. In Ottawa's marine clays, the OCR is in the range 1.4-7.1 (Nader, 2014; Taha, 2010).

2.2.5.2 Shear Strength of Sensitive Marine Clays

The shear strength of a given soil is its capacity under stress to resist failure and sliding along some plane within its structure (Das and Sobhan, 2014). If the soil is subjected to stresses that exceed its shear strength, failure occurs (Ural, 2018). One of the major components of marine clay shear strength is *soil cohesion*, which is the result of the electrostatic bonds between the clay particles, and the cementation resulting from the deposition of minerals dissolved in the pore water. Additional factors contributing to cohesion are negative capillary pressure in the pore water, and pore water pressure, which produce *apparent cohesion* (Allaby and Allaby, 2013; Lapidus, 2003). The other component of shear strength is friction, specifically the angle of internal friction (Das and Sobhan, 2014). The greater the cohesion and angle of internal friction, the greater the shear strength. The shear strength of a given soil can be calculated using the *Mohr-Coulomb failure criterion*, which is expressed mathematically in the equation:

$$\tau = c + \sigma \tan \phi$$

where τ = shear strength, c = cohesion, σ = normal stress on the shear plane, and ϕ = angle of internal friction (Blume, 2016; Das and Sobhan, 2014; Gillott, 1987; Taha, 2010).

In the case of marine clays, the soil is generally saturated; thus, the total normal stress is the sum of the effective stress and the pore water pressure. The effective stress is borne by the clay particles (Das and Sobhan, 2014). The initial response of saturated marine clays to stress from the overburden is the generation of excess pore water pressure and the consequent maintenance of a constant volume. In this phase, the stress on the clay is the total normal stress. Eventually, the excess pore water pressure dissipates and the effective stress increases (Das and Sobhan, 2014; Ural, 2018). It is

only in this phase that the Mohr-Coulomb criterion expresses the actual long-term shear strength of the clay. It should be noted that depending on the degree of saturation, the pore water pressure may be negative. Negative pore water pressure may also occur in overconsolidated clays (Blume et al., 2016; Nader, 2014).

A soil's drained shear strength is its shear strength after the pore water pressure generated during shearing has had a chance to dissipate. The term is also applicable to dry soils, in which the absence of pore water means that pore water pressure is not a significant factor. Drained shear strength is contrasted with *undrained* shear strength, which depends on soil anisotropy (i.e., directional dependence, discussed below), strain or penetration rate, and stress history (Blume et al., 2016; Das and Sobhan, 2014; Nader, 2014; Taha, 2010). Undrained shear strength is estimated using tip resistance, corrected tip resistance and/or excess pore water pressure. Methods for measuring undrained shear strength include the direct shear test, *in-situ* and laboratory vane tests, compression or tension triaxial tests, and penetration tests (Nader, 2014; Ural, 2016).

As noted above, when clay soils are disturbed, their original stable fabric structure, held together by electrostatic bonds and cementation, is destroyed. Consequently, their angle of internal friction and their cohesion decrease significantly, resulting in a corresponding drop in their shear strength. Thus, for geotechnical purposes, a distinction is made between undisturbed shear strength and remoulded shear strength. The remoulded shear strength of sensitive marine clays is considerably lower than their undisturbed shear strength. Both undisturbed and remoulded shear strength increase with depth; however, remoulded shear strength increases at a lower rate than undisturbed shear strength, as shown in Figure 2-17 (Das and Sobhan, 2014; Nader, 2014). This lower rate for remoulded shear strength means that soil sensitivity (discussed below) increases with depth (Nader, 2014).

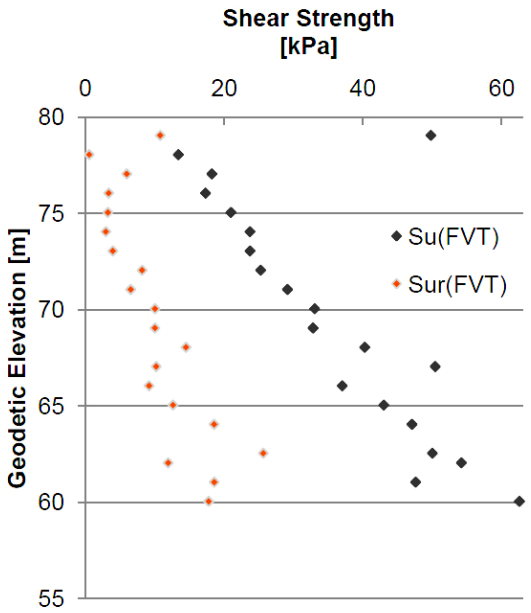

Figure 2-17 Undisturbed shear strength and remoulded shear strength with depth, as determined by field vane tests.
S_u = undisturbed undrained shear strength; S_{ur} = remoulded undrained shear strength (adapted from Nader, 2014).

In sensitive marine clays, the loss of strength with remoulding is not entirely irreversible. If the remoulded clay is left undisturbed after remoulding, it will gradually regain strength over time, as electrostatic bonds and cementation are re-established. This property of soils to regain strength after remoulding is known as *thixotropy*. Most soils, however, are only partially thixotropic, that is, they do not regain their full original strength following remoulding. The amount of strength regained depends on the composition of the soil (e.g., the amount of silt and/or sand mixed in with the clay) (Das and Sobhan, 2014).

It is worth noting that just as shear strength increases with depth (as mentioned above), it also increases with the salinity of the pore water—and, as discussed earlier, salinity increases with depth. Saline pore water is rich in ions, which establish strong electrostatic bonds between the clay particles and aggregates and thus increases the soil's stiffness. In addition, dissolved salts in the pore water may be precipitated and coalesce to form cementation bonds between the clay particles and aggregates. These strong bonds will break only under greater shear stress. Thus, higher salinity confers greater shear strength on the soil (Pindea et al., 2013; Ajalloeian et al, 2013).

The drained and undrained shear strengths of marine clay deposits in northern Quebec (similar to clays in the Ottawa area) was determined using the direct shear test, triaxial drained and undrained tests, and *in-situ* vane shear tests. The results of these tests revealed that the undisturbed

marine clay exhibited brittle behaviour and higher shear strength than normally consolidated or remoulded clay. The tests also confirmed the anisotropic structure of the clay (discussed below) and demonstrated that the shear strength increases as the effective stress increases (Taha, 2010).

2.2.5.3 Anisotropy

Anisotropy is the phenomenon by which directionally dependent variations occur in the geotechnical properties of a given soil (Allaby and Allaby, 2013). In other words, the values of a given property are not the same in all directions. If the value of a given property varies along one axis, the anisotropy is termed *zonal anisotropy*. If the value varies along two or more axes, the anisotropy is *geometrical anisotropy* (Asfanjani, 2013). Anisotropy is a significant feature of Ottawa's sensitive marine clays and it affects many of the marine clays' geotechnical properties (Alshawmar, 2014).

Anisotropy is the result mainly of the way sediments are deposited. As noted above, when marine clays consolidate under the pressure of overlying deposits, the random ordering of the clay particles in the "card-house" structure is dismantled, and the particles assume an orientation that is parallel to each other but perpendicular to the direction of the major principal stress. It should be noted that consolidation stress is itself anisotropic: the major principal stress, which is in the vertical direction, is many times greater than the minor principal stress, which is in the horizontal direction. This produces anisotropic one-dimensional consolidation in the vertical direction (Alshawmar, 2014; Das and Sobhan, 2014; Delage and Lefebvre, 1984; McEniry, 1978; Quigley and Thompson, 1966; Taha, 2010). Consequently, anisotropy is also observed in the microstructure of the soil as a result of progressive consolidation resulting from one-dimensional compression in the vertical direction. With increasing depth, the pores are oriented preferentially in the horizontal direction, being elongated horizontally and compressed vertically, with greater density in the vertical direction than in the horizontal direction. The pore-size distribution and compressibility also vary with depth, since consolidation pressure increases with depth. Furthermore, in the case of Ottawa's silty marine clays, because of pore anisotropy, the ratio of clay to silt increases in the vertical direction but not in the horizontal direction with increasing depth (Alshawmar, 2014; Delage and Lefebvre, 1984; Nader, 2014).

The preferential orientation of clay particles in one particular direction as a result of anisotropic stress is known a "*inherent*" or "*fabric*" *anisotropy*. The inherent anisotropy of marine clays affects several of the soil's geotechnical properties, notably soil compressibility, undrained shear strength, plasticity, porewater pressure, both of which vary with direction (McEniry, 1978; Mitchell and Klugman, 1979). Besides the inherent anisotropy resulting from one-dimensional consolidation,

marine clays developed another kind of anisotropy, known as *stress system induced anisotropy*. Marine clays operate in a stress system environment, in which the amount of shear stress necessary to produce failure varies from location to location within the soil. This is because the direction of the major principal stress at failure varies from vertical to horizontal. The two types of anisotropy are usually combined under the term "*overall anisotropy*" (McEniry, 1978).

Of special interest is the anisotropy observed in soil composition, which varies with depth as a result of erosion and leaching. For example, in Ottawa's marine clays, chlorite in the surface layers of the soil is oxidized over time into smectite as a result of erosion and leaching, which does not affect the underlying layers. Consequently, the surface layers are richer in smectite than the lower layers. This is significant because smectite is an expandable mineral and its concentration in the soil affects the soil's activity and swelling and shrinking potential (discussed below). As a result, Ottawa's marine clays have a higher activity index and swelling-shrinking potential at the surface, and the index decreases with depth (Nader, 2014). Thus, anisotropy in soil composition produces anisotropy in the activity index and the swelling-shrinking potential as well.

Another major property of marine clays that exhibits anisotropic behaviour is hydraulic conductivity, also known as "permeability" (discussed below). Directional variations in hydraulic conductivity are, as with other geotechnical properties, the result of the anisotropic structure of the fabric of marine clays and anisotropic consolidation, with the vertical values exceeding the horizontal values, and both sets of values varying with depth (Alshawmar, 2014; Freeland, 2013). Other geotechnical properties and processes that are subject to anisotropy are: preconsolidation pressure, elasticity, compressibility, porewater pressure, shrinkage and swelling, and possibly tensile strength. In addition, anisotropy bears an inverse relationship to the plasticity index: clays of low plasticity exhibit the highest degree of anisotropy, and as plasticity increases, anisotropy increases (Alshawmar, 2014; McEniry, 1978, Blume et al. 2016).

Like several other geotechnical properties, anisotropy is not static, but is subject to change over time. It has been observed that anisotropy is in a positive feedback relationship with the processes of soil formation. In this type of relationship, geophysical processes (such as deposition, consolidation, infiltration, and leaching) lead to the emergence of anisotropy, which in turn influences the geophysical processes, producing further anisotropy (Freeland, 2013).

2.2.5.4 Sensitivity

Soil sensitivity (discussed briefly above) is the phenomenon by which soils lose strength when they are disturbed or remoulded. Thus, it is expressed as the ratio of the undrained undisturbed

shear strength to the remoulded shear strength (Das and Sobhan 2014Nader, 2014; Taha, 2010). While most clays have a sensitivity ratio between 1 and 8, highly flocculated marine clays have a sensitivity ratio in the range 10 to 80. Clays of high sensitivities turn into viscous liquids when remoulded and are known as *quick* clays. Soils are generally classified on the basis of their sensitivity. The most comprehensive of the various classification systems proposed is the one by Rosenquist (1953), which is presented in Table 2-3 (Das and Sobhan, 2014). Rosenquist's system is used in areas where the soils exhibit a wide range of sensitivities (Abuhajar et al., 2010). The marine clays in the Ottawa area range widely in their sensitivity (Nader, 2014) and are therefore best classified under this system.

Table 2.3 Classification of clays based on their sensitivity (Das and Sobhan, 2014; Abuhajar et al., 2010)

Sensitivity	Classification
1	Insensitive
1–2	Slightly sensitive
2–4	Medium sensitive
4–8	Very sensitive
8–16	Slightly quick
16–32	Medium quick
32–64	Very quick
>64	Extra quick

It should be noted that the remoulded shear strength decreases as salinity decreases; therefore, sensitivity increases as salinity decreases (Nader, 2014; Taha, 2010). In conditions of low salinity, sensitivity varies widely and can range as high as 1000; however, at higher levels of salinity, the higher degree of flocculation keeps the sensitivity below 75. Given that salinity is inversely related to the zeta potential, it follows that sensitivity increases consistently with an increase in zeta potential. Sensitivity increase also correlates with an increase in concentration of monovalent ions (Na^+ and K^+) and a decrease in concentration of divalent ions (Ca^{2+} and Mg^{2+}) (Nader, 2014).

2.2.5.5 Expansion Potential, Shrinkage Potential, Erosion Resistance, and Activity Index

An *expansive soil* is one that undergoes increase in its volume as its moisture content increases. Expansive soils have a high clay content, but not all clay soils are expansive, such soils are considered problematic, since they pose a threat to the stability of the engineering structures that are built upon

them. The expansive nature of expansive clays arises from the expandable lattice-type structure of certain clay minerals (such as montmorillonite (a clay mineral of the smectite group) and vermiculite), the very weak van der Waals forces between the clay particles, their very high negative surface charges, their very high cation exchange capacity, and their large specific surface (Barton and Karathanasis, 2006; Asuri and Keshavamurthy, 2016; Nader, 2014). The capacity of a given soil to expand is designated its *expansion potential* (also referred to as "potential expansiveness" or "swelling potential").

Expansive soils experience shrinkage and volume decrease when their water content decreases as a result of drying. Their capacity for shrinking is referred to as their *shrinking potential*. As noted earlier, when the water content is above the liquid limit, the soil is in viscous liquid state. As the water content falls below the liquid limit, the soil changes from a liquid to a plastic state and its volume decreases. A further decrease in water content brings the soil to the plastic limit, and the soil makes the transition from the plastic state to the semi-solid, state, and undergoes further shrinkage. It should be noted that the shrinkage is not consistently linear, but occurs in three stages, which will be discussed below. With still further reduction, the water content eventually reaches the shrinkage limit and the soil turns from semi-solid to solid. At this point, any further reduction in water content does not produce a corresponding decrease in volume (Ural, 2018). The four states and the transition points at the three limits are presented in Figure 2-18.

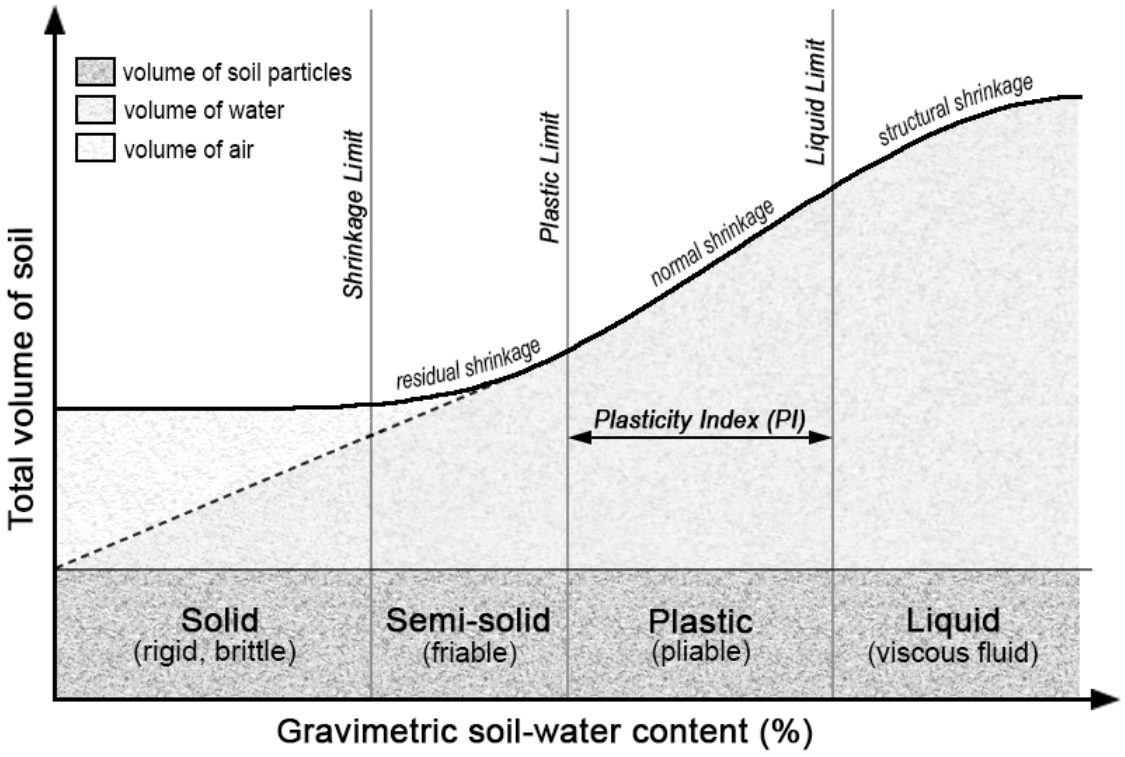

Figure 2-18 Water content, soil volume, the three limits, and the four states of clay soils (adapted from Das and Sobhan, 2014; McBride, 2006]; McGarry and Yule, 2006; and Ural, 2018).

As the volume line in Figure 2-18 shows, the three limits are closely associated with volume increase and are therefore significant factors in the expansion potential and shrinkage potential of a given soil. Various systems for classifying soils on the basis of their expansion potential have been proposed based on either the liquid limit, the plasticity index, or the shrinkage limit, but each has its own limitations. The most comprehensive and most commonly used metric for estimating the swelling and shrinkage potential of a given clay soil is an index known as *activity* (Asuri and Keshavamurthy, 2016; Das and Sobhan, 2014; Pruska and Sedivy, 2015). As discussed above, the high plasticity of marine clays is a consequence of the adsorbed water that envelops the clay particles. Thus, it follows that the concentration of clay particles in a given soil will determine its plastic and liquid limits. It has been demonstrated that a soil's plasticity index is positively correlated with the percentage of the clay-size fraction. As discussed earlier, the clay-size fraction is the percentage by dry weight of soil particles that have a diameter of <2 μm.

Activity is the ratio of the plasticity index to the percentage of clay-size fraction of the soil, but it is also influenced by the mineralogy of the clay and the geological history of the soil, as well as by the percentage of the soil's shear strength that is derived from true cohesion (Das and Sobhan, 2014;

Özdemir and Gülser, 2017; Paaswell, 1973; Skempton, 1953). In its simplest terms, activity is a measure of a soil's capacity to hold water. In general, the higher the water content of a given soil, the higher its plasticity index, and therefore the higher its activity index and its expansion and shrinkage potential (Pruska and Sedivy, 2015). However, as just noted, a soil's capacity to hold water—and therefore its activity index—is influenced partially by the clay's mineral content. Thus, at a more advanced level, activity is an index of the clay's ability to attract, hold, and replace surface ions (Paaswell, 1973). Different clay minerals produce different soil activity ratios because each type of mineral has its own expansion and shrinkage characteristics (Das and Sobhan, 2014; Gillott, 1987).

Clay particles have a plate-like structure consisting of either two or three layers held together by hydrogen bonds in a crystalline lattice. Some clays (the non-expandable clays), such as kaolinite, are two-layer clays, consisting of a sheet of silica and a sheet of alumina held together by strong hydrogen bonds. These strong bonds resist ion replacement and water absorption between the layers, thus preventing expansion and restricting activity to only the outer surfaces of the clay particles. Other clays (the expandable clays), such as montmorillonite and illite, are three-layer clays, consisting of a sheet of alumina sandwiched between two outer sheets of silica, held together by weak bonds. Because of these weak bonds, ionic substitution can occur within the crystal lattice of the clay particle, with ions from the dissolved salts in the pore water replacing ions in the crystal lattice. This replacement of ions increases the particle's ability to absorb water and thus swell or expand. Montmorillonite (a member of the smectite group) exhibits the highest degree of ion substitution and therefore the highest expansion potential and therefore the greatest level of activity. Illite is similar to montmorillonite in its crystalline structure, but the presence of potassium ions between the sheets produces strong bonding which resists water absorption, and this limits the clay's expansion potential and hence its activity (Asuri and Keshavamurthy, 2016; Barton and Karathanasis, 2006; McGarry and Yule, 2006; Paaswell, 1973). As noted earlier, Ottawa's marine clays are composed predominantly of illite with only minor amounts of smectite and vermiculite (Nader, 2014), and their activity index and expansion potential are therefore relatively low. Typical values for the liquid limit, the plastic limit, and the activity index of kaolinite, illite, and montmorillonite are given in Table 2-4.

Table 2.4 Typical values for the liquid limit, the plastic limit, and the activity index of kaolinite, illite, and montmorillonite (adapted from Das and Sobhan, 2014)

Mineral	Liquid Limit	Plastic Limit	Activity Index
Kaolinite	35-100	20-40	0.3-0.5
Illite	60-120	35-60	0.5-1.2
Montmorillonite	100-900	50-100	1.5-7.0

In effect, then, the activity index of a given soil is an indicator of the expansion (or swelling) potential of that soil, and the swelling pressure, the swelling strain, and the swelling time can all be predicted using the activity index (Das and Sobhan, 2014; Özdemir and Gülser, 2017; Pruska and Sedivy, 2015). If lower valence ions in the lattice are replaced by higher valence ions from the pore water, an overall negative charge develops on the clay particle's surface, thus increasing the attractive or repulsive forces between adjacent clay particles. Thus, the greater the percent by weight of clay particles in a given soil, the greater will be the overall effect on the soil's expansion (or swelling) behaviour on account of the potential increase in the number electrically charged particles present (Paaswell 1973). This aspect of soil dynamics is a key factor in determining a given soil's activity.

The expansion potential of a soil is, of course, associated with its shrinkage potential, and the two are thus related to each other through the soil's activity index. Highly active soils, that is, soils containing expandable minerals such as the smectites (of which montmorillonite is a member) have a high shrinkage potential and a correspondingly high tendency towards cracking. Soils whose smectite content is greater than 5 percent experience a marked increase in shrinkage cracking as the internal angle of friction and the soil cohesion decrease with a reduction in the soil's moisture content and the consequent reduction in the thickness of the diffuse double layer (Ren et al., 2019).

Shrinkage also occurs as air enters the pores to replace the moisture that is lost through drying. Surface tension acting at the interface of air, water, and soil particles creates negative pressure, also known as "matric suction," in the pore water still present. This negative pressure (lower than atmospheric pressure) causes the soil to shrink, producing microscopic vertical cracks within the soil when the limit of the soil's tensile strength is exceeded (Chertkov, 2000; Deshpande, 2016; Shi et al., 2014).

Ottawa's marine clays have a high shrinkage potential because of their high void ratio and easily collapsible fabric structure. The shrinkage is, for the most part, irreversible since the collapsed fabric structure cannot be restored and also because the expandable minerals are present in only minimal

amounts (Law and Bozozuk, 1988). Kaolinite displays virtually no residual shrinkage; montmorillonite, on the other hand, experiences a high degree of residual shrinkage (Warkentin, 1961). This indicates that shrinking, like swelling, is influenced by the mineral composition of the clay and the mechanics associated with the crystalline structure of these minerals. This association with mineral composition applies to the shrinkage limit as well. As noted above, the shrinkage limit is the moisture content (given in percent) at which the volume of the soil stops decreasing with decreasing moisture content. Typical values for the shrinkage limit of the three dominant clay minerals, kaolinite, illite, and montmorillonite, are given in Table 2-5. As mentioned earlier, Ottawa's marine clays consist predominantly of illite.

Table 2.5 Typical values for the shrinkage limit of kaolinite, illite, and montmorillonite (adapted from Das and Sobhan, 2014).

Mineral	Shrinkage limit
Kaolinite	25-29
Illite	15-17
Montmorillonite	8.5-15

In saturated clayey soils, shrinkage occurs in three distinct stages. As the water content begins to diminish with drying, initially the decrease in soil volume is less than the volume of water lost, since the large pores do not initially collapse with water loss. This is known as *structural shrinkage*. As further water loss occurs, the decrease in soil volume becomes equal to the volume of water removed from the soil. Water is lost from inter-aggregate pores, and the shrinkage is isotropic, producing cracks in the soil. Such shrinkage is termed *normal shrinkage*. When the water content falls below the liquid limit with further drying, however, and the soil becomes unsaturated, and the shrinkage tapers off such that the decrease in soil volume becomes increasingly less than the volume of the water lost. Water loss now occurs in the inter-particle pores, which do not collapse easily, thus maintaining the soil's fabric structure. This type of shrinkage is *residual shrinkage*, Eventually, a point is reached at which further reduction in water content produces no further shrinkage. This point is known as the shrinkage limit, as noted above (Chertkov, 2000; Law and Bozozuk, 1988; McGarry and Yule, 2006; Warkentin, 1961; Warkentin and Bozozuk, 1961). The three stages of shrinkage are shown in Figure 2-18, above.

The shrinkage limit is lower for remoulded clays than for undisturbed clays. This is because remoulding breaks down the original "card-house" structure of the soil's fabric and gives the clay

particles a more parallel orientation, which reduces the pore size and porewater content. For Ottawa marine clays, the average shrinkage limit for undisturbed soil is 27%, while for remoulded soil it is 20% (Warkentin and Bozozuk, 1961).

After water loss and shrinkage have occurred, the soil does not regain its original water content and volume upon rewetting. The degree of regain of water content and the amount of expansion is determined by the amount of water loss and shrinkage that was experienced initially. This is partially because shrinking and swelling causes an adjustment in the orientation of the clay particles and an alternation in the structure of the soil fabric. Furthermore, the expansion is anisotropic, with greater expansion occurring in the vertical direction than in the horizontal direction (Warkentin, 1961; Warkentin and Bozozuk, 1961). Similarly, shrinkage is also anisotropic, with horizontal shrinkage exceeding vertical shrinkage, thus producing vertical cracking. This anisotropy in shrinkage affects the soil's hydraulic properties, such as hydraulic conductivity (discussed below), and transport phenomena, even in the absence of cracking from shrinkage, though cracking of course amplifies the effect (Deshpande, 2016; Chertkov, 2013; Quigley and Thompson, 1966; Towner 1986).

In addition to indicating the expansion and shrinkage potential of a given soil, activity is also an indicator of a soil's ability to resist erosion. The higher a soil's activity index, the lower its resistance to erosion. The factor that links these two parameters is the soil's expansion potential. Undisturbed soil is in a stable state at its existing void ratio. As the water content of the soil increases, the presence of expandable clay in the soil means that the clay particles will absorb water and expand, thus increasing the soil's void ratio. An increase in the void ratio results in a weakening of the original interparticle electrostatic forces, with a net increase in the repulsive forces and a corresponding increase in the soil's tendency to dispersion. A greater tendency to dispersion increases the soil's susceptibility to erosion. Thus, swelling of the soil has a negative effect on the soil's erosion resistance. In general terms, the activity index of a given soil is negatively correlated with its dispersion ratio, its erosion ratio, and its erodibility factor, whereas it is positively correlated with the soil's structural stability index. However, since other factors are involved in a soil's erodibility, activity is best used as an identifier of soil type and as a predictor of a soil's ability to resist erosion (Özdemir and Gülser, 2017; Paaswell, 1973).

From this understanding of the effect of clay mineralogy on soil dynamics, it can be concluded that soils containing quartz are totally inactive and non-expandable; soils containing illite (e.g., Ottawa's marine clays) are moderately active with a limited expansion and shrinkage potential; and soils containing montmorillonite are highly to extremely active with an enormous expansion and shrinkage potential (Skempton, 1953). A recent study, cited by Ren et al. (2019) has shown that a soil

similar to the Ottawa marine clays, containing illite and a small amount of smectite, has an activity index ranging from 0.33 to 0.48, and a correspondingly limited expansion potential, in addition to low shear strength and high compressibility. Similarly, Taha (2010) reported an activity index of 0.48 for the Ottawa marine clays used in his study. Clays are classified according to their degree of activity, as follows: (1) *inactive* (activity <0.75); (2) *normal* (activity 0.75-1.25); and (3) *active* (activity >1.25) (Skempton, 1953). Based on the activity index data cited above, illite-smectite clays are in the inactive range.

Marine clays in the Ottawa area have a percentage of clay-size fraction as high as 84% (Taha, 2010). An analysis by Nader (2014) of samples from 7 sites in the Ottawa area led him to conclude that Ottawa's marine clays range in activity from inactive to normal, according to the classification system described above. Nader's findings are presented in Figure 2-19. As the data in Nader's graph indicates, activity may vary widely within a given site and may even span all three activity categories (as is the case with Site 1 in the graph), depending on the manner in which the sediments are deposited at that particular site (Nader, 2014).

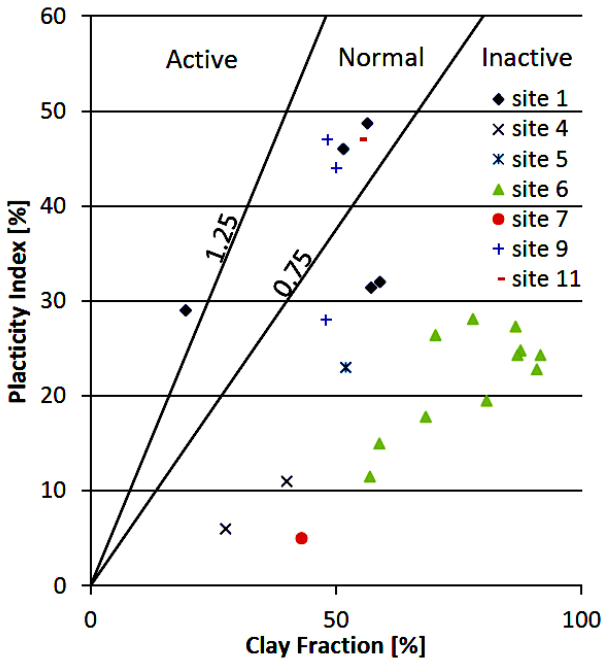

Figure 2-19 Activity ratios for marine clays at 7 sites in the Ottawa area (Nader, 2014).

2.2.5.6 Hydraulic Conductivity

In its most basis sense, hydraulic conductivity, sometimes referred to as the *coefficient of permeability*, is a measure of the rate at which water flows though the soil, and it is generally expressed in centimeters per second (or meters per second). The higher a soil's hydraulic conductivity, the lower its water retention (Chesworth, 2008).

It is important to distinguish between permeability and hydraulic conductivity. Permeability is a property of the *soil structure* whereby water or other fluids are allowed to pass through the soil, whereas hydraulic conductivity is a property that focuses on the *fluid that permeates the soil structure*; thus, permeability is one component of hydraulic conductivity. Permeability is related broadly the interconnectivity of pores and to pore size (the larger the pores, the higher the permeability), and it is, consequently, affected by pore-size distribution. Hydraulic conductivity, on the other hand, especially in marine clays, takes into account pore water density and viscosity, grain-size distribution, void ratio, roughness of clay particle surfaces, ion concentration (i.e., salinity), the thickness of the water layer adhering to the clay particles, and the amount of undissolved gas in the pore water (Chesworth, 2008; Das and Sobhan, 2014; Rao and Matthew, 1995; Ural, 2018).

Clays generally have relatively low hydraulic conductivity (Asfanjani, 2013; Ural, 2018). For marine clays, specifically, hydraulic conductivity is controlled by the valency of the exchangeable cations in the pore water. Adsorbed monovalent cations produce a lower hydraulic conductivity than adsorbed divalent and trivalent cations. The higher the valency of the adsorbed cations, the higher the hydraulic conductivity. Conversely, within a given valency, the larger the size of the hydrated cation, the lower the hydraulic conductivity. The lower valency and larger cation radius cause repulsive forces in the diffuse double layer to predominate, and this promotes deflocculation and dispersion of clay particles, Deflocculation and dispersion, in turn, bring about a reduction in hydraulic conductivity through a plugging up of the soil pores with the loose clay particles released by deflocculation (Rao and Matthew, 1995).

The degree of saturation of a given soil affects its hydraulic conductivity; thus, a distinction is made between *saturated* and *unsaturated* hydraulic conductivity (Chesworth, 2008). For marine clays under saturated conditions, the hydraulic conductivity is controlled by the microstructure of the soil rather than the macrostructure (Rao and Matthew, 1995). In addition, if tensile cracks form in the soil as a result of shrinkage, as discussed above, they create preferential flow paths and thus bring about a considerable increase in the soil's hydraulic conductivity. Observations have confirmed that the hydraulic conductivity of a cracked soil is much higher than it is when the same type of soil with the same water content has not undergone cracking (Deshpande, 2016).

In marine clays, hydraulic conductivity generally decreases as stress increases, but there may also be an initial increase in the hydraulic conductivity before the decrease sets in. Initially, when there is an increase in stress, the load is borne by the "card-house" structure and the pore water, and compression is therefore resisted. During this early phase, hydraulic conductivity may increase, since pore volume remains unchanged even as pressure increases. There comes a point, however, when the soil structure can no longer withstand the strain and it collapses, resulting in a significant reduction in pore size and a corresponding decrease in hydraulic conductivity (Nader, 2014).

As noted above, hydraulic conductivity is anisotropic. In other words, there is generally a preferential flow direction in soils, which is influenced by particle size, shape, and orientation, and by soil consolidation, among other factors. Partly on account of one-dimensional consolidation and the parallel orientation of clay particles in consolidated soils, the preferential flow direction is horizontal. Measurements have confirmed that hydraulic conductivity is generally higher in the horizontal direction than in the vertical direction. Furthermore, hydraulic conductivity decreases with depth as a result of increasing geostatic pressure from the overburden. As a general principle, vertical conductivity (i.e., perpendicular to a given soil's layers) is lower than horizontal conductivity (i.e., parallel to the soil's layers). However, in clays that develop large cracks from periodic shrinking and swelling, as noted above, the vertical conductivity may be much higher than the horizontal conductivity. Other soil phenomena, such as the downward leaching of dissolved minerals in pore water and the upward transport of mineral through capillary action, also have anisotropic effects on the soil's hydraulic conductivity (Asfanjani, 2013; Freeland, 2013). A further factor that produces anisotropic hydraulic conductivity is anisotropic shrinkage (as discussed earlier). Since shrinkage upon drying is anisotropic, the cracking that results from the shrinkage is also anisotropic, and since cracking increases hydraulic conductivity, anisotropic cracking increased hydraulic conductivity anisotropically (Chertkov, 2013).

For most sites in the Ottawa area, the hydraulic conductivity ranges between 5.52×10^{-10} and 1.09×10^{-6} cm/s. However, it varies considerably at various depths depending on the moisture content of the soil and on the amount of sand and/or silt mixed in with the clay (Nader, 2014).

2.3 Background on GIS

Geographic Information System (GIS) is a framework for recording, storing, manipulating, analyzing, managing, and presenting in visual form any set of spatial or geographical data. GIS integrates different types of data format: point, line, polygon, or raster. GIS organizes data in a layers-based schema using information pertaining to geographical location (geospatial data); results from

the data analysis can be presented visually in the form of a map in 2 or 3 dimensions. GIS mapping is an excellent tool to enhance decision-making, and it has the added advantage of saving time and money. GIS is also capable in modelling natural processes regardless of the scale of the process. There are many spatial analyses that can be performed to study trends, relationships, and patterns using different interpretation methods or tools. Also, different types of maps can be developed to suit the purpose and audience for which the map is being prepared. The ability of GIS to perform different types of analysis depends on the software and platform that is used. There are many GIS software platforms available, such as ArcGIS, MapInfo, GRASS GIS, QGIS, etc.

The main concept underlying GIS is that the physical locations that are inherent in various bodies of data and the information associated with these locations can be mined profitably to gain insight into the way natural and human systems operate. The data is stored in a database, where it can be managed, manipulated, transformed, and analyzed. Data can be stored locally or in the cloud. Spatial data or geospatial data can be anything around us that has a physical location, such as houses, road networks, park areas, migration routes, etc. GIS data can be inputted into the system either in vector or in raster format.

Spatial data is typically collected in the field using devices such as the Global Positioning System (GPS), total stations, drones, satellites, etc. Data can be collected by human surveyors or obtained through mechanical means such as satellites, airplanes, drones, or data collection stations. Data that is collected through these various means is usually recorded and stored in a number of different formats, including Excel spreadsheets, database tables, delimited text, blueprints, or printed maps. In order for this data to be inputted into GIS, it needs to be converted into the GIS format. GIS has a tool for converting data that is recorded in non-GIS formats into the GIS format. Global Positional System (GPS) units are a common format in which geospatial data from satellites is recorded. GPS data recorded in GPS units have varying degrees of accuracy. Some locations are identified to within centimeters of their actual position on the globe, while others can be within a 5-10 m radius. Thus, there is some uncertainty surrounding data obtained from GPS satellites. Uncertainty in geospatial data may also arise from human error, lack of reference points when digitizing data originally recorded on paper, malfunctioning of data collection tools, etc. Having accurate data is crucial in GIS analysis, since inaccurate data will skew the results of the analysis and thus lead to decisions that could have detrimental and costly consequences. This must be kept in mind during the data collecting and inputting phase.

Once the data has been collected and entered into the system, it can be analysed in a number of ways, using methods such as buffer analysis, proximity analysis, and cluster analysis. GIS also has

various tools for managing and manipulating data, such as the Interpolation tool (for predicting values for areas that do not have sampled values but lie between areas that do have sampled values), the Cut/Fill tool (for estimating the volume of soil displaced from one area and deposited in another as a result of, for example, erosion or landslides, both of which are common problems with Ottawa's marine clays), and the Resample tool (for changing the spatial resolution of a raster dataset and specifying how the new resolution is to be accommodated with aggregation and interpolation). The various tools and functions of GIS can be used to determine the density of a given dataset, identify potential problems that may arise in the area in which the data was gathered, uncover hidden relationship within the dataset, identify features that change over time, etc. GIS can be used in a wide variety of domains to conduct operations such as flooding analysis, traffic analysis, flow analysis, risk assessment, landslide assessment, etc.

GIS manages data in the form of points, lines, polygons, and raster or grid formats. Point data can be anything that contains one specific location such as the location of a school, a gas station, a tree, a weather station, etc. Features with many locations can be captured in multiple points. The line form can be used to represent linear feature such as a road network, a transmission line, a watermain, a drainage system, etc. The polygon form is used to represent areas with boundaries, such as a city, a recreation area, a region with a specific soil type, an area that is prone to landslides, etc. Points can be converted to lines or polygons using the Production Points to Line or Polygon tool. There are also tools for converting lines and polygons to points. The Conversion toolbox contains tools for converting to and from various file formats, such as GPS, Excel, text, ASCII, among others. Some other toolboxes are the Spatial Analyst toolbox, the Network Analyst toolbox, and the 3D Analyst toolbox. The Spatial Analyst toolbox contains various toolsets, such as the Density toolset, the Groundwater toolset, the Hydrology toolset, the Solar Radiation toolset, which are of special relevance to the present study. In this study, the Spatial Analysis tools were used to interpolate point data in order to create raster or grid data, to perform raster calculations, and to extract raster data to specific shapes, i.e., areas containing sensitive marine clays.

Each dataset is laid out in a layer. Maps are created by stacking several layers of related data one on top of another. GIS can be used to get answers to questions such as: How many people live within the limits of the City of Ottawa? Where are the potholes located on Ottawa's Elgin Street? What is the extent of the 100-year floodplain?

Given its versatility and flexibility and its ability to analyse large bodies of geospatial data, GIS is an ideal system for modelling and predicting the behaviour of Ottawa's sensitive marine clays under a wide variety of condition, and particularly under conditions of significant global climate change.

2.4 Background on TRIGRS

Transient Rainfall Infiltration and Grid-Based Regional Slope-Stability Analysis (TRIGRS) is a FORTRAN program, originally developed in 2008 by a research team at the U.S. Geological Survey and updated in 2014 in conjunction with a team from Italy, to facilitate the prediction of the timing and distribution of shallow, rainfall-induced landslides (Baum et al., 2008; Raia et al, 2014). The program computes transient pore-pressure changes caused by rainfall infiltration and predicts the resulting changes in the factor of safety. These changes can be observed as they progress over time, once the TRIGRS analysis is completed. The program uses a simple infinite-slope model that calculates the factor of safety on a cell-by-cell basis for both saturated and unsaturated soils. The purpose of the cell-by-cell computation is to allow for the anisotropic properties and behaviour of various soils: input parameter values such as rainfall intensity, slope, soil depth, initial water-table depth, saturated vertical hydraulic conductivity, hydraulic diffusivity, cohesion for effective stress, angle of internal friction for effective stress, total unit weight of soil, etc. can vary from cell to cell. (Alvioli and Baum, 2016; Baum et al., 2008; Raia et al, 2014),

The program distinguishes between two types of data: *time-invariant* data and *time-dependent* data. Time-invariant data are the type of data for which the parameter values are assumed to remain constant over time. Generally, the mechanical and hydrological properties of the soil are assumed to be time-invariant. They include: unit weight, cohesion, angle of internal friction, water content, and saturated hydraulic conductivity. Also assumed to be time-invariant are the geometrical features of the sliding mass, namely, the gradient of the slope, the angle of the sliding plane, and the depth of the sliding plane. Conversely, time-dependent data are data that are in flux and change with the passage of time. They include the intensity and duration of rainfall and the pressure head (i.e., the pressure exerted by the infiltrated water on the sliding mass). Not only do these parameters change over time, but they change in a non-linear fashion, and they therefore have to be processed using a probabilistic approach and different equations from the deterministic ones used for time-invariant data. This produces approximate solutions (Alvioli and Baum, 2016; Raia et al., 2014).

Data is inputted into the program in the form of ASCII text files. Analysis of the data is controlled through an initialization file that specifies the names of all other input and output files and includes values for the geotechnical parameters that are needed to run the program as well as the rainfall intensity-and-duration pattern. Required inputs are: (1) a Digital Elevation Model; (2) the corresponding slope grid; (3) a rainfall intensity-and-duration pattern; and (4) the numerical values for the geotechnical parameters (just mentioned above). Additional information may be inputted optionally, such as delineation of specific zones that are isotropic for a given parameter, and

additional grids to specify initial conditions, soil depth, and values for other parameters that may affect the accuracy of the analysis. However, the more the data that the program has to process, the longer it will take for the operation to be completed. It is also possible to specify the type and number of outputs, and the intermediate points during the simulation at which outputs are to be generated. The program was designed to be used in conjunction with Geographic Information System (GIS) software. Output from TRIGRS is saved to a series of text files, which can then be imported into GIS for visual display or further analysis (Alvioli and Baum, 2016; Baum et al., 2008).

One problem in modelling rainfall-induced landslides over large areas, such as the Ottawa area, is the difficulty involved in obtaining sufficient and accurate spatially distributed data for the soil's mechanical and hydrological properties that reflects variations in localized areas. The use of a single blanket value to cover a large area may result in an inaccurate representation of conditions in localized cells. To overcome this problem, the program uses a probabilistic approach by sampling randomly from a given probability distribution to assign a more realistic value to each individual cell. The program employs two types of probability distribution: (1) normal, or Gaussian, distribution; and (2) uniform distribution. The Gaussian distribution is used for predicting the occurrence of landslides in localized areas of limited size, where sufficiently detailed data exists for the various soil parameters. The uniform distribution is used for large areas, for which detailed localized information on the soil properties is not available. This approach increases the sensitivity of the model to the random variations that are inherent in the model's time-dependent parameters as well as possible localized variations in the time-invariant parameters when a large area is the subject of the analysis (Raia et al, 2014).

2.5 Background on the Climate Model Used

There is a growing body of evidence that increases in greenhouse gas emissions, changes in land-use, runaway population growth, the steep rise in energy production, and the expansion of global and regional economies are bringing about major changes in the chemical composition of the Earth's atmosphere at a rapid rate, and these changes are in turn causing the planet's climate to change on a global scale. Early attempts to model the planet's climate assumed that the climate of the past was a good indicator of what climate will be like in the future. However, in light of the growing body of evidence just mentioned, it has become clear over the past few decades that the past is not a reliable guide in predicting the climate of the future, and new models need to be developed to study and predict the nature and intensity of the systemic changes in climate that can be expected in the coming decades (Schardong et al., 2018).

Global Climate Models (GCMs), also known as General Circulation Models, are a set of complementary models designed to represent the physical processes operating in the Earth's atmosphere, oceans, cryosphere, and land surfaces, and, additionally, to simulate the response of these processes to ongoing systemic change—in particular, the rapidly increasing concentration of greenhouse gases in the atmosphere (IPCC, n.d.). The key elements of GCMs are: (1) land-ocean-atmosphere coupling; (2) greenhouse gas emissions; and (3) various sets of initial conditions as the starting state of the climate system. There are more than 40 GCMs created by various climate research centres that can be used individually or in conjunction with one another in various combinations (Schardong et al, 2018). GCMs provide advanced tools that assist in the effort to understand current and future climate dynamics on both global and regional scales. GCMs are therefore the most suitable framework within which to assess and predict the impact of climate change on the natural and human environment in the Ottawa area.

GCMs depict dynamic climatic conditions in the form of a three-dimensional grid that spans the globe. The grid has a horizontal resolution of between 250 and 600 km, with 10 to 20 vertical layers upwards in the atmosphere and up to 30 layers downwards in the oceans. The coarseness of this grid introduces an element of uncertainty into the results of GCM-generated simulations of future climate patterns, given that many physical process, such as those involved in cloud activity, operate at much smaller scales. GCMs are also not particularly good at simulating various feedback mechanisms in such interactive processes as: water vapour and planetary warming; clouds and radiation; and circulation in the oceans and ice-and-snow albedo. These uncertainties and limitations need to be kept in mind when interpreting the results of GCM analyses, particularly with regard to regional projections (IPCC, n.d.).

An important tool in predicting future weather patterns is the Rainfall Intensity-Duration-Frequency (IDF) curve. An IDF curve is a probability curve that represent the likelihood that a rainfall with occur at a given intensity for different durations, based on past patterns of rainfall gleaned from rainfall records of data collected at rainfall monitoring stations. Since existing IDF curves are based on historical rainfall data, they need to be modified and updated to take into account the possible effects of global warming—a problem already mentioned above with regard to climate models in general. However, consensus is lacking on the best method to achieve this updating, since there is a wide range of distribution functions, future climate model datasets, downscaling methods, bias correction methods, and future climate scenarios that can be employed in reworking the IDF curves. This wide range of options may cause considerable variability in the outputs, and this in turn increases the level of uncertainty (Coulibaly et al., 2016; Fadhel et al., 2017; Schardong et al. 2018).

One tool that takes these various uncertainty-producing factors into account is the IDF_CC tool, a simple web-based tool developed in 2016 at the Institute for Catastrophic Loss Reduction at the University of Western Ontario, in London, Ontario. It combines a user-friendly interface with a powerful database system and a sophisticated, highly efficient methodology for updating IDF curves (Simonovic et al., 2016). The tool was constructed as a decision support system (DSS), and as such it contains a database and a model base, which contains a set of mathematical models and procedures for updating IDF curves. In 2018, a module was added to the tool, which allows the user to obtain IDF curves for any location in Canada, especially in areas for which no rainfall observations are available (Schardong et al, 2018).

As noted above, GCMs have a resolution larger than 250 km. Regional Climate Models (RCMs) have a resolution of between 25 and 50 km. Both scales are too large for the kind of data used in IDF curves, which focus on local conditions. This problem of scale is addressed through a technique known as *downscaling*. There are two types of downscaling: (1) *dynamic*; and (2) *statistical*. While dynamic downscaling uses more complex physics, statistical downscaling is generally the procedure of choice because it is quicker and can use a wider range of GCM outputs (Schardong, 2016).

As noted above, one of the problems associated with updating IDF curves is the number of different future climate scenarios. These scenarios are based on future greenhouse gas emission and concentration scenarios, known as Representative Concentration Pathways (RCPs). The RCPs contain time series of projected emissions and concentrations of the entire range of greenhouse gases, aerosols, and chemically active gases, as well as projections relating to land use and land cover.). There are four RCPs available to IDF_CC users: RCP2.6, RCP4.5, RCP6.5 and RCP8.5 (Schardong et al., 2018). Each RCP represents one of many possible scenarios in which a certain pattern of radiative forcing is achieved within a certain timeframe. Radiative forcing is a quantitative measure of the strength of climate change drivers, such as greenhouse gases and solar radiation. It is expressed in watts per square metre (Wm^{-2}) and indicates the change in energy flux caused by a given climate change driver at the top of the atmosphere. RCP2.6 represents a future in which radiative forcing reaches its maximum level at approximately 3 Wm^{-2} before 2100 and then declines. RCP4.5 and RCP 6.0 are intermediate scenarios in which the radiative forcing stabilizes at approximately 4.5 Wm^{-2} and 6.0 Wm^{-2} respectively sometime after 2100. RCP8.5 is the most pessimistic scenario, in which radiative forcing reaches higher than 8.5 Wm^{-2} by 2100 and continues to rise for some time thereafter (Schardong et al., 2018; Stocker et al. 2013). A more detailed discussion of the IDF_CC tool will be presented in Chapter 5.

For the current study, IDF data for 2010 to 2100 for a rain gauge station in Ottawa area were obtained through the IDF_CC tool mentioned above. The future emissions scenarios used in the IDF_CC tool were based on RCP4.5 and RCP8.5.

2.6 Summary

The sensitive marine clays of the Ottawa area, located in basin of the former Champlain Sea, are the result of pre- and post-glacial deposition in the St. Lawrence Lowlands. The clays exhibit a "card-house" fabric structure, the pore of which contain a high water content with a high salt concentration. The clays' open flocculated structure gains strength from electrostatic bonding through cation exchange with mineral present in the porewater. The electrostatic bonds are easily broken, and when they break under pressure or other stresses, such as those caused by extreme weather events, the "card-house" structure collapses, causing the soil to become unstable and prone to landslides, which have been fairly frequent in the Ottawa area. An understanding of the geotechnical characteristics and properties of Ottawa's marine clays, as discussed in this chapter, is essential to investigating the potential effects of climate change (and the likely increase in the number of extreme weather events) on the future behaviour of these clays and the possible increase in the incidence of landslides and the consequences for the engineering structures in the area.

Geographic Information System (GIS) is a computer-based framework for analyzing and presenting in visual form relationships and patterns in data that is linked to specific locations in geographical space. As such, it is the ideal framework within which to analyse soil data in association with climate change data, and with projected future rainfall occurrence in particular.

TRIGRS is modeling software used in assessing and predicting the timing and distribution of shallow, rainfall-induced landslides. The program calculates the changes in transient pore-pressure that occur when rainfall enters the soil and then predicts variations in the factor of safety that will occur as a result of these pressure changes. The TRIGRS software was used in the current study, in conjunction with ArcGIS software, to assess the likelihood of landslides occurring in Ottawa's sensitive marine clays in the face of climate change using future climate model rainfall intensity data.

Global Climate Models (GCMs) are a set of computer-based models used in the prediction of changes in weather patterns and the occurrence of severe weather events that can be expected in the wake of climate change. GCMs can be used in conjunction with an online tool known as IDF_CC to look specifically at changes in rainfall intensity and duration that might be expected as a result of climate change. The rainfall data for the Ottawa area used in the current study was obtained through the IDF_CC tool.

2.7 References

Abuhajar, O., El Naggar, M. H., and Newson, T. (2010). Review of Available Methods for Evaluation of Soil Sensitivity for Seismic Design. *International Conferences on Recent Advances in Geotechnical Earthquake Engineering and Soil Dynamics, 27*. Available at: https://scholarsmine.mst.edu/icrageesd/05icrageesd/session01b/27.

Ajalloeian, R., Mansouri, H. and Sadeghpour, A. H. (2013). Effect of saline water on geotechnical properties of fine-grained soil. *Electronic Journal of Geochemical Engineering, 18*, 1419-1435.

Allaby, M. and Allaby, A. (2013). *A Dictionary of Geology and Earth Sciences* (4th ed.). Oxford: Oxford University Press.

Alshawmar, F. (2014). Evaluation of compressibility, anisotropy and at-rest lateral earth pressure in Champlain Sea clay. Master's thesis. Carleton University, Ottawa, Canada. Alvioli, M., and Baum, R. L. (2016). Parallelization of the TRIGRS model for rainfall-induced landslides using the message passing interface. *Environmental Modeling & Software 81*, 122-135.

Andrews, J. T., and Retherford, R. M. (1978). A reconnaissance survey of late Quaternary sea levels, Bella Bella/Bella Coola region, central British Columbia coast. *Canadian Journal of Earth Sciences, 15*, 341-350.

Andrews, J. T. (1972). Post-glacial rebound. In G. Fremlin (Ed.), *The National Atlas of Canada*. Ottawa: Department of Energy, Mines, and Resources, Surveys and Mapping Branch. Plate 35-36.

Asfanjani, D. K. (2013). Determination of homogeneity and isotropy of soil using geophysical methods. Master's Degree Project. Royal Institute of Technology, Stockholm, Sweden.

Asuri, S. and Keshavamurthy, P. (2016). Expansive soil characterisation: An appraisal. *INAEL Letters, 1*(1), 29-33.

Ballivy, G., Loiselle, A. A., and Pouliot, G., (1975), Quelques caractéristiques géotechniques des dépôts d'argile de la baie James: les coulées d'argile de Fort Rupert, Québec. *Canadian Geotechnical Journal*, 12, pp. 498-509.

Barton, C. D. and Karathanasis, A. D. (2006). Clay minerals. In: R. Lal, ed. *Encyclopedia of Soil Science*, 2nd ed. New York: Taylor & Francis, pp. 276-280.

Baum, R. L., Godt, J. W. , and Savage, W. Z. (2010). Estimating the timing and location of shallow rainfall-induced landslides using a model for transient, unsaturated infiltration. *Journal of Geophysical Research—Earth Surface*, 115, F03013. doi:10.1029/2009JF001321.

Baum, R. L., Savage, W. Z., and Godt, J. W. (2008). TRIGRS—A Fortran program for transient rainfall infiltration and grid-based regional slope-stability analysis, version 2.0: U.S. Geological Survey Open-File Report, 2008-1159. Reston, VA: U.S. Geoogical Survey.

Bechai, M. (1974). Determination of the Preconsolidation Pressure for a Sensitive Marine Clay. Master's thesis. University of Ottawa, Ottawa, Canada.

Bennett, R. H., Bryant, W. R., and Keller, G. H. (1978). Clay fabric and geotechnical properties of selected submarine sediment cores. In: H. B. Stewart, ed. *Collected Reprints 1977*. Boulder, Colorado: U.S. Department of Commerce, National Oceanic and Atmospheric Administration, pp. 691-784.

Blume, H.-P., Brümmer, G. W., Fleige, H., Horn, R., Kandeler, E., Kögel-Knabner, I., … Wilke, B.-M. (2016). *Scheffer/Schachtschabel Soil Science*. Heidelberg: Springer.

Brydon, J. E. and Patry, L. M. (1961). Mineralogy of Champlain Sea sediments and a Rideau Clay soil profile. *Canadian Journal of Soil Science,* 41 (2), 169-181.

Chertkov, V. Y. (2000). Modeling the pore structure and shrinkage curve of soil clay matrix. *Geoderma, 95,* 215-246.

Chretkov, V. Y. (2013). Shrinkage anisotropy characteritics from soil structure and initial sample/layer size. *Geoderma*, 200-201, 1-8.

Chesworth, W. (Ed.). (2008). *Encyclopedia of Soil Science*. Dordrecht: Springer.

Coulibaly, P., Burn, D. H., Switzman, H., Henderson J., Fusto, E. (2016). A comparison of future IDF curves for Southern Ontario. Toronto and Region Convervation Authority and Essex Region Conservation Authority. Available at: https://climateconnections.ca/app/uploads/2014/01/IDF-Comparison-Report-and-Addendum.pdf.

Das, B. M. and Sobhan, K. (2014). *Principles of Geotechnical Engineering.* 8th ed., SI. Stamford, CT: Cengage Learning.

Dejong, J. T., Asce, M., Yafrate, N. J., Degroot, D. J., (2011), Evaluation of Undrained Shear Strength Using Full-Flow Penetrometers , pp. 14–26.

Delage, P. and Lefebvre, G. (1984). Study of the structure of sensitive Champlain clay and of its evolution during consolidation. *Canadian Geotechnica Journal*, 21 (1), pp. 21-35. doi. 10.1139/t84-003

Deshpande, S. S. (2016). Tensile strength of soil. A seminar report presented to the Government College of Engineering, Amarvati, India. doi: 10.13140/RG.2.1.1263.9123

Fadhel, S., Rico-Ramirez, M. A., and Han D. (2017). Uncertainty of Intensity-Duration-Frequency (IDF) curves due to varied climate baseline periods. *Journal of Hydrology 547*, 600-612.

Freeland, J. (2013). Soil anisotropy: Mechanisms and hydrologic consequences. Terra Central, July 1. Available at: https://blogs.agu.org/terracentral/2013/07/01/soil-anisotropy-mechanisms-and-hydrologic-consequences/.

Gillott, J. E. (1987). *Clay in Engineering Geology*. Amsterdam, the Netherlands: Elsevier Science Publishers,.IPCC (Intergovermental Panel on Climate Change). (n.d.). *What is a GCM?* IPCC Data Distribution Centre. Available at: https://www.ipcc-data.org/guidelines/pages/gcm_guide.html.

Lapidus, D. F. (2003). Collins Dictionary of Geology (new ed., rev. and updated by James MacDonald and Christopher Burton). Glasgow: HarperColins.

Law, K. T. nd Bozozuk, M. (1988). Engineering problems in Leda Clay. In: *Proceedings of the International Conference on Engineering Problems of Regional Soils, Beijing, China, 11–15 August 1988*. Beijing, China: International Academic Publishers, pp. 775-792.

Leroueil, S. (1999). Geotechnical characteristics of eastern Canada clays. In: A. Nakase and T. Tsuchida (Eds.), *Characterization of Soft Marine Clays: Proceedings of the International Symposium on the Characterization of Soft Marine Clays*. Rotterdam: CRC Press, pp. 3–32.

Lo, K. Y., Bozozuk, M., Law, K. T. (1976). Settlement analysis of the Gloucester test fill. *Canadian Geotechnical Journal*, 13 (4), pp. 339-354.

Locat, J. (1995). On the development of microstructure in collapsible soils. In: E. Derbyshire, T. Dijkstra, and I.. J. Smalley (Eds.), *Genesis and Properties of Collapsible Soils*. Dordrecht: Kluwer Academic Publishers, pp. 93-128.

Locat, J., Lefebvre, G., and Ballivy, G. (1984). Mineralogy, chemistry, and physical properties interrelationships of some sensitive clays from Eastern Canada. *Canadian Geotechnical Journal*, 21 (3), pp. 530-540. DOI: 10.1139/t84-055

Logan, C., Cummings, D. I., Pullan, S., Pugin, A., Russell, H. A. J., and Sharpe, D. R. (2009). Hydrostratigraphic model of the South Nation watershed region, south-eastern Ontario. Geological Survey of Canada, Open File 6206. Available at: https://10.4095/248203.

McBride, R. (2006). Consistence. In R. Lal (Ed.), *Encyclopedia of Soil Science* (2nd ed., pp. 335-337). New York: Taylor & Francis.

McEniry, G. P. (1978). The estimation of the effective shear strength parameters of Leda clay. Master's thesis. University of Ottawa, Ottawa, Canada.

McGarry D. and Yule D. F. (2006). Soil shrinkage. In R. Lal (Ed.), *Encyclopedia of Soil Science* (2nd ed., pp. 1633-1636). New York: Taylor & Francis.

Mhashhash, A., Bockelmann-Evans, B., and Pan, S. (2018). Effect of hydrodynamics factors on sediment flocculation processes in estuaries. *Journal of Soils and Sediments, 18*, 3094-3103.

Mitchell, R. J. (1970), On the yielding and mechanical strength of Leda clays. *Canadian Geotechnical*

Journal, 7 (3), pp. 297-312.
Mitchell, R. J. and Klugman, M. A. (1979). Mass instabilities in sensitive Canadian soils. *Engineering Geology, 14*, 109-134.
Nader, A. (2014). Engineering Characteristics of Sensitive Marine Clays—Examples of Clays in Eastern Canada. Master's thesis. University of Ottawa, Ottawa, Canada. ProQuest Dissertations Publishing, MS26684.
Nastev, M., Parent, M., Ross, M., Howlett, D., and Benoit, N. (2016). Geospatial modelling of shear-wave velocity and fundamental site period of Quaternary marine and glacial sediments in the Ottawa and St. Lawrene Valleys, Canada. Soil Dynamics and Earthquake Engineering, 85, pp. 103-116.
Newland, P. L. and Allely, B. H. (1957). A study of sensitivity resulting from consolidation of a remolded clay. *Proceedings of the Fourth International Conference on Soil Mechanics and Foundation Engineering*, Vol. 1, pp. 83-86.
Özdemir, N and Gülser C. (2017). Clay activity index as an indicator of soil erodibility. *Eurasian Journal of Soil Science 6*(4), 307-311.
Paaswell, R. E. (1973). Causes and mechanisms of cohesive soil erosion: The state of the art. In: *Soil Erosion: Causes and Mechanisms; Prevention and Control: Proceedings of a Conference-Workshop Held January 26, 1973, Washington, D.C.*. Washington, D.C.: Highway Research Board, pp. 52-74.
Penner, E. (1965). A study of sensitivity in Leda clay. *Canadian Journal of Earth Sciences*, 2 (5), pp. 425-441. Available at: https://doi.org/10.1139/e65-037.
Pineda, J. A., Kelly, R., Bates, L., Sheng, D., and Sloan S. (2013). Effects of pore fluid salinity on the shear strength of a soft clay. In: C. Hellmich, B. Pichler, and A. Dietmar, eds. *Poromechanics V: Proceedings of the Fifth Biot Conference on Poromechanics*. New York: American Society of Civil Engineers, pp. 1460-1469.
Pruska, J. and Sedivy, M. (2015). Prediction of soil swelling parameters. *Procedia Earth and Planetary Science 15*, 219-224.
Quigley, R. M. (1980). Geology, mineralogy, and geochemistry of Canadian soft soils: a geotechnical perspective. *Canadian Geotechnical Journal*, 17 (2), pp. 261-285. Available at: https://doi.org/10.1139/t80-026
Quigley, R. M. (1983). Glaciolacustrine and glaciomarine clay deposition: A North American perspective. In: N. Eyles, ed. *Glacial Geology: An Introduction for Engineers and Earth Scientists*. Oxford, UK: Pergamon Press, pp. 140-167.
Quigley, R. M. and Thompson, C. D. (1966). The fabric of anisotropically consolidated sensitive marine clay. *Canadian Geotechnical Journal,* 3 (2), pp. 61–73. Available at: https://doi.org/10.1139/t66-008
Raia, S., Alvioli, M., Rossi, M., Baum, R. L., Godt, J. W., and Guzzetti, F. (2014). Improving predictive power of physically based rainfall-induced shallow landslide models: A probabilistic approach. *Geoscientific Model Development 7*(2), 495-514.
Rao, S. N. and Matthew, P. K. (1995). Effects of exchangeable cations on hydraulic conductivity of a marine clay. *Clays and Clay Minerals 43*(4), 433-437.
Rasmussen, K. K. (2012), An Investigation of Monotonic and Cyclic Behaviour 0f Leda Clay. Master's thesis. The University of Western Ontario, London, Ontario, Canada..
Ren, J., Li, X., Li, S., Zhu, H., and Zhao, K. (2019). Quantitative analysis of spectral response to soda saline-alkali soil after cracking process: A laboratory procedure to improve soil property estimation. *Remote Sensing 11*(12), 1-18. doi. 10.3390/rs11121406.
Sangrey, D. A., and Paul, M. J., (1971), A regional study of landsliding near Ottawa. *Canadian Geotechnical Journal*, 8 (2), pp. 315-335. Available at: https://doi.org/10.1139/t71-026.
Schardong, A., Gaur, A., Simonovic, S. P. and Sandink, D. (2018). Computerized Tool for the Development of Intensity-Duration-Frequency Curves Under a Changing Climate, Technical Manual v. 3., Water Resources Research Report No. 103. Department of Civil and Environmental

Engineering and Institute for Catastrophic Loss Reduction, The University of Western Ontario, London, Ontario, Canada.

Shi, B. X., Chen, S. S., Han, H. Q., & Zheng, C. F. (2014). Expansive soil crack depth under cumulative damage. *The Scientific World Journal*, *2014*, 498437. doi:10.1155/2014/498437.

Simonovic, S. P., Schardong, A., Sandink, D., and Srivastav, R. (2016). A web-based tool for the development of Intensity Duration Frequency Curves under changing climate. *Environmental Modelling & Software Journal, 81*, 136-153.

Skempton, A. W. The colloidal "activity" of clays. In: *Proceedings of the Third International Conference on Soil Mechanics and Foundation Engineering*, Vol. 1. Zurich: Organizing Committee, ICOSOMEF, pp. 57-61.

Stocker, T. F., Qin, D., Plattner, G-K., Tignor, M. M. B., Allen S. K., Boschungm Judith … Midgley P.M. (2013). Climate Change 2013: The physical science basis. Geneva: Intergovermmental Panel on Climate Change.

Sutherland, B. R., Barrett, K. J. and Gingras, M. K. (2015). Clay settling in fresh and salt water. *Environmental Fluid Mechanics, 15*(1), 147-160.

Taha, A. M. (2010), Interface Shear Behavior of Sensitive Marine Clays—Leda Clay. Master's Thesis. Department of Civil Engineering. The University of Ottawa, Ottawa, Canada.

Taha, A. M. and Fall, M. (2013). Shear behavior of sensitive marine clays—concrete interface. *Journal of Geotechnical and Geoenvironmental Engineering*, 139 (4), pp. 644–650.

Tavenas, F., Jean, P., Leblond, P., and Leroueil, S. (1983), The permeability of natural soft clays. Part II: Permeability characteristics. *Canadian Geotechnical Journal*, 20 (4), pp. 645-660. Available at: https://doi.org/10.1139/t83-073.

Torrance, J. K. (1979). Post-depositional changes in the pore-water chemistry of the sensitive marine clays of the Ottawa area, eastern Canada. *Engineering Geology*, 14 (2-3), pp. 135-147.

Towner, G. D. (1986). Anisotropic shrinkage of clay cores, and the interpretation of field observations of vertical soil movement. *European Journal of Soil Science 37*(3), 363-371.

Ural, N. (2018). The importance of clay in geotechnical engineering. In: M. Zoveidavianpour, ed. *Current Topics in the Utilization of Clay in Industrial and Medical Applications*. London: IntechOpen, pp. 83-102.

Warkentin, B. P. (1961). Studies on shrinking and swelling of Leda clay and of a prairie clay. Internal Report No. 226 of the Division of Building Research. Ottawa: National Research Council of Canada.

Warkentin B. P. and Bozozuk, M. (1961). Shrinking and swelling properties of two Canadian clays. In: *Proceedings of the Fifth International Conference on Soil Mechanics and Foundation Engineering: Paris, 17th to 22nd July, 1961*. Paris: Dunod, pp. 851-855.

Yong, R. N., Sethi, A. J., and LaRochelle, P. (1979). Significance of amorphous material relative to sensitivity in some Champlain clays. *Canadian Geotechnical Journal*, 16 (3), pp. 511-520. Available at: https://doi.org/10.1139/t79-057.

3 Literature Review

The most notable feature of Ottawa's sensitive marine clays is its proneness to landslides, particularly in exceptionally wet weather conditions. The frequency with which landslides occur in the Ottawa area prompted researchers early on to investigate the mechanisms underlying landslides, and slope failure in general. One early attempt to do this was that of Eden and Mitchell (1970), who outlined the features common to the landslides that had occurred in the Ottawa area during the previous decade with special attention to the landslides at Breckenridge (1963), Orleans (1965), and Rockcliffe (1967), all three of which occurred during heavy rainfalls. All three slides had been documented and discussed in earlier literature—the Orleans slide by Eden and Jarrett (1970), and the Breckenridge and Rockcliffe slides by Mitchell (1970). From their analysis of the data, the authors concluded that groundwater mechanics play a critical role in the slope instability of Ottawa's marine clays. A temporary increase in groundwater pressure tends to produce slope deformation without triggering complete collapse, whereas extended periods of high groundwater pressure tend to produce strains that cause tension cracks to develop near the top of the slope. If surface water is present from snowmelt or spring rains (as was frequently the case in the Ottawa landslides under consideration), it enters the soil through these tension cracks, raising the groundwater table to the critical level at which slope failure is triggered. Furthermore, the clay structure in this region is uniquely characterized by the presence of microfissures, which develop in response to stress relief from overburden removal or slope cutting, or in response to seasonal changes in temperature and/or groundwater pressure. The presence of these microfissures gives the clay structure the ability to dilate (expand in volume), and this in turn increases the permeability of the soil. In fact, significant dilation was observed in the study's triaxial compression tests before and during failure. The main contribution of this study was that it discredited the then-prevailing view that slope failure in Ottawa's marine clays occurred in a brittle manner, in which the clay is remoulded into a quasi-liquid state during flowslides, and it demonstrated that an appreciation of the microfissured nature of the clay fabric is instrumental in understanding the mechanics of slope failure and landslides in these clays.

In the decade that followed, Mitchell and Klugman (1979) undertook a broad review of the latest developments that had occurred in the analysis and management of slope instabilities in the St. Lawrence Lowlands, and in particular the Ottawa area. They noted that the clays of the St. Lawrence Lowlands are not uniform throughout the region, but display significant local variations in terms of composition, geologic history, and deposition—and thus vary considerably in geotechnical

properties and behaviour from one locality to the next. Consequently, no clear pattern is discernible in the hundreds of landslides and related phenomena (i.e., earthflows and flowslides) that have occurred there within recorded history. There are, however some common features that emerge. The surface layer of the soil is generally highly pervious and thus facilitates a high rate of infiltration. In the spring, snow melt and rainfall enter the soil through this pervious crust and saturate the soil, causing a significant rise in groundwater levels. Thus, the bulk of the landslides, large and small, occur between February and May each year, especially on riverbanks, where erosion plays a major part in the process. For any given slope, initial rotational instability is initiated by an exceptionally high groundwater level and/or erosion at the toe of the slope. Dilative failure occurs when microfissures in the clay's fabric widen during failure and take in large amounts of excess free water. Dilative failure releases most of the gravitational energy the moment instability is reached, creating a flow in which remoulding of the clay occurs and the clay is transformed from small chunks into a frictional fluid, which launches into a retrogressive flowslide. Retrogression depends not so much on soil sensitivity as on slope height and the undrained strength of the slope soil. The landslide will come to an end at this stage, unless the average shearing stress exceeds the undrained strength of the clay. Thus, failure may occur in several stages. The size of a landslide does not appear to be related to the sensitivity of the soil and may be influenced by a variety of factors. The frequent occurrence of landslides in the region and the resulting catastrophic loss incurred in the preceding decades prompted renewed interest in slope monitoring and management. The authors review various then-current instruments and mechanisms for monitoring the stability of slopes, and go on to recommend the development of a warning system in areas where loss of life could ensue if failure should occur. A prototype of such a system was being tested at the site of the Rockcliffe landslide (mentioned above) at the time of writing. The authors also mention a six-category classification system that was then being prepared as a guide to geotechnical engineers. The system would identify a given site as either unsuitable for development; suitable, pending site investigation and the application of remedial measures; or suitable, but with routine site inspection post-development. Slope management involves the use of slope-stabilization techniques. Traditionally, these had been applied after the fact; however, the authors note that with the increase in geotechnical input, before-the-fact application was beginning to be implemented.

Early attempts to identify the mechanics of landslides, and slope instability in general, relied on attempts to replicate historical landslides in the laboratory, using reduced-scale models with soil samples obtained from the location of the landslide in question. In particular, the mechanics of slope instability and failure in Ottawa's sensitive marine clays were poorly understood and there was

considerable disagreement on the roles played by uplift, strain-softening, and time effect in triggering failure. In an attempt to resolve the dispute, Goodings and Schofield (1984) undertook to replicate the well-documented Rockcliffe landslide, which had occurred in 1967 on the south bank of the Ottawa River, on the northern periphery of the City of Ottawa, and which had been described and analysed earlier by Eden and Mitchell (1970). The attempt was largely unsuccessful in replicating the behaviour of the original landslide. Some of the models in the study displayed some form of slope instability, including deep intact soil movement, slope degradation, and flowsliding. These inconclusive results prompted the authors to make some tentative speculative conclusions. First, the dense network of microfissures in the freshwater layers of Ottawa's clay sets it apart from other cemented sensitive clays with respect to slope instability and failure. In less fissured marine clay, failure occurs through shearing. However, in densely fissured clay it is the dilation (or widening) of the fissures that triggers the failure. Second, the presence of fissures may explain why slope failure in Ottawa's clays does not exhibit the conventional circular rotational pattern, but is characterized by a toppling and buckling of soil columns, which is suggestive of interacting wedges. Third, uplift does not trigger slope failure, but it does play a role in what occurs after the failure has been triggered. Fourth, the time-dependent horizontal stress release resulting from natural slope cutting may precede slope failure. Finally, reduced-scale modelling is of limited utility in understanding the mechanics of slope failure in fissured clays.

More recently, with the introduction of sophisticated computer modelling software, the study of slope instability and landslides has entered a new phase and has shifted away from reduced-scale laboratory modelling. Quinn et al. (2010) investigated the relationship between key features of the terrain (such as elevation, flow accumulation, soil type, overburden soil thickness, and land use) and the characteristics of historical large landslides in the sensitive marine clays of the St. Lawrence Lowlands. For this purpose, they developed a landslide susceptibility model, to be applied at the regional scale. The model used the "weights of evidence" method, a bivariate statistical approach in which, for each point in the terrain of the study area, a weight is assigned to each variable of a given terrain feature that is known to be associated with a precondition or a trigger of landslides. For example, "clay" is a variable in the terrain feature "soil type." Weights are either positive or negative: a positive value for a variable indicates the likelihood of a landslide occurring when that variable is present; a negative value indicates the likelihood of occurrence when that variable is absent. A positive weight of zero indicates an equal probability for occurrence and non-occurrence in the presence of that variable. The higher above zero the positive weight, the more likely is the landslide occurrence in the presence of that variable; the lower below zero the weight, the less likely the

occurrence. The weighting was calculated and maps prepared for each terrain feature as well as for a digital inventory of historical landslides in the study area (created previously from recorded landslide data) using ArcMap and the GIS framework. The maps were then combined to produce an overall susceptibility map, based on a combined weight assigned to each point on the map. The combined weights represent the susceptibility to landslides of each point in the map. These susceptibility values were grouped broadly into three categories; (1) low; (2) low to moderate; and (3) moderate to high. A Monte Carlo simulation using randomly selected points provided probabilities for landslide occurrence in these three category areas, based on historical landslide data. For example, at any given point in the moderate to high susceptibility areas, there is a 15% chance of a landslide occurring within 500 m of that point, a 26% chance of an occurrence with 1km, and a 44% chance of an occurrence within 2 km. The model was validated by comparing the predicted levels of susceptibility with actual historical landslides in the study area: all such landslides were located within areas designated "low to moderate" or "moderate to high." However, the authors note that the model does tend to overpredict landslide susceptibility, given that in some areas designated susceptible by the model, no landslides had occurred. Since the susceptibility model was intended to be used as a screening tool in the construction or maintenance of infrastructure, the study tested the model using selected railway river crossings in the study area. The analysis revealed that 26 percent of the selected river crossings had large retrogressive landslides within 2 km, which was slightly lower than what might be expected from the model's prediction of the susceptibility of the locations in question. Nevertheless, the authors conclude that the model is a useful tool in identifying areas of susceptibility and earmarking them for further study.

Since the focus of the current study is the effect that currently changing weather patterns will have on the behaviour of Ottawa's sensitive marine clays and, consequently, on the engineering structures built in and on those clays, a Master's degree project by Taha (2010), published later by Taha and Fall (2013), is of special interest. His study investigated the shear behavior of sensitive marine clays at the interface with building materials such as steel and concrete. The study found that under consolidated, drained, and saturated conditions, the clay's angle of friction at the interface increases as the clay's overconsolidation ratio increases; that the higher the dry density of the remoulded clay, the greater its shear resistance at the interface, and that the higher the clay's salinity, the greater its shear strength at the interface. Conversely, as the clay's level of saturation increases, the shear resistance at the interface decreases.

As recently as the beginning of the current decade, there was still no clear consensus on the precise mechanisms by which landslides in sensitive marine clays occur. Several triggers had been

investigated, including heavy precipitation, piezometric pressure distributions, groundwater flow and pressure, riverbank erosion, and localized slope failure—and conflicting findings had been obtained. It was against this backdrop that Gauthier and Hutchinson (2012) undertook an investigation into the role of precipitation and other possible meteorological triggers in the occurrence of large landslides in the sensitive marine clays of eastern Canada. They selected five large landslides that occurred in the St. Lawrence Lowlands between 1971 and 2010 for their study. All five occurred during the spring months (April to June), during which heavy rainfall and snowmelt are expected. All but the 2010 landslide were associated with these weather-related triggers; the 2010 landslide occurred shortly after a magnitude 5.0 earthquake struck the area. For each of the five landslides, precipitation data for the year immediately preceding the landslide event (recorded at weather stations in the vicinity of each landslide site) were analyzed to reflect short-term, long-term, seasonal, and annual weather patterns. The expectation was that if the trigger for landslides is heavy precipitation, then the data would show that the landslides occurred during the wettest periods on record. To assess the role of snowmelt as a trigger, winter snowfall intensity and snow accumulation were taken into consideration. The study also examined the role that ground frost played in the occurrence of the five landslides. If, during the winter months, there is not a substantial layer of snow on the ground to insulate the soil, the groundwater in the soil freezes and remains sequestered in the soil until the spring thaw. When the thaw is complete the melted groundwater would have the same effect on the soil as water infiltrating from a heavy rainfall. In such a scenario, the point at which critical instability is reached and a landslide is triggered depends on the timing of the ground thaw and some as-yet-unidentified combination of the amount of water trapped in the soil over winter, the amount of water from snowmelt, and the amount of water from springtime rainfall. These amounts need not necessarily to be large, as the study discovered in its analysis of the relevant meteorological data. Thus, the timing of frost formation and thaw are significant factors, but were beyond the scope of the study. The findings of the study were mixed and somewhat inconclusive with regard to establishing causation between precipitation and landslides in sensitive marine clays, but there were sufficient grounds for the authors to conclude that periods of heavy precipitation over both the short and long term are not the sole trigger for a landslide event. However, a steady supply of surface water from precipitation or snowmelt is a necessary precondition for the occurrence of marine-clay landslides, Precipitation appears to be just one of a complex set of preconditions, which includes ground frost conditions and seismic activity. These preconditions must be met for a landslide to be triggered. The authors also concluded that a better understanding of how ground frost interacts with rainfall and snowmelt in triggering landslides in sensitive marine clays requires more detailed

information on the timing of frost formation and thaw. Furthermore, more precise modelling of air temperatures and snow cover in relation to ground frost conditions in landslide-prone areas would greatly enhance the ability to predict more precisely when a large landslide is likely to occur.

In the field of geotechnical engineering, accurate information on a soil's geotechnical properties is essential, and this is particularly true when assessing the effect of climate change on the behaviour of various soils, and the response of the engineering structures built on them. In the case of Ottawa's marine clays, however, there has long been a concern about the accuracy of the data obtained using the standard penetration test equipment employed in the determination of these properties. Negative readings and incorrect estimations of the geotechnical properties of the soil were routinely observed in the Ottawa area. It was suspected that temperature, which varies widely in the Ottawa area on a seasonal basis, might be responsible for the observed inaccuracies. At any given time of year, there is a temperature differential of up to 18° C between the soil's surface layer and soil at a depth of 6 m, where the temperature remains at a constant 8-9° C throughout the year. To address this question of the effect of temperature on the penetrometer readings, Nader (2014) undertook an investigation for a Master's degree project. The results were later published by Nader et al. (2015). Tests were conducted at the Canadian Geotechnical Research Site No. 1, southeast of the City of Ottawa, using various measuring instruments, and also in the laboratory, where the penetrometer that was used in the field tests was assessed for its performance under various temperature change conditions. The findings of these investigations confirm that temperature variations do in fact compromise the accuracy of the readings taken by the instrument in various ways, to various degrees, at various depths, and under various conditions. The study applied temperature corrections to the penetrometer recordings to compensate for the drift in the test results and thus improve their accuracy and standard deviation. The study recommended that the correlations between penetrometer test values and the values of the various geotechnical parameters of the marine clay that are given in the literature should be verified and modified if necessary in accordance with local and site-specific conditions.

With the increasing use of computer modelling, researchers have begun devising new and better models for increasingly specific purposes. Al-Umar (2018) investigated the influence of rainfall and snowmelt on shallow landslides in the sensitive marine clays of the Ottawa area using the TRIGRS model within the GIS framework, the overall objective of the study being to demonstrate the validity and reliability of the GIS-TRIGRS model developed for the purpose. The study fed topographic, geologic, hydrologic, and geotechnical data for the Ottawa area into the computer program along with rainfall and snowmelt intensity data drawn from historical records. The program used this data to

calculate the factor of safety for each pixel in the area in question and then determine the susceptibility to landslides from rainfall and snowmelt for each of those points on the landscape. The results were presented in the form of maps. These maps were then compared with maps marking the locations of historical landslides that had occurred the area. The study found a high degree of correlation between the predictions of the model and known historical landslides. The model was run to simulate landslide susceptibility in three typical scenarios: (1) an optimistic scenario, in which the most favourable values for the various geotechnical parameters (e.g., the highest values for cohesion and angle of internal friction) were used; (2) a normal scenario, in which the average values for the geotechnical parameters were used; and (3) a worst-case, or pessimistic, scenario, in which the most unfavourable values for the geotechnical parameters (e.g., the lowest values for cohesion and angle of internal friction) were used. All three scenarios assumed a constant, steady maximum-intensity rainfall for a 24-hour period. The results of the analysis showed that the number of sites susceptible to landslides increased as the pessimism of the scenario increased, thus confirming that the model being used was sensitive to variations in the geotechnical parameters. Furthermore, the landslide-prone sites predicted by the model for all three scenarios were matched up against the locations of actual historical landslides and the two were found to correlate well. This close agreement between the model's predictions and the distribution of historical landslides once again confirmed the model's ability to predict accurately the susceptibility of Ottawa's marine clays to rainfall-induced landslides. Further investigations of the study revealed that there is a slight increase in the number of sites susceptible to rainfall- and snowmelt-induced landslides as the duration of rainfall increases from 24 to 48 hours and the steepness of the slope increases. The study concluded that the model developed by the researcher can be used effectively to assess landslide probability and provide useful geotechnical data for slope management and land-use planning.

3.1 References

Al-Umar M. (2018), GIS based assessment of climate-induced landslide susceptibility of sensitive marine clays in the Ottawa region, Canada. Unpublished doctoral dissertation. University of Ottawa, Ottawa, Canada. Available at: http://dx.doi.org/10.20381/ruor-21490.

Eden W. J. and Jarrett, P. M. (1970). Landslide at Orleans, Ontario. Technical Paper No. 321, Division of Building Research, National Research Council of Canada, Ottawa.

Eden, W. J. and Mitchell, R. J. (1970). The mechanics of landslides in Leda clay. *Canadian Geotechnical Journal, 7*, 285-296.

Gauthier, D. and Hutchinson, D. J. (2012). Evaluation of potential meteorological triggers of large landslides in sensitive glaciomarine clay, eastern Canada. *Natural Hazards and Earth System Sciences, 12*, 3359-3375.

Goodings, D. J. and Schofield, A. N. (1985). A centrifugal model study of slope instability in Ottawa area Champlain Sea clay. *Canadian Geotechnical Journal, 22*(1), 102-109.

Mitchell, R. J. (1970). Landslides at Breckenridge, Pineview Golf Club, and Rockcliffe. Technical Paper No. 322, Division of Building Research, National Research Council of Canada, Ottawa.

Mitchell, R. J. and Klugman, M. A. (1979). Mass instabilities in sensitive Canadian soils. *Engineering Geology, 14*, 109-134.

Nader, A., Fall, M., Hache, R. (2015). Characterization of Sensitive Marine Clays by using Cone and Ball Penetrometers – Example of Clays in Eastern Canada. *Journal of Geotechnical and Geological Engineering* 33(4), pp. 841-864.

Nader, A. (2014). Engineering characteristics of sensitive marine clays—Examples of clays in Eastern Canada. Master's thesis. University of Ottawa, Ottawa, Canada. ProQuest Dissertations Publishing, MS26684.Nader, A., Fall, M., and Hache. R. (2015). Characterization of sensitive marine clays by using cone and ball penetrometers: Example of clays in Eastern Canada. *Geotechnical and Geological Engineering*, *33*(4), 841–864.

Quinn, P. E., Hutchinson, D. J., Diederichs, M. S., and Rowe, R. K. (2010). Regional-scale landslide susceptibility mapping using the weights of evidence method: An example applied to linear infrastructure. *Canadian Geotechnical Journal, 47*, 905–927.

Taha, A. M. (2010). Interface shear behavior of sensitive marine clays—Leda Clay. Master's thesis. Department of Civil Engineering, University of Ottawa, Ottawa, Canada.

Taha, A. M. and Fall, M. (2013). Shear behavior of sensitive marine clays—concrete interface. *Journal of Geotechnical and Geoenvironmental Engineering*, 139(4), pp. 644–650.

4 The Study Area

4.1 Introduction

This chapter presents a detailed profile of the study area, namely, the City of Ottawa and its immediate surroundings. The profile includes the area's geographical and geomorphological characteristics, its geologic history and composition, the geotechnical properties of the soils in the area, and the climate and population of the region.

4.2 Geographical and Geomorphological Characteristics

4.2.1 Location of the Study Area

The City of Ottawa, the capital of Canada, is located in the northern part of Eastern Ontario, between latitudes 45.54° N and 44.96° N, and longitudes 75.25° W and 76.36° W with a total area of just over 2,800 km^2. On the north, the city is bounded by the Ottawa River for 8.6 km, with Gatineau, Quebec on the other side of the river.

The City of Ottawa as it exists today was brought into existence by *The City of Ottawa Act* of 1999, which authorized the amalgamation, to be completed in 2001, of the then-existing Regional Municipality of Ottawa-Carleton and the then-existing cities of Cumberland, Gloucester, Kanata, Nepean, Ottawa, and Vanier, along with the then-existing townships of Goulbourn, Osgoode, Rideau, and West Carleton, and the Village of Rockcliffe Park (City of Ottawa Act, 1999). These names often appear in the literature in relation to the study area.

Currently, the City of Ottawa is divided into 23 electoral districts or wards and is surrounded by smaller towns, municipalities, and townships as illustrated in Figure 4-1. On the west are the towns of Arnprior, Mississippi Mill, and Carleton Place and the Township of Beckwith. On the south are the Township of Montague, the Village of Merrickville-Wolford and the Municipality of North Grenville. On the east are the townships of North Dundas and Russell, the Municipality of the Nation and the City of Clarence-Rockland.

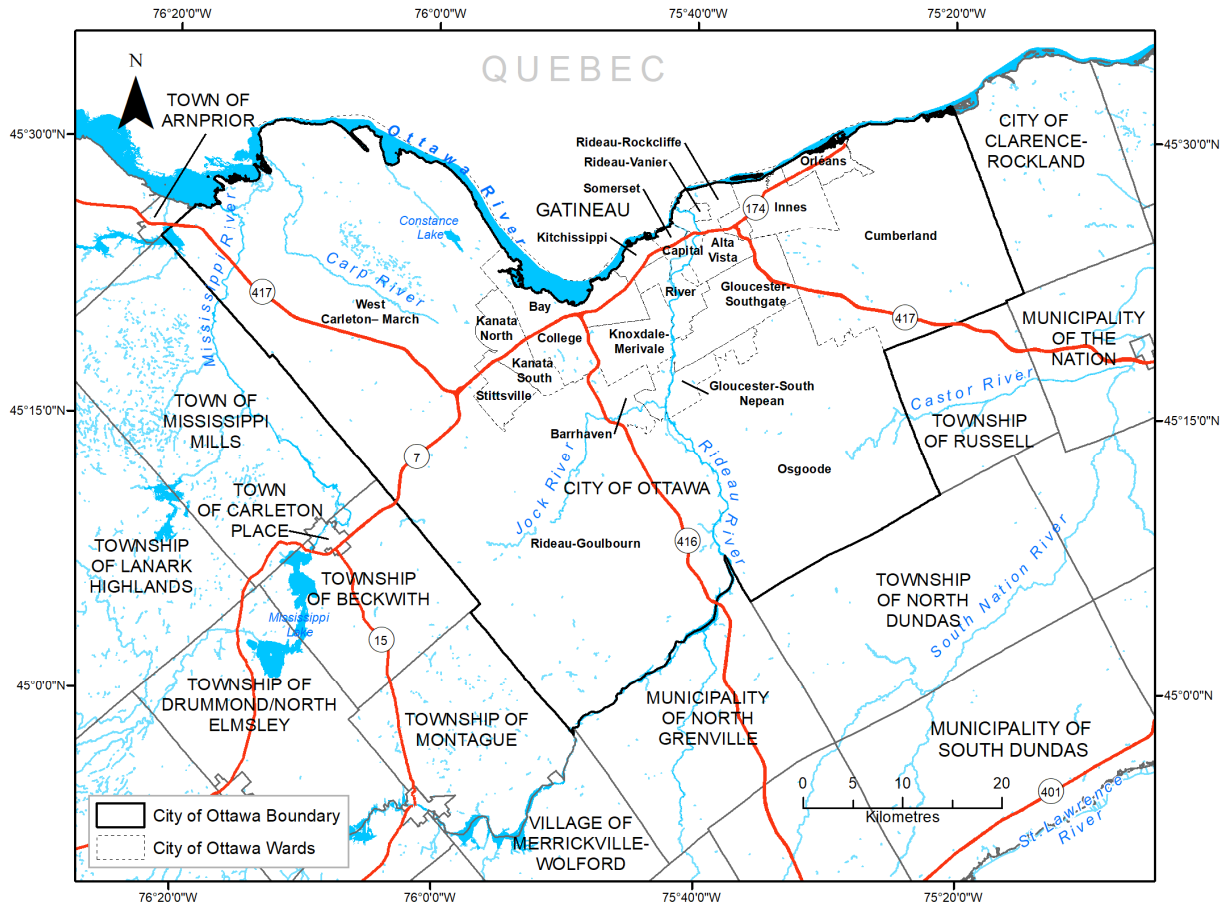

Figure 4-1 City of Ottawa: boundary, wards, and surrounding municipalities.

Ottawa's downtown area lies on the south bank of the Ottawa River, west-southwest of the Rideau Canal. The older part of the city, known as Lower Town, lies across the Canal to the north and east, and extends eastwards to the Rideau River. The city and its surroundings are served by a network of highways (see Figure 4-1). The main artery in this network is the Trans-Canada Highway (designated Highway 417 in the Ottawa area), which runs across the width of the northern part of the city in an east-west direction. Highway 7 branches off the Trans-Canada Highway just west of Kanata in a southwesterly direction and Highway 416 (also known as Veterans Memorial Highway) branches off the Trans-Canada Highway just east of Kanata in a south-southeasterly direction.

4.2.2 Geographic Setting and Geomorphology

The Ottawa region consists of flat and gently sloping plains with elevations ranging between 39 and 168 mASL. The overall slope runs from the highest point (168 mASL) near Manion Corners, in

the west, to the lowest point (39 mASL), in the bed of the Ottawa River, to the north and east in the vicinity of Clarence-Rockland (see Figure 4.2).

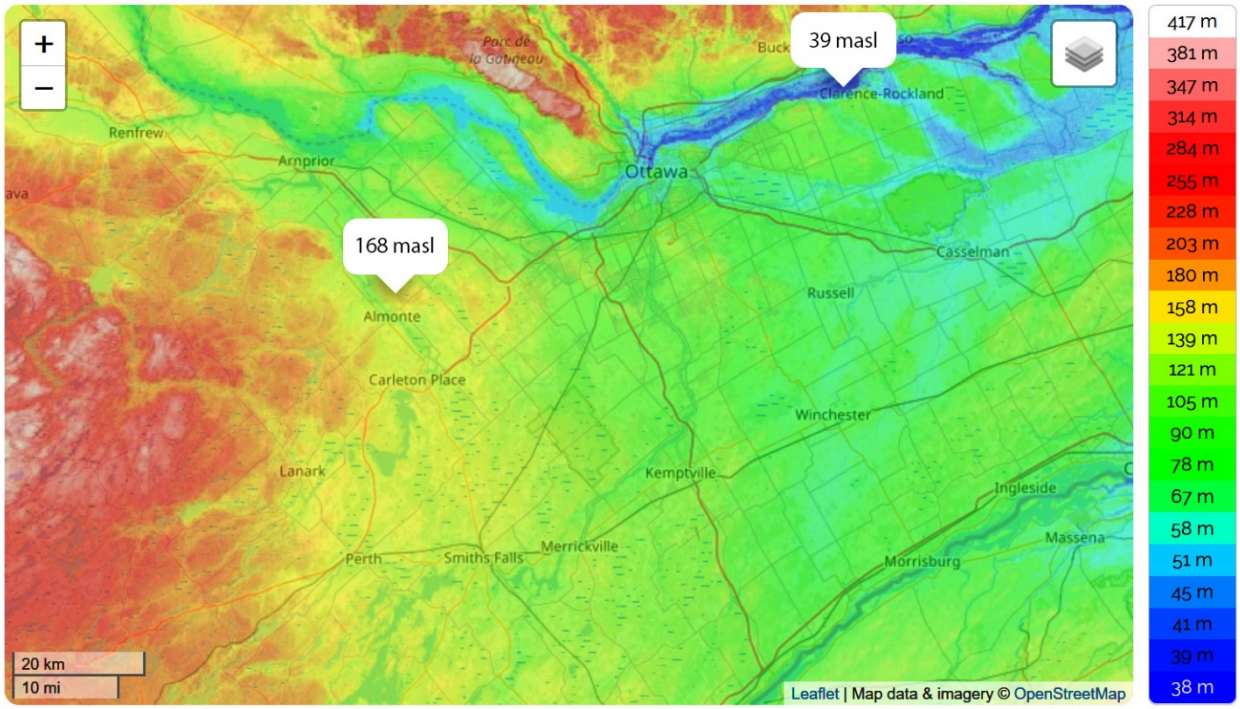

Figure 4-2 Elevation map of the Ottawa area (adapted from topographic-map.com, 2019).

Across the study area, the plains are cut into river valleys by the many rivers, tributaries, and creeks that drain the region. Several of these river valleys are marked visibly with the scars of historic and prehistoric landslides, scars that form a permanent part of the area's topography (Brooks, 2014; Brooks et al., 1994; McEniry, 1978; Quinn et al., 2010). Individual slopes are in the range of 0-40 degrees, the steepest slopes being found in the western sector of the city in river valleys along the Mississippi and Carp Rivers. A unique and notable feature of the topography of the study area is the alluvial terraces created, in prehistoric times, by the erosional and depositional activity of the proto-Ottawa River (also known variously as the "ancestral Ottawa River," the "paleo Ottawa River," or the "pre-Ottawa River"), which was as much as 5 km wider than it is today on average. The proto-Ottawa River cut wide channels and subsequently left high terraces and abandoned channels and banks as it receded (discussed below), following the isostatic uplift that resulted from glacial melting; these abandoned banks later experienced frequent, very large landslides (Al-Umair, 2018; Brooks, 2014; Brooks, et al, 1993; McEniry, 1978; Marshall et al., 1979; Mitchell and Klugman, 1979; Nader, 2014; Quinn et al, 2010); Schut and Wilson, 1987).

The Ottawa River is the major body of water in the area and it serves as the city's northern boundary. It flows eastwards and drains into the St. Lawrence River at Montreal. It is fed by a number of tributaries, some of which are rivers in their own right, which flow northwards through the study area. The main tributary is the Rideau River, which bisects the study area from top to bottom into two roughly equal halves. Its main sub-tributary is the Jock River, which enters it about 3.2 km north of Manotick. Approximately 18 km farther north, after flowing past Nepean, the Rideau River feeds into the Rideau Canal on its western bank at Hog's Back. Past Hog's Back, the Rideau River flows to the east of the Rideau Canal (and roughly parallel to it) and enters the Ottawa River at Rideau Falls. The Rideau Canal meets the Ottawa River in a series of 8 locks east of Parliament Hill in downtown Ottawa. In the west of the study area, the Mississippi River flows north out of Mississippi Lake through the Town of Mississippi Mills and enters the western corner of the City of Ottawa before draining into the Ottawa River between Fitzroy Harbour and Arnprior. To the immediate east of the Mississippi River, the Carp River flows northwest from Kanata and enters the Ottawa River at Fitzroy Harbour. To the east of the Rideau River, the Castor River and Bearbrook Creek and its tributaries flow eastwards into the South Nation River, which eventually empties into the Ottawa River about 15 km east of Clarence-Rockland (Marshall, et al. 1979). The banks of the South Nation River have been the location of numerous landslides over the past century. The most notable of these occurred on June 20, 1993, following a heavy rainfall, in the vicinity of the former town of Lemieux, about 60 km east of Ottawa. The town had been abandoned about 3 years earlier in response the severity of the landslide hazard in the area. Approximately 3 million cubic metres of sand, silt, and clay flowed into the South Nation Valley, filling the valley bottom with spoil up to 12 m deep and damming the river for three days (Brooks et al., 1994).

The area's major rivers do not undergo significant seasonal variations. However, as a general pattern, by mid- to late-summer, the Jock River (which has only a few tributary streams) and the area's major creeks and small drainage channels are reduced to a trickle or run dry for lack of sufficient runoff (Marshall et al., 1979).

The rivers of Ottawa and their respective watersheds are shown in Figure 4-3.

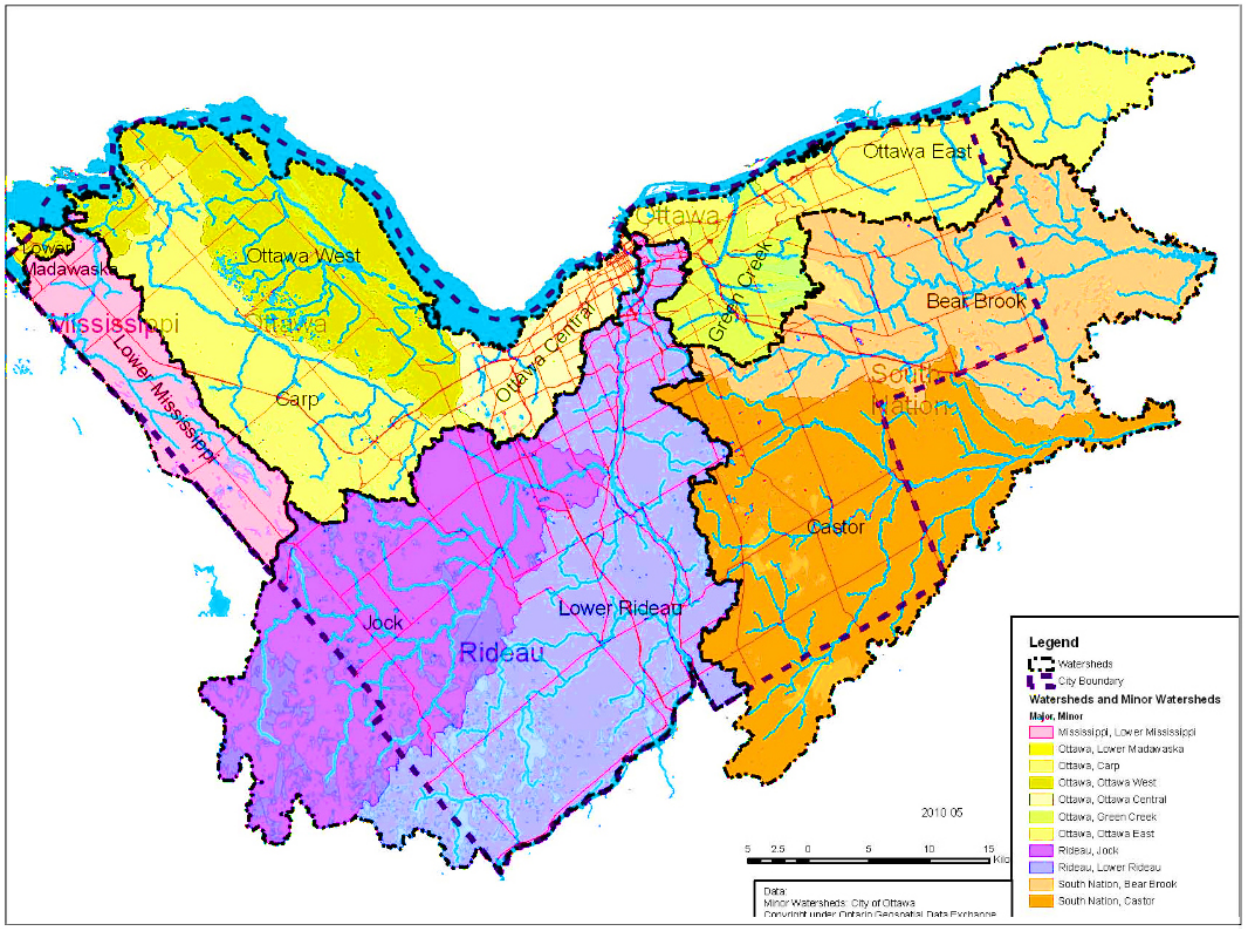

Figure 4-3 The major rivers of Ottawa and their respective watersheds (City of Ottawa, 2011b).

4.2.3 Physiography

There are five physiographic regions within the City of Ottawa limits, as shown in Figure 4-4. These are: (1) the Ottawa Valley clay plains; (2) the Smiths Falls limestone plains; (3) the Edwardsburg sand plains; (4) the Russell and Prescott sand plains; and (5) the North Gower drumlin field (Chapman and Putnam, 2007; Schut and Wilson, 1987).

The Ottawa Valley clay plains region sits directly on the south bank of the Ottawa River, which serves as its northern boundary. The region encompasses West Carleton, Goulbourn, Kanata, and the northern part of Cumberland (see Figure 4-4). In the south of Cumberland, the clay plains come to an end at the edge of an abandoned channel of the proto-Ottawa River, most of which consists of clay plains mixed in with modified till plains and sandy deposits. This abandoned channel is also the site of the large 7,700-year-old Mer Bleue peat bog, southeast of Blackburn Hamlet. In terms of

physiography, the region consists of a combination of clay plains and bedrock uplands created by faulting and upthrust. One such fault is the Hazeldean fault, which separates Carp Ridge from Carp Valley. The region is drained by the Ottawa River, the Mississippi River, the Carp River, the Jock River, the Rideau River, and minor creeks and brooks, such as Bear Brook in Gloucester and Cumberland (Marshall et al., 1979; Schut and Wilson, 1987).

The Smiths Falls limestone plains region covers most of the southwest part of the City, and include parts of Rideau-Goulbourn and Carleton (see Figure 4-4). The region sits on the limestone and dolomite Ottawa and Oxford bedrock formation and is therefore largely flat. Overlying this bedrock is a thin layer of till. The region has been subjected to mining for bedrock aggregate. The region is also characterized by large areas of wetlands—mainly stream and basin swamps and a few fen deposits. A minor feature of the region's physiography is the scattered patches of deeper clays and sands. Drainage is provided almost entirely by the Jock River along the southeast margin of the region (Schut and Wilson, 1987).

The Edwardsburg sand plain region lies to the immediate east of the Smiths Falls limestone plains region in a narrow corridor in the southern part of Rideau-Goulbourn on the northwestern bank of the Rideau River (see Figure 4-4). In this region, the bedrock is overlain with a layer of boulder clay, which is in turn, mostly covered with a layer of sand, which is predominantly level, with occasional undulations. Drainage for the region is provided by the Rideau River.

The North Gower drumlin field region lies to the north and east of the Edwardsburg sand plain region and covers the eastern part of Rideau-Goulbourn and the southern half of Osgoode (see Figure 4-4). The dominant physiographic features of this region are drumlins and gently undulating and moderately sloping till plains. Adjacent to these features are low-lying, poorly drained deposits of finer clays and silts that were laid there by the Champlain Sea. A unique feature is the esker deposit that lies in a north-south orientation on the west bank of the Rideau River. The esker is flanked intermittently by gently sloping sand plains. In addition, the region is dotted with stream swamp deposits and occasional limestone plains. Drainage is provided mainly by the Rideau River in the south and central part of the region and by the smaller South Castor and Castor Rivers in the east. In general, the region is not well drained by natural means and this has made necessary the introduction of artificial drainage ditches connected to the natural drainage system to carry away excess spring runoff and lower the water table (Marshall et al., 1979; Schut and Wilson, 1987).

Sandwiched between the North Gower drumlin field region and the Ottawa Valley clay plains region is the Russell and Prescott sand plains region (see Figure 4-4), which encompasses the northern reaches of Osgoode, the southern half of Gloucester-Southgate, with a narrow east-west

corridor through Knoxdale-Merivale, and the southern fringe of Cumberland, as far north as the abandoned channel of the proto-Ottawa River (see Figure 4-4). The sands that characterize this region were originally deposited in a delta of the proto-Ottawa River. Subsequently, with isostatic uplift, the waters of the delta receded and the river was rerouted, leaving behind a layer of sand about 5 to 10 m thick. The sands are generally level or undulate gently and are dotted with occasional dunes. The area is drained by the North Castor River, and by Shaws Creek and the South Indian Creek, both of which are tributaries of Bear Brook (Schut and Wilson, 1987).

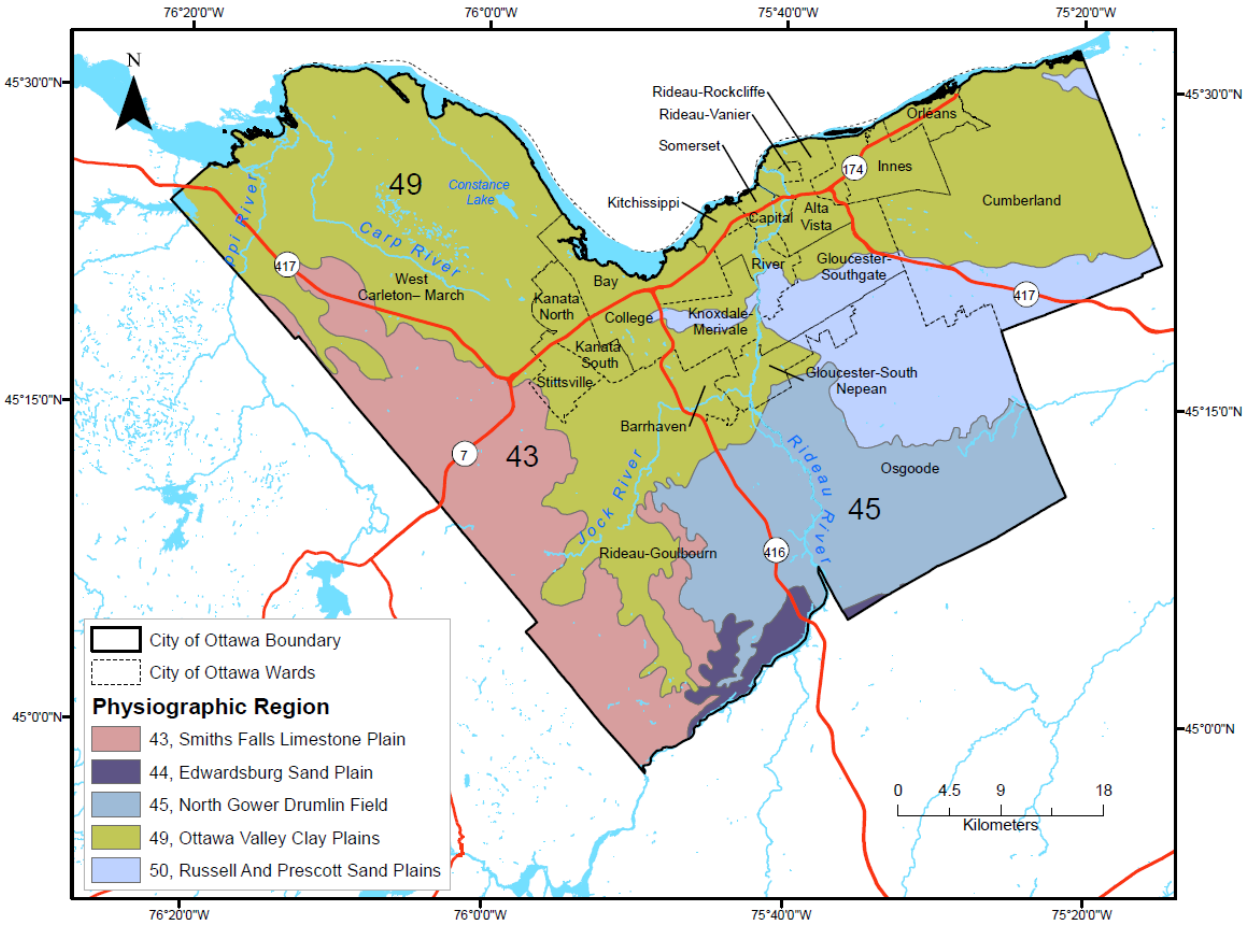

Figure 4-4 Physiographic Regions of Ottawa (modified from Physiography of Southern Ontario MRD288; Chapman and Putnam, 2007).

4.3 Geological Characteristics of the Study Area

4.3.1 Introduction

The City of Ottawa is situated in the Ottawa-St. Lawrence Lowlands geological region of Ontario. The region covers the western part of the former Champlain Sea. In the 1980s, the Ontario Ministry of Natural Resources, in collaboration with the Federal Department of Regional Economic Expansion, sponsored efforts to update the then-current geological maps of this region, which had been prepared by the Geological Survey of Canada and the Ontario Department of Mines in the 1940s. A final report combining the findings of the various preliminary field studies was published by the Ontario Geological Survey in 1991 (Williams, 1991). The 1991 report covered an area bounded on the north by the Ottawa River, on the south by latitude 44° 30' N and the St. Lawrence River, on the east by the Ontario-Quebec border, and on the west by longitude 76° 30' W. An update of the earlier maps and nomenclature was made necessary by the fact that several surface exposures and drill-cores were not in existence in the 1940s, and recent excavations at quarries, roadbuilding sites, and the site of the TransCanada Pipeline (now known as the Canadian Mainline) had exposed new bedrock and other stratigraphic features, indicating that the structural geology of the region, particularly in the northern reaches of the Lowland, in the Ottawa area, was more structurally complex than had previously been thought (Williams, 1991).

4.3.2 Geologic Overview

The geology of the study area was profoundly affected by the glaciation of the last Ice Age, which ended about 11,500 years ago, giving rise to the former Champlain Sea. The geologic history of the region can thus be divided into three broad time periods: (1) the pre-Champlain Sea period, which extends backwards in time from the formation of the Champlain Sea; (2) the Champlain Sea period, which lasted about 2,000 to 3,000 years; and (3) the Post-Champlain Sea period, which extends from the recession of the Champlain Sea to the present. Pre-Champlain Sea geology includes bedrock plains, glacial till plains, and glaciofluvial ridges. Champlain Sea geology is characterized by the deposition of marine clays, fine-textured deltaic deposits, and organic matter over the existing material. Post-Champlain Sea geology includes the formation of abandoned river channels, peat bogs, and eroded river and stream channels (Marshall et al., 1979).

The geologic history of the Pre-Champlain Sea period is marked by five major occurrences: (1) the formation of the Gatineau Hills, on the north and northwest of the study area; (2) a long period

of erosion; (3) a sinking and rising of the Lowland accompanied by successive invasions by the sea; (4) a second period of erosion; (5) the descent of glaciers from the north (Wilson, 1956).

(1) The Gatineau Hills were formed during the Precambrian Era on the eastern edge of the Canadian Shield, over 1 billion years ago. They consist of gneisses and crystalline Grenville limestone, which are the oldest rocks in the region, and form the underlying bedrock for the Ottawa-St. Lawrence Lowlands. In the present-day, outcroppings of this Precambrian bedrock occur in the northwest corner of Nepean (Marshall et al., 1979; Wilson, 1956).

(2) The long period of erosion occurred in the early part of the Paleozoic Era, during the Cambrian Period, over the next 500 or 600 million years. Rock from the Gatineau Hills was worn away through the usual processes of weathering and distributed in lower-lying areas, forming the sedimentary basin between the Canadian Shield on the west and the Adirondack Mountains on the east. It was a time of great geological disturbances, when enormous faults and cracks developed in the Precambrian bedrock. The three major faults in the area are: (1) the Hazeldean Fault, which runs from the Connaught Rifle Range in the northwest, on the south bank of the Ottawa River, heading in a southeasterly direction, to Barrhaven; (2) the Gloucester Fault, which runs to the immediate east of the Hazeldean Fault, from Gatineau, Quebec in the north, across the Ottawa River and into the City of Ottawa in a south-southeasterly direction, curving eastwards towards the Village of Russell, near the eastern boundary of the City of Ottawa; and (3) a segment of the Grenville Front, which runs in an east-west direction along the northern bank of the Ottawa River, across from the northeast corner of the City of Ottawa. These and other minor faults are shown in Figure 4-5). The complex pattern of block faulting created the basin that would later receive the deposits of marine clay during the Champlain Sea period (Marshall et al., 1979; Williams, 1991; Wilson, 1956).

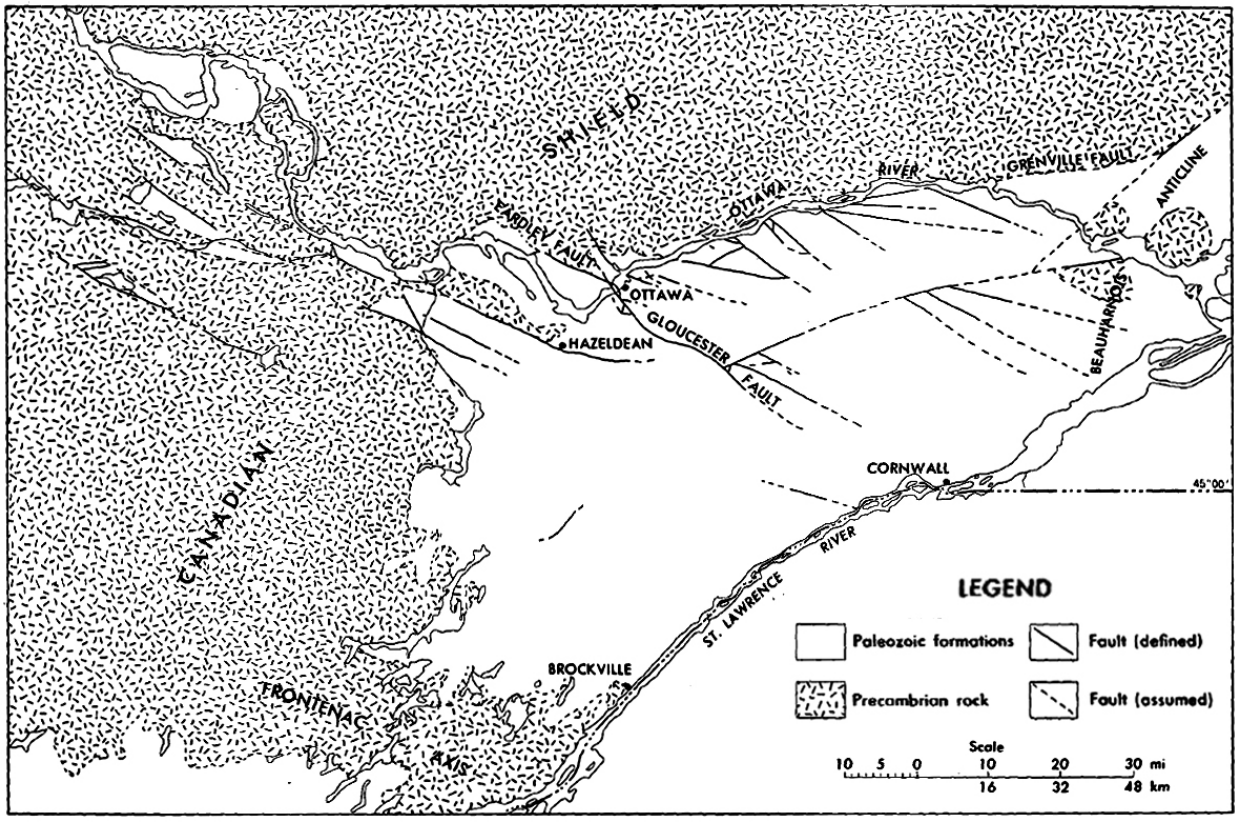

Figure 4-5 Structural Geology Map of Ottawa - St. Lawrence Lowland showing major faults in the Precambrian bedrock (modified from Marshall et al., 1979).

(3) The sinking and rising of the Lowland occurred during the Ordovician period, immediately following the Cambrian. There were seven successive instances in which this part of the continent, which was originally above sea level, subsided and was subsequently raised, and in all instances, the ocean invaded the basin on subsidence and retreated as the land rose above sea level once again. With the first invasion, the ocean water acted on the loose material that was scattered across the basin during the preceding period of erosion. The insoluble sand was carried westward as the waters advanced from the Gulf of St. Lawrence and was deposited unevenly across the uneven surface of the basin. The deposits eventually consolidated as Nepean sandstone. The soluble materials dissolved in the ocean waters and became increasingly concentrated as the sea advanced westward. Eventually, the solubles were deposited as limestone or dolomite (a kind of magnesium-laced limestone) on top of the sandstone. On subsequent invasions, shale or a mixture of shale and limestone were deposited in the basin. The third inundation came from the southwest and flowed eastwards, depositing predominantly limestone. The fourth invasion brought black shale, which now underlies a large area of the City of Ottawa to the south of the Parliament Buildings. The fifth invasion brought grey shales

from the Gulf of Mexico. The sixth inundation brought grey limestone and dolomitic limestone interbedded with some shale. The final invasion brought red shale with a few layers of green shale. The various materials brought in by these successive invasions were not deposited uniformly across the basin but were localized to specific areas depending upon the direction in which the inundation proceeded, the presence of fault lines along the path of the water's advance, and other factors. They all do, however, appear as outcrops at various location in the study area (Wilson, 1956).

(4) The second long period of erosion, which lasted for 300 million years, occurred after the basin was once again raised and remained above sea level. This period is characterized not only by erosion, but also by considerable faulting in the sediments laid down in the preceding period triggered by as the gradual rise of the Appalachian Mountain to the east and south of the Lowland. One such fault of major proportions is the Gloucester fault. The block to the east of this fault dropped, such that the main part of the City of Ottawa in the present day stands on the northwest corner of the block that dropped. Weathering following faulting smoothed out the jagged edges of the faults, and rivers carved valleys out of the floor of the basin.

(5) The descent of the glaciers from the north caused major changes in the topography. The tops of the Gatineau Mountains were sheared off, ground up, and borne southwards into the Lowland. The rock surfaces below the glaciers were gouged by boulders embedded in the glacial ice. This left deep scars when the ice melted. As the glaciers melted, they deposited the debris they had collected at random points across the Lowland, often miles from where the debris had originated. Where melting water flowed under the ice, the debris was deposited in long snaking trails known as "eskers." One such is the esker on the west bank of the Rideau River, mentioned earlier. The movement of glaciers is also responsible for the formation of drumlins (mentioned above). Drumlins are dome-shaped mounds of debris shaped like an inverted spoon, narrower at one end than at the other. They form around a large obstacle, such as massive boulder, that the glacier is unable to move. Loose debris collects at the impact-end of the obstacle, then spreads out along either side of it, and as the flow gets past the obstacle, the debris unites once again into a single stream which gradually tapers off. Large areas of the Lowland are dotted with drumlins, as discussed above. With the continued melting of the icecaps, the meltwater formed large freshwater lakes along the margins of the melt. Sedimentation in these lakes resulted in the deposition of large amounts of varved clays. Clays deposited in summer were thicker and browner than those deposited in winter, owing to oxidation. Given these dynamics of glaciation, the pattern of deposition resulting from glacial action is glacial boulder till topped with a layer of varved clays (Wilson 1956).

The melting of the glaciers ushered in the Champlain Sea period. As discussed earlier, the immense weight of the glaciers, which were a mile thick in some places, had depressed the land mass under them, causing the low-lying areas to sink below sea level. When the glaciers melted, the sea rushed in once more from the Gulf of St. Lawrence, advancing up the St. Lawrence Valley, into the Champlain Valley and eventually into the St. Lawrence Lowlands. The expansive body of water that was created by this influx is known as the Champlain Sea, the influx of sea water brought with it large amounts of marine clay and silt, which were eventually deposited all across the Ottawa-St. Lawrence Lowland. These new waters, through the actions of their waves, also modified areas of elevated sedimentary bedrock and reworked and redistributed the glacial tills and debris that were left behind by the glacial lakes and the retreating ice. Eventually, the Earth's crust responded to the easing of the weight of the glaciers by gradually rebounding. This isostatic rebound raised the Lowlands above sea level, causing the Champlain Sea to retreat. During the slow process of retreat, the Sea was transformed from a marine environment into an estuarine coastal environment—one in which a relatively thin layer of sand was deposited over the early deposits of clay. With further uplift and retreat, the estuarine environment became a freshwater environment. During the long period of retreat, the steeply sloping glaciofluvial ridges were transformed by the action of waves and longshore drift into gently sloping upland plains through the deposition of successive layers of sand along the flanks of the ridges. The Champlain Sea was not, however, the only factor influencing the geology of the basin during this period. Rivers, fed by the waters of the melting ice sheet deposited large quantities of sand, which created extensive deltas, especially in the Russell and Prescott sand plains region, as discussed earlier (Marshall et al., 1979; Wilson, 1956).

The Post-Champlain Sea period was marked by the shifting of the channels of the Ottawa River. The proto-Ottawa River was much wider than it is at present, as noted earlier. It flowed farther south from its present route, taking in present-day Bells Corners and Dows Lake in the west and splitting into two channels at present-day Blackburn Hamlet in the east, with one channel going north, the other south. As a result of isostatic uplift and erosion upstream from Ottawa, the river abandoned the southern channel and shifted northwards into the pre-glacial valley, settling into what is the current Ottawa River channel. The abandoned south channel contains fluvial sands overlying marine clay. Some of its sub-channels still host small streams, but the major portion of the channel southeast of Blackburn Hamlet is currently the site of the Mer Bleue Bog (mentioned earlier). In addition to the abandoned channels, the isostatic uplift left a series of high terraces at various elevations between 46 and 76 mASL, marking successive stages in the progression of the proto-Ottawa River on its way to its current location. It was also during this period that the area's organic peat deposits were formed

(Marshall et al., 1979). Given the geotechnical characteristics of the abandoned channels and banks of the Ottawa River, these channels are a particularly fertile ground for landslides, and several have occurred along them over the course of the area's long geologic history.

The abandoned channels and banks of the proto-Ottawa River and the landslides that have occurred along them are shown in Figure 4.6.

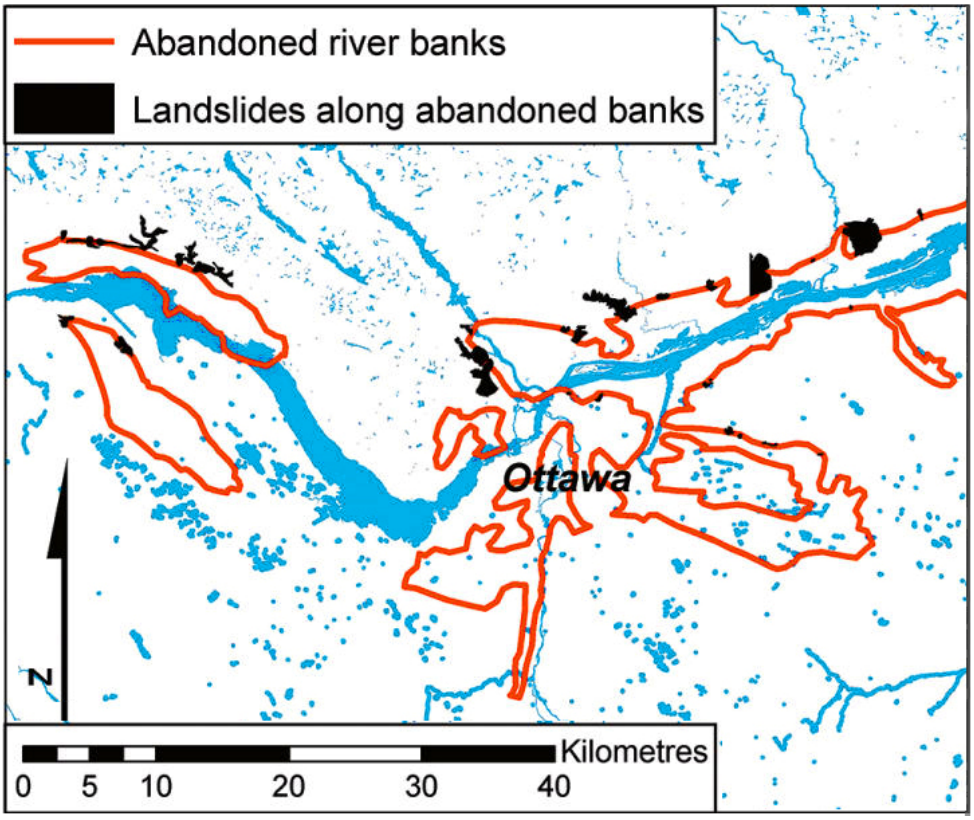

Figure 4-6 Abandoned channels and banks of the proto-Ottawa River, and the landslides that occurred in and around them (modified from Quinn et al, 2010).

4.3.3 Surficial Geology

The surficial material of the study area can be categorized into five groups, based on the period of deposition: (1) bedrock; (2) Pre-Champlain Sea deposits; (3) Champlain Sea deposits; (4) Post-Champlain Sea deposits; and (5) recent deposits.

4.3.3.1 Bedrock

The oldest surficial materials in the City of Ottawa are those found in the bedrock, which appears at the surface in the form of outcrops. They date back to the Precambrian Era and the early Paleozoic

Era. The Precambrian bedrock consists of intrusive rock, predominantly granite, and metamorphic rocks such as quartzites, crystalline limestone, and granite-gneiss. It is found in the western part of the city, from Galetta and Fitzroy Harbour to the Carp Ridge and Kanata, and occurs primarily as bare, isolated hilly rock knob uplands, or occasionally under a thin layer of unconsolidated sediments less than 1 m thick. The Paleozoic bedrock, which overlies the Precambrian bedrock for the most part, dates from the early Paleozoic, namely the late Cambrian or Ordovician Period. It occurs in a number of "formations," localized to specific parts of the city, and consists variously of limestone, dolomite, shale, sandstone, and quartzite. It appears at the surface chiefly as bare, flat, tabular outcrops, occasionally covered with a thin layer of unconsolidated sediments up to 1 m thick. The dominant formation is the Oxford Formation, which underlies most of Rideau and Osgood and parts of West Carleton and Kanata. At the surface, it is found in outcrops in southwestern Rideau and northeastern Osgoode. It consists chiefly of dolomite, grey limestone, and magnesian limestone. The oldest Paleozoic rock in the area, however, is the Nepean Formation, which appears at the surface as outcrops in parts of Kanata. It consists generally of cream-coloured coarse-grained sandstone. In northern Cumberland, along the Ottawa River, are found outcrops of the St. Martin Formation, consisting mainly of limestone. Surficial bedrock is found in two physiographic regions: the Ottawa Valley clay plains and the Smiths Falls limestone plans (Marshall et al., 1979; Schut and Wilson, 1987, Williams, 1991).

4.3.3.2 Pre-Champlain Sea Deposits

In the Pre-Champlain Sea period, surficial materials were added to the bedrock topography by the action of moving glaciers and the rivers and streams that formed with glacial melting and retreat. Thus, the surficial materials are of two broad types: (1) glacial till deposits; and (2) glaciofluvial deposits. The glacial deposits consist of tills, sand, and a heterogeneous mixture ranging from clay to large Paleozoic boulders, laid out in flat, undulating, or hummocky plains, or heaped up into elongated drumlin ridges (discussed above). The composition of the till is related to the material of the bedrock where the deposition occurred. In the area of the Oxford Formation, for example, the till material is predominantly limestone and dolomite. Around Fitzroy Harbour, the till deposits are dominated by sandstone. Till deposits derived from various types of shale bedrock are generally distinguished from each other by their colour: Queenston, derived from red shale; Billings, from black shale; Carlsbad, from grey shale, Rockcliffe, from grey-green shale. The largest body of shaly till is found in southern Cumberland. In contrast to the glacial tills, the glaciofluvial deposits consist of gravel and sand, occurring in the form of eskers (discussed above). The retreat of the ice sheet also

produced ice-frontal deposits, in the form of esker-like ridges and kames (irregularly shaped hills or domes) consisting of non-fossiliferous sand, gravel, cobbles, and intermittent till lenses, found chiefly in Goulbourn, West Carleton, Rideau, Osgoode and Cumberland. The surficial materials deposited during this period are found in the North Gower drumlin field physiographic region (Schut and Wilson, 1987; Marshall et al., 1979).

4.3.3.3 Champlain Sea Deposits

Deposition during the Champlain Sea period occurred in three locations: (1) the sea floor, that is, deep water; (2) the sub-littoral zone, that is, the shallow waters near the shores of the Champlain Sea; and (3) the littoral zone, that is, the shores of the Champlain Sea.

Deposits in the deep water zone consist of alternating layers of blue-grey and reddish-grey clay, silt, and silty clay (i.e., Leda clay). These deposits are calcareous, fossiliferous, and non-oxidized in the lower layers but not in the upper layers to a depth of about 2 m. The lower layers were deposited early during the marine phase of the Champlain Sea, when its waters were saline or brackish. The upper layers were deposited during the freshwater phase of the Champlain Sea. The deep-water deposits are found in the Ottawa Valley clay plains physiographic region, mainly in the Carp Valley (West Carleton) and the Richmond plains (Goulbourn) and in parts of Cumberland. The sub-littoral and littoral deposits were laid down towards the end of the Champlain Sea period, when the waters began to recede on account of isostatic uplift. Both of these two types of deposits are found in the North Gower drumlin fields and the Smiths Falls limestone plains physiographic regions. Deposits in the sub-littoral zones consist of uniform, fossiliferous, medium-to-fine, buff-to-grey sand with some silt, which forms nearly level to gently sloping plains in areas such as Huntley, Stittsville, and Stanley Corners (Goulbourn), Kars and Waterson Corners (Rideau), and between Osgood and Manotick Station. Deposits in the littoral zone are the result of Champlain Sea waves reworking earlier glaciofluvial eskers, drumlins, and shallow till deposits covering Paleozoic bedrock. They consist of gravel, coarse sands, and cobbles, with occasional slabs of Paleozoic bedrock, in some areas overlying earlier glaciofluvial deposits. Reworked eskers are found in Stittsville and Manotick Station; reworked drumlins are found in Rideau and Osgoode; reworked shallow till deposits are found in West Carleton, Goulbourn, and Rideau (Schut and Wilson, 1987; Marshall et al., 1979).

4.3.3.4 Post-Champlain Sea Deposits

The Champlain Sea period came to and end when the Sea's marine environment was gradually transformed into an estuarine environment with the influx of freshwater from the melting ice sheet.

Eventually, with isostatic rebound, the estuarine waters began to recede and at the same time the proto-Ottawa River began to form and go though its various stages. Thus, the Post-Champlain Sea period is characterized by both estuarine and river channel deposits. The estuarine deposits are found in the Russell and Prescott sand plains physiographic region along with river channel deposits. Both types of deposits in this region consist of stratified, grey-to-buff, medium-to-fine-grained sand, reworked locally by wind into dunes. Abandoned river channel deposits are of two types in terms of content: (1) sandy; and (2) clayey; and of two types in terms of mode of deposition: (1) fluvial; and (2) erosional. The sandy abandoned river channel deposits are found in the Russell and Prescott sand plains and the Ottawa Valley clay plains physiographic regions. They are fluvial and consist of stratified, grey-to-buff, medium-grained, non-fossiliferous sand, with some silt, deposited on the channel floors, banks, and terraces, and reworked into dunes. They often take the form of spits, bars, or terraces. The clayey abandoned river channel deposits are found only in the Ottawa Valley clay plains physiographic region. They are erosional and consist of silt and silty clay with sand lenses, overlying unmodified marine clay. In some of these abandoned channels, such as the one in northern Cumberland, which runs adjacent and parallel to the Ottawa River, erosion along the floor and sides of the channel and on terraces in the channels has exposed the underlying marine clays, and in some places even the till deposits that underlie the eroded clays. However, there are large areas that remain covered with a thin intermittent layer of fluvial sediments. Along the banks of the abandoned channels of the proto-Ottawa River are found deposits from numerous landslides, consisting primarily of the Champlain Sea sensitive marine clays that make up the banks. These landslide deposits are also considered erosional.

4.3.3.5 Recent Deposits

Recent deposits are of two types: (1) organic deposits; and (2) modern river deposits. The organic deposits are found in the Smiths Falls limestone plain and the North Gower drumlin field physiographic regions and consist of mulch and peat in the form of bogs, fens, and swamps in very poorly drained areas. The organic materials are predominantly decaying plant matter, which has a loose, extremely soft consistency, and is dark brown or black in colour, Peat is usually formed under a relatively thin layer of high-moisture-content fill and over a bed of clay. Extensive organic deposits are found in Goulbourn and Rideau, between Greely and West Osgoode, and central Cumberland, where it is represented most notably by the Mer Bleue peat bog. The modern river deposits consist of stratified sand, silty sand, silt, silty clay, and disseminated organic matter, deposited on the flood

plains of present-day rivers and streams, especially along the current Ottawa River in northern Cumberland (Al-Umar, 2018; Marshall et al., 1979; Schut and Wilson, 1987).

The surficial geological landforms of the study area are shown in Figure 4-7 and the surficial materials are presented in Figure 4-8.

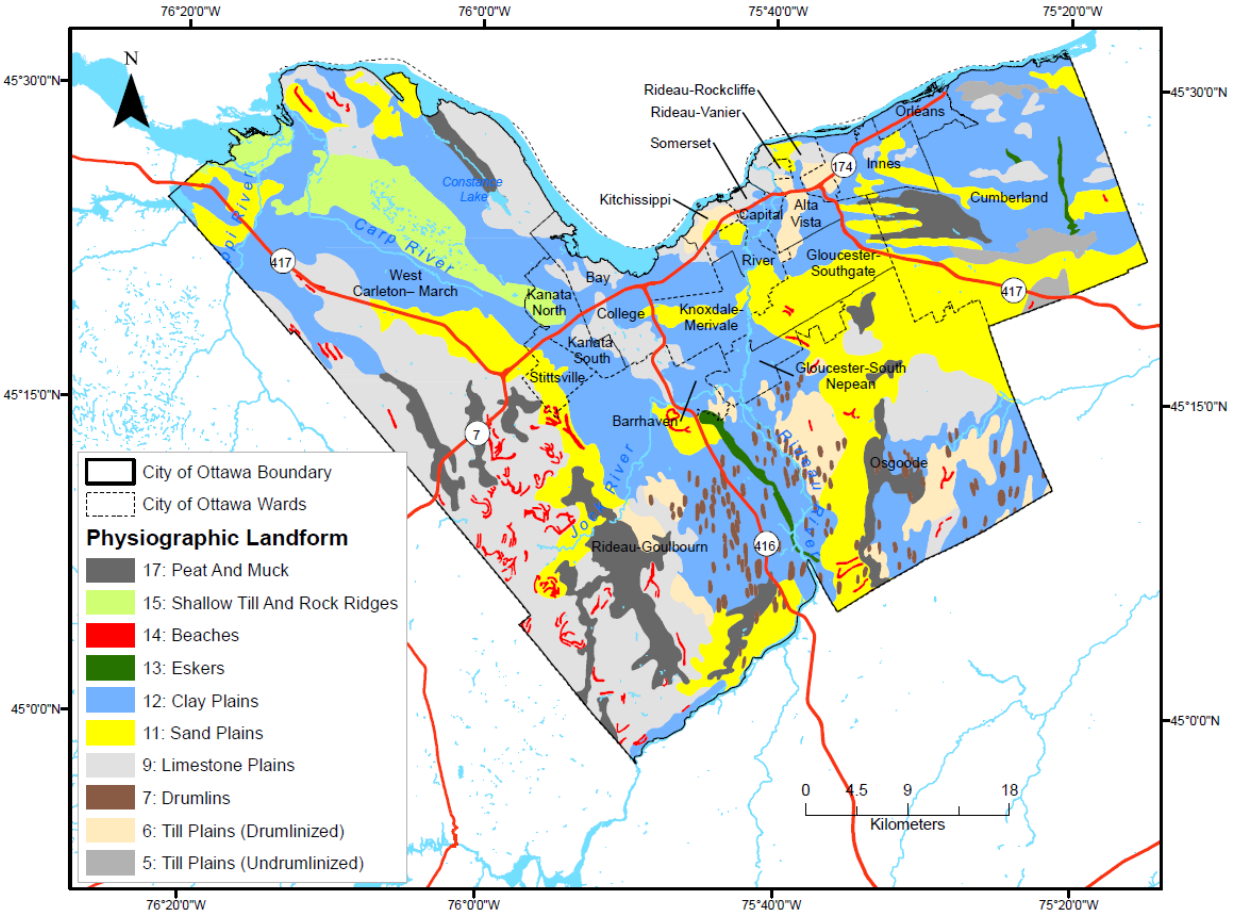

Figure 4-7 Surficial geological landforms of the City of Ottawa (Physiography of Southern Ontario MRD228; Chapman and Putnam, 2007).

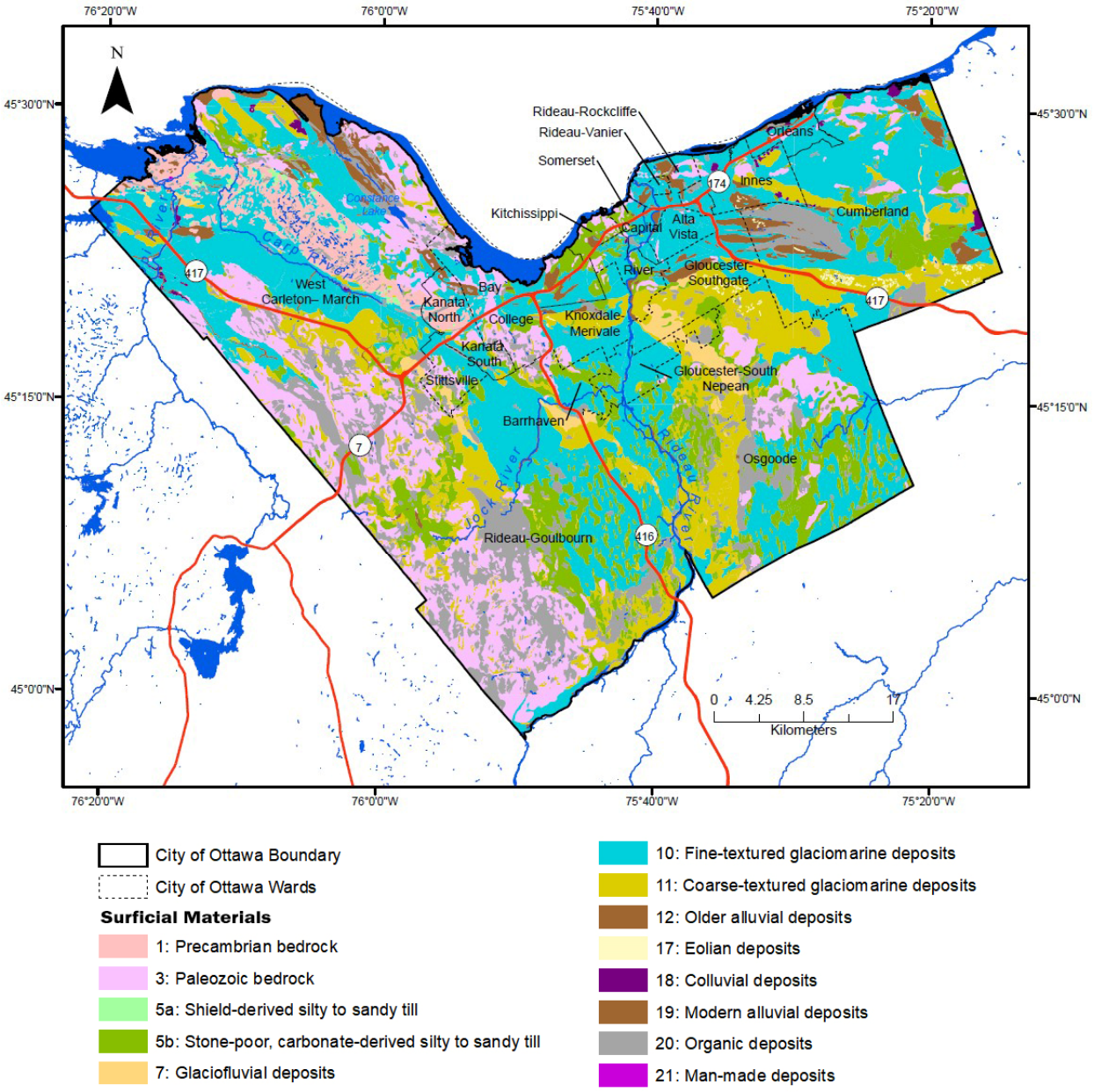

Figure 4-8 Surficial materials within the City of Ottawa (Surficial Geology of Southern Ontario MRD128-REV; Ontario Geological Survey, 2010).

4.3.4 Land Forms and Surface Features

The study area is characterized, in the present day, by a number of unique landforms and surface features, which are broad classifications of the surficial geology discussed in the previous section. The following forms and features will be discussed below: (1) rocklands; (2) recent alluvium; (3) eroded channels; (4) escarpments; (5) landslides; and (6) marshlands.

4.3.4.1 Rocklands

Rocklands are areas in which 25 percent of the surface or more is either exposed bedrock or bedrock topped with 10 cm or less of surficial material. They represent either outcrops of Precambrian metamorphic or igneous bedrock, or Paleozoic sedimentary bedrock. The majority of the Paleozoic sedimentary bedrock areas are composed of limestone and dolomite, the rest being sandstone. In the study area, these Paleozoic outcrops are found predominantly in the areas adjacent to the Hazeldean and Gloucester faults and around the block fault northeast of Blackburn. Smaller exposures occur in the abandoned channels of the proto-Ottawa River. However, the Paleozoic sedimentary type of rockland accounts for only a fraction of the total rockland areas, which are dominated by Precambrian outcrops. West Carleton hosts the largest outcrop Precambrian bedrock in a ridge of granite and gneiss which runs in a northwest-southeast direction. The surficial materials that overlie the bedrock in these rockland areas are composed of moderately coarse to coarse undifferentiated drift materials laid out in nearly level to gently sloping or undulating plains (Marshall et al., 1979; Schut and Wilson, 1987).

Areas of recent alluvium contain soils that have formed on recent alluvial deposits. They are found in floodplains or river bars in areas that are poorly drained and are subject to regular and frequent flooding. Their mineral content varies considerably and may include sand, silt, and clay, with additional amounts of organic matter. Generally, the alluvial deposits overlie deposits of marine clay (Marshall et al., 1979; Schut and Wilson, 1987).

4.3.4.2 Eroded Channels

Eroded channels are the result of erosion that is either recent or geologically ancient. They take the form of steep-sided valleys, gullies, or creek beds with embankments. The steepest valley slopes range from 20 to 40% and are associated with major rivers. Gullies and creekbed embankments are generally associated with smaller tributaries traversing level marine plains, which have been cut to a depth of 2 to 5 m. They are shorter and tend to have less-steep slopes ranging from 5 to 15%. Soil material on the slopes commonly slump or move down the slope, particularly when the channels have been cut into thick layers of marine clay or clay overlaid with sand. The steep channels cut to depths more than 20 m are particularly prone to landslides (Marshall et al, 1979; Schut and Wilson, 1987).

4.3.4.3 Escarpments

Escarpments are of two types: (1) bedrock; (2) clay, with or without a sand overlay. Bedrock scarps are the result of local block faulting in which a steep vertical face of bedrock is left exposed on one side of the fault. The escarpments in the study area are closely related to the Hazeldean and Gloucester faults, and the block fault northeast of Blackburn. Bedrock scarps are found in the limestone and dolomite bedrock plains in Cumberland, West Carleton and Kanata. Sandstone carps are found in Kanata. The most prominent of bedrock scarps tend to face north and run parallel to the Ottawa River. They vary in height from 5 to 25 m where surface materials are present, they generally cover less than 50 percent of the bedrock face and are composed to thin, flaggy till-like materials or undifferentiated drift. Clay and sand over clay scarps tend to occur on the banks of the Ottawa and Rideau Rivers, and in the abandoned channels and terraces of the proto-Ottawa River, and are associated with landslides. They are usually long, narrow, and continuous and no more than 12 m in elevation. If the clay is topped with sand, the topping is generally 1 to 3 m of sandy estuarine or fluvial material (Marshall et al, 1979; Schut and Wilson, 1987).

4.3.4.4 Landslides

Landslide areas contain material that has migrated downslope from a higher elevation, usually as a result of oversaturation of the unstable, highly sensitive marine clays typical of such areas. These areas tend to be poorly drained, a factor that contributes to the oversaturation of the soil. Landslide areas are typically found along active riverbanks or along the banks and terrace bluffs of abandoned river channels. They contain fine-textured marine material occasionally overlain with coarser marine or fluvial materials. The original material of the landslide is typically an undifferentiated, tilted or slumped block of clay containing vertical and horizontal lenses of sand. A typical landside area consists of a head scarp footed by a downslope apron and fan. The head scarp has a slope in the range of 5 to 15%. Downslope aprons and fans have a slope in the range of 2 to 9% and may be nearly level to undulating, or irregular. In the study area, landslides areas are found in the northeast of Gloucester, as well as along the Ottawa and Rideau Rivers, the Green and Ramsay Creeks, and Bear Brook (Marshall et al., 1979; Schut and Wilson, 1987).

Landslides may be classified into four types, based on their mode of failure: (1) simple rotational slides; (2) retrogressive rotational slides; (3) translational slides; and (4) flows. A simple rotational slide has a concave surface of rupture, and the mass rotates along the concave shear surface. Such a slide involves only one shear surface, whereas a retrogressive slide involves multiple or successive

shear surfaces. A translational slide, also known as a "sheet slide" or a "surficial slide", has a planar or gently undulatory surface of rupture and tends to be shallow. A flow or "flow slide" is one in which the material behaves like a fluid. It may start as a rotational slide, but the displaced material becomes liquefied and this hastens evacuation of debris from the scar (Hugenholtz and Lacelle, 2004).

Landslides have occurred in the sensitive marine clays of the Ottawa region in both prehistoric and historic times. With the help of radiometric dating it has been possible to date some of the early landslides that have been discovered. One early slide that has been dated to 4,550 B.P. was caused by a series of earthquakes. Another, discovered in 1960 in the Beacon Hill area in the Green's Creek Valley, was dated to 1,140 B.P. It was the largest ancient landslide in the Green's Creek Valley, involving 1.5 million m^3 of material (Al-Umar, 2018; Hugenholtz and Lacelle, 2004). In more recent times, several landslides have been recorded and some have been studied. A major rainfall-induced landslide occurred in Orleans in 1965. The area is particularly prone to landslides, and several had occurred earlier in the terrace bluffs above Orleans but their traces were obscured by urban sprawl and spreading housing development, their existence being attested to only by pre-development aerial photographs (Al-Umar, 2018). As noted above, riverbanks are prime locations for the occurrence of landslides. The massive Lemieux landslide of 1993 on the banks of the South Nation River was mentioned and discussed at some length earlier. A similarly large slide involving nearly 70 acres took place along the South Nation River, 6.4 km north of Casselman, on the night of May 16, 1971 during a heavy thunderstorm. The soil was already oversaturated with snowmelt from a record snowfall of 432 cm during the winter of 1970-71. Debris from the slide was carried both upstream and downstream (Eden et al., 1971). Hugenholtz and Lacelle (2004) created an inventory of 52 landslides that occurred in the Green's Creek Valley between 1928 and 2001, by scanning archival aerial photographs of the area provided by the City of Ottawa and the National Air Photo Library, and then digitizing the landslide scars and channel geometry in a GIS. Scars from prehistoric and historical landslides are found all over the current study area, but many have been covered over or obscured by human activity.

4.3.4.5 Marshlands

Marshland areas are found in low-lying depressional basins that are periodically or permanently flooded on account of extremely poor natural drainage and the discharge of precipitation and groundwater into the marsh from the surrounding areas. They contain standing water or organic soils with wetland vegetation. The organic soils vary considerably in composition, depth, and stage of decomposition. Marshland organic materials include leaf and needle fragments, grasses, woody

fragments, sedges, reeds, and stumps. In the study area, the organic matter ranges in depth from 15 cm to 200 cm. Marshland conditions give rise to the formation of peat, which is found in some abundance in the study area (Al-Umar, 2018; Marshall et al., 1979; Schut and Wilson, 1987).

4.4 The Geotechnical Properties of Sensitive Clays in the Study Area

This study builds on the findings of an earlier study by Al-Umar (2018), which undertook a GIS-based assessment of the rainfall-induced landslide susceptibility of sensitive marine clays in the Ottawa region. The data for the geotechnical properties of the soil in the study area that are used in the current study were obtained from Al-Umar (2018), who complied them from six geotechnical investigation reports prepared for various engineering and development projects in the City of Ottawa by local engineering firms between 2008 and 2014. One additional engineering report from 2017 was also later added to the study. The locations of the seven sites investigated for these reports are shown in Figure 4-9. The addresses of the seven sites with the respective years of the investigations and the names of the engineering firms are provided in Table 4-1.

Table 4.1 Sources of the geotechnical data used in the current study

No.	Investigation site	Year	Engineering Firm
1.	1455 Youville Drive	2008	Golder Associates Ltd.
2.	280-282 Crichton Street	2010	Trow Associates Inc.*
3.	Johnston Road	2010	Stantec Consulting Ltd.
4.	2710 March Road	2013	Houle Chevrier Engineering*
5.	1358 Coker Street	2013	Kollaard Associates Engineers
6.	2717 Stevenage Drive	2014	Inspec-Sol Inc.
7.	6909 Notre Dame Street	2017	LRL Associates Ltd.

* *These firms currently go by different names. Trow Associates Inc. is now known as EXP Services Inc. and Houle Chevrier Engineering is now GEMTEC Consulting Engineers and Scientists Ltd.*

Figure 4-9 Sites at which the geotechnical data used in the current study were obtained.

The geotechnical investigations were conducted using standard procedures. At each site, boreholes were drilled at multiple locations, standard penetration tests and in-situ vane shear tests were performed, soil sample cores were extracted and examined on site, then logged and identified visually, and groundwater conditions were noted. In some cases, test pits were dug and selected soil samples were taken. The core and test-pit samples were then taken to the investigating firm's laboratory and subjected to various laboratory tests to obtain data on their geotechnical properties, such as hydraulic conductivity, clay fraction, specific gravity, plasticity, moisture content, unit weight, shear strength parameters, and porosity. From the six reports on the investigations, Al-Umar (2018) extracted and collated the data for the geotechnical properties relevant to sensitive marine clays and used them in his study, additional geotechnical data from LRL report (2017) were also added to the dataset.

According to the soil stratigraphy from borehole logs from these studies, there are two layers of sensitive marine clays found on the sites. The shallow layer of silty clay – clay is at about 1.8 to 5.25 m below the surface and the deeper layer of clay – clayey silt is at a depth of about 6.5 to 12 m. The standard penetration tests (SPT) resulted in 5 to 10 blows for the shallow layer and 5 to 20 blows for the deeper layer. Shallow layer Liquid Limit (LL) ranges from 22 to 80 percent and 50 to 70 percent in the deeper layer. The Plasticity Index (PI) ranges between 8 to 48 percent in shallow layer and 28

to 52 percent in deeper layer. Unit weight ranges between 14 to 22 kN/m^3, clay fraction ranges between 56 – 87 percent, and specific gravity is between 2.70 to 2.80 in all sites (Al-Umar, 2018). These values align with values published in the literature (Taha and Fall, 2014; Quinn, 2009).

4.5 Climate

The study area has a humid, cool, continental climate, characterized by short, warm summers and long, severe winters, with weather conditions varying considerably through the year. In 2019, the mean annual temperature was 5.9° C. July is the hottest month with the most hours of sunlight: in July 2019, the hourly mean temperature was 22.8° C, and there were 473.2 hours of sunlight. January is the coldest month: in January 2019, the hourly mean temperature was -11.6° C (Al-Umar, 2018; Marshall et al., 1979; Ottawa Weatherstats, 2019 b, 2019c, 2019d). However, winter may begin as early as three months before the peak month and end three months after. Generally, it starts snowing in November, and the snowfall continues well into April. However, three times in the past 10 years, the first snowfall occurred in October (i.e., in 2010, 2016, and 2018). The typical Ottawa winter has long-lasting snow cover with repeated freeze-thaw cycles, as daytime temperatures rise above freezing but nighttime temperatures return to the sub-zero range, and frequent occurrences of freezing rain and high windchill (Al-Umar, 2018; Ottawa Weatherstats, 2019a).

Precipitation levels remain fairly constant through the year, with a slight peaking in July and August. The annual rainfall over the past 25 years has ranged from a low of 748.3 mm in 2015 to a high of 1,348.8 mm in 2017, with a 25-year average of 942.83 mm as of 2018 (Ottawa Weatherstats, 2019e). This average appears to have risen by more than 100 mm since 1979, when the mean annual rainfall was reported to have been 820 mm (Marshall et al., 1979; Dumanski et al., 1979). The average snowfall over the same period has ranged from a low of 111.1 cm in 2010 to a high of 374.1 cm in 2008, with a 25-year average of 228.86 cm as of 2018 (Ottawa Weatherstats, 2019a). This appears not to have changed significantly since 1979, when the mean annual snowfall was reported to have been 230 cm (Dumanski et al., 1979).

Data recored at the Ottawa CDA weather station between 1960 and 2004 shows that the annual maximun 24-hour rainfall has increased at the rate of of 0.57 millimetre per year over this period (Auld et al., 2009; Al-Umar, 2018). The year-by-year annual maximum 24-hour rainfall from 1960 to 2004 is presented in Figure 4-10.

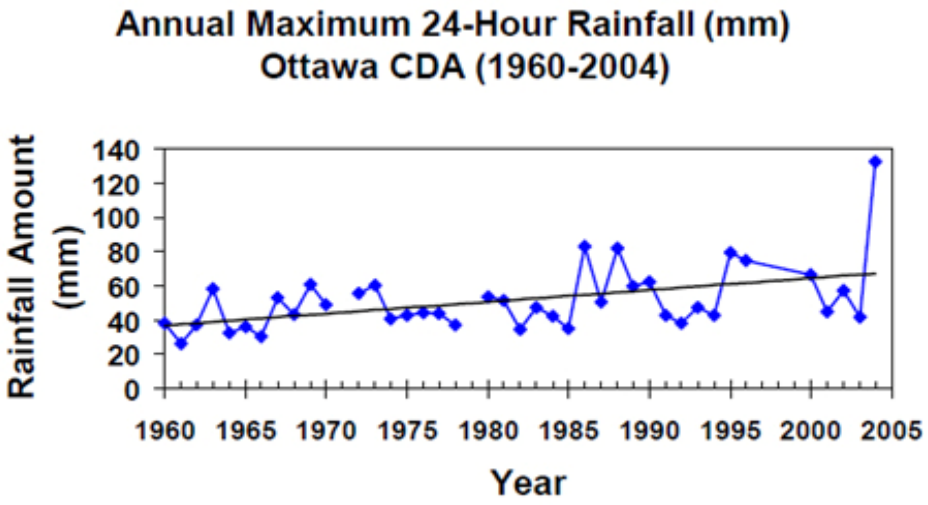

Figure 4-10 Annual maximum 24-hour rainfall (mm) at Ottawa CDA (1960-2004) (Auld et al., 2009; Al-Umar, 2018).

The climate of the City of Ottawa has already begun to feel the effects of climate change. Summers are becoming hotter and winters less severe. Average annual precipitation is increasing, and precipitation is experiencing greater variation with regard to the location and time of occurrence. Extreme heat, wind, rain, and snow events have increased in frequency, and, in general, Ottawa's weather patterns are becoming increasingly variable and unpredictable. For example, in July 2018, a six-day spell of extreme heat and desiccation was followed by four days of record-breaking rainfall that cause flooding in several neighbourhoods across the city. Severe flooding along the Ottawa River occurred in the spring of 2017 following days of persistent rain combined with large volumes of melting snow. In February 2016, a record-breaking 51 cm of snow descended on the city in a single day, despite the general trend towards less severe winters. And also against the trend towards increased precipitation, there have been dry spells, such as the fairly severe drought in the summer of 2016. Extreme wind events have become increasingly destructive. In September 2018, a tornado swept through the city with winds measured at 265 km/h, causing power outages and extensive damage to property and city infrastructure. Similar damage occurred in the fall of 2017 and the spring of 2018, when wind gusts reached 100 km/h. High winds in April 2018 were accompanied by freezing rain (City of Ottawa, 2019).

4.6 Population

Based on population alone, the City of Ottawa, Canada's capital city, is the country's fourth largest city after Toronto, Montreal, and Vancouver, and the second largest city in Ontario. Its population

density, however, is relatively low on average, given that it covers an area of 2,796 km^2, which is larger than the combined areas of Toronto, Montréal, Vancouver, Calgary and Edmonton. Based on data from the 2016 census, Ottawa's population density is 334.8 per km^2. The same census data indicates that in 2016, the City of Ottawa had a population of 934,243, representing a 5.8% increase since 2011, a rate higher than that of Toronto over the same period. In fact, Ottawa's population growth rate is higher than the average growth rate of the entire province of Ontario (4.6%), and of Canada as a whole (5%). Immigration is a major factor influencing Ottawa's high growth rate. For instance, Ottawa receives a higher number of refugees than any other metropolitan area in the country. A 2011 survey indicated that one in five residents of the Capital Region is a first-generation immigrant. Ottawa's population growth is expected to continue, and the city's population is projected to approach 1.2 million by 2031, as shown in Figure 4-11 (City of Ottawa, 2006a; National Capital Commission, 2017).

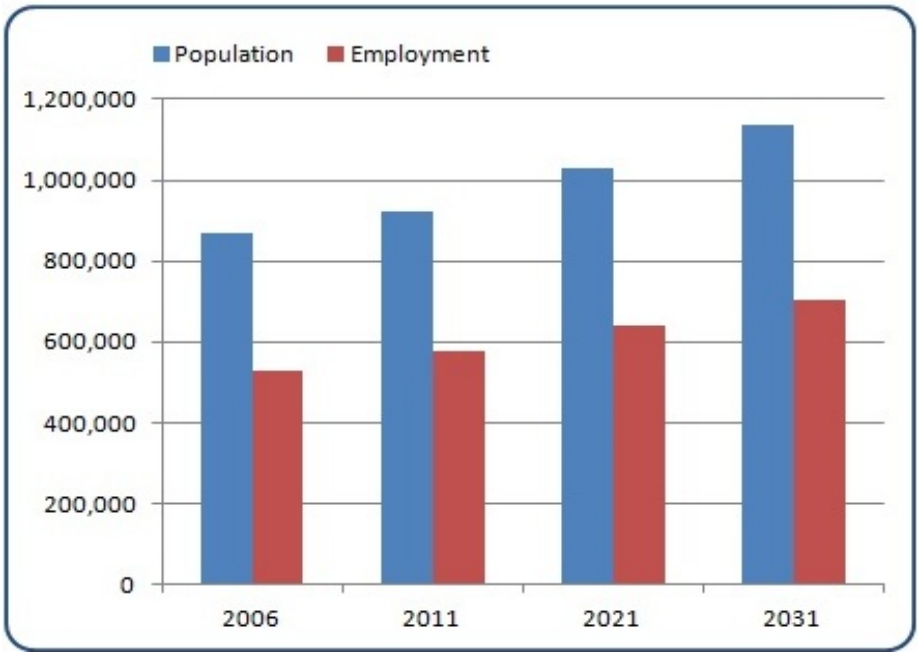

Figure 4-11 Projected population and employment growth for the City of Ottawa, 2006-2031 (City of Ottawa, 2006).

The projections are based on current trends and changes in demographic patterns observed over the past five or so decades. Since the 1960s, the city's population has been aging steadily, with the number of children declining and the number of senior citizens increasing as the baby boom generation ages into seniorhood. This trend is expected to continue over the next decade or so, but will be moderated by factors such as migration and birthrate. Three sets of projections for age

distribution are proposed: (1) A low scenario, in which migration and birthrate are estimated conservatively, producing a population heavily weighted towards the elderly; (2) A medium scenario, in which migration and birthrate increase moderately; and (3) A high scenario, in which migration and birthrate are expected to be high, and the population is less heavily weighted towards the elderly (City of Ottawa, 2015a). The three scenarios are presented in Figure 4-12.

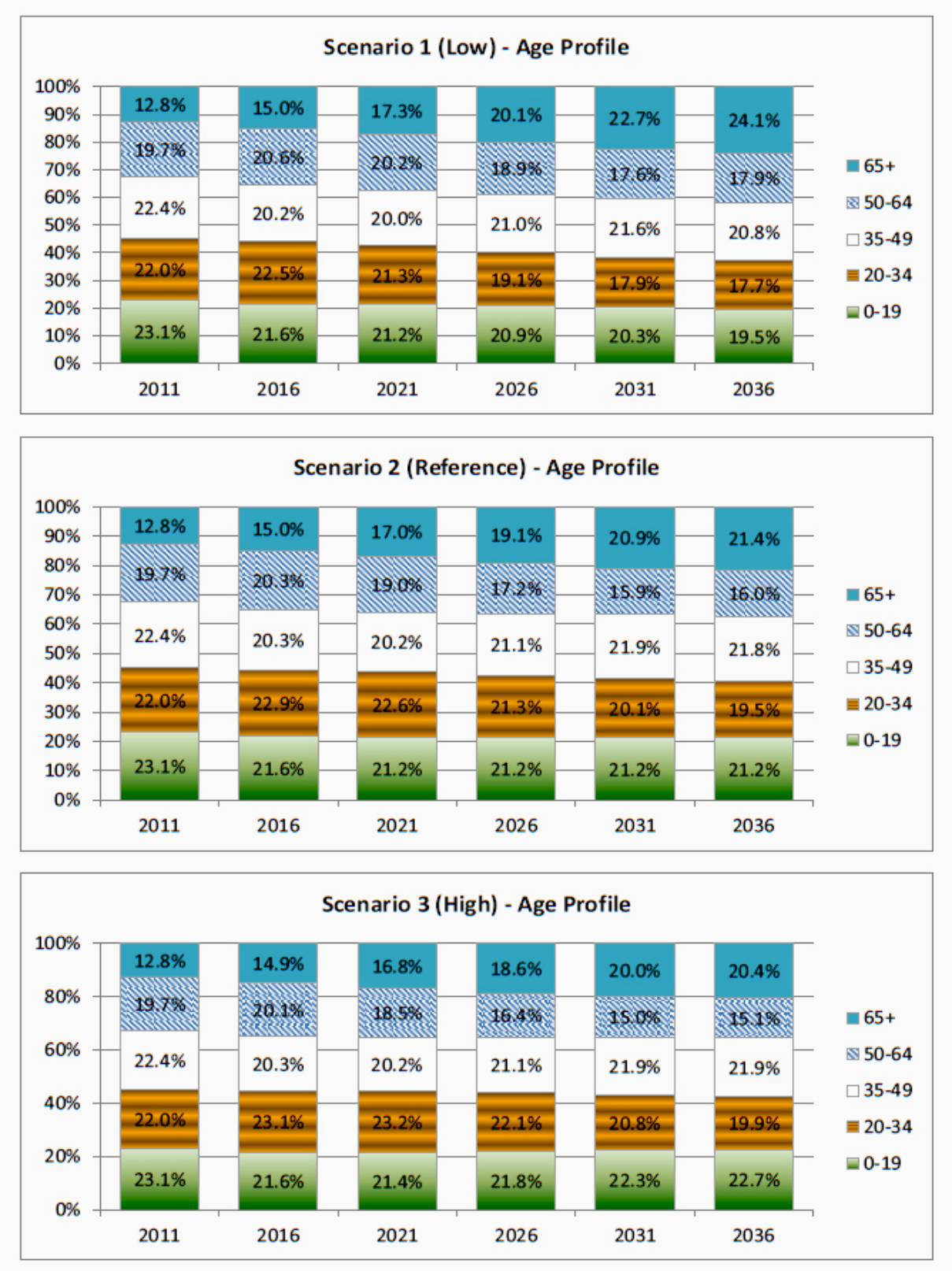

Figure 4-12 Three projected scenarios for changes in age distribution for the population of the City of Ottawa, 2011-2036 (City of Ottawa, 2015a).

4.7 The Future of the Study Area

In 2017, on the occasion of the 150th anniversary of Confederation and the formation of Canada as a country, the National Capital Commission published a Strategic Plan for the next 50 years, looking forward to Canada's bicentennial in 2067. The Plan outlined policies that would guide the development of federal lands, buildings, and public spaces as the country's Capital strives to deal with urban growth and densification, major demographic changes and increasing diversity, climate change, and other current and emerging challenges of the 21st century (National Capital Commission, 2017).

In earlier, more modest municipal-level plans dating back to 2006, which looked forward to the 2030s, the projected growth in Ottawa's population and the projected increase in the proportion of elderly residents had been taken into account by the city's Planning, Infrastructure, and Economic Development Department in planning for long-term development, including housing, land-use, infrastructure, and financial planning. The City's plan involved converting employment land to residential land to accommodate the need for increased housing over the next 20 years, and it was not anticipated that any additional land supply would be needed to meet the projections into the 2030s (City of Ottawa, 2015b). As they plan for the City's future, city planners are taking into account the inevitable population densification that will occur beyond the dense urban core, with special attention being paid to investment in environmentally friendly transportation infrastructure, and in particular to integrated rapid public transit (National Capital Commission, 2017). The projected increase in the elderly population, which is expected to more than double by the 2030s, and especially the increase in the "very elderly" (85 years old and over) population will result in high demands on health and long-term care facilities, as well as on several other services (City of Ottawa, 2011a).

An important component of the long-term Strategic Plan for the nation's capital is the focus on preparedness for the effects of climate change. The National Capital Commission's 50-year Plan states that the strategic objectives with regard to nature, climate, and sustainability are, in part, to:

- adapt to warmer temperatures, increased weather variability and increased impact on existing infrastructure during major weather events;
- address climate changes that affect Canadians' health, safety and economic well-being and require adaptation, such as water level changes, the potential for increased seasonal flooding along shores and the viability of some forms of winter recreation;

- develop strategies to counter susceptibility to invasive species and the loss of the urban forest canopy;
- focus on greening infrastructure, increasing energy efficiency and the proactive reversal of environmental deterioration (National Capital Commission, 2017).

In March 2019, the City of Ottawa published its updated official plan for adapting to climate change and developing resiliency. The plan addressed issues such as the reduction of flood risk, temperature shifts and the mitigation of extreme heat, and the effects on infrastructure, with an emphasis on developing infrastructure resilience, and it presented guidelines for city planning considerations beyond 2036. The report cited the forecast of climate scientists that Ottawa's climate will continue its warming trend, with a significant rise in the incidence of extreme heat events and increasingly variable and unpredictable precipitation, with more frequent occurrences of drought and heavy rain. The report also noted that the elderly are particularly vulnerable to extreme heat and other extreme weather events (City of Ottawa, 2019). As noted above, the elderly population of the City of Ottawa is expected to more than double over the next decade, and this poses an additional challenge for city planners in their effort to prepare for the effects of climate change.

A notable omission in all the projections for the future of the City of Ottawa and the plans for addressing ongoing and emerging challenges is the likely increase in the occurrences of landslides in the wake of climate change.

4.8 Summary

In this chapter, the geographical, physiographical, geological, and geotechnical characteristics of the study area were reviewed, and the area's climate, population, and future prospects were outlined, in order to understand in greater detail the role of these ancillary factors in the landslide phenomenon, and to incorporate them into the landslide susceptibility model. Ottawa's sensitive marine clays do not operate in isolation, but interact with a variety of other geological materials and landforms, including bedrock, sand, silt, boulders, faults, escarpments, and so on. It is within the network of these interrelated and interrelating geological features that landslides occur. Another key element in the occurrence of landslides is precipitation. The Ottawa area experiences heavy rainfall and snowfall, and long winters followed by abundant spring snowmelt, all of which raise groundwater levels and thus contribute to landslide susceptibility. Two major factors are of importance in considering future landslide occurrence in the Ottawa area. One of these is climate change, which threatens to exacerbate the area's already adverse climatic conditions that trigger the frequent landslides that plague the region. In the past, maps and written records of historical

landslides have helped to identify areas prone to slope failure and landsides, and they have thus informed decision making regarding damage mitigation and future development. However, in the wake of climate change, past landslide activity is no longer a reliable guide to future landslide occurrence, and new approaches need to be found. The other factor of importance in considering the future of the Ottawa area is its enormously high rate of population growth and the rapidly changing demographics of the nation's capital. Given that the population is increasing and that the elderly population will more than double over the coming decade, significant changes will occur in land use patterns, and there will be greater demands in the areas of housing, infrastructure, and services. This means that not only will the likelihood of landslide occurrence increase, but more people will be at risk of suffering damage or loss of life and property as a result of the landslides when the do occur.

4.9 Reference

Al-Umar M. (2018), GIS based assessment of climate-induced landslide susceptibility of sensitive marine clays in the Ottawa region, Canada. Unpublished doctoral dissertation. University of Ottawa, Ottawa, Canada.

Auld, H., MacIver, D., Klaassen, J., Cheng, S., Comer, N., Fernandez, S. (2009). *Adaptation by Design: Climate, Municipal Infrastructure & Buildings in the Ottawa Area*. Adaptation and Impacts Research Division, Environment Canada, Ottawa, Ontario.

Brooks, G. R. (2014). Prehistoric sensitive clay landslides and paleoseismicity in the Ottawa Valley, Canada. In: J-S. L'Heureux, A. Locat, S. Leruiel, D. Demers, and J. Locat, (eds.), *Landslides in Sensitive Clays: From Geosciences to Risk Management*, pp. 119-131. Springer, Dordrecht.

Brooks, G. R., Aylsworth, J. M., Evans, S. G., and Lawrence, D. E. (1994). The Lemieux landslide of June; 20, 1993, South Nation Valley southeastern Ontario—a photographic record. Geological Survey o Canada Miscellaneous Repert 56. Natura Resources Canada, Ottawa. Available at: https://doi.org/10.4095/193534.

Chapman, L. J. and Putnam, D. F. (2007). Physiography of Southern Ontario; Ontario Geological Survey, Miscellaneous Release Data 228.

City of Ottawa. (2006). *Long-Range Financial Plan III—Part I and Part II: Economy and Demographics*. Available at: https://ottawa.ca/en/city-hall/budget/financial-reports-and-statements/long-range-financial-plans/long-range-financial-plan-iii-part-1-and-part-2/economy-and-demographics#population.

City of Ottawa, (2011a). *A Portrait of Ottawa Older Adults: Demographic and Socio-Economic Characteristics*. Available at: https://app06.ottawa.ca/calendar/ottawa/citycouncil/cpsc/2011/08-18/07 - Document 3 Demographic and Socio-Economic Characteristics EN.pdf

City of Ottawa. (2011b). *Characterization of Ottawa's Watersheds: An Environmental Foundation Document with Supporting Information Base*. Available at: https://documents.ottawa.ca/sites/documents/files/documents/cap083402.pdf

City of Ottawa. (2016a). *Growth Projections for Ottawa: Prospects for Population, Housing, Employment and Land, 2014-2036*. Available at: https://documents.ottawa.ca/sites/documents/files/growth_projections_2014to36_en.pdf.

City of Ottawa. (2016b). *Growth Projections for Ottawa, 2014-2036 Addendum: Inclusion of Recommended Conversions of Employment Land Supply*. Available at:

https://documents.ottawa.ca/sites/documents/files/growth_projections_add_2014to36_en.pdf.
City of Ottawa, (2019). *New Official Plan: Climate Adaptation and Resiliency*. Available at: https://documents.ottawa.ca/sites/documents/files/op_discuss_paper_climate_en.pdf
City of Ottawa Act. (1999). S.O. 1999, Chapter 14, Schedule E. Government of Ontario. Available at: https://www.ontario.ca/laws/statute/99c14e. Geological Survey of Canada Miscellaneous Report 56. Ottawa, Geological Survey of Canada
Dumanski, J., Marshall, I. B., and Huffman, E. C. (1979). Soil capabiity analysis for regional land use planning—a study of the Ottawa urban fringe. *Canadian Journal of Soil Science*, 59 (4), pp. 363-379.
Eden, W. J., Fletcher, E. B., and Mitchell, R. J. (1971). South Nation River Landslide, 16 May 1971. *Canadian Geotechnical Journal*, 8, pp. 446-451. Available at: https://nrc-publications.canada.ca/eng/view/accepted/?id=aacc9d19-c4ad-4ccc-9c92-97e4616bbd71.
Golder Associates Ltd. (2008). *Report on Geotechnical Investigation: Proposed Commercial Building, 1455 Youville Drive, Ottawa, Ontario*. Available at: http://webcast.ottawa.ca/plan/All_Image Referencing_Site Plan Application_Image Reference_D07-12-12-0132 Geotechnical Investigation.PDF.
Houle Chevrier Engineering Ltd. (2013). *Report on Geotechnical Investigation: Proposed Garden Centre, 2710 March Road, Ottawa, Ontario*. Available at: http://webcast.ottawa.ca/plan/All_Image Referencing_Site Plan Application_Image Reference_D07-12-13-0162 Geotechnical Report.PDF.
Hugenholtz, C. H. and Lacelle, D. (2004). Geomorphic controls on landslide activity in Champlain Sea clays along Green;s Creek, Eastern Ontraio, Canada. Géographie physique et Quaternaire, 58(1), pp. 9-23.
Inspec-Sol Inc. (2014). *Technical Memorandum – Geotechnical Update: Commercial Development, 2717 Stevenage Drive Ottawa, Ontario*. Available at: http://webcast.ottawa.ca/plan/All_Image Referencing_Site Plan Application_Image Reference_D07-12-14-0053 Geotechnical Report.PDF.
Kollaard Associates. (2014). *Report on: Additional Geotechnical Investigation: Proposed Light Industrial Building, 1358 Coker Street, Osgoode Ward, Greely, City of Ottawa, Ontario*. Available at: http://webcast.ottawa.ca/plan/All_Image Referencing_Site Plan Application_Image Reference_D07-12-13-0086 Additional Geotechnical Investigation - Revised.PDF.
LRL Associates Ltd., 2017, *Slope Stability Analysis, 6909 Notre Dame Street*, Ottawa.
Marshall, I. B., Dumanski, J., Huffman, E. C., and Lajoie, P. G. (1979). *Soils, Capability and Land Use in the Ottawa Urban Fringe*. Report No. 47, Ontario Soil Survey. Ottawa: Research Branch, Agriculture Canada and Ontario Ministry of Agriculture and Food. .
McEniry, G. P. (1978). The estimation of the effective shear strength parameters of Leda clay. Master's thesis. University of Ottawa, Ottawa, Ontario.
Mitchell, R. J. and Klugman, M. A. (1979). Mass instabilities in sensitive Canadian soils. *Engineering Geology, 14*, pp. 109-134.
National Capital Commission. (2017). *The Plan for Canada's Capital, 2017-2067*. Available at: http://capital2067.ca/wp-content/uploads/2017/05/PFCC-English-complete-optimized.pdf.
Ottawa Weatherstats. (2019a). Snowfall—Annual data for Ottawa (Kanata-Orléans). Available at: https://ottawa.weatherstats.ca/charts/snow-yearly.html
Ottawa Weatherstats. (2019b). Sunlight—Monthly data for Ottawa (Kanata-Orléans). Available at: https://ottawa.weatherstats.ca/charts/sunlight-monthly.html
Ottawa Weatherstats. (2019c). Temperature—Annual data for Ottawa (Kanata-Orléans). Available at: https://ottawa.weatherstats.ca/charts/temperature-yearly.html.
Ottawa Weatherstats. (2019d). Temperature—Monthly data for Ottawa (Kanata-Orléans). Availale at: https://ottawa.weatherstats.ca/charts/temperature-monthly.html

Ottawa Weatherstats. (2019e). Total Precipitation—Annual data for Ottawa (Kanata-Orléans). Available at: https://ottawa.weatherstats.ca/charts/precipitation-yearly.html.

Quinn, P. E. (2009). Large landslides in sensitive clay in eastern Canada and the associated hazard and risk to linear infrastructure. Doctoral dissertation. Queen's University, Kingston, Ontario, Canada.

Nader, A. (2014). Engineering Characteristics of Sensitive Marine Clays—Examples of Clays in Eastern Canada. Master's thesis. University of Ottawa, Ottawa, Canada. ProQuest Dissertations Publishing, MS26684.

Quinn, P. E., Hutchinson, D. J., Diederichs, M. S., and Rowe, R. K. (2010). Regional-scale landslide susceptibility mapping using the weights of evidence method: An example applied to linear infrastructure. *Canadian Geotechnical Journal,* 47, pp. 905–927.

Schut, L. W. and Wilson, E. A. (1987). The soils of the Regional Municipality of Ottawa-Carleton (excluding the Ottawa Urban Fringe) Vol.1. Ontario Institute of Pedology, Report No. 58, Ottawa: Ministry of Agriculture and Food.

Stantec Consulting Ltd. (2010). *Geotechnical Inventory and Evaluation, Johnston Road Land Use Study*. Available at: https://app06.ottawa.ca/calendar/ottawa/citycouncil/ec/2011/03-29/Geotechnical Inventory and Evaluation Report – April 2010 (2).pdf.

Taha, A. and Fall, M., (2014), Shear behavior of sensitive marine clay–steel interfaces. *Acta Geotechnica*, 9(6), pp. 969-980.

topographic-maps.com. (2019). Ottawa. Available at: https://en-ca.topographic-map.com/maps/q4e/Ottawa/.

Trow Associates Inc. (2010). *Updated Geotechnical Investigation: Proposed Residential Development, 280-282 Crichton Street, Ottawa, Ontario*. Available at: http://webcast.ottawa.ca/plan/All_Image Referencing_Site Plan Application_Image Reference_Geotechnical Study D07-12-10-0219.PDF.

Williams, D. A. (1991). Paleozoic Geology of the Ottawa-St. Lawrence Lowland, Southern Ontario. Ontario Geological Survey, Open File Report 5770. Toronto: Ontario Ministry of Natural Resources.

Wilson, A . E., (1956). A Guide to the Geology of the Ottawa District, *Canadian Field Naturalist*, 70. (1), pp. 1-68.

5 Climate Change Effects on Rainfall in the Ottawa Area

5.1 Climate Change on a Global Scale

Observational data and studies clearly indicate that the Earth's climate is changing on a global scale. The major factor driving global climate change is human activity resulting from exponential population growth, activity such as large-scale land use modification and dramatic increases in greenhouse gas (GHG) emissions being released into the atmosphere. Increasing concentrations of the chief greenhouse gases (GHG)—carbon dioxide, methane, and nitrous oxide—have produced a rapid rise in the respective mean temperatures of the atmosphere, the oceans, and land surfaces, accompanied by the rapid melting of polar ice and a corresponding rise in sea level and ocean acidity (IPCC, 2015). These trends are shown graphically in Figure 5-1. The most recent IPCC Climate Change Report projects an increase in the global mean surface temperature within the range of 0.3°C and 4.8°C (depending on the optimism or pessimism of the GHG emissions scenario used) by the year 2100 relative to 1986-2005 (IPCC, 2015). This projected range for the anticipated rise in mean global temperature is shown in Figure 5-2, along with the projected range for sea-level rise.

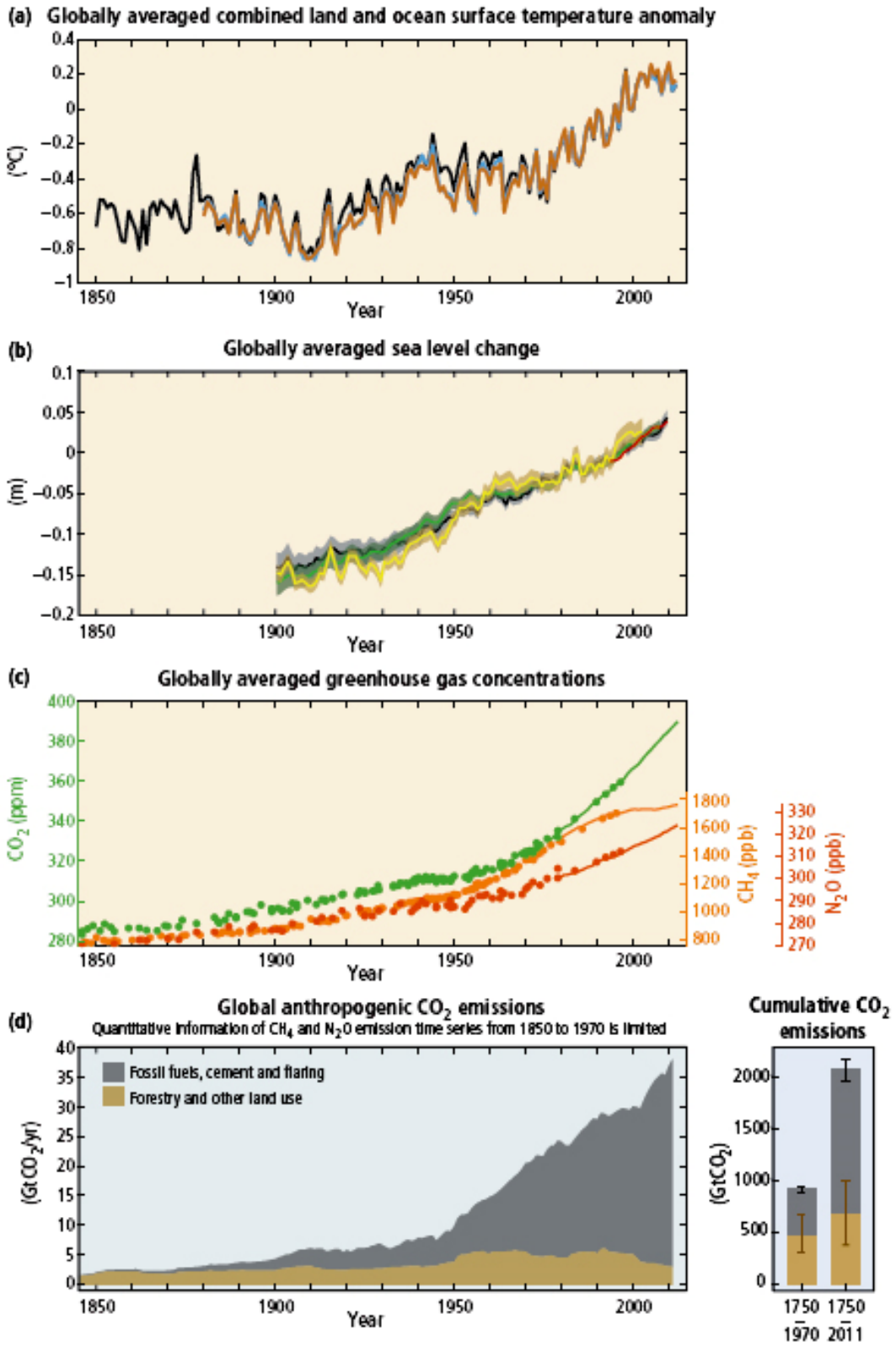

Figure 5-1 Rise in mean global temperature, sea level, and greenhouse gas concentrations between 1850 and 2000 (IPCC, 2015).

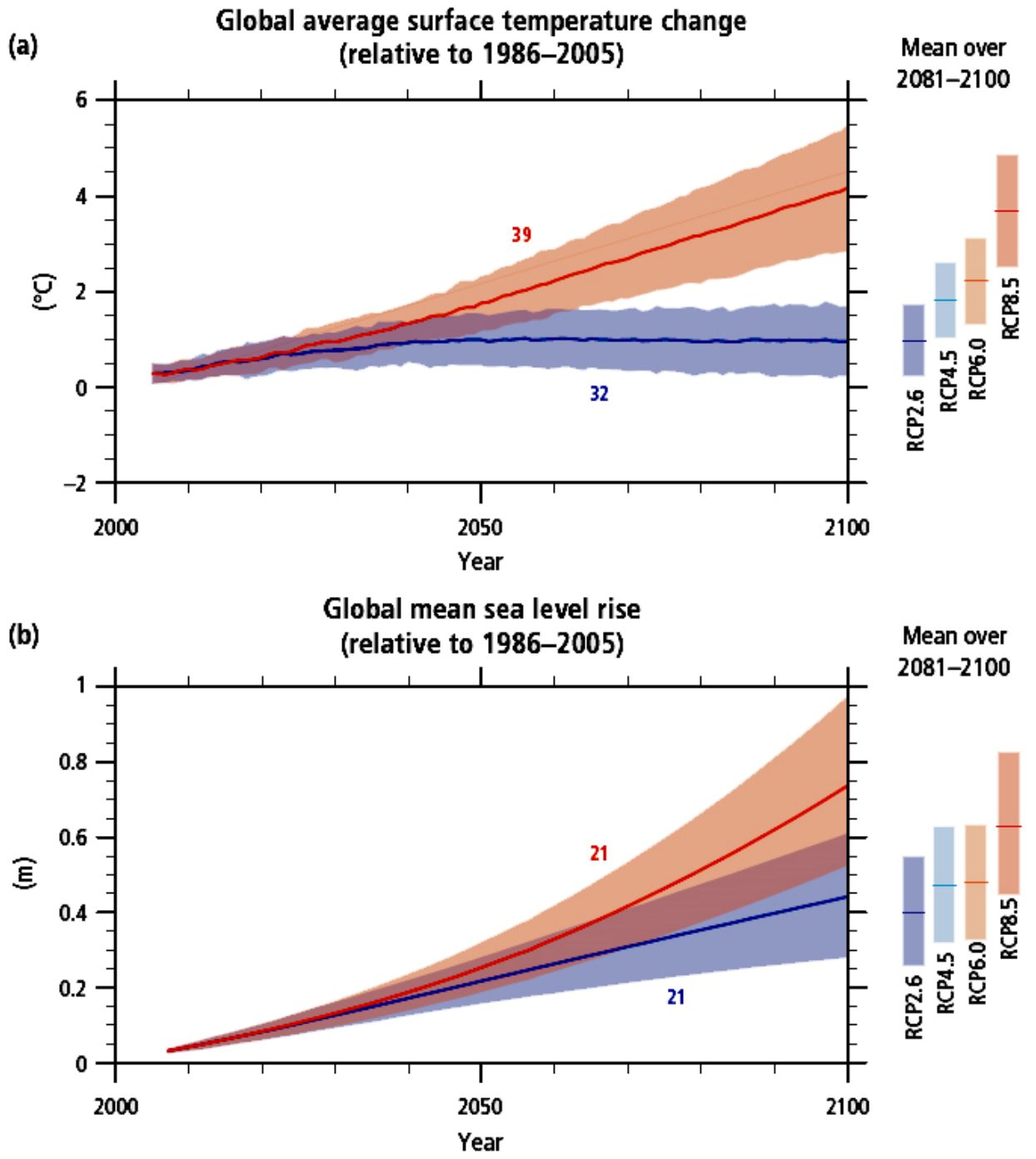

Figure 5-2 Projected rise in mean global surface temperature and sea level to 2100 (IPCC, 2015).

The projected rise in mean global temperature is expected to be accompanied by an increase in average global precipitation. There is a close interrelationship between temperature and precipitation, and changes in one can induce changes in the other. A consistent, sustained rise or drop

in temperature can increase or decrease the likelihood of rainfall during the winter; it can alter the timing and extent of snowpack development, soil freezing, and the freeze-thaw cycle; and above all, it can disrupt current patterns in the timing, duration, quantity, and phase (rain vs. snow) of precipitation events (McNeil, 2019). The projections for precipitation increase to the end of the current century are based on high-confidence trends in historical over-land precipitation since the middle of the last century. Figure 5-3 shows the projected change in average surface temperature and average precipitation for 2081-2100 relative to 1986-2005 under the most optimistic scenario (RCP2.6) and the most pessimistic scenario (RCP8.5).

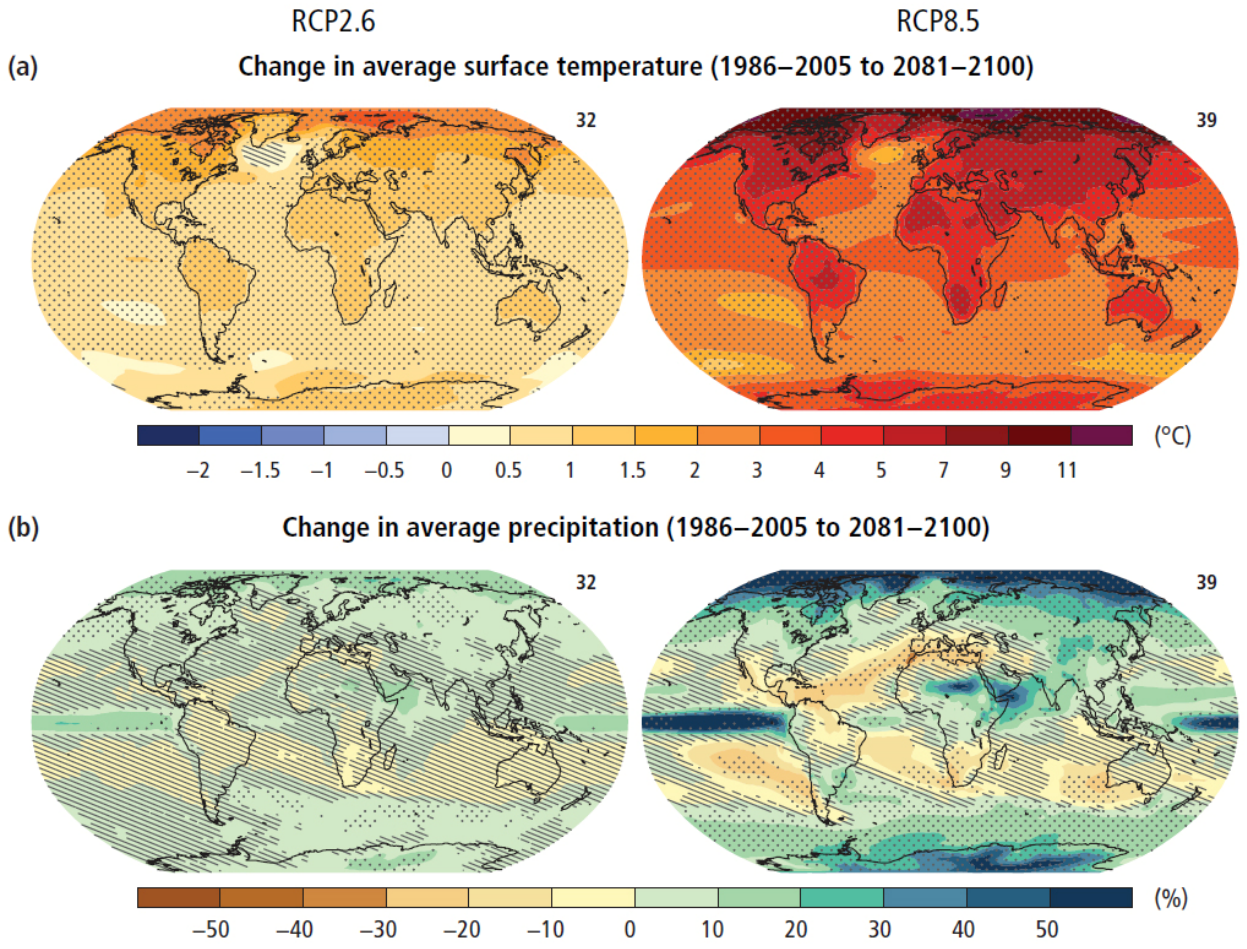

Figure 5-3 Change in average surface temperature (a) and change in average precipitation (b) based on multi-model mean projections for 2081-2100 relative to 1986-2005 under the RCP2.6 (left) and RCP8.5 (right) scenarios.
The number of models used to calculate the multi-model mean is indicated in the upper right corner of each panel. Stippling (i.e., dots) shows regions where the projected change is large compared to natural internal variability and where at least 90% of models agree on the sign of change. Hatching

(i.e., diagonal lines) shows regions where the projected change is less than one standard deviation of the natural internal variability (IPCC, 2015).

Even under the most optimistic scenarios, the rise in surface temperature is expected to have a marked effect on the magnitude and frequency of extreme weather and climate events in several areas (Schardong et al., 2018). Under all the current scenarios, whether optimistic or pessimistic, there is a high likelihood that the frequency and duration of heat waves and drought will increase and the intensity and frequency of extreme precipitation events will rise correspondingly. Global warming, through changing patterns of precipitation and snow-and-ice melting, has affected both the hydrological and the ecological systems of the earth (IPCC, 2015). Landslides, erosion, and flooding (both coastal and inland) are among the major consequences of global-warming-induced extreme precipitation events, and these are expected to increase throughout the 21st century (IPCC, 2015; McNeil, 2019).

5.2 Climate Change in Canada

Canada has not been immune from these adverse effects of climate change, and, in fact, the most recent climate change report issued by the Government of Canada indicates that Canada's climate is warming at twice the rate of the global average, with the highest level of warming occurring in winter, the increase in the mean annual temperature between 1948 and 2016 being estimated at 1.7°C (McNeil, 2019; Zhang et al., 2019). Evidence suggests that across the Great Lakes Basin (which includes the Ottawa region) there has been a steady increase in precipitation, along with more frequent extreme weather events and consequent flooding, which have caused damage to infrastructure and have adversely affected the lives of the region's inhabitants. A recent development in Ontario is the sporadic occurrence of so-called "ninja" storms. These are short-duration, high-intensity rain events over a small area that are not forecast and are not adequately recorded by the existing rainfall gauge network (McNeil, 2019).

With the increase in precipitation and more frequent extreme precipitation events has come a rise in the incidence of flooding and the occurrence of extreme flooding events. The Ottawa area has recently experienced two 100-year flood events within a span of three years. In the spring of 2017, the Ottawa River experienced a peak flow of over 9,000 m^3 per second. The river overflowed its banks, causing widespread flooding and damage across the Ottawa area. The event was dubbed "the flood of the century." However, just two years later, in the spring of 2019 the same thing happened on a more severe scale. The size and scale of the flooding was unprecedented. As a result of seven consecutive months of below-normal temperatures, from October 2018 to April 2019, the

ground froze solid and did not thaw until quite late in the spring, thus preventing infiltration of snowmelt and rain. To compound the problem, there were several bouts of heavy spring rains over a five-week period, from mid-April to mid-May, and two storms from the Gulf of Mexico that brought the equivalent of a month's worth of rain. In Ottawa itself, 150 mm of rain fell between April 10 and May 10. On May 1, the Ottawa River at peak was 30 cm above the peak of the 2017 flood. Homes were evacuated, bridges and roads were closed, and ferry services were suspended. Damage to property and infrastructure was extensive. (Government of Canada, 2020).

In light of this recent history, predictions for the future are necessarily grim. Under a low-emissions scenario (RCP2.6), average surface warming across Canada is projected to be about 2°C higher relative to 1986-2006, and is expected to remain relatively steady after 2050. Under a high-emissions scenario (RCP8.5), the temperature increase is projected to continue steadily, reaching over 6°C by the end of the 21st century (Zhang et al, 2019). Annual precipitation is expected to increase all across Canada through the 21st century. Under a low-emissions scenario (RCP2.6), the increase is projected to be 7% by the end of the 21st century; under a high-emissions scenario (RCP8.5), it is projected to be 24%. This increase is accounted for primarily by increases in winter precipitation. Summer precipitation will be affected in a slightly more complex way. Under a high-emissions scenario, southern Canada (which includes the Ottawa region) is expected to experience a decrease in summer precipitation towards the end of the 21st century; however, under a low-emissions scenario, summer precipitation is projected to change only minimally (McNeil, 2019; Zhang et al., 2019). Along with increased precipitation, there is expected to be an increase in the frequency of extreme weather events. For example, an extreme precipitation event that occurs on average once every 20 years will become a once-in-five-years event by the end of the 21st century. Put another way, the amount of 24-hour precipitation associated with a 20 -year event is expected to increase by about 5% under the low-emissions scenario (RCP2.6) and by about 12% under the high-emissions scenario (RCP8.5) by 2031-2050. By 2081-2100, the increase will be as high as 25% under the pessimistic scenario. The projected increases over the 21st century in 24-hour precipitation for 10-year, 20-year, and 50-year events under the two scenarios are presented in Figure 5-4.

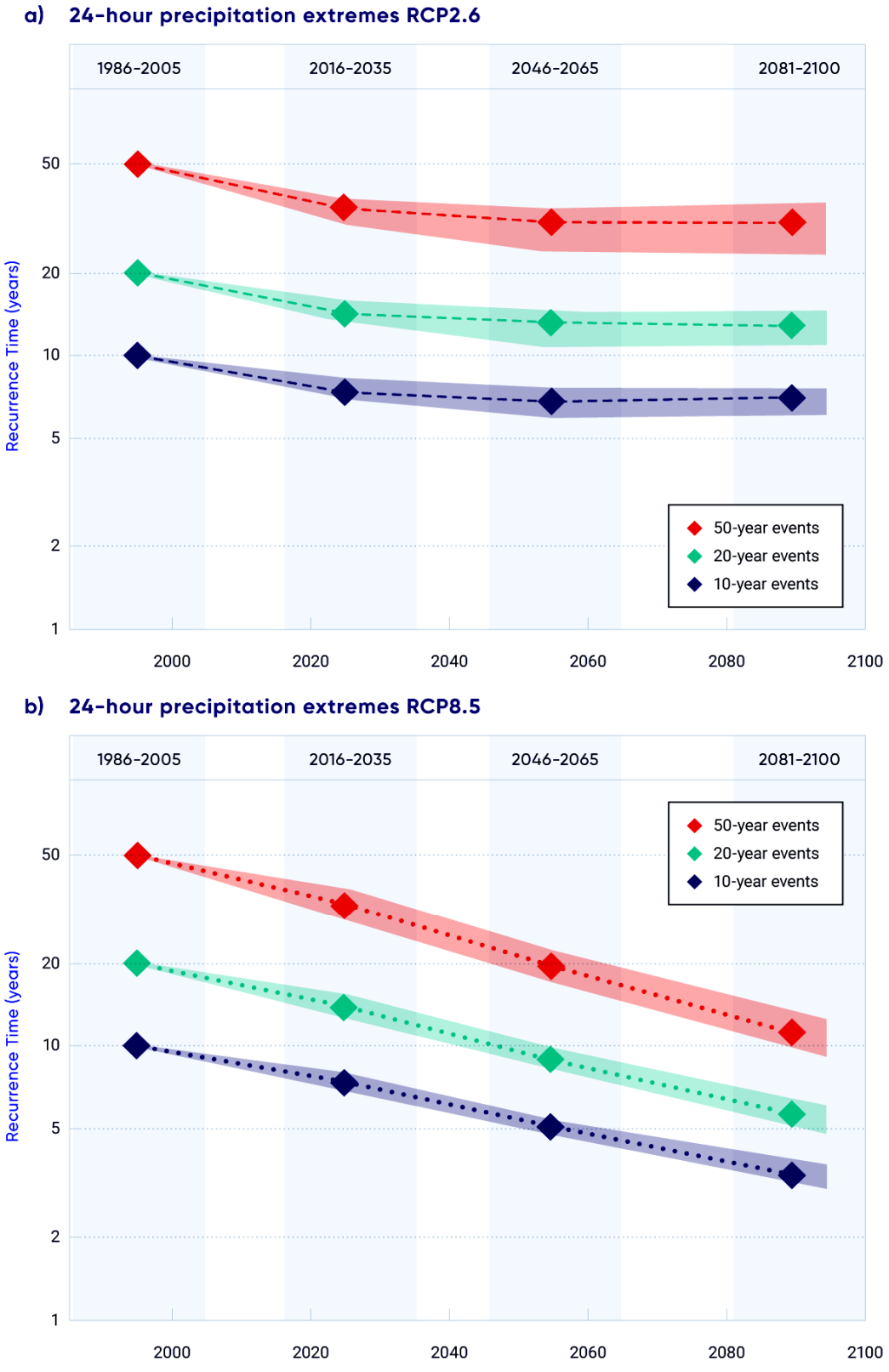

Figure 5-4 Projected changes through the 21st century in recurrence time for three categories of extreme precipitation events under two emissions scenarios (Zhang, et al., 2019).

To prepare for these dire projections, it is necessary to understand how climate mechanisms work globally. The Global Climate Models (GCMs) system was developed to represent the earth's climate as we know it historically and to predict the sort of climate we can expect in the future. The data produced by these models can be used by scientists, engineers, and decision makers in their planning to meet the challenges of climate change the formulation of adaptation responses and the development of resilient and sustainable designs for future infrastructure projects.

5.3 Tools for Studying Climate Change

Climate scientists have developed a wide range of tools and mechanisms for studying climate change and predicting the changes in weather patterns that might be expected, both globally and on a local scale, as a result of this global phenomenon. This section will discuss the tools and methods that were used in the current study to derive data for analysis in determining the effect of climate change on rainfall in the Ottawa region. These tools and methods include general tools for studying climate change and specific tools for examining rainfall patterns.

5.3.1 Global Climate Models and Representative Concentration Pathways

Global Climate Models (GCMs) represent in digital and graphic form the activity that goes on in the earth's atmosphere. The system provides tools that can be used to gain a better understanding of the dynamics of current and future climate. As such, the GCMs system is the ideal platform for assessing the impact of climate change. GCMs provide projections for future climate under a set of four future greenhouse gas (GHG) emissions scenarios, known as Representative Concentration Pathways (RCPs). All the models are based on land-ocean-atmospheric coupling, amount of GHG emissions, and different initial conditions representing the state of the climate system. The major input in generating future climate scenarios is the level of GHG emissions. Other factors that may influence future climate include changing land-use patterns, increased energy production and consumption, intensified global and regional economic activity, and population growth (Schardong et al., 2018). However, only some of these additional factors are taken into consideration in creating the four scenarios.

The four RCP scenarios are: RCP2.6, RCP4.5, RCP6.5 and RCP8.5. RCP2.6 is based on the possible implementation of stringent emissions mitigation measures resulting in low levels of GHG emissions and accumulation in the atmosphere; RCP4.5 and RCP6.5 are based on less stringent measures resulting in moderate emissions and accumulation; RCP8.5 assumes virtually no mitigation and

consequently very high levels of emissions and accumulation (IPCC, 2015). Based on these emissions assumptions, each RCP provides a possible scenario that leads to a specific level of radiative forcing (IPCC, 2015; Schardong et al., 2018).

Radiative forcing is a measure of the strength of the drivers of climate change. The physical drivers of climate change are the natural and human-generated substances and processes that alter the Earth's energy budget. Thus, radiative forcing is the change in energy flux caused by climate change drivers as observed and calculated to be occurring at the tropopause (i.e., at the top of the atmosphere). It is expressed in watts per square meter (W/m^2). Radiative forcing values higher than zero produce near-surface warming, whereas values lower than zero produce cooling (IPCC, 2015). The following definitions of each RCP in terms of radiative forcing are taken directly from the IPCC Climate Change 2014 Synthesis Report (IPCC, 2015);

- **RCP2.6**: One pathway where radiative forcing peaks at approximately 3 W/m^2 before 2100 and then declines (the corresponding Extended Concentration Pathway (ECP) assuming constant emissions after 2100).
- **RCP4.5 and RCP6.0**: Two intermediate stabilization pathways in which radiative forcing is stabilized at approximately 4.5 W/m^2 and 6.0 W/m^2 after 2100 (the corresponding ECPs assuming constant concentrations after 2150).
- **RCP8.5**: One high pathway for which radiative forcing reaches > 8.5 W/m^2 by 2100 and continues to rise for some amount of time (the corresponding ECP assuming constant emissions after 2100 and constant concentrations after 2250).

The projected radiative forcing levels expected by 2100 for the four RCPs are shown in Figure 5-5, along with projected concentrations of GHGs and other forcing agents (i.e., climate change drivers).

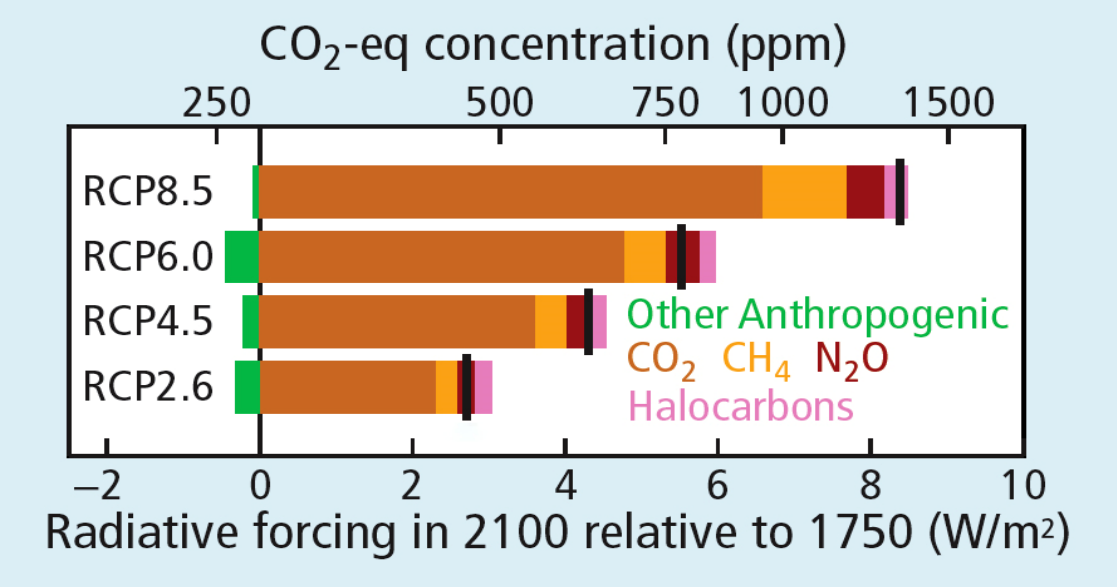

Figure 5-5 Projected radiative forcing levels expected by 2100 relative to 1750 (W/m²) and concentrations (ppm) of major forcing agents (adapted from IPCC, 2015).

The outputs of the GMCs are projection for future climate from 2006 to 2100. However, the projections are not all presented with equal certainty or confidence. High-confidence projections include projections for temperature, precipitation, and average wind speeds. Uncertainty arises from a number of factors. One factor is the lack or insufficiency of observed and recorded meteorological data for past and present weather, especially for rare events. Another is the difficulty of assigning causation in complex or multi-component processes that may involve interacting physical, biological, and human systems. Not all of these processes are well understood, though many are. When multiple climatic and non-climatic forces interact in a complex manner and change over time, uncertainties are bound to persist (IPCC, 2015). Another source of uncertainty is the widely divergent results that may be produced by several models looking at the same phenomenon or process, divergences arising from differences in the dataset inputted into the model and the algorithms used to analyse that data. Downscaling of data is yet another source of uncertainty, given that the resolution of the data in a given dataset may not be fine-grained enough to provide an accurate picture of local of regional conditions. Thus, there is generally higher confidence for larger-scale or longer-term effects than for smaller-scale or shorter-term effects. For example, projections for rainfall intensity over a 12-hour period are more reliable than projections for rainfall intensity over a 1-hour period or less.

5.3.2 Rainfall Intensity-Duration-Frequency (IDF) Curves

Rainfall intensity-duration-frequency (IDF) curves are important tools, traditionally used in the design and management of water-related infrastructure such as storm sewers, catch basin, etc. , but they can also be used in addressing issues that arise from the increased precipitation and extreme precipitation events that are expected to occur as a result of climate change (Schardong et al., 2018). For example, IDF curves are a key source of data used in assessing factor of safety in the analysis of slope stability with regard to rainfall-induced landslides using TRIGRS (discussed in detail in Chapter 2, Section 2.4).

The projected IDF curves used in this study were obtained using the Computerized Tool for the Development of Intensity-Duration-Frequency Curves Under a Changing Climate (the IDF_CC tool) developed by the Department of Civil and Environmental Engineering and Institute for Catastrophic Loss Reduction at the University of Western Ontario in London, Ontario. The data was downloaded from the IDF_CC website.[1]

GCMs provide climate change projections on large scales, both spatially and temporally. The coarse-grained three-dimensional grids used by GCMs typically have a resolution of between 250 and 600 km (IPCC, n.d.). This resolution is not fine enough to represent local-scale weather conditions and atmospheric dynamics accurately at the local level, nor is it suitable for use in IDF-curve analysis in the projection of future weather patterns for such small-scale areas. The ideal scale in the application of IDF curves is one that operates on the level of watersheds, such as the Ottawa River watershed, with a resolution of about 300 arc-second (approximately 10 km). In order to incorporate GCM data into IDF-curve analysis, the data has be downscaled, both spatially and temporally, using one of several methods (Schardong et al., 2018).

The IDF_CC tool is a web-based user interface that provides IDF data for gauged and ungauged locations throughout Canada. The tool contains an embedded database of precipitation data with mathematical models that are used for updating historically based IDF curves to reflect the impact of climate change on future climate patterns under various future climate change scenarios. The tool incorporates 33 GCMs from various climate research centres, chosen because they contain complete sets of future GHG emissions scenarios. Of these 33 GCMs, 9 were downscaled using the Bias Correction/Constructed Analogues (BCCA) with Quantile mapping reordering (BCCAQ) method. The BACCAQ method combines outputs from BCCA and QMAP (Quantile Mapping). The BCCA method retrieves spatial information from a linear combination of historical analogues for daily large-scale

[1] https://www.idf-cc-uwo.ca/home.

fields, thus avoiding the use of monthly aggregates. QMAP applies quantile mapping to the daily climate model outputs that have been interpolated into the high-resolution grid using the climate imprint method developed by Hunter and Meentemeyer (2005) (Schardong et al., 2018). The outputs of the GCM models are downloaded in netCDF format, which is widely used to store large scientific datasets such as climate data. The IDF_CC tool then converts the netCDF files into a more efficient space-saving, time-saving format and stores the files in the tool's database (Schardong et al., 2018).

In creating Intensity Duration Frequency (IDF) curves, the IDF_CC tool typically fits a theoretical probability distribution to an annual maximum precipitation (AMP) time series using extreme value distributions such as Gumbel, Generalized Extreme Value (GEV), Log Pearson, and Log Normal. The GEV distribution is used for both historical and future AMP data, whereas the Gumbel distribution is used only for historical data. For the GEV distribution, parameter estimation is accomplished through the use of the L-Moments method; for the Gumbel distribution, the method of choice is the conventional method of moments. The resulting IDF curves provide precipitation accumulation depths for various return periods and for a range of durations, generally 5, 10, 15, 20, and 30 minutes, and 1, 2, 6, 12, and 24 hours. Longer durations can also be included when necessary (Schardong et al., 2018).

5.4 Projected Changes in Rainfall Patterns in the Ottawa Area to 2100

As noted above, the IDF_CC tool version 3 provides IDF curves for both gauged locations and ungauged locations. However, since the data for the ungauged locations does not provide separate datasets for RCP4.5 and RCP8.5, it is not applicable to the current study, which focuses specifically on these two future climate scenarios. As such, the data from the ungauged locations can be disregarded for current purposes. The data from the gauged locations is presented in tabular form as well as in IDF curves for historical rainfall and the two future scenarios, RCP4.5 and RCP8.5.

Historical IDF data collected at the Ottawa CDA RCS gauged weather station are presented in Table 5-1, along with two sets of IDF projections for the period 2006-2100 based on RCP4.5 and RCP8.5. IDF curves for the two projections are presented in Figures 5-6 and 5-7. As can be seen in the two figures, the IDF curves indicate that the probability of extreme precipitation events is slightly higher under RCP8.5 than under RCP4.5. The raw data in Table 5.1 shows a consistent trend towards increases in rainfall intensity for all five durations and all six return periods under both scenarios. For example, it can be observed from the data in the table that the rainfall intensity for the 24-hour, from 100-yaer-return event under RCP4.5 (5.9 mm/h) is projected to be 20% higher than the historical intensity for the same type of event (4.93 mm/h), and under RCP8.5, the projected intensity

(7.05 mm/h) is projected to be 43% higher than the historical value. It is worth noting that under RCP8.5 there is significantly greater probability than under RCP4.5 that high-intensity short-duration precipitation events will occur for the longer return periods (i.e., 50 and 100 years).

Projections for both RCP scenarios show that extreme precipitation events will occur more frequently from the present until the end of the current century. For example, under RCP4.5, the projected intensity for a 5-minute, 5-year-return event (162.92 mm/h)) is within the same range as the intensity of a historical 5-minute, 25-year-return event (165.98 mm/h) (see Table 5-1). Under RCP8.5, the projected intensity for the 5-minute, 5-year-return event (170.62 mm/h) is in the range of the intensity of a historical 5-minute, 50-year event (177.68 mm/h) (see Table 5-1). In other words, under RCP4.5, the kind of storm that occurred once every 25 years historically can be expected to occur once every 5 years between the present and 2100. Similarly, under RCP8.5, the kind of storm that occurred once every 50 years historically can be expected to occur every 5 years over the coming century. A more dramatic example is the historical 30-minute, 100-year-return event (intensity: 81.08 mm/h), which is projected to recur every 25 years between the present and 2100 under RCP4.5 (projected intensity: 81.28 mm/h) (see Table 5-1). As noted above, in Section 5.2, the Ottawa area experienced two 100-year floods within a span of 3 years, between 2017 and 2019, an occurrence which lends credibility to the projections.

Another way to look at the effect that climate change will have on rainfall in the Ottawa area is to single out one specific return period, say 25 years, and compare the historical IDF curves for that period only with the corresponding curves for the RCP scenarios. Figure 6-8 shows the historical IDF curve for 25-year-return events at the Ottawa CDA station for the period 1905-2007 along with the projected IDF curves for 25-year-return events under RCP2.6, RCP4.5, and RCP8.5 for the period 2006-2100. As the graph shows, all the projected intensities across all durations and all RCP scenarios are consistently higher than the corresponding historical intensities.

Table 5.1 Rainfall intensity (in mm/h) at the Ottawa CDA station, comparing historical rainfall for five return periods and six durations with projections for RCP4.5 and RCP8.5 for 2006-2100.

Table 5-1 Rainfall intensity (in mm/h) at the Ottawa CDA station, comparing historical rainfall for five return periods and six durations with projections for RCP4.5 and RCP8.5 for 2006-2100.

Duration	Return period (T) in years											
	2			5			25			50			100		
	Historical	RCP4.5	RCP8.5	Historical	RCP4.5	RCP8.5	Historical	RCP4.5	RCP8.5	Historical	RCP4.5	RCP8.5	Historical	RCP4.5	RCP8.5
5 min	106.56	123.24	127.43	132.96	162.92	170.62	165.98	202.00	224.61	177.68	209.77	246.71	188.29	223.08	268.09
30 min	38.99	45.17	46.70	49.91	61.25	64.13	66.74	81.28	90.26	73.89	86.51	102.68	81.08	97.06	115.81
1 h	23.59	27.39	28.27	30.25	37.18	38.95	42.89	52.53	57.91	49.25	58.51	68.42	56.34	67.36	80.57
6 h	6.09	7.07	7.31	8.23	10.09	10.57	12.29	15.05	16.60	14.34	17.14	19.92	16.63	19.98	23.77
12 h	3.52	4.09	4.22	4.69	5.76	6.03	7.13	8.74	9.67	8.44	10.20	11.71	9.86	11.81	14.10
24 h	1.95	2.26	2.33	2.53	3.11	3.26	3.68	4.50	4.97	4.26	5.10	5.92	4.93	5.90	7.05

NOTE: The increasing frequency of extreme precipitation events is indicated through colour-coded highlights for selected types of events under various scenarios: yellow shows a historical 5-minute, 25-year-return event projected to occur every 5 years under RCP4.5; green shows a historical 5-minute, 50-year-return event projected to occur every 5 years under RCP8.5; blue shows a historical 30-minute, 100-year-return event projected to occur once every 25 years.

Source of data: IDF_CC tool version 3 at: https://www.idf-cc-uwo.ca/home.

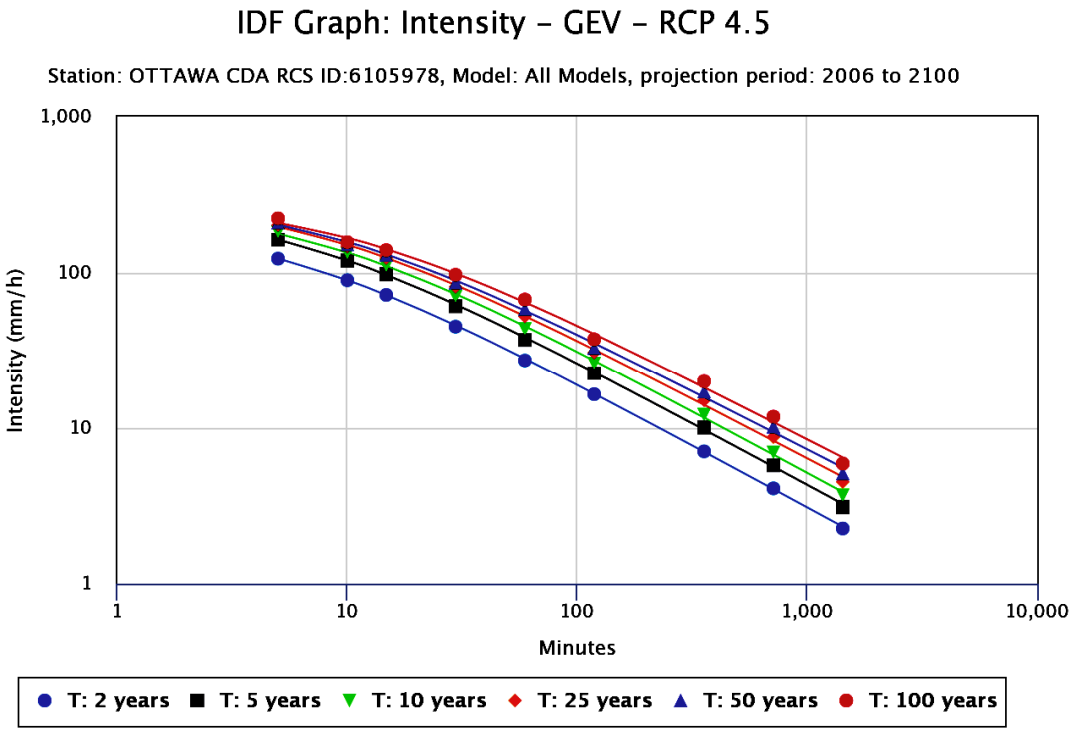

Figure 5-6 IDF Curves for six return periods at the Ottawa CDA station, projected under RCP4.5 for the years 2006-2100 (Schardong et al., 2018)

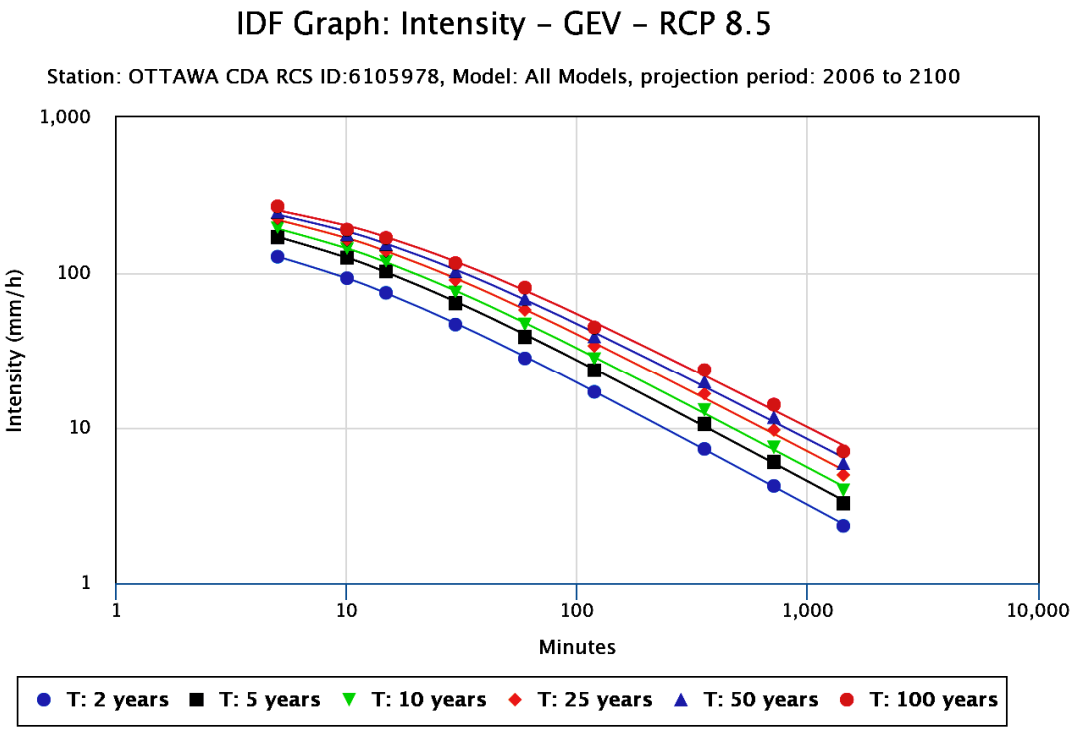

Figure 5-7 IDF Curves for six return periods for the Ottawa CDA station, projected under RCP8.5 for the years 2006-2100 (Schardong et al., 2018).

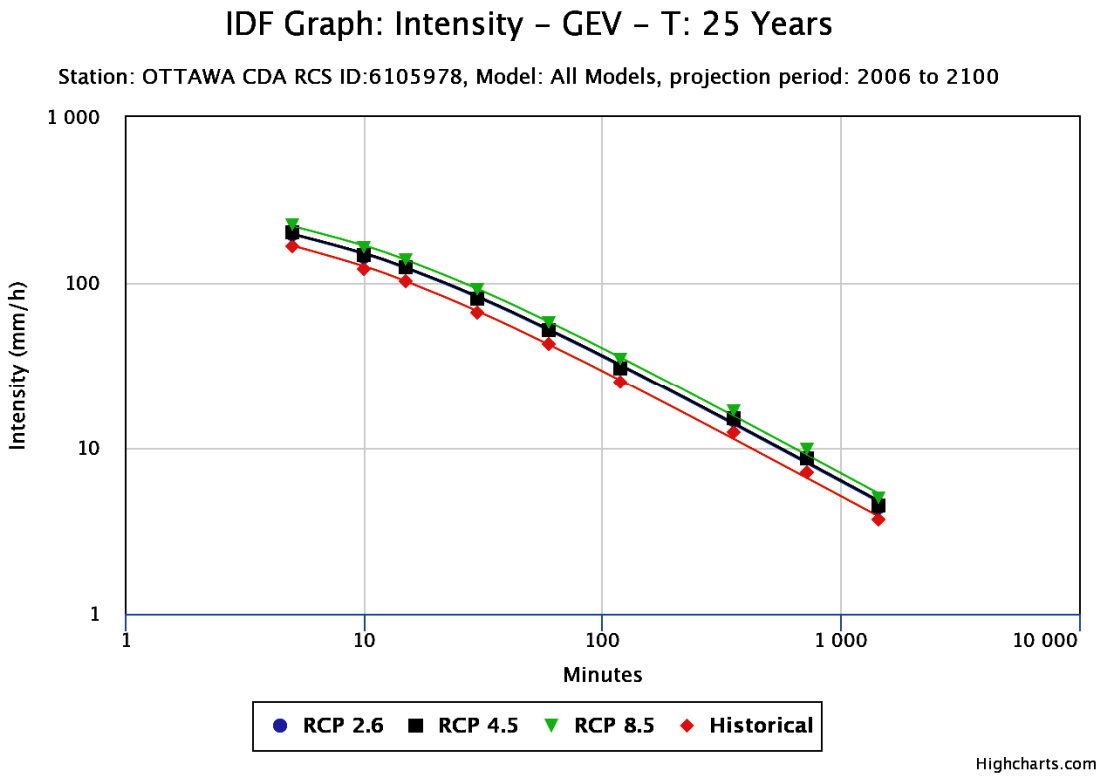

Figure 5-8 IDF curves for the 25-year return period for historical rainfall for 1905-2007 and projected rainfall for 2006-2100 under three RCP scenarios (Schardong et al., 2018).

5.5 Climate Change, Rainfall, and Landslide Occurrence

Climate-change-induced alterations in rainfall patterns in the Ottawa area over the coming century are relevant to the current study because rainfall appears to be causally linked to the frequent occurrence of landslides in this area (and to the triggering of landslides generally around the world). However, the precise relationship between rainfall and landslide occurrence is not fully understood and is still under investigation.

Rainfall-induced slope failure is thought to be induced by one of two processes; (1) infiltration of the soil by rainwater creates a wetting front (the boundary between infiltrated and non-infiltrated soil), which advances downwards through the soil producing loss of matric suction behind the wetting front and thus reducing the soil's factor of safety until it drops below the critical level; (2) infiltrated rainwater produces a rise in the water table (i.e., groundwater level), which not only adds weight to the slope, but also raises the soil's porewater pressure, thus reducing its shear strength to the point at which slope failure is inevitable (Li et al, 2013; Zhang et al., 2011).

Of special interest in recent investigations is the role played by rainfall intensity and duration and the infiltration capacity of the soil in the initiation of slope failure. Infiltration capacity is determined by the degree of saturation of the soil, and when the soil reaches full saturation, infiltration is controlled by the soil's saturated permeability (Li et al, 2013). Saturated permeability (or, saturated hydraulic conductivity) is an important consideration in analyzing landslide susceptibility in the Ottawa area, given that landslides in this area often occur in the spring, following heavy spring rains, when the soil is already saturated from several months of snow cover and weeks of copious snowmelt.

The mechanics of slope failure by loss of matric suction during infiltration is governed by the soil's saturated hydraulic conductivity. If rainfall intensity is lower than the soil's permeability, matric suction decreases as the wetting front advances. The higher the ratio of rainfall intensity to the soil's saturated hydraulic conductivity, the lower the matric suction behind the advancing wetting front. If the rainfall intensity is higher than the soil's saturated hydraulic conductivity, the matric suction will be completely dissipated under the advance of the wetting front. The depth at which slope failure occurs is determined by the degree of matric suction behind the wetting front, which (as just pointed out) is itself controlled by the intensity of the rainfall. High-intensity rainfall produces low matric suction behind the wetting front, which results in a shallow failure plane (or curved slip surface, in the case of rotational slides, which are not uncommon in the Ottawa area [see: Eden and Mitchell, 1970; Brooks, 2019]), and the shallowest failure plane (or slip surface) is achieved when the matric suction is completely dissipated. Conversely, low-intensity rainfall is likely to generate a deep failure plane (or slip surface). In fact, both rainfall intensity and saturated hydraulic conductivity influence the depth of the failure plane (or slip surface). The higher the ratio of rainfall intensity to saturated hydraulic conductivity, the shallower the failure plane (or slip surface). However, regardless of rainfall and hydraulic conductivity considerations, a slope will never fail from loss of matric suction during the advance of the wetting front if the soil's internal angle of friction is greater than the angle of the slope. That is to say, a lower angle of internal friction is a prerequisite for slope failure by loss of matric suction, with the additional provision that the depth of the soil above the impermeable layer must be sufficient for the development of a failure plane (or slip surface) (Li et al., 2013, Qiu et al., 2008; Zhang et al, 2011). Figure 5-9 presents four distinct scenarios for the formation of a curved slip surface, each scenario producing a different depth for the rotational landslides that are associated with various rainfall intensities.

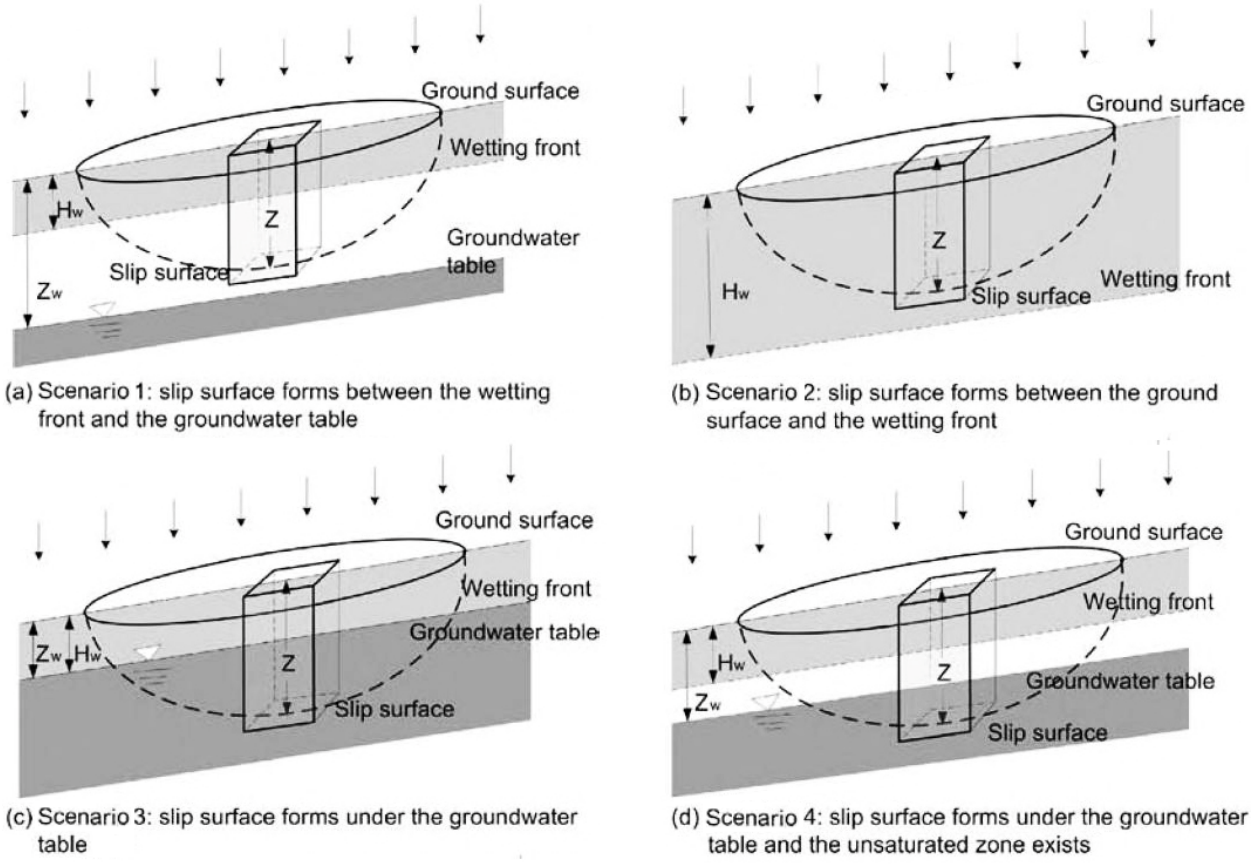

Figure 5-9 Four scenarios producing different depths of the failure plane (or slip surface) associated with different rainfall intensities (modified from Qiu et al., 2008). Z = depth of the failure; H_w = depth of the wetting front; Z_w = depth of the groundwater table.

As noted above, slope instability and slope failure may also be induced by a rise in the water table, if failure is not triggered by the advance of the wetting front. As the water table rises, the positive hydrostatic porewater pressure increases, and as the positive porewater pressure rises at the surface of the impermeable layer, the factor of safety drops and approaches the critical value of 1. The higher the rainfall intensity, the more rapid is the rise of the water table. 2. Low-intensity rainfall over a prolonged period produces a slow rise in positive porewater pressure and therefore a gradual reduction in the factor of safety. High-intensity rainfall causes the positive porewater pressure at the impermeable layer to rise rapidly and this produces a sudden drop in shear resistance, causing the factor of safety to plummet and triggering sudden slope failure. If rainfall intensity exceeds the soil's saturated hydraulic conductivity, the rise of the water table is almost instantaneous, and slope failure occurs almost immediately. Water table rise (rather than loss of matric suction) is the most likely means of slope failure when the soil's internal angle of friction is greater than the angle of the slope (Li, et al., 2013, Qiu et al., 2008).

In addition to rainfall intensity, rainfall duration is also a factor in the occurrence of landslides. Typically, low-intensity rainfall is of long duration. If the duration is sufficiently long to cause an appreciable rise in the water table and in positive porewater pressure, failure will occur at a plane near the surface of the impermeable layer. High-intensity rainfall is generally of short duration. Depending on the intensity of the rainfall and the depth of the water table, short duration rainfall may not be sufficient to cause an appreciable rise in the water table. Thus, high intensity, short-duration rainfall is more likely to cause a shallow failure induced by the advance of the wetting front (Li et al., 2013).

From the foregoing discussion, it is clear that rainfall-induced landslides are a complex phenomenon involving several interrelated and interrelating factors, and as such no single simple model can be created to express the relationship between the various components of the phenomenon. In very general terms, it might be said that high-intensity, short-duration rainfall is associated with shallow landslides and that moderate-intensity, long-duration rainfall is more likely to produce deep landslides. Furthermore, deep landslides are more likely to occur when the soil's saturated hydraulic conductivity is low and shallow landslides are more typical in soils having high saturated hydraulic conductivity (Li et al., 2013).

Al-Umar (2018) developed a model for determining landslide susceptibility, which he used to conclude that landslides in the Ottawa area are most likely to be triggered by rainfall events of low intensity (4.5 mm/h) and long duration (24 hrs) rather than by events of high intensity of short duration. The model makes the explicit assumption that the upper layers of Ottawa's marine clays are initially unsaturated and it uses this assumption as one of its initial conditions. The model further assumes that the instrumental factor in the initiation of slope failure is loss of matric suction, and it does not take into consideration elevation of the water table and rise in positive porewater pressure as a possible trigger. It is important to note that several of the historical rainfall-induced landslides that occurred in the area were associated with high-intensity rainfall and high soil saturation, and many of them involved an excessively elevated water table. Some of these historical landslides are described below.

At about 10:00 p.m. on 20 April, 1963, in a ravine near Breckenridge Station, Quebec, just north of the Ottawa River, off the extreme northeastern tip of the City of Ottawa, during a heavy rainstorm accompanied by high winds, a slide involving about 30,000 cu yd (about 23,000 cu m) of clay began and continued intermittently for the next three days. The slide occurred in a natural clay bank, about 90 ft (27.4 m) high, with an average slope of about 17°, an average water content of 79 %, a factor of

safety of the original slope at about 1.12, and a "dished" (i.e., curved) failure surface (Crawford and Eden, 1967; Eden et al. 1963; Eden and Mitchell, 1970; Mitchell, 1969).

On 10 October 1965, a minor landslide occurred in Orleans, in the northeast corner of the City of Ottawa, following three days of heavy rainfall, totalling 1.4 in. (36 mm) over that three-day period. Two weeks later, on 23 October 1965, a second slide occurred on the perimeter of the first slide during a heavy rainstorm, with an overnight accumulation of 1.14 in. (29 mm). Between December 1965 and February 1966, a third slide occurred, but it was more contained than the two previous slides (Eden and Jarrett, 1971).

During the month of April in 1967, the south bank of the Ottawa River in the Rockcliffe area was the scene of several landslides. The largest one, which relocated about 30,000 cu ft (about 23,000 cu m) of sensitive marine clay, occurred on 3 April at the Rockcliffe Air Base. Significant snow melt (about 20 in [508 mm]) occurred during the last week of March 1967, accompanied and followed by heavy rainfall, such that the slope was fully saturated and had a factor of safety of 0.92 when the slide occurred (Mitchell, 1969).

The large 70-acre Casselman landslide of May 16, 1971 (discussed in Chapter 4, Section 4.3.4.5) occurred during a heavy thunderstorm (Eden et al., 1971). Eden et al. (1971), who reported on the slide a couple of weeks after it occurred, noted that the soil was already heavily saturated from the snowmelt of a long, gradual melting season following a record winter snowfall of 432 cm. Likewise, the massive Lemieux landslide of June 20, 1993 (discussed in Chapter 4, Section 4.2.2), located just about 4 km north of the 1971 landslide, occurred in the aftermath of a heavy rainfall and involved the displacement of about 3 million cubic metres of soil (Brooks et al., 1994). Reporting within weeks of the slide, Brooks et al. (1994) noted that an elevated water table appears to have been a prime factor in the occurrence of the slide. They also note that the period of January to June 1993 was the wettest first six months of the year on record since 1947. Prior to the landslide, in the month of June the area had received 73.6 mm of rain, and 15.8 mm of that fell on the day of the slide, prior to the slide. Heavy snowfall occurred during March and early April. Total precipitation between January 1 and June 20, as measured at the Ottawa International Airport, exceeded the 47-year January-to-June average of 406.3 mm by 36%. Record January-to-June precipitation combined with rapid spring melting and heavy spring rainfall produced water tables at or near ground level, and at the time of the slide, there were areas of standing water in the surrounding fields, indicating the excessive height of the water table (Brooks et al., 1994). To these major historical rainfall- induced landslides may be added the series of minor landslides that occurred in and around the small Ottawa River Valley community of Combermere, about 180 km west of Ottawa (CTV Ottawa, 2017), following two heavy

rainfall events across the Ottawa River Basin in the first week of May 2017, during Ottawa's "flood of the century" mentioned earlier, in Section 5.2.

The historical landslides described above are typical of landslides that occur in the Ottawa area in the spring, during or immediately after a heavy spring rainfall under conditions of high soil saturation from copious spring snowmelt and early spring rains. Such landslides clearly do not fit the profile that Al-Umar (2018) used to create his model, and it is therefore important to keep in mind that no one single set of rainfall and soil conditions is typical for the occurrence of rainfall-induced landslides in the Ottawa area. As van Westen et al. (2006) have noted, "different landslide types have different meteorological triggers" (p. 171). With this in mind, the current study has selected projected rainfall intensities under RCP4.5 and RCP8.5 for return periods of 10 and 50 years and durations of 12, 24 and 48 hours, to be used in the TRIGRS model. The selected durations are believed to be sufficient to generate reliable values for the factor of safety throughout the Ottawa area in the worst-case scenario. The selected return intervals ensure that a wide range of rainfall intensities are represented in terms of their probability of occurring, from high probability (10-year return, or 10% probability) to fairly low probability (50-year return, or 2% probability).

5.6 Summary

The steady increase in greenhouse gas emissions over the past century and a half has resulted in an accumulation of these gases in the atmosphere to the level at which serious changes are occurring in climate patterns on a global scale. The global mean temperature has been rising steadily, as has mean sea level, and extreme weather events have been increasing in frequency. Rise in global mean temperature is positively correlated with an increase in average global precipitation. Canada has felt the effects of climate change in a more accelerated manner than any other country, since its climate is warming at twice the mean global rate. The Ottawa area is particularly prone to the effects of climate change, having experienced two one-hundred-year floods within a span of three years (2017-2019) as a result of excessively high levels of precipitation.

Global Climate Models (GCMs) and Intensity-Duration-Frequency (IDF) curves are tools that are used to study climate change and predict future weather patterns based on projections for the levels of greenhouse gas emissions that might be expected over the rest of the current century. The Intergovernmental Panel on Climate Change (IPCC) has established four emissions scenarios, known as Representative Concentration Pathways (RCPs), to represent varying degrees of optimism or pessimism regarding whether emissions will be reduced to relatively safe levels by the end of the century. IDF_CC is a tool that is designed to update IDF curves taking into account the effects of

climate change and projecting IDF curves for future precipitation under the four RCP scenarios. Version 3 of this tool was used in the current study to obtain projections for rainfall in the Ottawa area to the end of the current century under the worst-case scenario (RCP8.5). Under this scenario rainfall intensity is expected to increase significantly across the board, and the probability of more frequent high-intensity rainfall events is also expected to increase.

Rainfall appears to be causally related to the occurrence of landslides, and it is therefore possible to use projections for changes in rainfall patterns to assess future landslide susceptibility in the Ottawa area under conditions of climate change. Rainfall intensity and duration are key factors in the initiation and mechanics of landslides, and therefore projected values for these parameters and a wide range of probabilities were used in the TRIGRS model to identify specific sites in the Ottawa area that will become susceptible to landslides under these projected rainfall conditions.

5.7 References

Al-Umar M. (2018), GIS based assessment of climate-induced landslide susceptibility of sensitive marine clays in the Ottawa region, Canada. Unpublished doctoral dissertation. University of Ottawa, Ottawa, Canada. Available at: http://dx.doi.org/10.20381/ruor-21490.

Brooks, G. R. (2019). Sensitive clay landslide inventory map and database for Ottawa, Ontario. Geological Survey of Canada Open File 8600. Natural Resources Canada, Ottawa. Available at: https://doi.org/10.4095/315024

Brooks, G. R., Aylsworth, J. M., Evans, S. G., and Lawrence, D. E. (1994). The Lemieux landslide of June; 20, 1993, South Nation Valley southeastern Ontario—a photographic record. Geological Survey o Canada Miscellaneous Repert 56. Natura Resources Canada, Ottawa. Available at: https://doi.org/10.4095/193534.

Crawford, C. B. and Eden, W. J. (1967). Stability of natural slopes in sensitive clay. *Journal of the Soil Mechanics and Foundations Division, A.S.C.E.*, 93 (SM4), pp. 419-436. Available at: https://nrc-publications.canada.ca/eng/view/accepted/?id=9423b1a4-170a-43fc-a151-7bbd1d5b996b

CTV Ottawa. (2017). Flooding across the region drives hundreds from their homes. *CTV News*, 3 May. Available at: https://ottawa.ctvnews.ca/flooding-across-the-region-drives-hundreds-from-their-homes-1.3396807.

Eden, W. J., and Jarrett, P. M. (1971). *Landslide at Orelans, Ontario*. Division of Building Research, Technical Paper No. 321. National Research Council of Canada, Ottawa. Available at: https://doi.org/10.4224/20373789.

Eden, W. J. and Mitchell, R. J. (1970). The mechanics of landslides in Leda clay. *Canadian Geotechnical Journal*, 7 (3), pp. 285-296. Available at: http://web.mit.edu/parmstr/Public/ NRCan/rp441.pdf.

Eden, W. J., Fletcher, E. B., and Mitchell, R. J. (1971). South Nation River Landslide, 16 May 1971. *Canadian Geotechnical Journal*, 8, pp. 446-451. Available at: https://nrc-publications. canada.ca/eng/view/accepted/?id=aacc9d19-c4ad-4ccc-9c92-97e4616bbd71.

Eden, W. J., Matyas, E. L., and Irwin, W. (1965). *The Breckenridge Landslide*. Division of Building Research Internal Report No. 316. National Research Council Canada, Ottawa. Available at: https://doi.org/10.4224/20337956.

Hunter, R. D. and R. K. Meentemeyer. (2005). Climatologically aided mappin god daily precipitation and temperature. *Journal of Applied Meteorology*, 44, pp. 1501-1510.

Goovernment of Canada. (2020). Canada's top 10 weather stories of 2019. Available at: https://www.canada.ca/en/environment-climate-change/services/top-ten-weather-stories/2019.html

IPCC (Intergovermental Panel on Clmate Change). (2013). *Climate Change 2013: The Physical Science Basis*. Available at: https://www.ipcc.ch/site/assets/uploads/2018/02/WG1AR5_all_final.pdf

IPCC (Intergovermental Panel on Clmate Change). (2015). *Climate Change 2014: Synthesis Report*. Available at: https://www.ipcc.ch/site/assets/uploads/2018/05/SYR_AR5_FINAL_full_wcover.pdf

IPCC (Intergovermental Panel on Climate Change). (n.d.) *What is a GCM?* IPCC Data Distribution Centre. Available at: https://www.ipcc-data.org/guidelines/pages/gcm_guide.html.

Li, W. C., Lee, L. M. Cai, H., Li, H. J., Dai, F. C., Wang, M. L. (2013). Combined roles of saturated permeability and rainfall characteristics on failure of homogeneous soil slope. *Engineering Geology*, 153, pp. 105-113.

McNeil, D. (2019). An Independent Review of the 2019 Flood Events in Ontario: A Report to the Hon. John Yakabuski, Minister of Natural Resources and Forestry. Available at: https://files.ontario.ca/mnrf-english-ontario-special-advisor-on-flooding-report-2019-11-25.pdf.

Mitchell, R. J. (1969). Landslides at Breckenridge, Pineview Golf Club, and Rockcliffe. Division of Building Research Internal Report No. 372. National Research Council Canada. Available at: https://doi.org/10.4224/20338133

Qiu, C., Esaki, T., Mitani, Y., and Xie, M. (2008). A GIS-based method for predicting the location, magnitude and occurrence time of landslides using a three-dimensional deterministic model. In: Z. Chen, J. Zhang, Z. Li, F. Wu, and K. Ho, (eds.). *Landslides and Engineered Slopes: From the Past to the Future,* Vol. 1, pp. 893-900. CRC Press, The Netherlands.

Schardong, A., Gaur, A., Simonovic, S. P. and Sandink, D., (2018), Computerized Tool for the Development of Intensity-Duration- Frequency Curves Under a Changing Climate, Technical Manual v. 3., Water Resources Research Report No. 103. Department of Civil and Environmental Engineering and Institute for Catastrophic Loss Reduction, The University of Western Ontario, Ontario, Canada.

Van Westen, C. J., van Asch, T. W. J., and Soeters, R. (2006). Landslide hazard and risk zonation—why is it still so difficult? *Bulletin of Engineering Geology and the Environment*, 65 (2), pp. 167-184.

Zhang, X., Flato, G., Kirchmeier-Young, M., Vincent, L., Wan, H., Wang, X., Rong, R., Fyfe, J., Li, G., Kharin, V. V. (2019). Changes in temperature and precipitation across Canada. In: E. Bush and D. S. Lemmen, eds., *Canada's Changing Climate Report*, pp. 112-193. Government of Canada, Ottawa, Ontario.

6 Assessing the Effects of Climate Change on Future Susceptibility to Rainfall-Induced Landslides in the Ottawa Area

6.1 Basic Principles and Techniques Used in Landslide Susceptibility Assessment

Ideally, any prediction of landslide susceptibility should provide three pieces of information about the potential future landslide: (1) its magnitude; (2) its location; and (3) the time of its occurrence. These components of a landslide's occurrence are governed by several factors, which can be grouped into two broad categories: (1) quasi-static variables; and (2) dynamic variables. The *quasi-static* variables are direct contributors to landslide susceptibility and include the site's surficial geology, slope gradient (i.e., angle of slope), slope aspect (i.e., directional orientation of slope face), geotechnical properties, and natural and artificial drainage. The *dynamic* variables are factors that induce landslides in a given area of susceptibility; they include rainfall and earthquakes. In predicting landslide susceptibility, then, it is necessary to examine the influence of both *quasi-static* and *dynamic* variables on slope stability (Dai and Lee, 2001; Qiu et al., 2008).

Another distinction worth making is the distinction between: (1) *determinative* (i.e., necessary) factors (also known as "discriminant factors"); and (2) *predisposing* (or, contributory) factors. Determinative factors are those elements that must be present for the development of slope instability, factors such as angle of slope. Predisposing factors are those elements that work in combination with other factors to contribute to the deterioration of slope stability to the point of slope failure, factors such as soil depth, land use, and land cover. Determinative factors are used to identify *potential areas of susceptibility*, whereas predisposing factors are used to assess the *degree of susceptibility* of the identified area (i.e., the probability that a landslide will occur in that area) (Leoni et al., 2015).

Slope stability (or instability) is determined and landslide susceptibility is assigned to a given site using one or more methods that may be either subjective or objective, and either qualitative or quantitative. For convenience, they are classified into the four broad approaches (Al-Umar, 2018; Dai and Lee, 2001; Fall et al., 2006; Pardeshi et al., 2013; Park et al., 2013; van Westen et al, 2006; Wahono, 2010). They are: (1) the *distribution* approach; (2) the *heuristic* approach; (3) the *statistical* approach; (4) the *deterministic* approach. A combination of two or more of these approach is considered a *mixed* approach.

6.1.1 The Distribution Approach

Also known as the "inventory" approach, this approach is the simplest of the qualitative methods and involves using maps and databases in inventories of historical landslides to identify local areas that have been prone to landslides in the past, based on the distribution of the historical landslides contained in the inventory. Ideally, such inventories would provide both spatial and temporal information about the distribution of landslides in a given area, along with type, direction and rate of flow, type of material displaced, etc. Such data may be obtained through field survey mapping, and aerial photography, and from satellite images, newspaper accounts, and other historical records. This approach is often used in combination with other appoaches, since it has certain limitations and disadvantages. Triggering events are generally not included in the inventories, and dynamic variables and some quasi-static variables cannot be determined accurately by this approach. Furthermore, each landslide in a given area may have its own unique set of characteristics, which may not be reflected in the inventory. Additionally, inventories are not exhaustive in that the time periods they cover are often limited, minor slides may not be included, and recorded data in the inventories often contain inconsistencies (Dai and Lee, 2001; Fall et al., 2006; Pardeshi et al., 2013; Stanley and Kirschbaum, 2017; van Westen et al., 2006). As an example of a landslide inventory map, the most recent (2019) landslide inventory map for the City of Ottawa is presented in Figure 6-1.

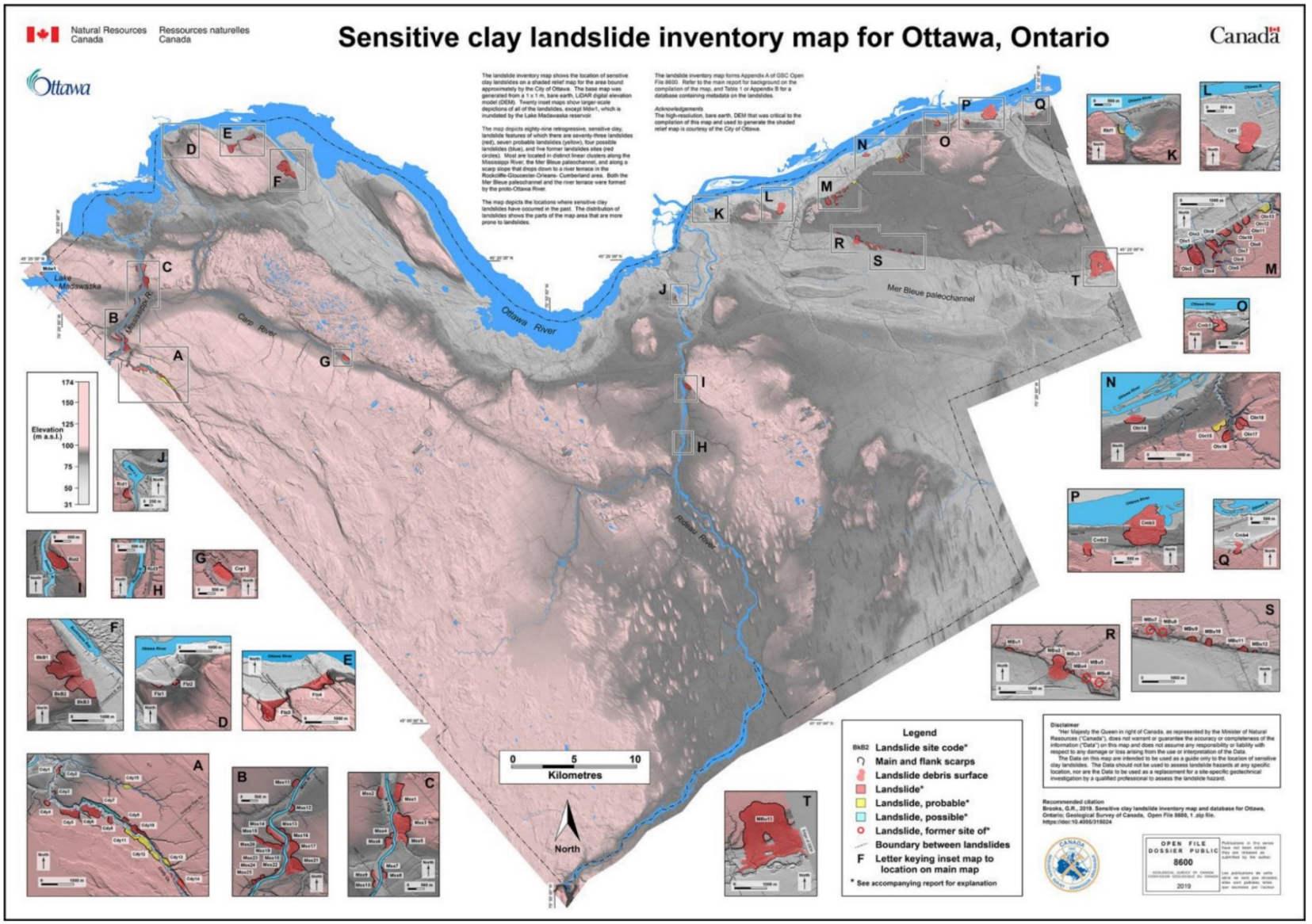

Figure 6-1 Sensitive clay landslide inventory map for Ottawa, Ontario (Brooks, 2019).

6.1.2 The Heuristic Approach

This is a knowledge-based approach that relies on the judgment of experts, such as geomorpholgists, who draw upon their knoweldge of the mechanics of landslides and the occurrence of historical landslides, and then use heuristic reasoning to assess risk. Expertise is developed through experience in the field, backed up by a thorough understanding of the theoretical bases of the physical processes involved. This approach uses only the quasi-static variables, and it is highly subjective in the assigning of relative weights and ratings to these variables. The higher the weight and rating (or score) assigned to a given variable, the greater its role or influence in the occurrence of the landslide. Risk or susceptibility is determined by adding up the assigned weights for all the variables in the analysis. Landslide distribution is not taken into consideration. Susceptibility is assessed in five broad categories: (1) very high; (2) high; (3) moderate; (4) low; and (5) very low. Because of the heuristic nature of the reasoning involved in the process, the assessed susceptibility is a *possibility* rather than a *probability* (as it is when using quantitative methods). The heuristic approach is most effective when a multi-disciplinary team of experts is involved and qualitative or semi-qualitative risk assessment is appropriate, such as when large areas are being assessed. For this reason, it is often used in combination with other approaches and methods (Dai and Lee, 2001; Fall et al. 2016; Kaur et al., 2018; Leoni et al. 2015; Pardeshi et al., 2013; Stanley and Kirschbaum, 2017; van Westen et al, 2006; Wahono, 2010; Wati et al., 2010).

6.1.3 The Statistical Approach

This is a quantitative or semi-quantitative approach in which statistical methods are used to determine the set of variables that are most likely to have contributed to a given historical landslide as ubducated on a landslide invetory map. Quantitative and semi-quantitative methods are then used to identify areas where the conditions represented by that set of variables prevail but where landslides have not yet occurred. The various methods employed under this approach can be divided into those that employ bivariate statistical analysis and those that employ multivariate statistical analysis. Some studies suggest that multivariate statistical analysis provides the best assessment of susceptibility for both rotational and translational landslides. The statistical approach is an objective approach to landslide susceptibility assessment, as opposed to the subjective nature of the previous two approaches. One drawback of this approach is that very few users of the approach create separate statistical models for different types of landslides, but treat all landslides as a generic phenomenon with one set of conditions, which is then used to generate statistical relationships.

However, each type of landslide has its own unique combination of environmental factors, with different landslide depths, and different landslide volumes. Furthermore, the statistical approach rarely takes into account the dynamic variables (i.e, the triggering factors), and when these variables are included, they are analysed for their spatial distribution and variation rather than for their temporal patterns. The general criticism of the statistical approach is that it often engages in an extreme oversimplification of the controlling and contributory factors involved in landslide occurrence (Dai and Lee, 2001; Fall et al., 2006; Pardeshi et al., 2013; van Westen et al., 2006; Wahono, 2010).

6.1.4 The Deterministic Approach

This approach involves slope stability analysis using the limit equilibrium method (LEM). In LEM, potential failure mechanisms are identified and factors of safety are then derived for a given set of geotechnical conditions. The deterministic approach is suitable for assessing landslide susceptibility in relatively small areas, where the ground conditions are failry uniform throughout the area or highly detailed data is available for points of variation within the area and the landslide types are known and can be analysed with relative ease. This is, perhaps, one of its greatest limitations. In the GIS enviornment, it is possible to apply the approach to larger areas, but only for an infinite slope stability model that has a slip plane parallel to the ground surface, since models that have complex slip planes or curved slip surfaces are difficult to implement. The primary advantage of the deterministic approach is that it allows for the factor of safety to be determined quantitatively (Dai and Lee, 2001; Fall et al., 2006; van Westen et al., 2006).

6.1.5 The Mixed Approach

Given the individual limitations and disadvantages of each of these approaches on their own, the most recent trend has been to combine the various approaches, particularly the statistical and deterministic approaches. In 2014, the creators of the TRIGRS model (discussed in detail in Chapter 2, Section 2.4) undertook the address the limitations of their original model by taking a "probabalistic" (the opposite of "deterministic") approach to improving the predictive power of their originally deterministic model. The problem they were encountering with their original model was the difficulty in obtaining accurate values for the variables related to the properties of the slopes where landslides were occurring. Additionally, their original model was not able to work with large areas, precisely because sufficient detailed geotechnical and hydrological data was not available at that scale. To address this problem, they introduced a probabilistic Monte Carlo approach into their

model. In the new version of TRIGRS (v. 2.1), parameters such as transient pore pressure are computed probabalistically on a cell-by-cell basis. Infiltration is modelled using analytical solutions of partial differential equations. The natural variability of the mechanical and hydrological properties of landslide-prone slopes is accommodated by allowing the values of the model's input parameters to be sampled randomly from a given probability distribution. In testing their modified model, the team ran the modified model several times, varying the input parameters, and then analysed the various outputs statistically. A comparison of the outputs of the modified model with the output of the original deterministic model indicated an improvement of between 10% and 16% in the overall model's predictive power (Alvioli and Baum, 2016; Baum et al., 2008; Baum et al., 2010; Raia et al., 2014).

As noted in Chapter 2, Section 2.4, the current study uses this mixed-approach version of TRIGRS to assess susceptibility to rainfall-induced landslides in the sensitive marine clays of the Ottawa area.

6.2 Methodology

The study proceeded in two broad stages involving the gathering and processing of various types of data, inputting this data into various computer models, and generating outputs in the form of maps. The sequence of step is presented diagrammatically in Figure 6-2.

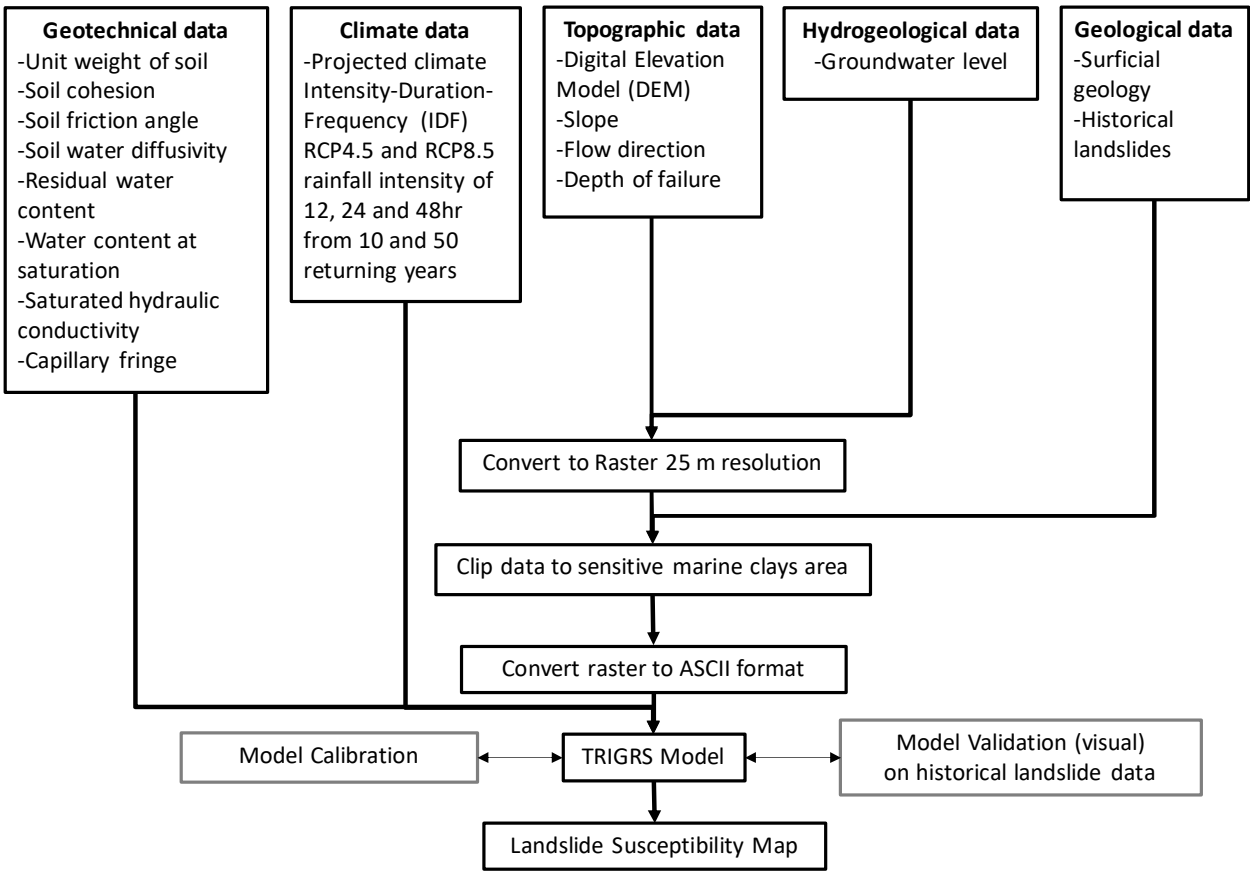

Figure 6-2 Methodology flowchart for landslide susceptibility assessment in this study

6.2.1 Collection and Processing of Data

The first stage was the collection (or extraction) and processing of data from various sources. The data thus obtained falls into five broad categories: (1) geological data; (2) geotechnical data; (3) topographical data; (4) hydrogeological data; (5) and projections for future rainfall patterns (IDF curves). The collected data was processed using ArcGIS software with ArcMap and the Spatial Analysis extension, and Microsoft Excel.

6.2.1.1 Geological Data Collection and Processing

Data collection began with accessing and analyzing the geological data for the study area in order to determine those zones within the study area that contain sensitive marine clays, and in particular those land units that have been designated "landside" zones, based on the occurrence of landsides in the past (as outlined in the discussion of surficial geology in Chapter 4, Section 4.3.4.5). The purpose

of this crucial first step was to establish limits for the collection and analysis of all other types of data. Those portions of the study area that do not contain sensitive marine clays as part of their surficial geology were not taken into consideration in this study, since the study's focus was limited to rainfall-induced landslide susceptibility specifically in sensitive marine clays. The surficial geology data was extracted from the Surficial Geology of Southern Ontario dataset (MRD 218-REV), complied by the Ontario Geological Survey (2010), which was downloaded from the Geology Ontario website.[2] The dataset is a GIS-based geological map in polygon format showing the distribution and characteristics of surficial units across Southern Ontario.

Land units containing sensitive marine clays (Leda Clay) and other fine-textured glaciomarine deposits were extracted from the dataset and mapped in ArcMap. Land units with landslide surface features were identified using data from the Geological Survey of Canada's *Surficial Geology, Lower Ottawa Valley, Ontario-Quebec* (2009), published by Natural Resources Canada, and downloaded from the GEOSCAN website.[3] The locations of these landslide land units were added to the map of the sensitive marine clay zones. The zones of sensitive marine clay with landslide surface features are shown in Figure 6-3.

[2] http://www.geologyontario.mndm.gov.on.ca/mndmaccess/mndm_dir.asp?type=pub&id=MRD128-REV

[3] https://geoscan.nrcan.gc.ca/starweb/geoscan/servlet.starweb?path=geoscan/fulle.web&search1=R=247486

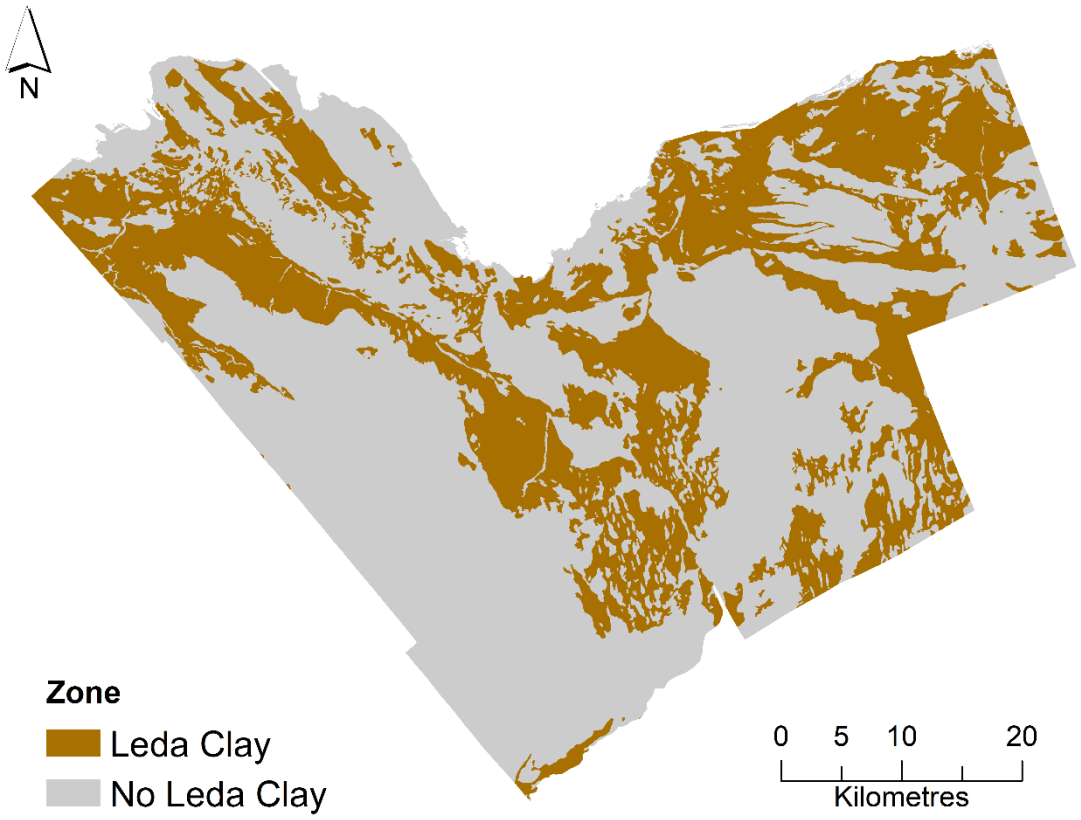

Figure 6-3 Sensitive marine clay (Leda Clay) zones in the City of Ottawa

6.2.1.2 Geotechnical Data Collection and Processing

The geotechnical data was obtained from a previous study by Al-Umar (2018), for his study, Al-Umar extracted and collated the relevant data from six geotechnical reports prepared between 2008 and 2017 by engineering firms in the City of Ottawa for engineering projects at six Ottawa sites characterized by the presence of sensitive marine clays (as discussed in Chapter 4, Section 4.4), and therefore already within the zones identified in the previous step. The locations of the six sites are shown in Figure 6-4. Additional Geotechnical data was obtained from previous study by Klugman and Chung (1976), for this study, they collected field geotechnical data in the Regional Municipality of Ottawa-Carleton to develop slope stability map for this area. Geotechnical data was also compared to the City of Ottawa Slope Stability Guidelines for development applications (2012)[4].

[4] https://documents.ottawa.ca/sites/documents/files/documents/cap137604.pdf

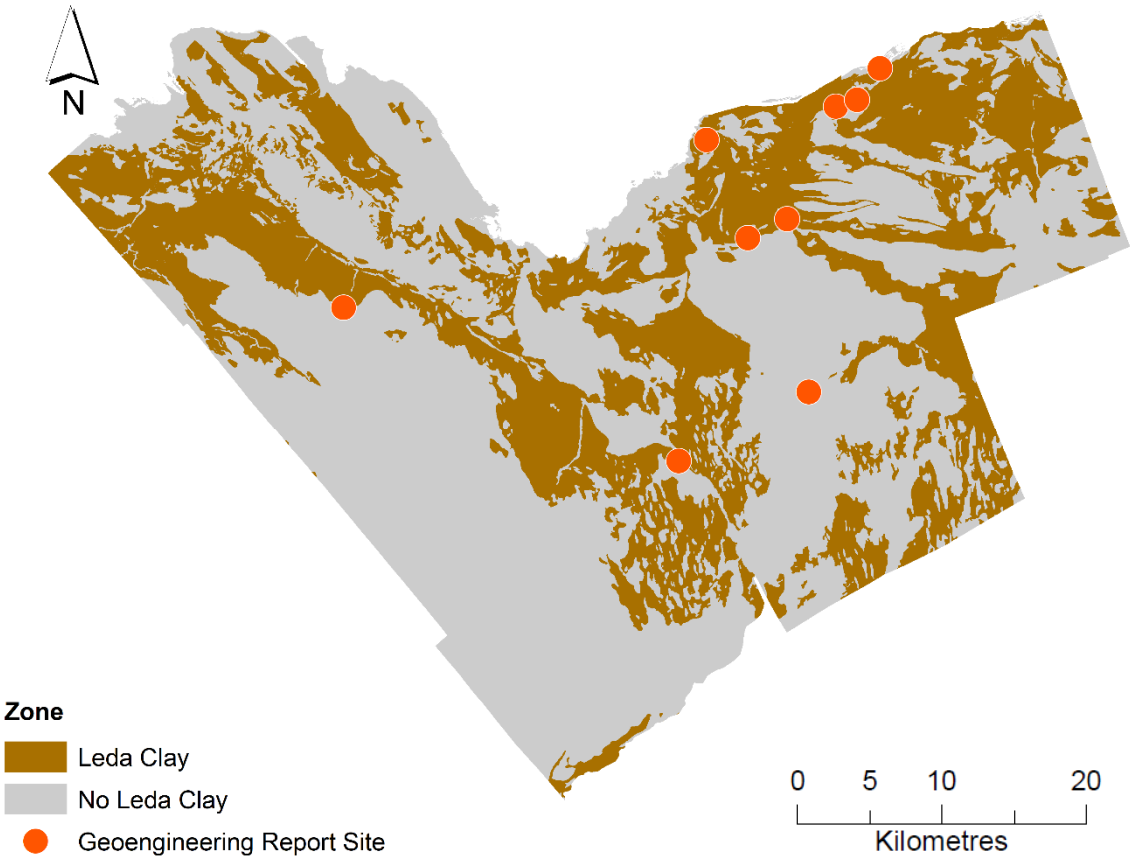

Figure 6-4 Locations of the six sites at which geotechnical data for the study were obtained.

The geotechnical properties for which data was obtained include: effective cohesion, effective internal angle of friction, volumetric water content at saturation, residual water content, saturated hydraulic conductivity, and soil water diffusivity. The value for the inverted capillary fringe was calculated using experimental data obtained by Taha (2010). Values for hydraulic pressure head, volumetric water content at saturation, and residual water content were extracted from Taha's Excel file and fitted to the Soil-Water Characteristic Curve (SWCC) using Eq. 10 (see Section 6.3 below). The calculation of the inverted capillary fringe value from the SWCC is explained in detail in Section 6.4.2 below.

6.2.1.3 Topographical Data Collection and Processing

The topographical data for the study area consists of elevation values extracted from LiDAR (Light Detection and Ranging) data collected by the City of Ottawa between 2006 and 2015, and

downloaded from the University of Ottawa Geospatial Data Library.[5] The LiDAR system provides highly accurate ground surface elevations at a 1 m resolution in raster format as Digital Elevation Models (DEMs) data. The extracted DEMs data was resampled down to a 25 m resolution for use in ArcGIS and clipped to the sensitive marine clay areas identified in the initial step (described in Section 6.2.1.1 above) to be used in conjunction with rainfall data. Elevations for the City of Ottawa derived from Ottawa LiDAR are shown in Figure 6-5.

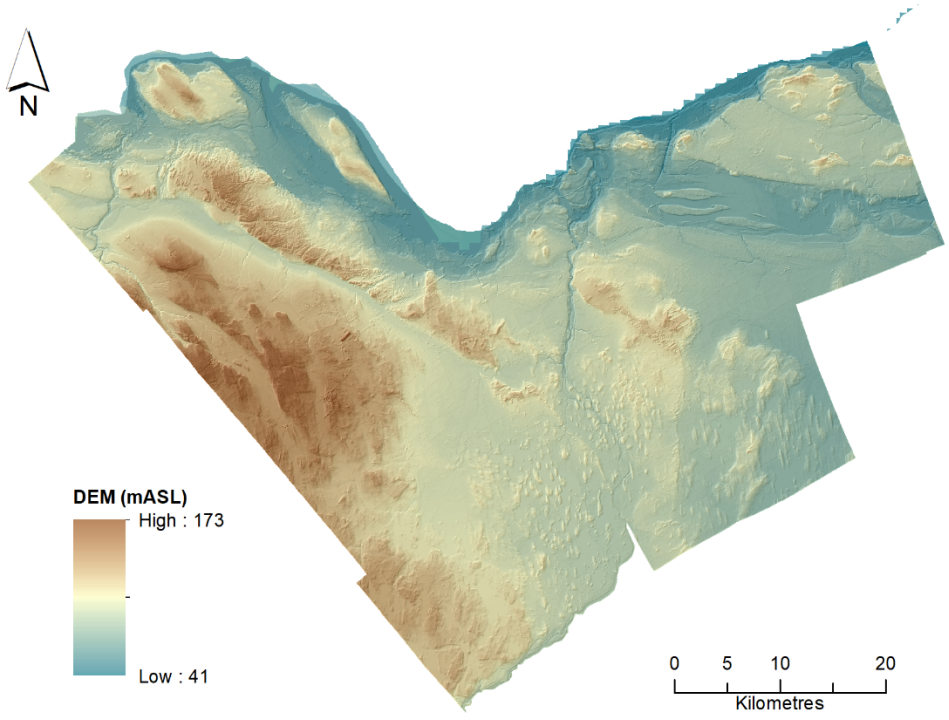

Figure 6-5 Elevation map for the City of Ottawa

Slope analysis was performed on the DEMs data using the ArcMap Spatial Analysis Extension to obtain slope values across the study area. Slope angles in degrees for the City of Ottawa are shown in Figure 6-6. Flow direction analysis was also performed on the DEMs data using the Spatial Analysis Extension, and values were obtained for the flow direction parameter.

[5] http://uottawa.libguides.com/geospatial-data/OttawaGatineau

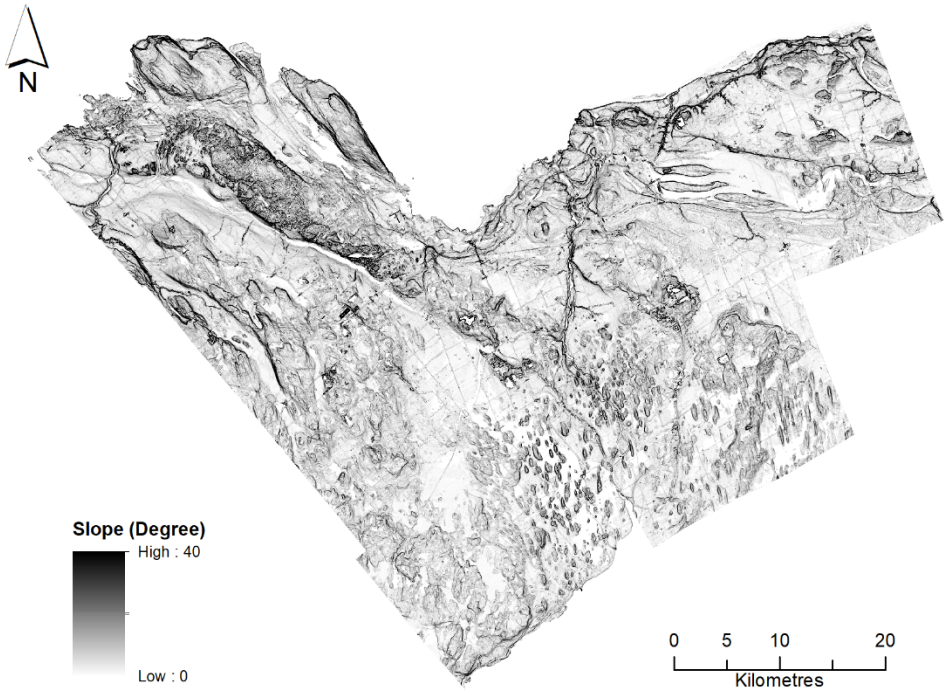

Figure 6-6 Slope map for the City of Ottawa

Values for depth of failure, that is, the predicted depth of the sliding plane, were also obtained, using the raster calculation tool in ArcMap, and applying the calculated slope values to Eq. (1), following Baum et al. (2010).[6] Predicted depths of failure for shallow landslides in the study area are presented in Figure 6-7.

$$d_{LZ} = 5.0e^{-0.04\delta} \quad (1)$$

Where: d_{LZ} = depth of failure
δ = slope angle

[6] Baum et al. (2010) note that depth of failure is inversely proportional to slope angle. Thus, d_{LZ} is at a minimum of about 0.5 m when the slope is angled at 58°, about 1.0 m when the slope is angled at 40°, and about 1.5 m when the slope is angled at 30°.

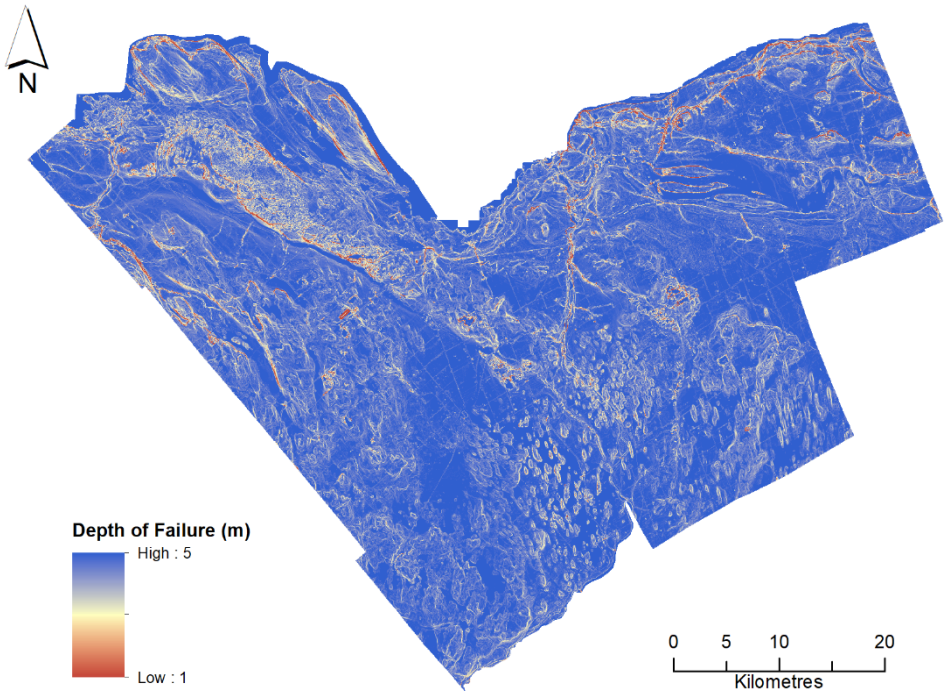

Figure 6-7 Predicted depth of failure for shallow landslides in the City of Ottawa

6.2.1.4 Hydrogeological Data Collection

The hydrogeological data collected for this study consisted of the water table levels in the study area, for the purposes of determining the depth of the groundwater below the ground surface. This data was obtained from water wells in the Provincial Groundwater Monitoring Network (PGMN) and the Water Well Information Systems (WWIS). The PGMN water wells are public monitoring wells that monitor groundwater levels on an hourly basis at various locations across the province. PGMN data is available for download at the official Government of Ontario website.[7] Data on well locations is in GIS shapefile format and consists of general information, such as the location's latitude, longitude, township, conservation authority, type of aquifer, depth of well, screening level, ground elevation, etc. Data on water levels at each well location (recorded as an elevation above mean sea level) is available from 2001 to 2015 and is downloadable in a separate file in .csv format. The WWIS represents well locations as point data in Ontario. The WWIS data provides detail information about

[7] https://www.ontario.ca/environment-and-energy/map-provincial-groundwater-monitoring-network.

the well's location, depth of well, static water level, ground surface elevation, etc. WWIS data is available for download at the official Government of Ontario website.[8]

As a preliminary step, the PGMN "Water Wells" and "Water Levels" files were downloaded from the website and 39 wells in and around the City of Ottawa within a 40-km radius of the city were selected for analysis. The static water level from 3,711 WWIS wells were extracted where the distribution of the PGMN wells are not present, this is to maintain water level in different topography as much as possible. Figure 6-8 shows the locations of the wells that were selected for the current study.

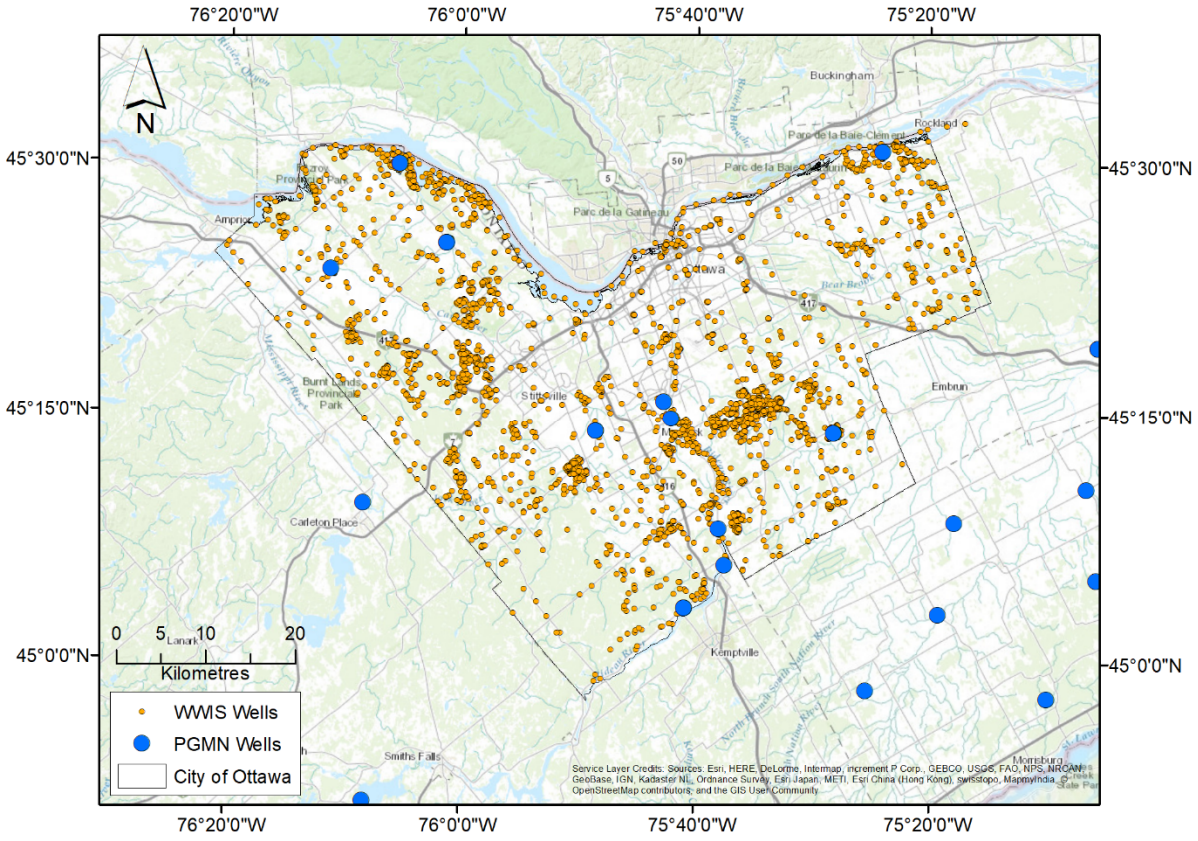

Figure 6-8 Locations of PGMN wells in Ottawa and the surrounding area

In order to allow for seasonal variations in groundwater levels, the data was grouped into the three relevant seasons for the Ottawa area, using the following groupings: (1) Spring: April, May and June; (2) Summer: July and August; (3) Fall: September, October, November. Data for these months were extracted from the Water Levels database and averaged for each of the three seasons for each well location, using Microsoft Excel. The seasonal averages and the overall averages of the three

[8] https://data.ontario.ca/dataset/well-records.

seasons combined are presented in Table 6.1. These averages were then entered into ArcGIS and associated to the well locations in the "Water Wells" shapefile for the next stage in the data analysis. In this stage, the average groundwater levels were compared with the ground surface elevation at each well location in order to determine the depth of the water table below the ground surface for that location. Interpolation in ArcGIS was used to obtain the depth of the water table in raster format at a 25 m resolution.

As Table 6.1 shows, there were no significant seasonal variations in groundwater level at any of the well locations. Consequently, the overall averages across the three seasons were used as the value for the water table depth parameter.

Table 6.1 Average water table levels (in mASL) during spring, summer, and fall at 39 PGMN wells in the Ottawa area, 2001 to 2015

PGMN Well ID	WL Spring (mASL)	WL Summer (mASL)	WL Fall (mASL)	WL AVG (mASL)
W0000081-1	78.83	78.66	78.65	78.71
W0000082-1	127.05	126.65	126.54	126.75
W0000085-1	84.00	83.71	83.22	83.64
W0000086-1	81.00	80.65	80.69	80.78
W0000087-1	85.69	85.59	85.61	85.63
W0000088-1	123.36	123.12	122.90	123.13
W0000094-1	75.30	74.89	74.68	74.96
W0000095-1	48.16	48.01	48.08	48.09
W0000096-1	100.00	99.30	99.37	99.56
W0000097-2	86.68	86.10	86.08	86.29
W0000097-5	83.06	82.52	82.72	82.76
W0000118-2	80.61	80.67	80.50	80.60
W0000119-2	95.13	94.59	94.36	94.69
W0000134-1	189.51	188.79	188.43	188.91
W0000156-2	91.28	90.72	90.56	90.85
W0000156-3	91.21	90.87	90.71	90.93
W0000157-2	86.49	86.13	86.14	86.26
W0000157-3	85.53	85.18	85.23	85.31
W0000186-1	81.54	81.48	81.48	81.50
W0000200-1	122.53	121.76	121.68	121.99
W0000268-1	71.77	71.16	70.97	71.30
W0000269-1	68.91	68.56	68.44	68.64
W0000278-1	142.52	140.56	139.73	140.94
W0000279-1	107.67	107.20	107.33	107.40
W0000282-3	44.53	43.75	43.01	43.76
W0000319-1	130.81	129.37	129.02	129.73
W0000331-1	205.96	204.61	204.59	205.06
W0000350-2	112.48	112.06	111.98	112.17
W0000350-3	113.18	112.71	112.65	112.85
W0000363-2	58.12	57.89	57.94	57.98
W0000363-3	58.29	58.05	58.02	58.12
W0000364-1	40.22	40.07	40.10	40.13
W0000378-1	75.62	75.07	74.79	75.16
W0000400-2	60.99	60.86	60.81	60.89
W0000400-3	61.05	60.89	60.84	60.92
W0000401-1	59.94	59.64	59.26	59.61
W0000402-1	94.02	93.88	93.72	93.87
W0000403-1	83.52	83.08	83.04	83.21
W0000458-1	41.66	41.60	41.62	41.63

6.2.1.5 Projected Rainfall Data Collection and Processing

As a preliminary step, projected rainfall data, in the form of IDF curves, were obtained from the IDF_CC tool (discussed in Chapter 5, Section 5.3.2) for the gauged weather stations in and around the City of Ottawa. Observed projected rainfall IDF curves from gauge stations surrounding City of Ottawa showing similar rainfall intensities, therefore the data from gauge weather station from Ottawa CDA RCS, 8 km north of the Ottawa International Airport were use for model input. The location of Ottawa CDA RCS is indicated in Figure 6-9. Rainfall intensities from IDF curves were obtained for durations of 12 hr, 24 hr, and 48 hr and for return periods of 10 and 50 years, under two emissions scenarios, RCP4.5 and RCP8.5 in excel table format. Each rainfall intensity is used for the model input. For example, for RCP4.5 rainfall duration of 12 hr under 10 years returning period, the stable value of 6.96 mm/h is used for the model. The model uses stable the rainfall intensity of 6.96 mm/h from start (0s) for the entire duration of 12 hr (model completed).

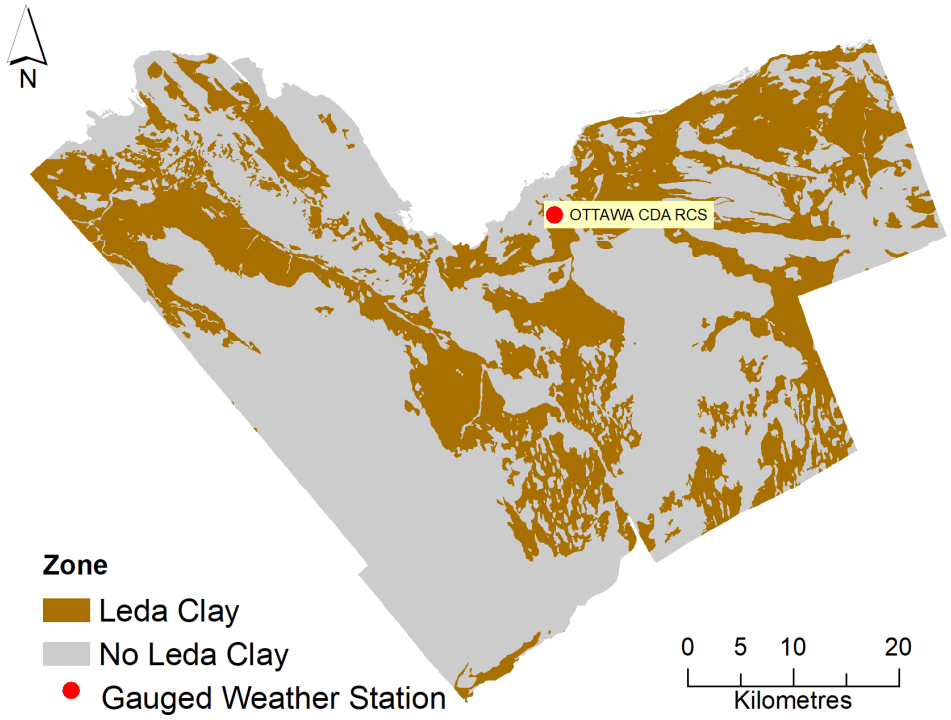

Figure 6-9 Location of gauged weather station Ottawa CDA RCS.

6.2.2 Application of Collected and Processed Data to TRIGRS Models

6.2.2.1 Introduction

The second stage involved running the suite of models contained in TRIGRS (discussed in Chapter 2, Section 2.5 above) for estimating the timing and location of shallow rainfall-induced landslides, using the data collected and processed in the first stage. In order to do this, the output data from ArcGIS had to be converted from raster format to ASCII format. Following this preparatory data conversion step, the ASCII data was inputted into TRIGRS and the models were run. The two general models are: (1) The Hydrological Model; and (2) The Slope Stability Model. The Hydrological Model simulates infiltrations patterns and consists of two sub-models, namely, the Infiltration Model for Saturated Initial Conditions and the Infiltration Model for Unsaturated Initial Conditions.

In rainfall-induced landslides, infiltration of rainwater into the soil is the central factor in the deterioration of slope stability and the eventual occurrence of slope failure. Hence the starting point in any assessment of landslide susceptibility is an analysis of infiltration patterns under various soil conditions. The Infiltration Models in TRIGRS set up the framework within which the Slope Stability Model operates. The model is based on a two-layer schema in which an unsaturated zone sits on top of a saturated zone (groundwater) and interacts with it in ways that affect slope stability. At the interface between the two zones, just above the water table is the capillary fringe, which serves as a sort of transition zone. The model links transient (i.e., time-variant), vertical infiltration into the unsaturated zone to porewater pressure changes in the saturated zone below the water table. The linkage is made through the transient rise in the water table that occurs as water collects at the base of the unsaturated zone. The porewater pressure changes that are computed in the Infiltration Models are then applied to the Slope Stability Model to compute the factor of safety of the slope under the specified infiltration conditions (Baum et al, 2010). This conceptual basis of the model is presented diagrammatically in Figure 6-10.

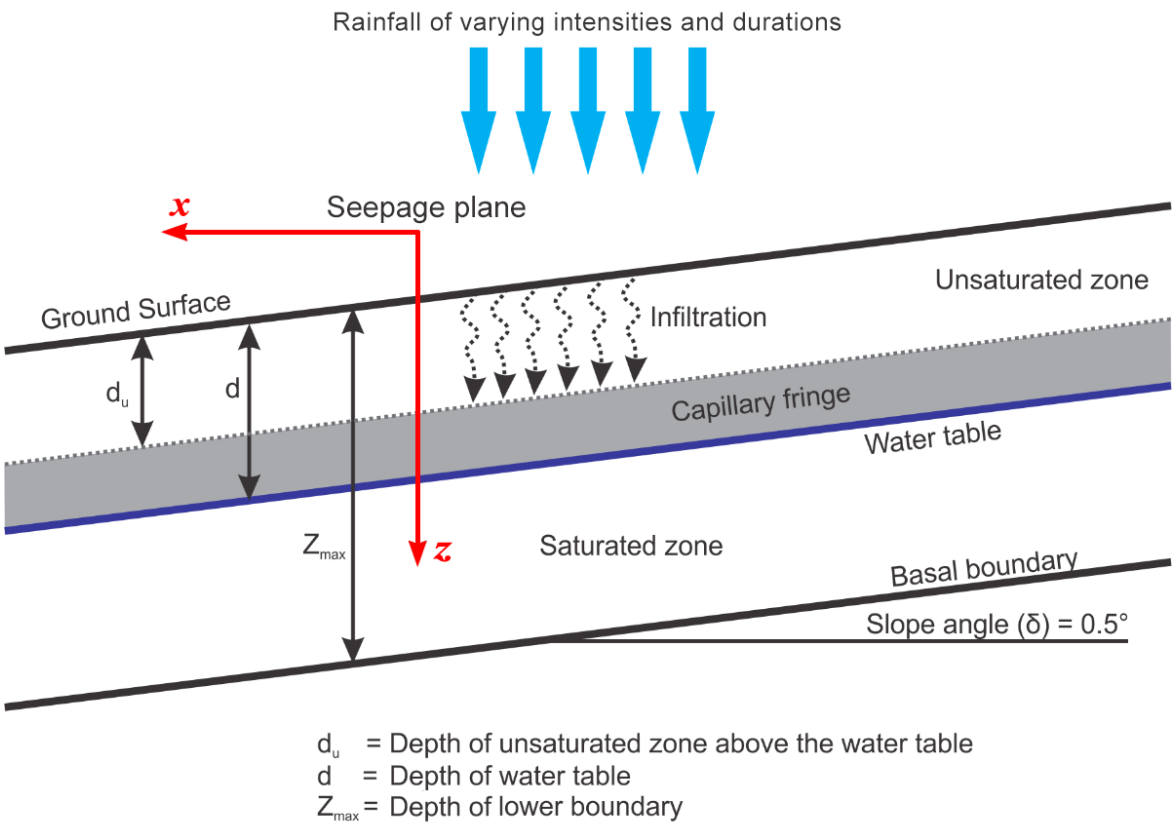

Figure 6-10 Diagrammatic representation of the conceptual basis of the TRIGRS Model (adapted from Baum et al., 2008 and Park et al., 2013).

6.2.2.2 The Hydrological Model

The TRIGRS hydrological model for rainfall-induced landslides consists of a set of models that simulate the movement of infiltrated rainwater through the soil and the effects this movement has on soil and slope dynamics.

There are two infiltration models for simulating infiltration and subsurface flow of rainwater and allowing for the routing of rainwater runoff, and two additional models for simulating water-table rise and pressure diffusion below the water table.

6.2.2.2.1 The Infiltration Models

How infiltration occurs in a given soil is governed in part by the initial conditions that prevail in that soil. Prior to a rainfall event, a given soil may be either saturated or unsaturated. Thus, one of the two infiltrations models simulates wet, saturated initial conditions; the other simulates moist, unsaturated initial conditions. It should be noted that infiltration patterns are also affected by the

hydrogeological properties of the soil in which the infiltration occurs. Both these sets of variables are taken into account in the models (Baum et al., 2008; Baum et al., 2010). The movement of water in saturated soils is two-dimensional (i.e., vertical and lateral), whereas in unsaturated soils, it is largely one-dimensional (vertical). The two-dimensional flow of water through saturated soil is generally referred to as "seepage", and the term "percolation" is usually used to signify the one-dimensional, vertical, downward movement of water through unsaturated soil.

6.2.2.2.1.1 Infiltration Model for Saturated Initial Conditions

The infiltration model for saturated initial conditions employs Iverson's linearized solution of the Richards equation with additional extensions added on by Baum and his collaborators over several years, beginning in 2002 (Baum et al., 2008, 2010). Iverson's solution incorporates a steady component and a transient component, representing the two modes by which water moves through soil (just mentioned above). The *steady seepage component* involves two key parameters: (1) the initial depth of the water table; and (2) a steady infiltration rate. In this component, the steady initial subsurface flow is two-dimensional and occurs along a plane perpendicular to the ground surface and parallel to the orientation of the slope (i.e., the *x*-*z* plane shown in Figure 6-10). The direction of this flow is determined by the steady infiltration rate, the soil's saturated hydraulic conductivity, and the slope angle). By contrast, the *transient component* presupposes a one-dimensional, vertical downward flow arising from a specified time-varying flux of fixed duration and intensity at the ground surface. A zero flux is specified for times greater than the starting time at a basal boundary of infinite depth (Baum et al., 2008).

Since this model is designed for saturated initial conditions, the flow is in the linear range for Darcy's law to apply and the hydraulic diffusivity is approximately constant. A series of Heaveside step functions is used to implement Iverson's suggested summation of his solution for rainfall of constant intensity to represent a general time-varying sequence of rainfall of varying intensities and durations. The modified solution used in TRIGRS, which superposes the transient solution on the steady-state solution, is given in Eq. (1). The equation, which returns the value for the pressure head, is applicable only to soils whose hydraulic properties are uniform in the vertical direction. The first term on the right-hand side of the equation represents the steady seepage component and the rest of the equation represents the transient component. This superposition of the steady-state and transient solutions is possible because both solutions satisfy the linearized partial differential equation for groundwater pressure head based on Richards equation (Alvioli and Baum, 2016; Baum et al. 2008; Baum et al. 2010; Park et al. 2013; Savage et al, 2004).

$$\psi(Z,t) = (Z-d)\beta + 2\sum_{n=1}^{N}\frac{I_{nZ}}{K_S}\left\{H(t-t_n)\,[D_1(t-t_n)]^{\frac{1}{2}}\,\text{ierfc}\left[\frac{Z}{2[D_{1(t-t_n)}]^{\frac{1}{2}}}\right]\right\} - 2\sum_{n=1}^{N}\frac{I_{nZ}}{K_S}\left\{H(t-t_{n+1})\,[D_1(t-t_{n+1})]^{\frac{1}{2}}\,\text{ierfc}\left[\frac{Z}{2[D_{1(t-t_{n+1})}]^{\frac{1}{2}}}\right]\right\} \quad (1)$$

Where: ψ = groundwater pressure head

t = time

Z = $z/cos\delta$

Where: Z = vertical coordinate direction (positive downward) and depth below the ground surface

z = slope-normal coordinate direction (also positive downward)

δ = slope angle

d = steady-state depth of the water table measured in the vertical direction

β = $cos^2\delta - (\frac{I_{ZLT}}{K_s})$

K_s = saturated hydraulic conductivity in the Z direction

I_{ZLT} = steady (initial) surface flux

I_{nZ} = rate of surface flux for the n^{th} time interval (usually corresponding to the average rainfall intensity during that time interval)

D_1 = $D_0/cos^2\delta$,

Where: D_0 = saturated hydraulic diffusivity, $D_0 = K_s/S_s$,

Where: K_s = saturated hydraulic conductivity

S_s = specific storage

N = total number of time intervals used to represent the sequence of time-varying surface fluxes

$H(t-t_n)$ = the Heaviside step function

Where: t_n = time at the n^{th} time interval in the rainfall infiltration sequence

The function $ierfc$ is of the form:

$$\text{ierfc}(\eta) = \frac{I}{\sqrt{\pi}}\exp(-\eta^2) - \eta\text{erfc}(\eta)$$

Where $erfc(\eta)$ is the complementary error function.

As an alternative to the infinite-depth model outlined above, TRIGRS provides a model that allows for a finite depth, d_{LZ} for the basal boundary. Pore pressure in this model is computed by the following equation (Baum et al. 2010):

$$\psi(Z,t) = (Z-d)\beta + 2\sum_{n=1}^{N}\frac{I_{nZ}}{K_S}H(t - t_n)[D_1(t - t_n)]^{\frac{1}{2}} \cdot \sum_{m=1}^{\infty}\left\{\text{ierfc}\left[\frac{(2m-1)d_{LZ} - (d_{LZ}-Z)}{2[D_1(t - t_n)]^{\frac{1}{2}}}\right] + \text{ierfc}\left[\frac{(2m-1)d_{LZ} + (d_{LZ}-Z)}{2[D_1(t - t_n)]^{\frac{1}{2}}}\right]\right\} - 2\sum_{n=1}^{N}\frac{I_{nZ}}{K_S}H(t - t_{n+1})[D_1(t - t_{n+1})]^{\frac{1}{2}} \cdot \sum_{m=1}^{\infty}\left\{\text{ierfc}\left[\frac{(2m-1)d_{LZ} - (d_{LZ}-Z)}{2[D_1(t - t_{n+1})]^{\frac{1}{2}}}\right] + \text{ierfc}\left[\frac{(2m-1)d_{LZ} + (d_{LZ}-Z)}{2[D_1(t - t_{n+1})]^{\frac{1}{2}}}\right]\right\} \quad (2)$$

Equation (2) is fundamentally the same as Equation (1) except for the addition of d_{LZ}, which represents the depth of the impermeable basal boundary measured in the Z direction. The two equations apply to two different subsurface conditions. Equation (1) assumes that the soil's hydraulic properties are isotropic in the vertical direction (i.e., uniform with depth), whereas Equation (2) models a slope in which there is a well-defined decrease in hydraulic conductivity to a finite depth.

The infinite series represented in Equations (1) and (2) soon converges, and consequently, for practical purposes, only the first several iterations of the series are sufficient. TRIGRS uses the minimum number of terms in each equation to ensure that accurate and consistent results are obtained. In the model, an additional physical limitation is imposed on the equation through the use of Iverson's β line limit, such that the pressure head value calculated by it cannot exceed the value that would result from steady-state seepage in a soil whose water table is at the ground surface and vertical infiltration at the surface is controlled by the ratio of surface flux to saturated hydraulic conductivity at the surface. This applies only to conditions of downward, gravity-driven flow. The β-line limitation is expressed by Eq. (3) (Baum, et al., 2008; Baum et al. 2010; Savage et al. 2004).

$$\psi(Z,t) \leq Z\beta \quad (3)$$

In other words, if Eq. (1) returns a value for the pressure head that is higher than $Z\beta$, TRIGRS automatically reduces the value to $Z\beta$. The value of β can be specified to represent either hydrostatic

flow ($\beta = 1$) or slope-parallel flow ($\beta = \cos^2 \delta$) (Baum et al. 2008). For the current study, slope-parallel flow was assumed. If, as an initial condition, the water table is at the ground surface, then exfiltration occurs and under rainfall conditions, the rainwater runs off along with the exfiltrating water. If, however, the water table is initially below the ground surface and the water table is rising as a result of infiltration, the flow is upward. In this scenario, TRIGRS allows infiltration to continue until the water table reaches the ground surface. In this case, Eq (3) is modified as follows:

$$\Psi(Z,t) = (Z - d_t)\beta \; ; \; Z > \; d_t \tag{4}$$

Where: d_t = depth to the transient water table

To summarize what has been stated above, Eq. (1) should be used, ideally, for saturated or nearly saturated soils in which the hydraulic diffusivity and hydraulic conductivity are approximately constant and are close or equal to their saturated values, and where transient infiltration is one-dimensional and *vertically downward*, the soil is homogeneous, and the depth is relatively shallow. Regardless of overall, soil conditions, the equation is always valid within the capillary fringe and below the water table, since water content and hydraulic conductivity are constant within these zones. If there is relatively minor transient *lateral* flow, the computed pore pressures will be sufficiently accurate for practical purposes. However, given that the steady seepage component allows flow in any direction consistent with allowable values of β, the superposition of the two components means that flow can be simulated in any arbitrary direction within the *x*-*z* plane (Baum et al., 2008; Baum et al., 2010; Savage et al., 2004).

6.2.2.2.1.2 Infiltration Models for Unsaturated Initial Conditions

The Infiltration Model for Unsaturated Initial Conditions invokes the two-layer schema described above in Section 6.2.2.2.1.1. The central feature of this schema is the unsaturated layer, which overlies the saturated zone below the water table, with a capillary fringe at the interface of these two layers, as shown in Figure 6-10. The unsaturated layer serves as a sort of filter, regulating the passage of infiltrated water to the water table. As infiltrated rainwater passes through the unsaturated zone, some of it is retained in the pores of the unsaturated zone, and the rest percolates through to the bottom of the zone, where it accumulates in the region of the capillary fringe, thus raising the water table. The load created by the weight of this accumulating water propagates downwards in the form of one or more diffusive pressure waves, thereby elevating porewater pressure in the underlying saturated zone. Given that on steeper slopes the saturated zone tends to be fairly thin, the pressure waves tend to reach the basal boundary in a relatively short time, and the

consequent rise of the water table and the elevation of the porewater pressure are therefore both initiated fairly rapidly (Baum et al. 2008; Baum et al., 2010). As discussed in Chapter 5 (Section 5.5), an elevation in positive porewater pressure below a rising water table contributes to a loss of shear strength and increases the likelihood of slope failure.

In this model, infiltration is simplified to a one-dimensional vertical flow through the unsaturated zone that is expressed in the form of Iverson's adaptation of the Richards equation to account for the slope of the ground surface and reduce the effect of gravity, as given in Eq. (5) (Baum et al., 2008; Baum et al., 2010).

$$\frac{\partial \theta}{\partial t} = \frac{\partial}{\partial Z}\left[K(\psi)\left(\frac{1}{\cos^2 \delta}\frac{\partial \psi}{\partial Z} - 1\right)\right] \tag{5}$$

Where: θ = the volumetric water content
Z = the vertical coordinate
$K(\psi)$ = the hydraulic conductivity function
ψ = the pressure head

Also in this model, hydraulic conductivity, and soil-water content in the unsaturated zone are variable and are determined by the pressure head. This relationship is expressed in Eq. (6) and Eq. (7).

$$K(\psi) = K_S \exp(\alpha \psi^*) \tag{6}$$

$$\theta = \theta_r + (\theta_s - \theta_r)\exp(\alpha \psi^*) \tag{7}$$

Where: ψ^* = $\psi - \psi_0$, where ψ_0 is a constant (defined below)
K_s = saturated hydraulic conductivity
θ_r = residual water content
θ_s = water content at saturation
α = a curve-fitting parameter approximately equal to the inverse of the air-entry suction

The parameter α in Eq. (6) and Eq. (7) is one of the two so-called "van Genuchten parameters". It is inversely proportional to the matric suction that exists at the point where air starts to enter the largest pores in a given soil, known as the "air-entry value" (AEV), or "bubbling pressure". The air-entry value for that soil is therefore dependent on the mean pore size (Fredlund and Xing, 1994). Thus, the AEV increases and α decreases as the size of the largest pores decreases. The value of α is obtained by fitting Eq. (6) to the soil-water characteristic curve (SWCC) for the soil under

consideration. A typical SWCC is shown in Figure 6-11. The SWCC for sensitive marine clays in the current study area is presented in Figure 6-16 below.

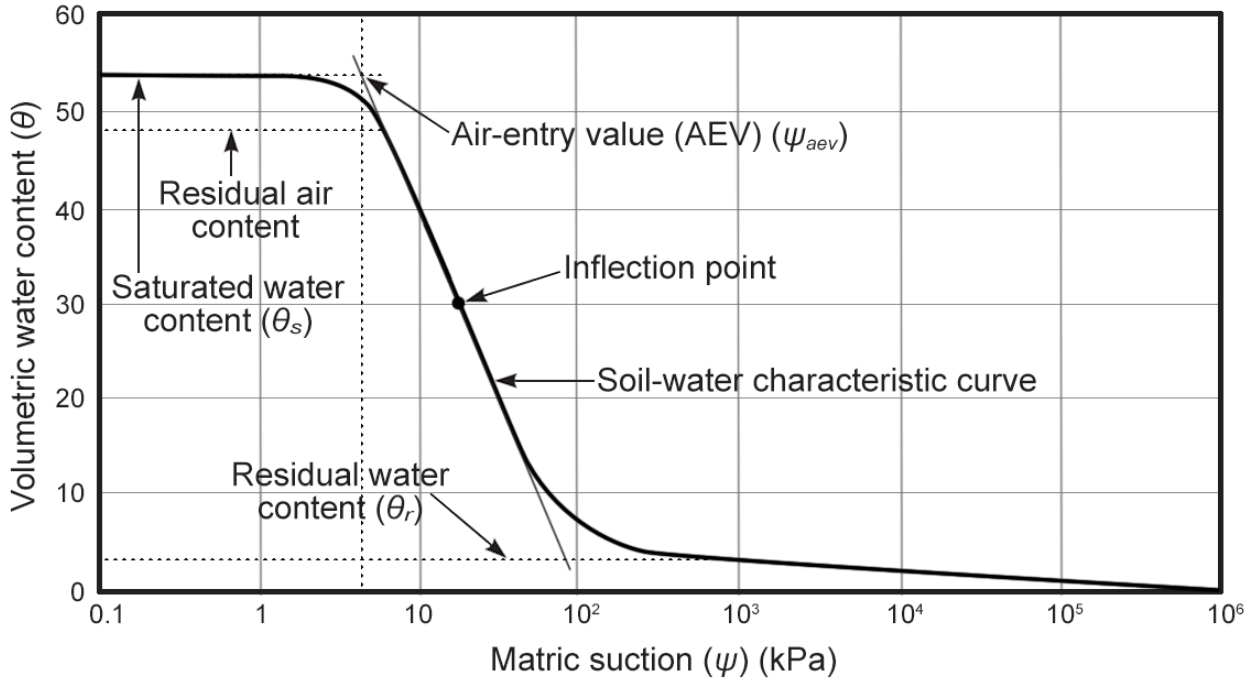

Figure 6-11 A typical soil-water characteristic curve (SWCC) (adapted from Fredlund and Xing, 1994).

In contrast to the unsaturated zone, in the capillary fringe and below the water table, hydraulic conductivity and soil-water content are constant and therefore independent of the pressure head, as noted earlier, briefly in Section 6.2.2.2.1.1. For practical purposes, hydraulic conductivity from the capillary fringe down to the basal boundary is equal to the soil's saturated hydraulic conductivity (K_s). The vertical height of the capillary fringe above the water table has been shown to be $1/\alpha$, and the pressure head at the top of the capillary fringe is, therefore, $\psi_0 = -1/\alpha$, as demonstrated by Savage et al, (2004). Eq. (6) and Eq. (7) can then be modified for the top of the capillary fringe, where $\psi = \psi_0$, by substituting $\psi_0 = -1/\alpha$ into the formula $\psi^* = \psi - \psi_0$, thus reducing Eq. (6) to $K(\psi) = K_s$ and Eq. (7) to $\theta = \theta_s$. It should be noted that one consequence of using $\psi_0 = -1/\alpha$ instead of $\psi_0 = 0$ is that the thickness of the unsaturated zone (that is, the depth to the top of the capillary fringe, d_u) is effectively reduced for calculation purposes, and this means that the time it takes for infiltrated rainwater to reach the saturated zone is correspondingly reduced in the simulation. To be specific, in Eq. (9) below, if the value of ψ_0 is taken as zero, then $d_u = d$, whereas if the value of ψ_0 is taken as $-1/\alpha$, then $d_u = d - 1/\alpha$ (Baum et al. 2008; Baum et al., 2010).

The final step in the calculation is the substitution of Eq. (6) and (7) into Eq. (5), which yields a linear partial differential equation in $K(Z,t)$, as shown in Eq. (8) (Baum et al. 2008; Baum et al. 2010).

$$\frac{\alpha_1(\theta_s - \theta_r)}{K_S}\frac{\partial K}{\partial t} = \frac{\partial^2 K}{\partial Z^2} - \alpha_1\frac{\partial K}{\partial Z} \tag{8}$$

To account for a sloping ground surface, coordinate transformation is applied with the formula: $\alpha_1 = \alpha\, cos^2\delta$ to account for the term $1/\cos^2\delta$ in Eq. (5) (Baum et al. 2008; Baum et al. 2010).

Assuming constant surface flux, the flux at the base of the unsaturated zone (q) is calculated using the following equations:

$$q(d_u,t) = \left\{ I_Z - 4(I_Z - I_{ZLT})\exp\left(\frac{\alpha_1 d_u}{2}\right)\exp\left(-D_\psi\frac{t}{4}\right) \cdot \sum_{m=1}^{\infty}\frac{\Lambda_m \sin(\Lambda_m\alpha_1 d_u)}{1 + \frac{\alpha_1 d_u}{2} + 2\Lambda_m^2\alpha_1 d_u}\exp\left[-\Lambda_m^2 D_\psi t\right] \right\} \tag{9}$$

Where: D_ψ = the soil-water diffusivity, which is calculated using Eq. (10) (below)
$D_\Psi t$ = the non-dimensional time
d_u = the vertical depth to the top of the capillary fringe
$\alpha_1 d_u$ = the non-dimensional depth
Λ_m = the roots of Eq. (11) (below)

$$D_\psi = \frac{\alpha_1 K_S}{(\theta_s - \theta_r)} \tag{10}$$

$$\tan(\Lambda\alpha_1 d_u) + 2\Lambda = 0 \tag{11}$$

As noted above, the hydraulic conductivity in the unsaturated zone depends on the pressure head and varies with depth. The initial condition, $K(Z,0)$. is given by the following equation:

$$K(Z,0) = I_{ZLT} - \left[I_{ZLT} - K_S\exp(\alpha_1\psi_0)\right]\exp[-\alpha_1(d_u - Z)] \tag{12}$$

TRIGRS takes into account the fact that during a rainstorm of varying intensities, the surface flux will be variable rather than constant, and therefore the flux at the base of the unsaturated zone will also be variable. To allow for variations in the flux at the base of the unsaturated zone, TRIGRS applies Heaviside series expansions to Eq. (9), as follows (Baum et al., 2008; Baum et al, (2010):

$$q(d_u,t) = \sum_{n=1}^{N} H(t-t_n) \left\{ \begin{array}{l} I_Z - 4(I_Z - I_{ZLT})\exp\left(\frac{\alpha_1 d_u}{2}\right)\exp\left(-D_\psi \frac{t}{4}\right) \\ \cdot \sum_{m=1}^{\infty} \frac{\Lambda_m \sin(\Lambda_m \alpha_1 d_u)}{1 + \frac{\alpha_1 d_u}{2} + 2\Lambda_m^2 \alpha_1 d_u} \exp\left[-\Lambda_m^2 D_\psi t\right] \end{array} \right\}$$
$$- \sum_{n=1}^{N} H(t-t_n) \left\{ \begin{array}{l} I_Z - 4(I_Z - I_{ZLT})\exp\left(\frac{\alpha_1 d_u}{2}\right)\exp\left(-D_\psi \frac{t}{4}\right) \\ \cdot \sum_{m=1}^{\infty} \frac{\Lambda_m \sin(\Lambda_m \alpha_1 d_u)}{1 + \frac{\alpha_1 d_u}{2} + 2\Lambda_m^2 \alpha_1 d_u} \exp\left[-\Lambda_m^2 D_\psi t\right] \end{array} \right\} \quad (13)$$

Hydraulic conductivity at the base of the unsaturated zone under variable surface flux is calculated using the following formula (Baum et al. 2010):

$$K(Z,t) = \sum_{n=1}^{N} H(t - t_n)$$
$$\cdot \left\{ \begin{array}{c} I_{nZ} - \left[I_{nZ} - K_s \exp(\alpha_1 \psi_0)\right] \exp[-\alpha_1 (d_u - Z)] \\ -4(I_{nZ} - I_{ZLT}) \exp\left(\frac{\alpha_1 Z}{2}\right) \exp\left[-D_\psi \frac{(t - t_n)}{4}\right] \\ \sum_{m=1}^{\infty} \frac{\sin[\Lambda_m \alpha_1 (d_u - Z)] \sin(\Lambda_m \alpha_1 d_u)}{1 + \frac{\alpha_1 d_u}{2} = 2\Lambda_m^2 \alpha_1 d_u} \exp\left[-\Lambda_m^2 D_\psi (t - t_n)\right] \end{array} \right\}$$
$$- \sum_{n=1}^{N} H(t - t_{n+1})$$
$$\cdot \left\{ \begin{array}{c} I_{nZ} - \left[I_{nZ} - K_s \exp(\alpha_1 \psi_0)\right] \exp[-\alpha_1 (d_u - Z)] \\ -4(I_{nZ} - I_{ZLT}) \exp\left(\frac{\alpha_1 Z}{2}\right) \exp\left[-D_\psi \frac{(t - t_{n+1})}{4}\right] \\ \sum_{m=1}^{\infty} \frac{\sin[\Lambda_m \alpha_1 (d_u - Z)] \sin(\Lambda_m \alpha_1 d_u)}{1 + \frac{\alpha_1 d_u}{2} + 2\Lambda_m^2 \alpha_1 d_u} \exp\left[-\Lambda_m^2 D_\psi (t - t_{n+1})\right] \end{array} \right\} \quad (14)$$

The pressure head in the unsaturated zone is calculated by solving Eq. (6) for ψ^* and then rearranging the equation to solve for $\psi(Z,t)$ and applying the coordinate transformation, as follows:

$$\psi(Z,t) = \frac{\cos\delta}{\alpha_1} ln\left[\frac{K(Z,t)}{K_S}\right] + \psi_0 \quad (15)$$

In Eq. (15), $K(Z,t) = K(\psi)$ from Eq. (8) and its values is calculated using Eq. (14). As noted earlier, TRIGRS adopts two values for ψ_0. For calculations at the water table, the value $\psi_0 = 0$ is used, and d, the depth of the water table, is substituted for d_u in all relevant equations. For calculations at the top of the capillary fringe, the value $\psi_0 = -1/\alpha$ is used, following Savage et al.

(2004). Using $\psi_0 = 0$ for the top of the capillary fringe returns a lower depth for the water table and also a slower rise of the water table (Baum et al. 2010). Calculation of the rate of rise of the water table is discussed below.

The volumetric soil-water content (θ) under variable surface flux is obtained by substituting the results of Eq. (15) into Eq. (7) (Baum et al. 2010).

6.2.2.2.2 The Model for Water-Table Rise

As noted earlier in this section, when infiltration occurs, under unsaturated initial conditions some of the infiltrated water is retained in the pores of the unsaturated zone and the rest percolates through the unsaturated zone until it reaches the water table. The amount of infiltrated water reaching the water table and the rate at which it accumulates is determined by the ratio of rainfall intensity to the soil's saturated hydraulic conductivity and other hydrogeological properties (Li et al, 2013). When the amount of this infiltrated water that has reached the water table exceeds the maximum amount of water that can be drained by gravity in the upper regions of the saturated zone, the water table rises (Baum et al. 2010). The water table is most likely to rise under one or more of the following conditions: (1) low-intensity, long-duration rainfall (rather than high-intensity, short-duration rainfall); (2) a shallow (rather than deep) water table; (3) a low (rather than high) groundwater recharge rate; and (5) an SWCC that shows high conductivity, and high soil-water content. The amount and duration of the rise and the time lag between the onset of the rainfall event and the onset of the resulting rise may vary widely from location to location depending on the angle and topology of the slope, the intensity and duration of the rainfall, the initial degree of saturation of the soil, and the saturated and unsaturated hydrogeological properties of the soil (Freeze and Cherry, 1979).

To determine the amount of rise of the water table in TRIGRS, the excess flux accumulating at the water table or at the top of the capillary fringe is compared with the available pore space directly above the water table or above the capillary fringe.

Excess flux at the water table or the top of the capillary fringe (q_{Zex}) is determined by either one of the two following equations (Baum et al. 2010):

$$\begin{aligned} q_{Zex} &= 0, \text{if } \mathrm{q}(d_u, t) \leq c_d(q_{Zmax} - I_{ZLT}) \\ \text{or:} \quad q_{Zex} &= \mathrm{q}(d_u, t) - c_{\mathrm{d}}(q_{Zmax} - I_{ZLT}), \text{if } \mathrm{q}(d_u, t) > c_d(q_{Zmax} - I_{ZLT}) \end{aligned} \tag{16}$$

Where: $\mathrm{q}(d_u, t)$ = the flux exiting from the base of the unsaturated zone, i.e., the value returned by Eq. (13)

c_d = a constant of value 1 when the basal no-flow boundary is at infinite depth, and 0.1 (set arbitrarily) when the basal no-flow boundary is at finite depth

q_{Zmax} = $K_S(\beta - 1)$, where: $\beta - 1$ is the long-term vertical hydraulic gradient

The volume of water arriving at the base of the water table, $V_A(t)$, is estimated by integrating the excess flux arriving at the water table over time, as determined by Eq. (16). The volume of fillable pore space, $V_f(Z,t)$, in the lower regions of the unsaturated zone is calculated as a function of height above the water table or the top of the capillary fringe, using the following equation, based on Eq. (6) and Eq. (7) (Baum et al. 2010):

$$V_f(Z,t) = (\theta_s - \theta_r)\left[d_u - Z + \frac{1}{K_S}\int_{d_u}^{Z} K(Z,t)dZ\right]$$
$$\text{and:} \quad T(Z,t) = \frac{1}{K_S}\int_{d_u}^{Z} K(Z,t)dZ \tag{17}$$

By integrating $K(Z,0)/K_S$ from Eq. (12) and $K(Z,t)/K_S$ from Eq. (14) with respect to Z, from the top of the saturated zone, , to Z, the following equations are obtained:

$$T(Z,0) = \frac{1}{K_S}\left\{I_{ZLT}(d_u - Z) - \left[I_{ZIT} - K_S \exp(\alpha_1 \psi_0)\right]\frac{1 - \exp[-\alpha_1(d_u - Z)]}{\alpha_1}\right\} \tag{18}$$

$$
\begin{aligned}
&T(Z,t)\\
&= \frac{1}{K_S}\sum_{n=1}^{N}\left\{\begin{array}{c} H(t-t_n)\left[I_{nZ}(d_u-Z)-\left[I_{nZ}-K_S\exp(\alpha_1\psi_0)\right]\dfrac{1-\exp[-\alpha_1(d_u-Z)]}{\alpha_1}\right]\\ -\left[\dfrac{2(I_{nZ}-I_{ZLT})}{\alpha_1}\exp\left(-D_\psi\dfrac{(t-t_n)}{4}\right)\right]\\ \left[\begin{array}{c}\displaystyle\sum_{m=1}^{\infty}\dfrac{\sin(\Lambda_m\alpha_1 d_u)\exp\left(-\Lambda_m^2 D_\psi(t-t_n)\right)}{\left(\Lambda_m^2+\frac{1}{4}\right)\left(1+\frac{\alpha_1 d_u}{2}+2\Lambda_m^2\alpha_1 d_u\right)}\\ \left[\begin{array}{c}2\Lambda_m\exp\left(\dfrac{\alpha_1 d_u}{2}\right)-\exp\left(\dfrac{\alpha_1 Z}{2}\right)\\ \left[\sin\left(\Lambda_m a_1(d_u-Z)\right)+2\Lambda_m\cos\left(\Lambda_m a_1(d_u-Z)\right)\right]\end{array}\right]\end{array}\right]\end{array}\right\}\\
&-\frac{1}{K_S}\sum_{n=1}^{N}\left\{\begin{array}{c} H(t-t_{n+1})\left[I_{nZ}(d_u-Z)-\left[I_{nZ}-K_S\exp(\alpha_1\psi_0)\right]\dfrac{1-\exp[-\alpha_1(d_u-Z)]}{\alpha_1}\right]\\ -\left[\dfrac{2(I_{nZ}-I_{ZLT})}{\alpha_1}\exp\left(-D_\psi\dfrac{(t-t_{n+1})}{4}\right)\right]\\ \left[\begin{array}{c}\displaystyle\sum_{m=1}^{\infty}\dfrac{\sin(\Lambda_m\alpha_1 d_u)\exp\left(-\Lambda_m^2 D_\psi(t-t_{n+1})\right)}{\left(\Lambda_m^2+\frac{1}{4}\right)\left(1+\frac{\alpha_1 d_u}{2}+2\Lambda_m^2\alpha_1 d_u\right)}\\ \left[\begin{array}{c}2\Lambda_m\exp\left(\dfrac{\alpha_1 d_u}{2}\right)-\exp\left(\dfrac{\alpha_1 Z}{2}\right)\\ \left[\sin\left(\Lambda_m a_1(d_u-Z)\right)+2\Lambda_m\cos\left(\Lambda_m a_1(d_u-Z)\right)\right]\end{array}\right]\end{array}\right]\end{array}\right\}
\end{aligned}
\tag{19}
$$

The conceptual basis of the water-table-rise model as discussed above is presented diagrammatically in Figure 6-12. As the diagram shows, the amount of water-table rise is estimated by linear interpolation on V_f between depths Z_k and Z_{k+1} to determine the height filled by volume V_A of infiltrated water.

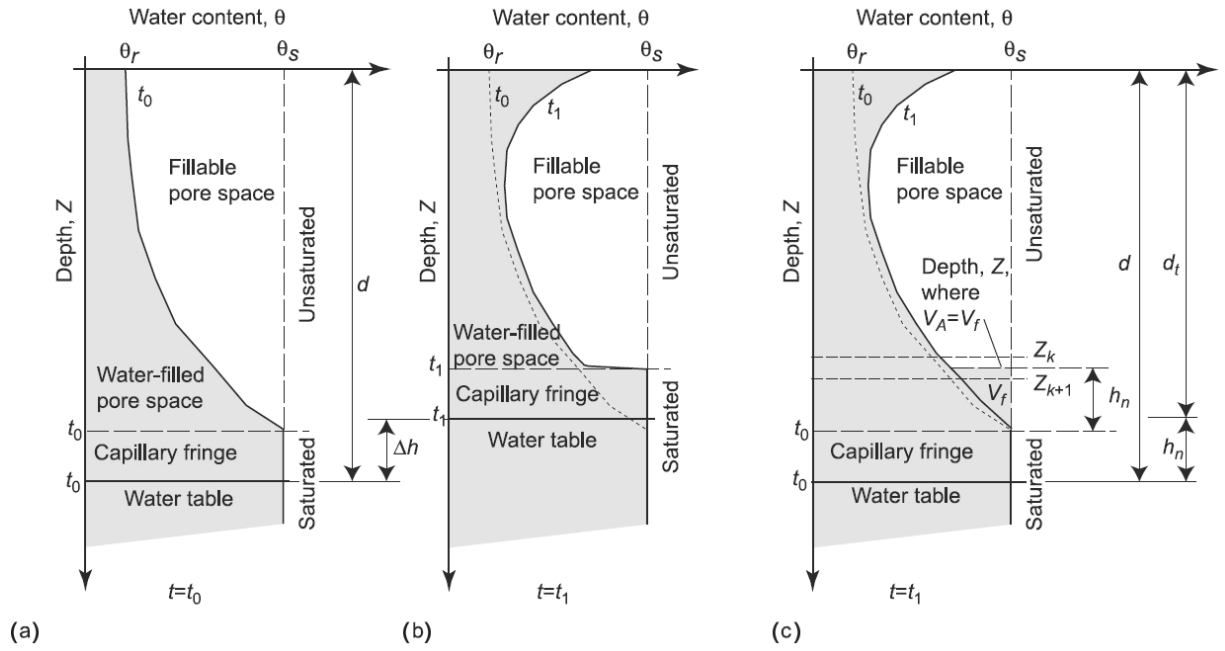

Figure 6-12 Water table rise resulting from infiltration as seen in a profile of soil-water content from the ground surface downward to an arbitrary depth (Z).
(a) Initial conditions at time (t_0), showing soil-water content (indicated by the shaded area) increasing with depth to the top of the capillary fringe (which is assumed to be saturated); (b) Conditions at some time after infiltration begins (t_1), showing the effect of infiltration on soil-water content and water-table rise (Δh). The shaded area between the dotted soil-water-content line marked t_0 and the solid line marked t_1 indicates the amount of infiltrated water absorbed by the soil in the unsaturated zone; (c) Approximations used by TRIGRIS in estimating water-table rise. The shaded area between the dotted soil-water-content line marked t_0 and the solid line marked t_1 indicates the computed amount of water absorbed by the soil, based on Eq. (6) and Eq. (14). The triangular area labelled V_A represents the cumulative volume of water computed to reach the water table (or the base of the unsaturated zone) between t_0 and t_1. The volume of fillable pore space, V_f, above the top of the capillary fringe (or the water table) is computed at evenly spaced depths using Eqs. (16) - (18). The water-table rise, h_n, is estimated by linear interpolation on V_f between depths Z_k and Z_{k+1} to estimate the height filled by volume V_A (modified from Baum et al. 2010).

6.2.2.2.3 Models for Pressure Diffusion below the Water Table

The final step of the hydrology model is the estimation of changes in the pressure head below the rising water table using one of the two models for pressure diffusion below the water table. For slopes with a relatively homogeneous soil, in which the saturated hydraulic conductivity is approximately constant with depth, the pressure rise is simulated using a model that has an impermeable basal boundary of infinite depth. The relevant equation is as follows (Baum et al., 2010):

$$\psi(Z_w,t) = \sum_{n=1}^{N} \psi_{hn}\, H(t - t_n)\mathrm{erfc}\left[\frac{Z_w}{2\sqrt{D_1(t - t_n)}}\right] - \sum_{n=1}^{N} \psi_{hn}\, H(t - t_{n+1})\mathrm{erfc}\left[\frac{Z_w}{2\sqrt{D_1(t - t_{n+1})}}\right] \quad (20)$$

Where: Z_w = the vertical distance below the initial water table, $Z_w = Z - d$.

For slopes that have a strong hydraulic conductivity contrast at shallow depth, the pressure rise below the water table is simulated by a model that has the impermeable basal boundary at a finite depth. The formula used is based on a Fourier series solution and employs the Heaviside step function, as follows (Baum et al., 2010):

$$\psi(Z_w,t) = \sum_{n=1}^{N} \psi_{hn}\, H(t - t_n) \cdot \left\{1 - \frac{4}{\pi}\sum_{m=1}^{\infty}(-1)^{m-1}\frac{1}{2m-1}\exp\left[-\frac{(2m-1)^2\pi^2 D_1(t - t_n)}{4d_{LZw}^2}\right] \cos\left[\frac{\pi}{2}(2m-1)\left(\frac{Z_w}{d_{LZw}} - 1\right)\right]\right\} - \sum_{n=1}^{N} \psi_{hn}\, H(t - t_{n+1}) \cdot \left\{1 - \frac{4}{\pi}\sum_{m=1}^{\infty}(-1)^{m-1}\frac{1}{2m-1}\exp\left[-\frac{(2m-1)^2\pi^2 D_1(t - t_{n+1})}{4d_{LZw}^2}\right] \cos\left[\frac{\pi}{2}(2m-1)\left(\frac{Z_w}{d_{LZw}} - 1\right)\right]\right\} \quad (21)$$

Where: d_{LZw} = the vertical height or thickness of the saturated layer, from the initial water table down to the impermeable basal boundary, $d_{LZw} = d_{LZ} - d$.

Eq. (20) and Eq. (21) contain *N* successive time steps to represent water-table rise from the initial base of the unsaturated zone. The time steps correspond to those in the unsaturated infiltration series (Baum et al., 2010).

6.2.2.3 The Slope Stability Model

The tool most commonly used in assessing slope stability and landslide susceptibility under conditions of infiltration from sustained rainfall is the Infinite Slope Model. It is incorporated into both GIS and TRIGRS (Dai and Lee, 2001; Fall et al. 2006; Raia et al. 2014; van Westen et al. 2006) The defining characteristic of the model is the estimation of the ratio of the downslope driving force (created by gravity) to the resisting force (created by friction). This ratio is referred to as the Factor of Safety (F_S). An $F_S > 1$ indicates stable conditions, and as FS drops below 1, instability begins to set in. That is to say, when the driving force exceed the resisting force, slope failure occurs. The depth (Z) at which F_S first drops below 1 is the depth at which the slip surface forms and the landslide is triggered (Baum et al., 2008; Baum et al. 2010; Park et al., 2013; Raia et al., 2014).

The model makes several simplifying assumptions that may not apply to all landslide-prone locations (Alvioli and Baum, 2016; Baum et al., 2008; Raia et al., 2014):

- that slope failure occurs at shallow depths and is translational (i.e., occurring along a plane);
- that the slip surface extends infinitely along the axis of the slope's gradient;
- that the slip surface is a plane at a fixed depth and parallel to the ground surface;
- that the slope is infinitely uniform and remains constant through time;
- that the thicknesses of the soil and the sliding mass are infinitely uniform and remain constant through time;
- that the geophysical and hydrological properties of the soil are infinitely uniform and constant through time;
- that porewater pressure is a function of only depth and time.

Baum et al. (2008), warn that if the infinite slope model is applied to locations where slope, thickness of soil, geophysical properties, or hydrological properties change abruptly, either spatially or temporally, (or where any of the other assumptions listed above are violated), the output is likely to contain errors. The infinite slope model is most accurate for locations whose geotechnical and hydrological conditions favour planar failure (i.e., translational landslides), which tend to occur at relatively shallow depths. Published studies of comparisons of various methods of slope stability analysis indicate that the infinite slope model calculates lower factors of safety than other, less simplistic (more rigorous), models when the location being assessed is prone to non-planar failures (i.e., rotational and other landslides) (Baum et al. 2008). It should be noted that non-planar landslides do occur in the study area and have occurred in the recent past (Brooks, 2019; Eden and Mitchell, 1970). A notable example of a non-planar landslide in the Ottawa area in recent history is the shallow rotational slip at Orleans in 1965 (discussed in some detail in Chapter 5, Section 5.5) (Eden and

Jarrett, 1971; Eden and Mitchell, 1970). Furthermore, like the Orleans rotational slip, the Breckenridge landslide of 1963 and the Rockcliffe landside of 1967 (also discussed in Section 5.5) occurred under conditions of high water table and heavy rainfall, which guaranteed fully saturated slopes in all three cases (Eden and Mitchell, 1970). Such landslides, it should be noted, are outside the scope of the current study, since they violate the assumptions of the infinite slope stability model.

As noted above, the factor of safety is the ratio of the driving force to the resisting force. During rainfall events, the primary process that contributes to an increase in the driving force and a decrease in the resisting force is infiltration of rainwater. The strength of the resisting force, also known as *shear resistance* or *shear strength*, is influenced by the porewater pressure and matric suction within the soil. As discussed in Chapter 5 (Section 5.5.), infiltration of rainwater can affect the shear strength of soils in one of two ways: (1) as rainwater enters the soil. a wetting front is formed, which advances downwards through the soil, creating a loss of matric suction (negative porewater pressure) behind the wetting front and causing a corresponding decline in unsaturated shear strength; (2) if infiltrated rainwater reaches the water table, the groundwater level rises, positive porewater pressure increases, and this reduces the soil's saturated shear strength. Thus, it should be noted, rainfall-induced slope failure takes into account both saturated and unsaturated shear strength, depending on the zone in which the failure occurs (Collins and Znidarcic, 2004; Li et al., 2013, Qiu et al., 2008; Rahardjo et al., 2019; Zhang et al. 2011; Zhang, et al, 2014). The mechanisms by which infiltration during rainfall events initiates slope failure are presented graphically in Figure 6-13.

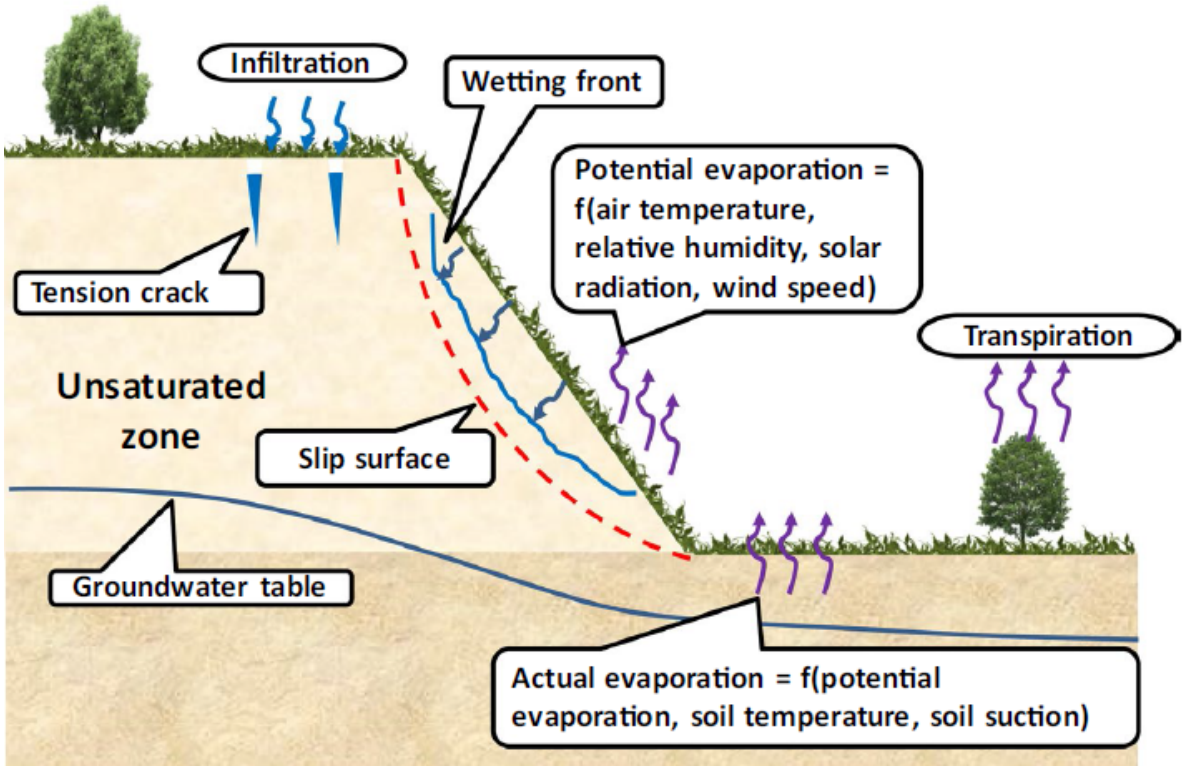

Figure 6-13 Mechanisms of rainfall-induced slope failure (Rahardjo et al., 2019).

Matric suction bears an inverse relationship to water content; thus, as water content increases, matric suction decreases. Changes in matric suction also affect the soil's hydraulic conductivity (or, permeability) in the same inverse manner: the lower the matric suction, the higher the hydraulic conductivity (Collins and Znidarcic, 2004; Rahardjo et al., 2019). Since the infiltration rate depends on the hydraulic conductivity, the higher the hydraulic conductivity, the higher the infiltration rate, and the shorter the time to a potential slope failure. A further variable that influences infiltration rate is rainfall intensity. If the rainfall intensity is less than the soil's hydraulic conductivity, the infiltration rate will be equal to the rainfall intensity, and consequently, all the rain that reaches the ground surface will enter the soil. If the rainfall intensity is greater than the soil's hydraulic conductivity, only part of the rain that reaches the ground surface will enter the soil, where it will eventually seep through into the groundwater, and the rest will travel downslope along the ground surface as runoff (Zhang et al, 2014). The higher the infiltration rate, the more rapid is the decline in shear strength, since the water content and porewater pressure increase—and the matric suction decreases—more rapidly. And the more rapid the decline in shear strength, the shorter the time it takes for potential slope failure to occur.

One way to understand the relationship between infiltration rate and slope failure is to consider the role played by hydraulic conductivity. When hydraulic conductivity tends to zero, infiltration does not occur and the infiltration rate is zero, so there is little likelihood of slope failure. At the other extreme, when hydraulic conductivity tends to infinity, the infiltration rate equals the rainfall intensity, infiltration is unimpeded, and the rainwater will pass right through the soil until the reaches the water table, at which point rainfall duration becomes the controlling factor in the likelihood of slope failure. However, between these two extremes there is a critical level of hydraulic conductivity at which the infiltration rate is sufficient to create the right conditions for slope failure, that is, loss of matric suction to the point at which the soil's shear strength is exceeded by the driving force (Collins and Znidarcic, 2004; Zhang et al, 2014). As noted earlier, the hydraulic conductivity of unsaturated soils varies, chiefly in relation to the soil-water content. However, the hydraulic conductivity of saturated soils is taken to be constant for all practical purposes.

TRIGRS calculates the factor of safety (F_S) for transient pressure heads (matric suction) at multiple depths (Z) and times (t) using the gravimetric soil-water content, as shown in Eq. (22) (Baum et al., 2008; Baum et al. 2010; Park et al., 2013).

$$F_S(Z,t) = \frac{\tan\varphi'}{\tan\delta} + \frac{c' - \psi(Z,t)\gamma_W \tan\varphi'}{\gamma_S Z \sin\delta\cos\delta} \tag{22}$$

Where: c' = soil cohesion for effective stress
φ' = soil friction angle for effective stress
$\psi(Z,t)$ = groundwater pressure head at depth Z and time t
δ = slope angle
γ_W = unit weight of water
γ_S = unit weight of soil

Failure is predicted if $F_S < 1$, and stability is indicated when $F_S > 1$. The depth Z at which F_S begins to drop below 1 is the depth of the slip surface and where the landslide is initiated. The time and depth at which slope failure occurs is determined by variations in the time and depth of the pressure head, which in turn is influenced by rainfall conditions on the slope.

A flowchart of the steps and procedures, along with the equations used in each step, that are involved in running TRIGRS through the various models described above is presented in Figure 6-14.

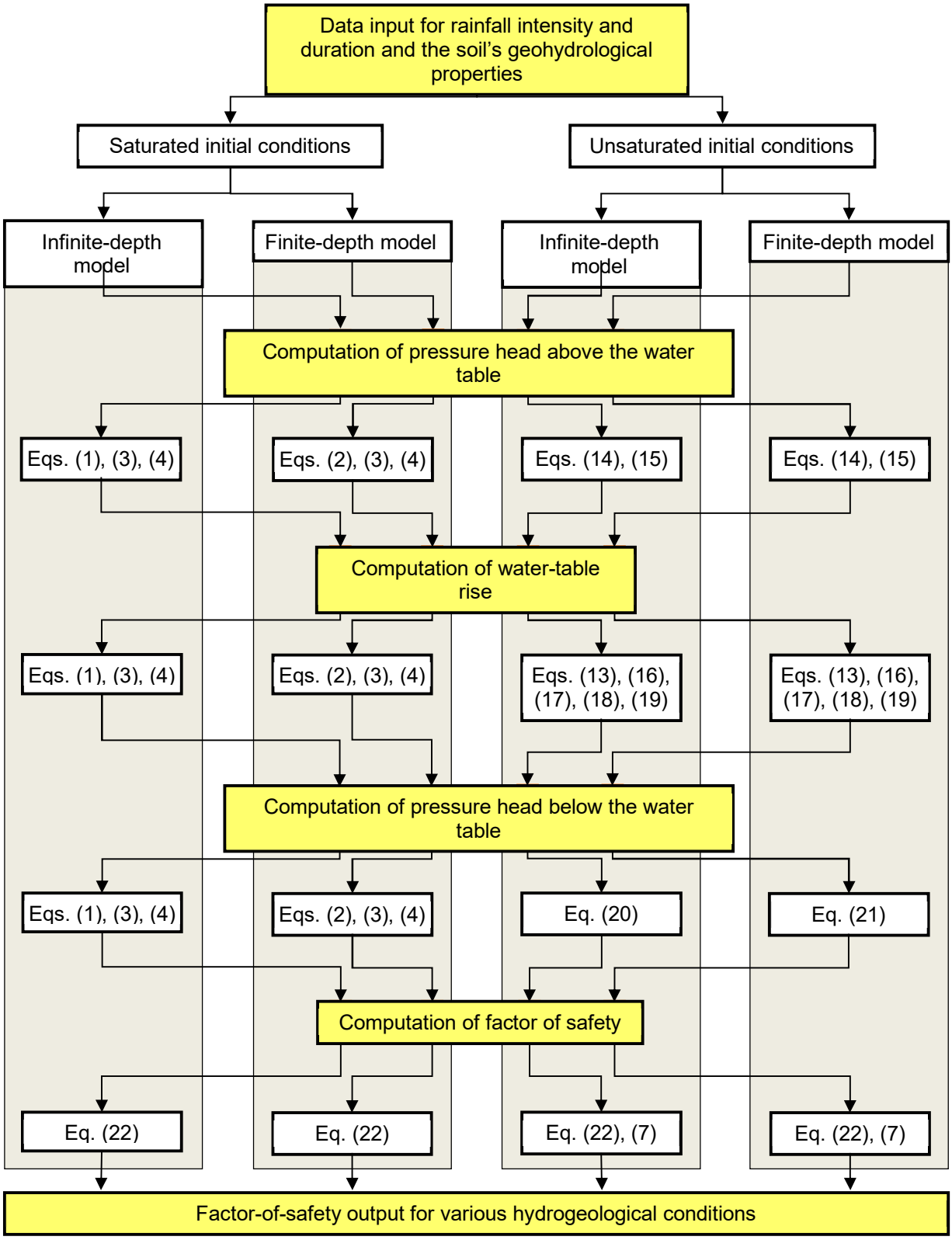

Figure 6-14 Flowchart of the steps and procedures used in TRIGIS with relevant equations (adapted from Baum et al. 2010).

6.3 Pilot Testing and Geotechnical Properties Sensitivity Analysis

In order to test the viability of the methodology chosen for the current study and to determine the limits of the study, a small area within the City of Ottawa with landforms and rainfall patterns typical of the general area was selected as the location in which to conduct a pilot study. The test site is located in Orleans, in the eastern part of Ottawa, as shown in Figure 6-15. It is 0.6 x 0.7 km (490,802 m^2), with elevations ranging from 53 to 88.7 mASL and slopes ranging from 3° to 58°. The average and water table level is 2.5 mBGS. This site was chosen because it is fairly representative of the range of topographical and geological features found in the Ottawa area

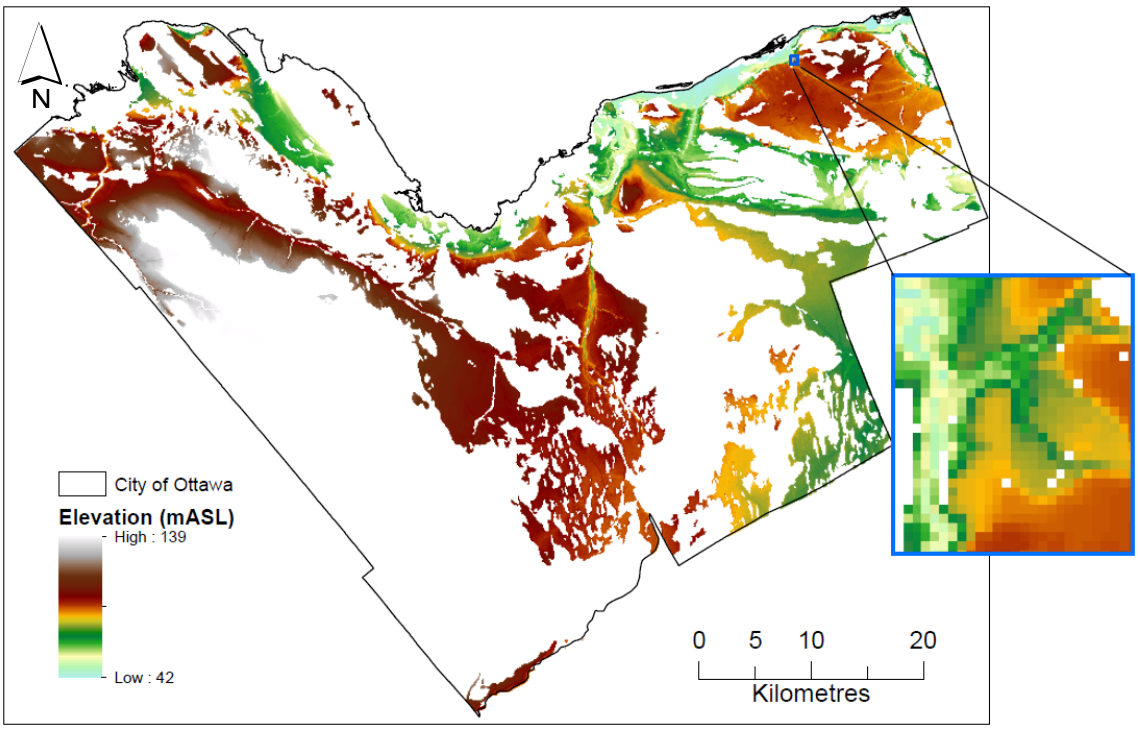

Figure 6-15 Location of the test area for the current study

The TRIGRS models were run using ranges of values for cohesion, effective internal friction, and unit weight of the soil. These ranges were obtained from recent geotechnical reports by engineering firms for engineering projects in the Ottawa area (as detailed earlier in Section 4.4 and Section 6.2.1.2), and from recent research papers, such as those by Al-Umar (2018), Nader (2014), and Taha (2010). These ranges and the values for other relevant parameters are listed in Table 6.2.

In order to simulate the most pessimistic outcome in the test run, the initial values used for the three geotechnical parameters with significant value ranges were the ones expected to return the lowest factor of safety, namely, the lowest values in the range for cohesion and effective internal angle

of friction, and the highest value for unit weight of soil. For the other parameters, such as soil water diffusivity and saturated hydraulic conductivity, average values were used, since the values for these parameters did not vary widely, and using ranges for them would not contribute significanlty to variations in the factor of safety. For volumetric water content at saturation and residual water content, data for these paramters collected by Taha (2010) were averaged, and the averages were used to plot the Soil-Water Characteristic Curve (SWCC), shown in Figure 6-16, from which the value for the inverted caillary fringe was determined.

Table 6.2 Input data for the TRIGRS model

Data Type	Values used	Unit
Geotechnical Data		
Effective cohesion (C')	5 - 12	kPa
Effective internal angle of friction (ϕ')	27 - 38	degrees
Saturated unit weight of soil (γ_s)	15.5 - 19	kN/m^3
Hydraulic diffusivity (D_0)	2.00025x10^{-6}	m^2/s
Saturated hydraulic conductivity (K_s)	5.08x10^{-8}	m/s
Volumetric soil-water content at saturation (θ_s)	0.6	-
Residual Water Content (θ_r)	0.03	-
Inverted Capillary Fringe (α)	-0.01221	-
Other input data		
Rainfall duration	12, 24, 48	hr
Rainfall return period	10, 50	years
Unit weight of water	9.8	kN/m^3
Water table depth (vertical)	0.6 – 36.4	mBGS
Slope angle	3 - 58	degrees
Elevation	53.0 - 88.7	mASL

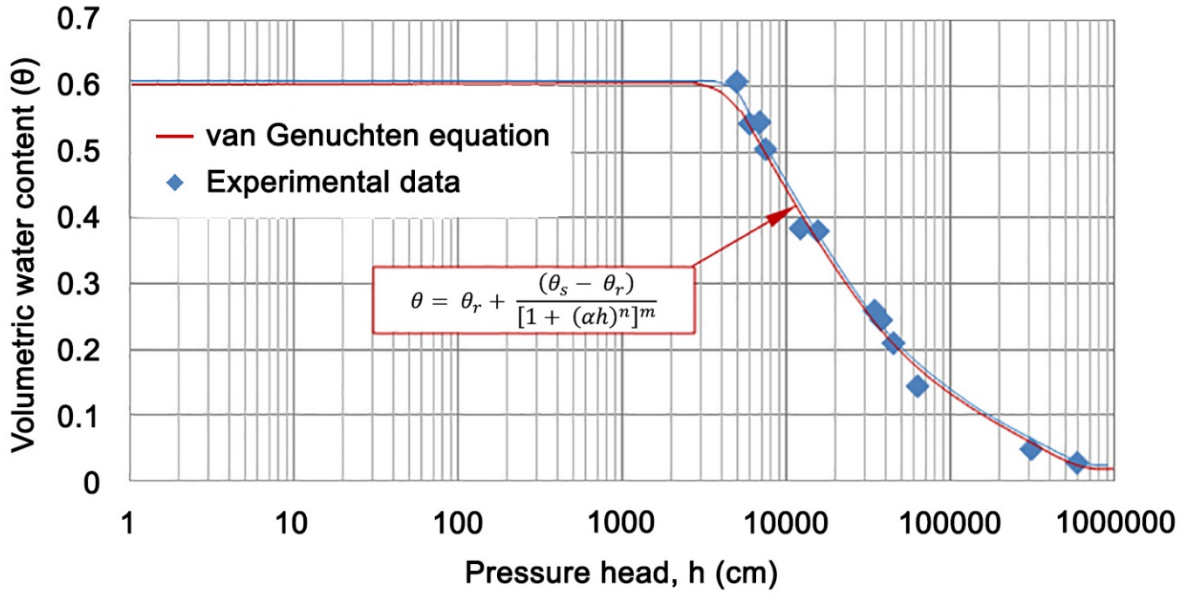

Figure 6-16 Soil-Water Characteristic Curve (SWCC) for sensitive marine clay in the Ottawa area (based on Taha, 2010).

The model was calibrated using the geotechnical properties from one of engineering slope stability analysis report in Orleans conducted by LRL Assosiated Ltd. in 2017. At initial condition (0s), the factor of safety result from TRIGRS (1.529) shows similar value comparing to the value in report (1.526) as shown in Figure 6-17.

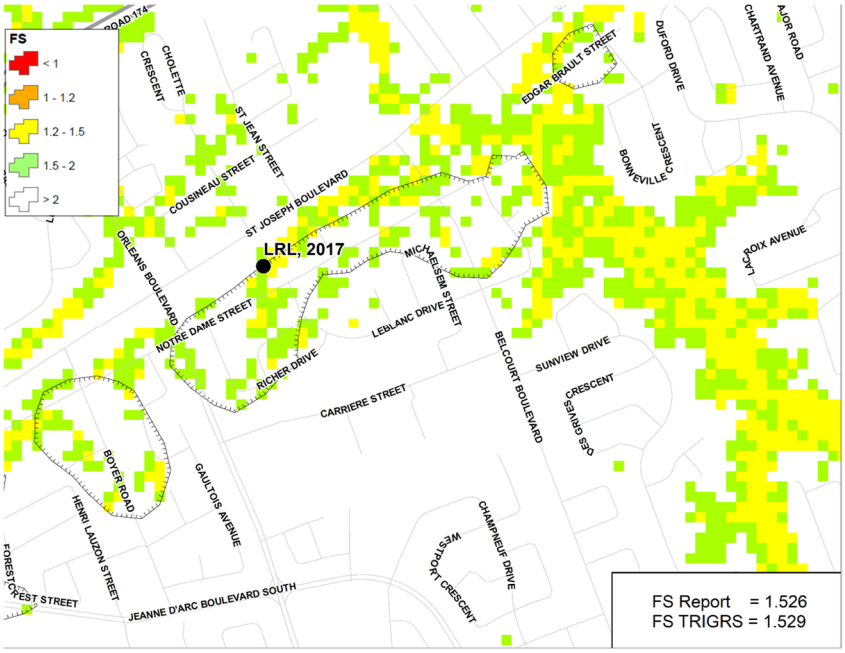

Figure 6-17 Model Calibration (LRL, 2017).

The test run began by inputting rainfall data derived from the IDF curves obtained by the procedures described in Section 6.2.1.5. above. Rainfall intensities for return periods of 2 years and for durations of 6, 12, and 24 hr from historical rainfall IDF and projected IDF from RCP 4.5 were used.

The results of the initial test run from rainfall durations of 6, 12, and 24 hr did not show any change to the FS for the test area. The rainfall duration of 48 hr interpolated from the IDF curves were added to the run. Results of the adjusted test run are presented in Figure 6-18. As the figure shows, the TRIGRS analysis returned a lowest value of 1.06 for the factor of safety in the test area after 48 hr of constant rainfall, the FS changes to very small area or only shows in few pixels. There were no changes to FS from rainfall duration of 6, 12, and 24 hr. Therefore the rainfall duration of 6 hr were dropped from the rest of the model simulations. It is to notice that the percentages of the rainfall runoff are decreasing as the rainfall duration is longer and slightly higher for projected rainfall from RCP 4.5 than the historical rainfall.

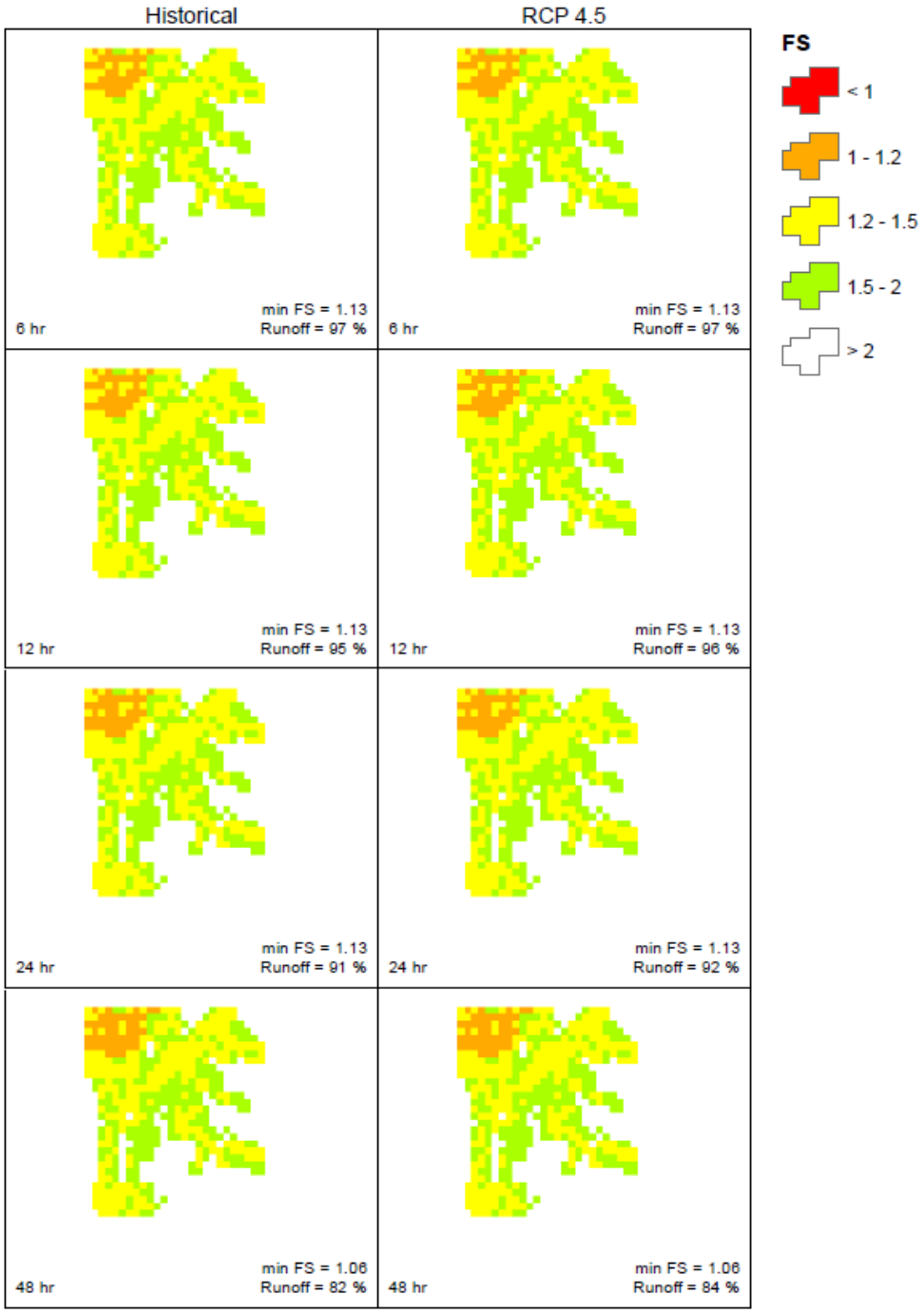

Figure 6-18 Results of the test run using a rainfall intensity from return period of 2 years and for duration of 6, 12, 24, and 48 hr from IDF of historical and projected rainfall RCP 4.5.

The infiltration rate for the test runs for each rainfall durations was the same, and it remained constant throughout both simulations, at 5.08×10^{-8} m/s (Figure 6-19). This is because the infiltration rate cannot exceed the soil's saturated hydraulic conductivity at the ground surface, and the

saturated hydraulic conductivity of Ottawa's sensitive marine clays is relatively low, at 5.08×10^{-8} m/s. These results of the infiltration rate analysis indicate that infiltration rate is not a significant factor in landslide susceptibility in Ottawa's sensitive marine clays. Regardless of the intensity of the rainfall, if the rainwater that reaches the ground surface exceeds the soil's hydraulic conductivity, the excess rainwater (that which does not enter the ground through infiltration) leaves the area in the form of runoff. The role of runoff in the development of slope instability and failure was not investigated in the current study.

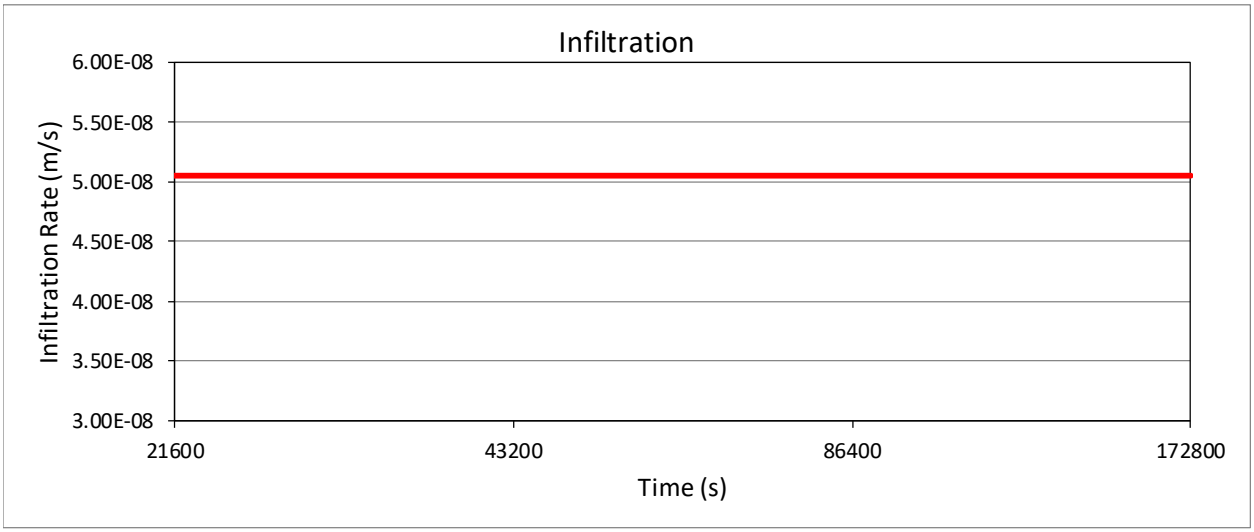

Figure 6-19 Infiltration rate over time

The independence of the factor of safety from rainfall intensity in the case of Ottawa's marine clays is presented in Figure 6-20. Note in the graph that for both historical rainfall intensities (lower intensities) and projected RCP4.5 rainfall (higher intensities), the change in the factor of safety over time is exactly the same.

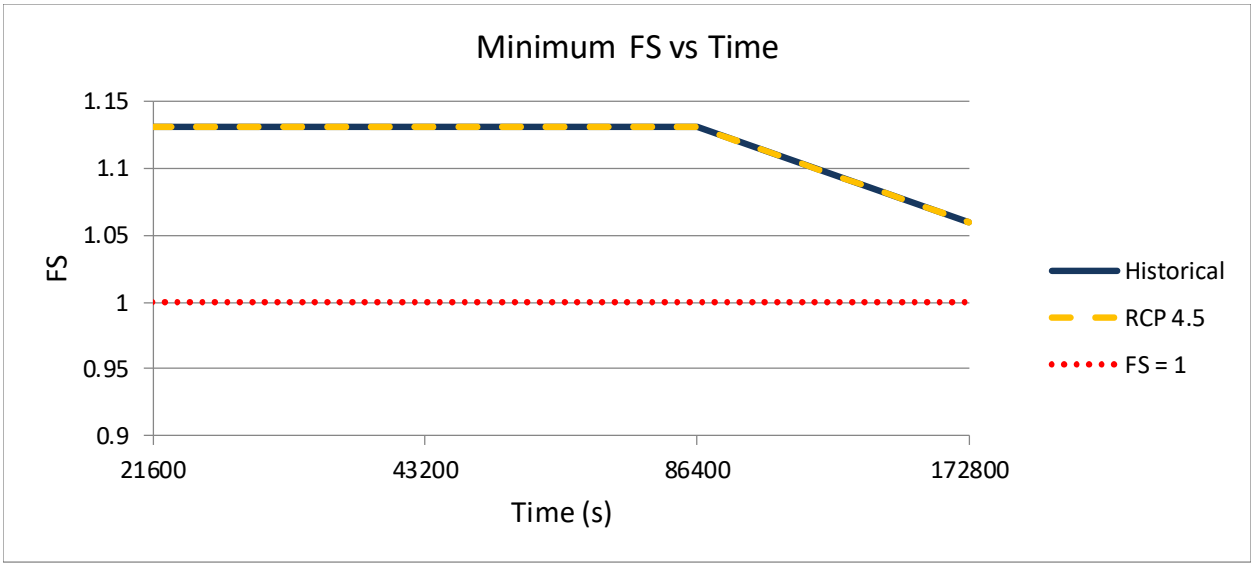

Figure 6-20 Factor of safety over time under return period of 2 years and for duration of 6, 12, 24, and 48 hr from IDF of historical and projected rainfall RCP 4.5.

As noted above, the three parameters with significant value ranges were: (1) cohesion; (2) effective internal angle of friction; and (3) unit weight of the soil. The next step in the pilot testing phase was to examine the ranges of these geotechnical properties with regard to the effect on factor of safety. The three parameters were each examined separately, varying the value of the parameter in question, while keeping the other parameters constant. The rainfall intensity in all cases was set at 1.13 mm/h, and the duration of rainfall was set to 48 hr. The purpose of examining each prameter separately was to determine whether varying the values within the obtained range for the parameter in question made any significant difference in the factor of safety.

6.3.1 Cohesion Test

As noted in previous sections, a decrease in soil cohesion causes a reduction in the soil's shear strength, and the lowering of shear strength contributes to slope instability, and therefore to the slope's susceptibility to landslides. It was also noted earlier that as soil-water content increases, soil cohesion decreases. Infiltration from rainfall increases the soil-water content, and the longer the duration of the rainfall, the greater the corresponding increase in soil-water content. Thus, it is vital to test the relationship between rainfall duration and soil cohesion in assessing landslide susceptibility under climate change.

The cohesion test started at the lower end of the range, with a cohesion value of 5 kPa, and proceeded in 1kPa increments up to 12 kPa, at the upper end of the range (see Table 6.2 above). The

resulting plot of factor of safety versus cohesion across the values range for various rainfall durations is presented in Figure 6-21. As expected, lower cohesion values result in lower FS values, or greater susceptibility to landslides. For example, a cohesion value of 5 kPa yields the lowest FS of 0.74.

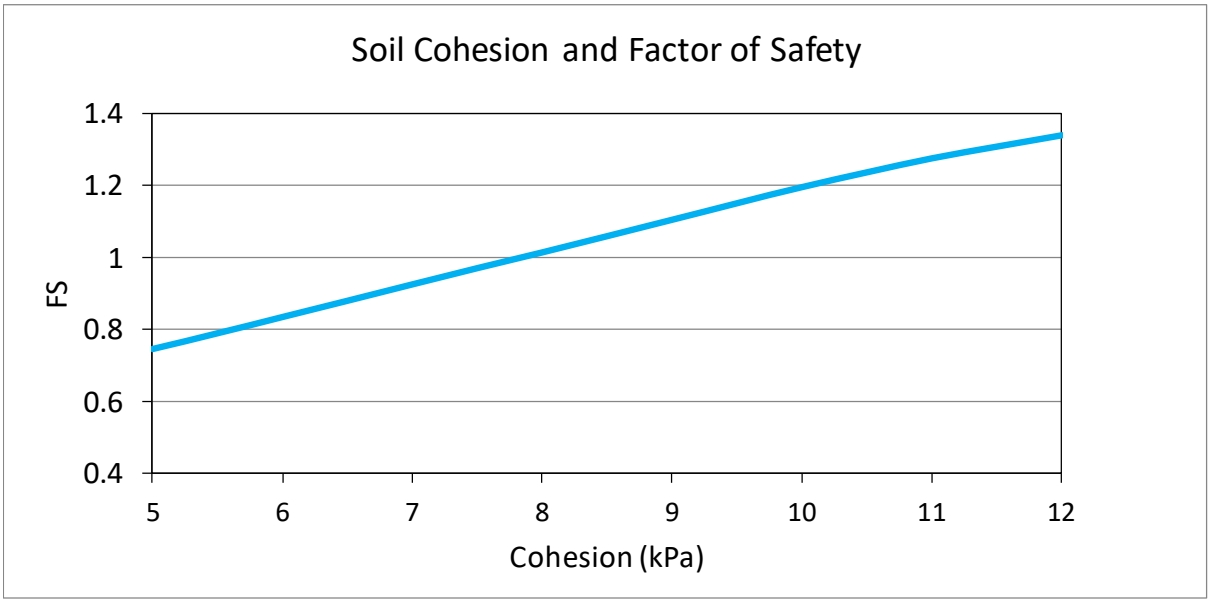

Figure 6-21 The relationship between soil cohesion and factor of safety.

6.3.2 Effective Internal Angle of Friction Test

The effective internal angle of friction is another crucial parameter that affects the factor of safety of a given slope, since it is also one of the properties that determine the soil's shear strength, as discussed in previous sections. The lower the internal angle of friction, the lower the soil's ability to resist shearing forces. In addition, as with soil cohesion, the internal angle of friction is in an inverse relationship to soil-water content. That is, the higher the soil-water content, the lower the angle of friction. As noted, before, soil-water content increases with an increase in the duration of rainfall. The purpose of the angle of friction test was to examine the effect of rainfall duration on the angle of friction across the range of values obtained for Ottawa's sensitive marine clays.

The results of the test are presented in Figure 6-22. The range of values obtained from the experimental data, as noted in Table 6.2 above, was 27° to 38°. As expected, at the bottom end of the range, an internal angle of friction of 27° returned the lowest value for FS. As the graph shows, the factor of safety is not greatly affected by changes in the internal angle of friction, with a 11° increase in the angle producing less than a 0.15 increase in FS.

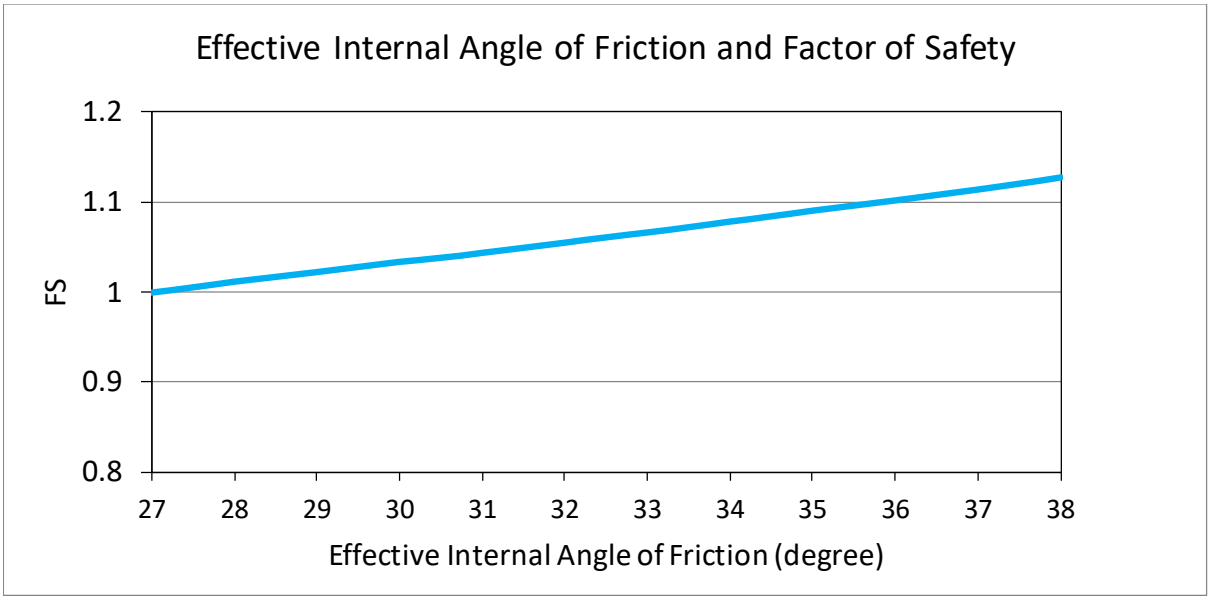

Figure 6-22 The relationship between effective internal angle of friction and factor of safety.

6.3.3 Unit Weight of Soil Test

The saturated unit weight of the soil is another parameter that contributes to a soil's shear strength and therefore to the factor of safety, slope failure, and landslide susceptibility. In addition, the unit weight of the soil has an inverse relationship to infiltration rate. That is, the higher the unit weight of the soil, the slower the infiltration rate and therefore the greater the amount of time taken for the factor of safety to drop below 1. The purpose of the unit weight of soil test was to investigate the effect of varying unit weight of soil obtained from the experimental on the factor of safety.

The results of this test are presented in Figure 6-23 below. From the graph it can be seen that unit weight of soil is negatively correlated with factor of safety, but the effect is small. At the bottom end of the range, a unit weight of 15 kN/m^3 returns a FS value of 1.12, while at the top end of the range, a unit weight of 19 kN/ m^3 returns an FS value of 1.02.

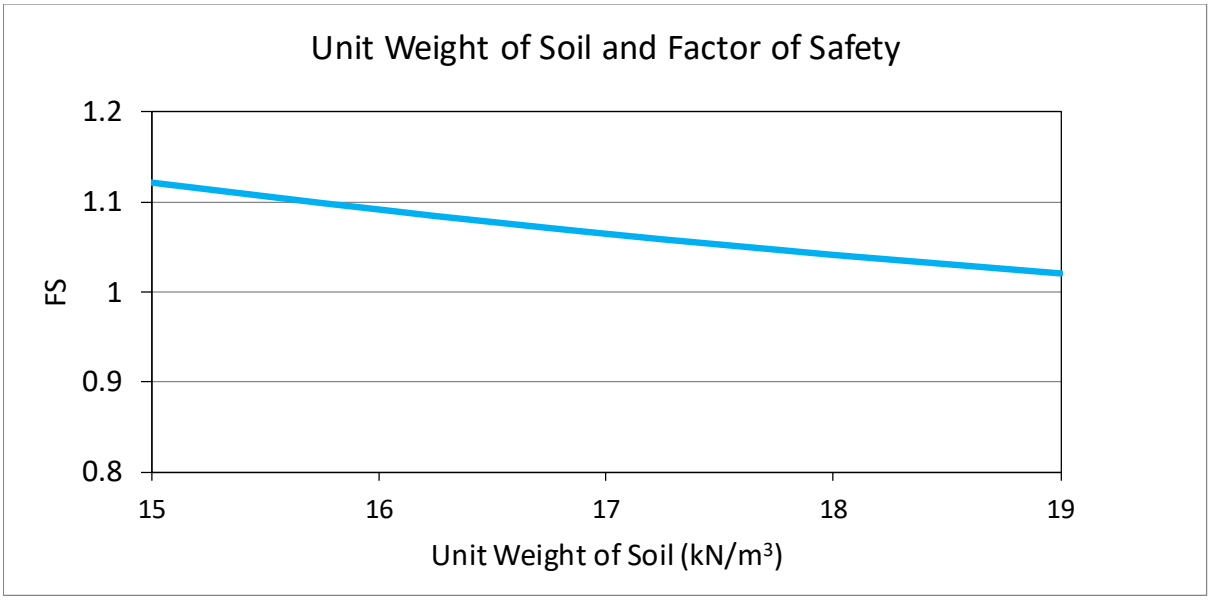

Figure 6-23 The relationship between unit weight of soil and factor of safety.

6.3.4 Results of the Pilot Tests

The tests described above confirm the relationship between effective cohesion, effective Internal friction, and unit weight of soil and factor of safety. Additionally, given that there were differences in factor of safety across the ranges of values for the three parameters tested, it was decided to create three categories (or "scenarios") for the values of these parameters: (1) low (or "ideal"); (2) medium (or "normal"); and high (or "worst-case"). The three "scenario" categories with their respective value ranges for the three parameters and the values for other geotechnical parameters are listed in Table 6.3, below.

Table 6.3 Parameters for the three scenarios used in the study

		Scenarios		
Geotechnical Properties	**Unit**	**Ideal**	**Normal**	**Worst-case**
Effective Cohesion (C')	kPa	12	8.5	5
Effective Internal Friction (ϕ')	degrees	38	32.5	27
Unit Weight of Soil (γ_s)	kN/m^3	15.5	17.25	19
Hydraulic Diffusivity (D_0)	m^2/s	2.00025E-06	2.00025E-06	2.00025E-06
Saturated Hydraulic Conductivity (K_s)	m/s	5.05E-08	5.05E-08	5.05E-08
Volumetric Water Content at Saturation (θ_s)	-	0.6	0.6	0.6
Residual Water Content (θ_r)	-	0.3	0.3	0.3
Inverted Capillary Fringe (α)	-	-0.01221	-0.01221	-0.01221

6.4 Results of the TRIGRS Simulation of Rainfall-Induced Landslides in Ottawa's Sensitive Marine Clays

The TRIGRS model was run for three rainfall durations (12 hr, 24 hr, and 48 hr) with the projected rainfall intensities from RCP4.5 and RCP8.5 IDF curves for return periods of 10 and 50 years. As mentioned in section 6.3, the rainfall duration of 48 hrs was added to the model and rainfall intensities were interpolated from the IDF curves due to the factor of safety value not showing any significant changes from rainfall duration of 24 hr results, taking into consideration that it is possible for future rainfall duration of more than 24 hours.

The factors of safety that were returned for the various simulations did not differ markedly from each other with variation in rainfall intensity. At the high end, a rainfall intensity of 7.07 mm/h produced similar factor-of-safety patterns as a rainfall intensity of 1.13 mm/h, at the low end. This is largely because in the simulations the infiltration rate is not affected by changes in rainfall intensity and remains constant at 5.05×10^{-8} m/s. The factor-of-safety patterns projected by the simulations for the three scenarios under RCP4.5 and RCP8.5 for the 10 year returning rainfall intensities are presented in the landslide susceptibility maps displayed in Figure 6-24 to Figure 6-26. Enlarge of individual results from Figure 6-24 to Figure 6-26 can be found in Appendix B-1-B-18. Results from the 50 year returning period are not present in this paper as the results of the factor-of-safety patterns being similar to the results presented from the 10 year returning period. The difference is the rainfall runoff which will be discussed later in this section.

The initial slope stability (at t = 0) is based on the geotechnical data, the slope, and water table levels that were input into the model as the initial conditions. At this initial stage, only the worst-case scenario returns some areas of slope instability (i.e., with FS < 1). These areas are located along the river valleys and along the banks of the Ottawa River in the eastern part of the city. As the simulation proceeds through longer and longer rainfall durations, the extent of these areas of slope instability increases.

For example, under the worst-case scenario, as the simulation progresses from 24 hours to 48 hours (see Figure 6-26), the factor of safety decreases. There is a slight increase in the areas with slope instability (see Figure 6-27). Thus, what the simulation shows is that the longer the duration of the rainfall, the greater the areas that become susceptible to rainfall-induced landslides. The relationship between factor of safety and rainfall duration is different for each area. Some areas may become unstable at a longer time (longer than 48 hours), however the IDF is unavailable for longer rainfall periods due to the high uncertainty.

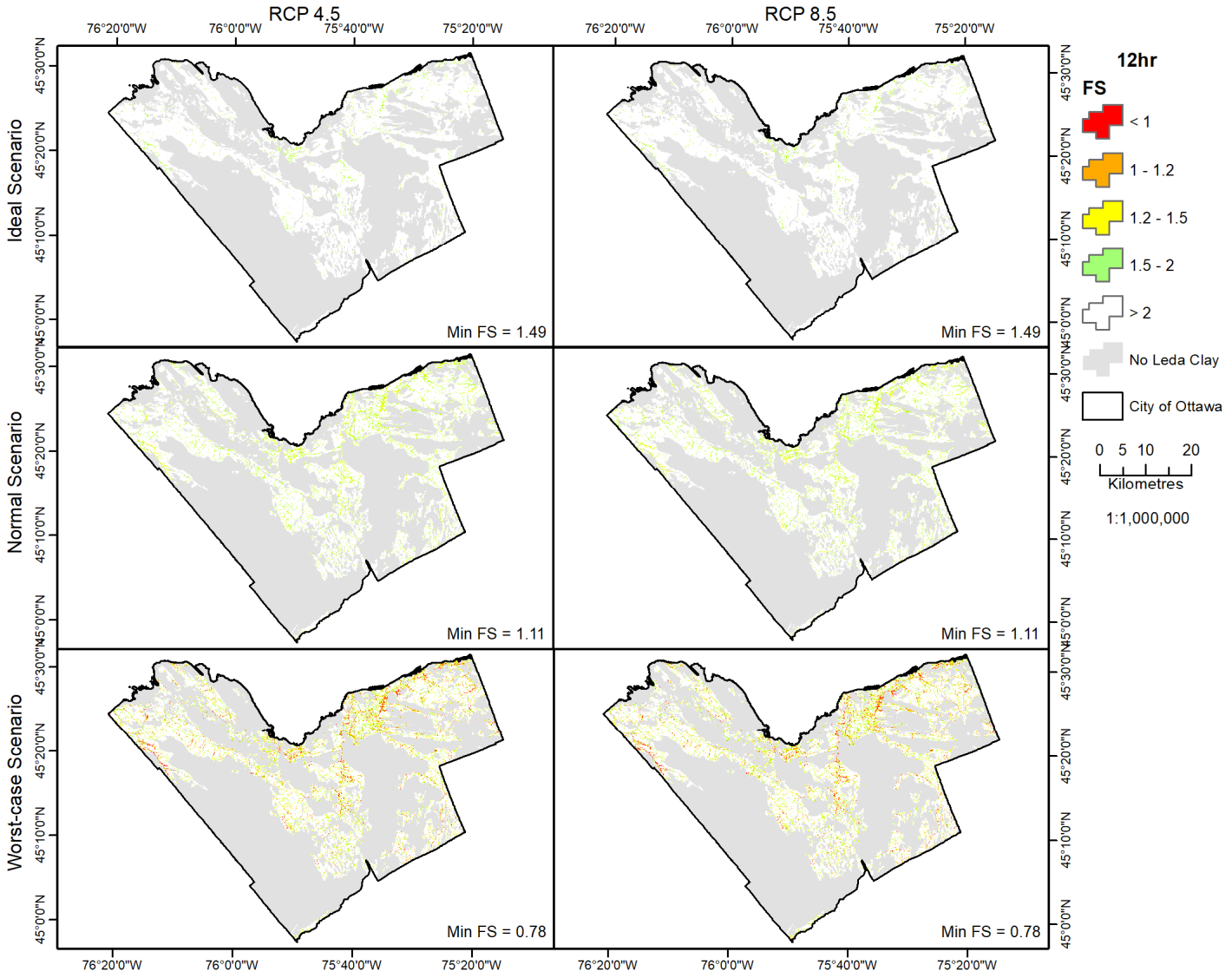

Figure 6-24 Factors of safety for sensitive marine clay in the study area computed by TRIGRS for time (t) = 12 hr under 10 years IDF RCP 4.5 and 8.5 for the ideal scenario, normal scenario, and the worst-case scenario. See enlarge figures in Appendix B1-B6

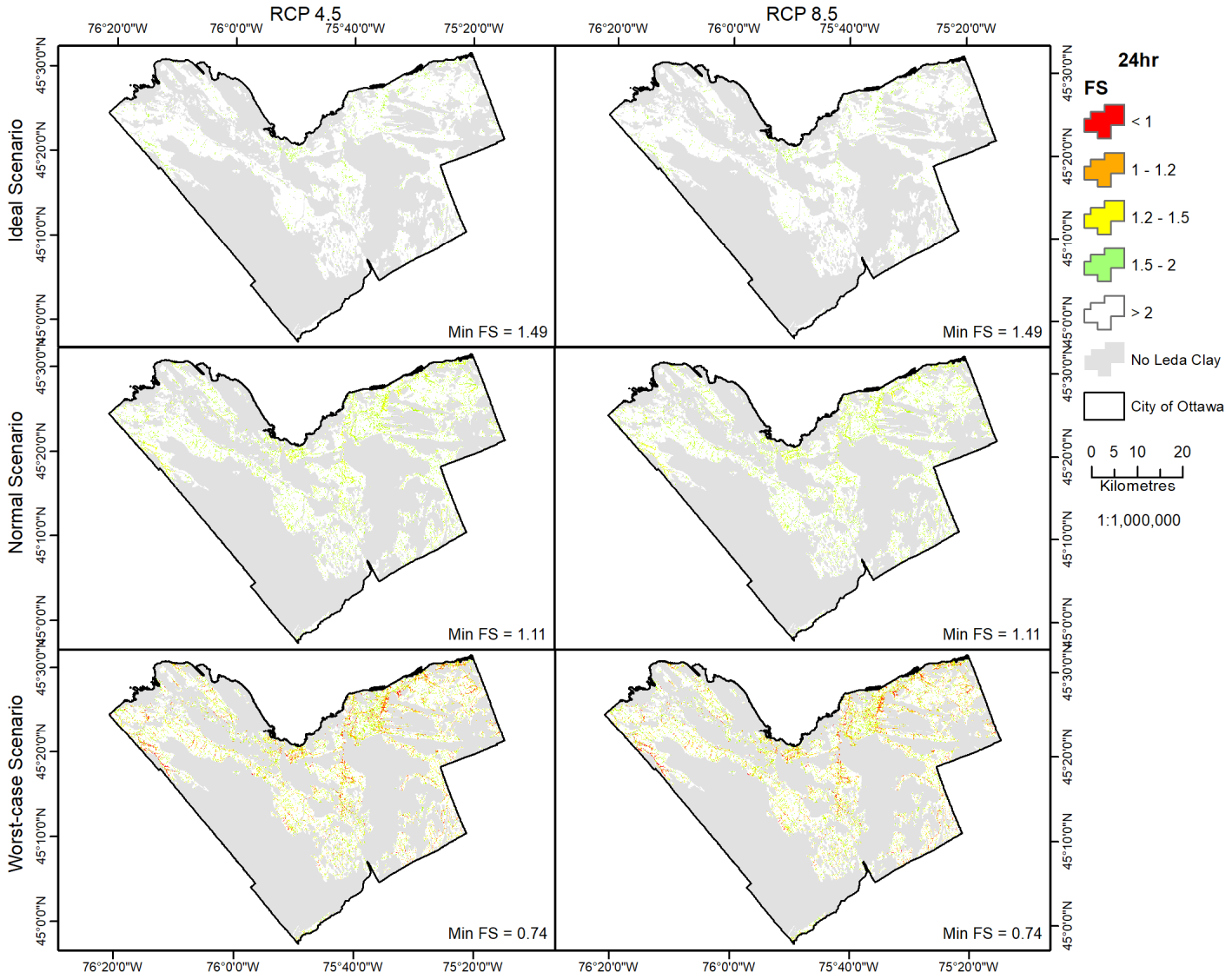

Figure 6-25 Factors of safety for sensitive marine clay in the study area computed by TRIGRS for time (t) = 24 hr under 10 years IDF RCP 4.5 and 8.5 for the ideal scenario, normal scenario, and the worst-case scenario. See enlarge figures in Appendix B7-B12

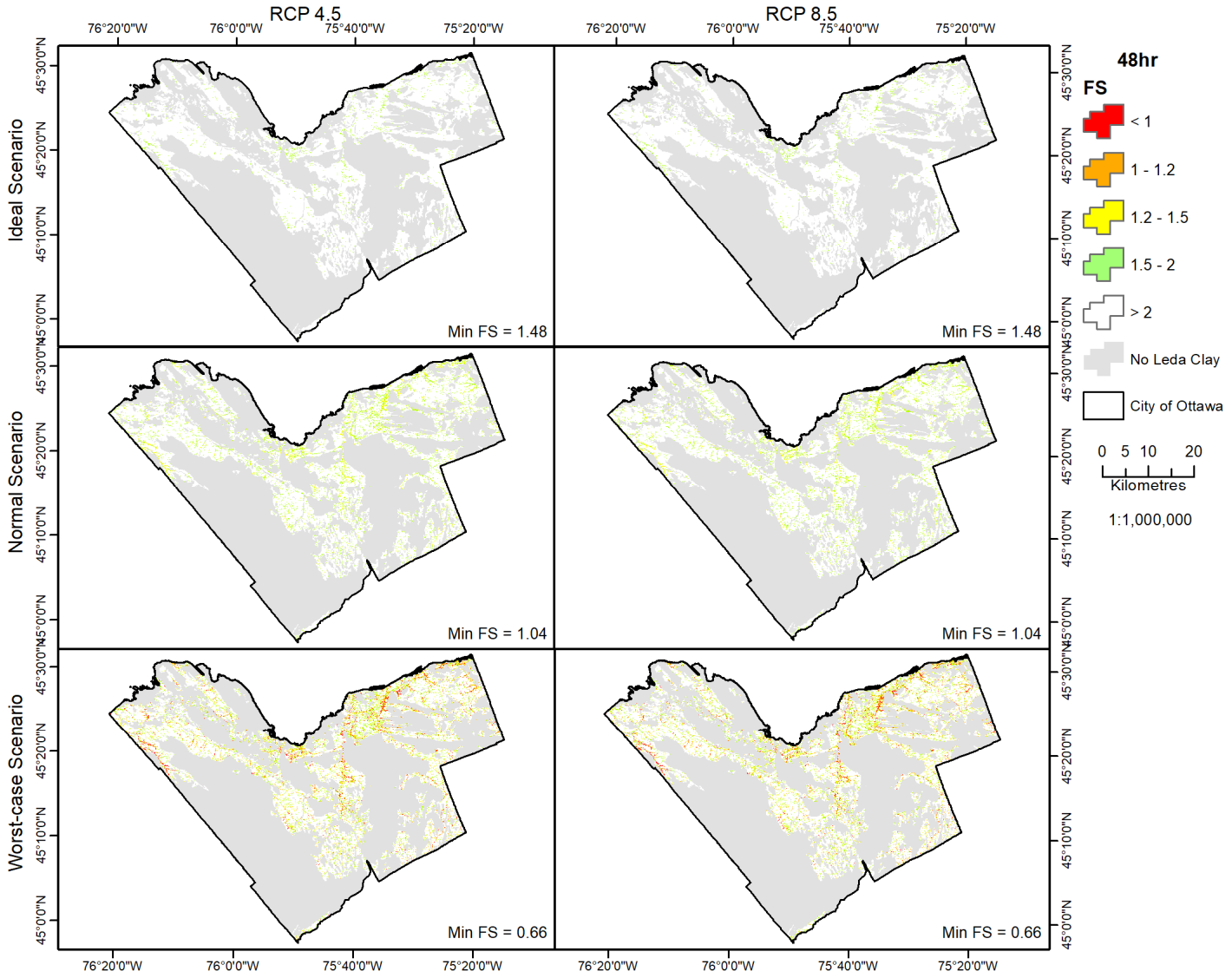

Figure 6-26 Factors of safety for sensitive marine clay in the study area computed by TRIGRS for time (t) = 48 hr under 10 years IDF RCP 4.5 and 8.5 for the ideal scenario, normal scenario, and the worst-case scenario. See enlarge figures in Appendix B13-B18

Changes in the distribution of various levels of factor of safety that occur as rainfall duration increases are presented in Figure 6-27. Under the worst-case scenario, the total area having FS < 1 is 24 km^2 (at t = 24 and 48 hours). The change of area having FS < 1 from t = 24 to t = 48 is insignificant. However, the minimum value of factor of safety is lower at longer rainfall durations as shown in Figure 6-24 to Figure 6-26. In other words, as the rainfall duration is longer, the lower the factor of safety, and the soil stability decreases. However, at rainfall duration of 48 hr the total area becomes susceptible to landslide (FS <1) does not change or only slightly changes.

The worst-case scenario shows some areas having FS < 1 at t = 0. Ideally, the simulation should not return FS < 1 at t = 0, since all slopes are assumed to be stable until slope failure actually occurs, and at t = 0 (i.e., the beginning of the simulation) there are no triggering factors at play that would initiate slope failure. The fact that under the worst-case scenario, the simulation identified an area of 24.5 km^2 as having FS < 1 at the beginning of the simulation may be explained by the fact that while the input for this scenario used the most unfavourable values for the various geotechnical and other parameters, it is unlikely that these values would all exist in that particular combination at the same time in any given location. The worst-case scenario is a hypothetical construct in which all the most unfavourable values come together in one location at the same time, a condition that is unlikely to exist in reality. In other words, if all the most unfavourable conditions were to exist at the same time at some locations in the study area, then 24 km^2 of this area would experience slope instability. What is of greater concern in these results is that it is only in the worst-case scenario that the simulation returns any areas with FS < 1. In the other two scenarios, the simulation does not identify any areas experiencing slope instability following any duration of rainfall, and therefore it predicts no susceptibility to rainfall-induced landslides anywhere in the marine clay zones of the study area. This may be explained by the fact that the geotechnical parameters from soil samples and the distribution of the soil samples is a crucial factor to the model in calculating the safety factor.

The comparison of areas for various levels of factor of safety between RCP4.5 and RCP8.5 is shown in Figure 6-27. The comparison of areas distribution for each range of factor of safety between RCP4.5 and RCP8.5 are identical. Note that the rainfall intensities from RCP8.5 projection is higher than the projected rainfall intensities from RCP4.5. This figure also confirmed that the factor of safety does not decrease with higher rainfall intensity due to very low infiltration rate. However, higher surface runoff is observed from the water balance calculation results from the model simulations as presented in Figure 6-28. The higher rainfall intensity the higher percentage of surface water runoff. For example, the RCP8.5 rainfall intensities are overall higher than rainfall intensities from RCP4.5, the percentage runoff from RCP8.5 is higher than runoff from RCP4.5. The percentage of surface

runoff is also lower for a longer rainfall intensity. As mentioned earlier, the impact of rainfall runoff to the slope stability is not covered in this study.

According to the overall results from the model simulations, it can be implied that the higher rainfall intensities are not the main trigger for landslides in sensitive marine clays in Ottawa, thus the projected rainfall from RCP4.5 and RCP8.5 or the climate change regarding rainfall intensities does not have impact or only slightly impacts the rainfall-induced landslides in sensitive marine clays in the Ottawa area.

The simulations, however, did not account for snowfall accumulation and thaw periods which could contribute to groundwater level changes and alter the soil properties as stated by the Gautier and Hitchinson (2012) study which concluded that the steady supply of surface water from precipitation or snowmelt as well as the ground frost conditions and timing of the thaw could be the triggering agent for large landsides in Eastern Canada. Moreover, the time to initiate slope failure may be reduced due to the sudden change in the hydraulic conductivity of the soil resulting from the ground thawing in early spring and the ice lens store in the fissures of the sensitive marine clays can also affect the soil stability when melted (Gautier and Hitchinson, 2012). An increase of the hydraulic conductivities allows a higher infiltration rate which contributes to groundwater levels rising faster. In sequence, the slope becomes unstable sooner and yields a higher probability of slope failure.

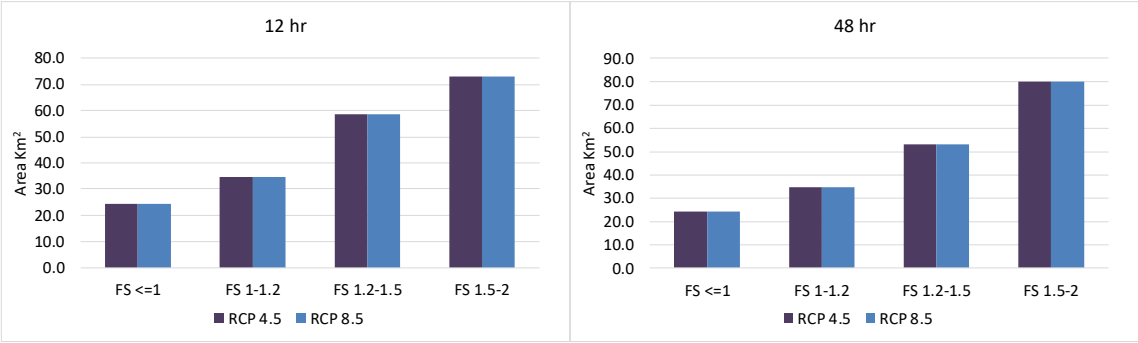

Figure 6-27 Projected changes in the extent of areas within the sensitive marine clay zones in the study area having a factor of safety under the worst-case scenario for RCP4.5 and RCP8.5.

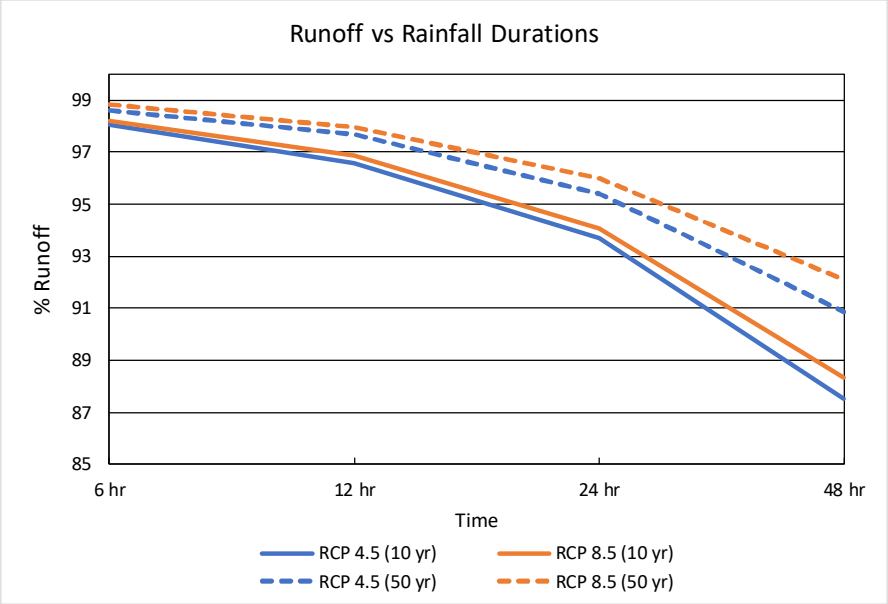

Figure 6-28 Surface runoff comparison for each rainfall duration

To see how the projected areas of susceptibility matched up with the land units designated "landslide" (based on surficial geology), the results of the simulation under the worst-case scenario returned at t = 48 hr for two selected areas, one in the northeast of the study area, the other in the northwest, were compared with the boundaries of the landslide units. The results of the comparison are presented in Figure 6-29 and Figure 6-30, larger scale of Figure 6-29 and Figure 6-30 can be found in Appendix C-1 and C-2 respectively. As the figures show, there is some degree of overlap between the projections and the areas known to have been prone to landslides in the past. An example of landslide susceptibility map for the City of Ottawa can be viewed in Appendix D

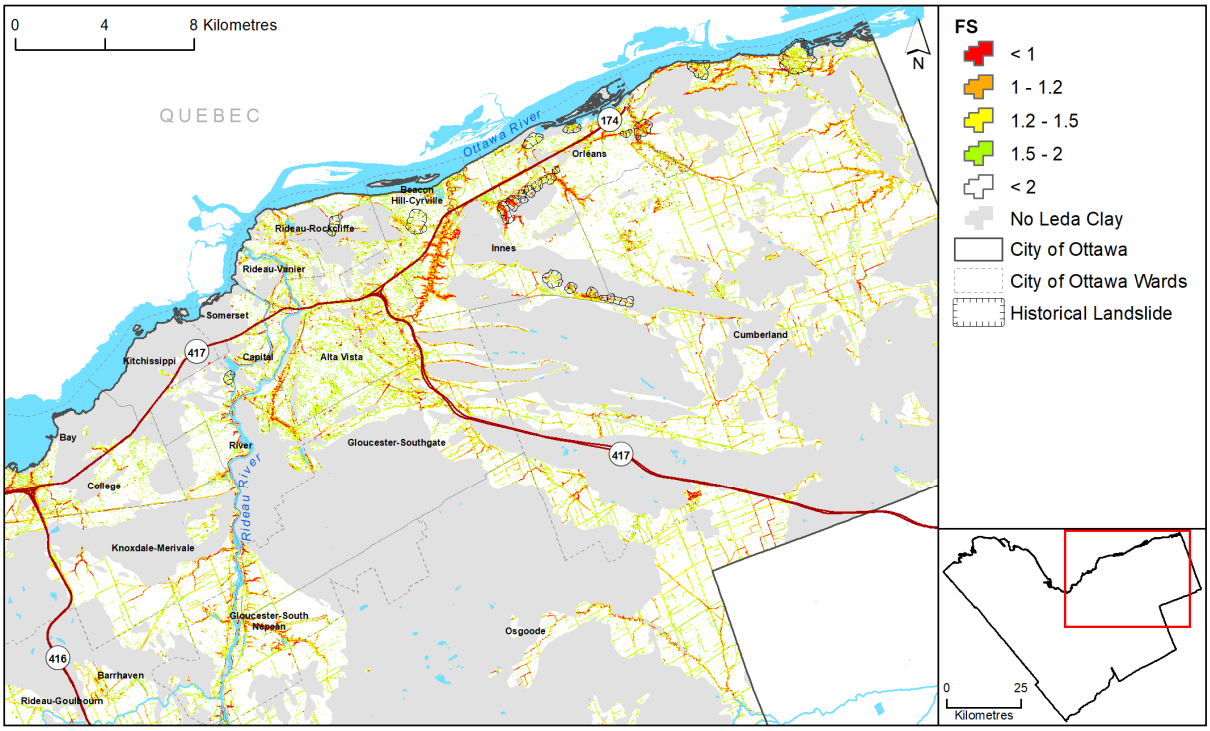

Figure 6-29 Projected factors of safety, under the worst case scenario, within the sensitive marine clay zones in the northeast sector of the study area at 48 hr of the simulation, compared with the study area's landslide land units (based on surficial geology). See Appendix C1 for larger scale.

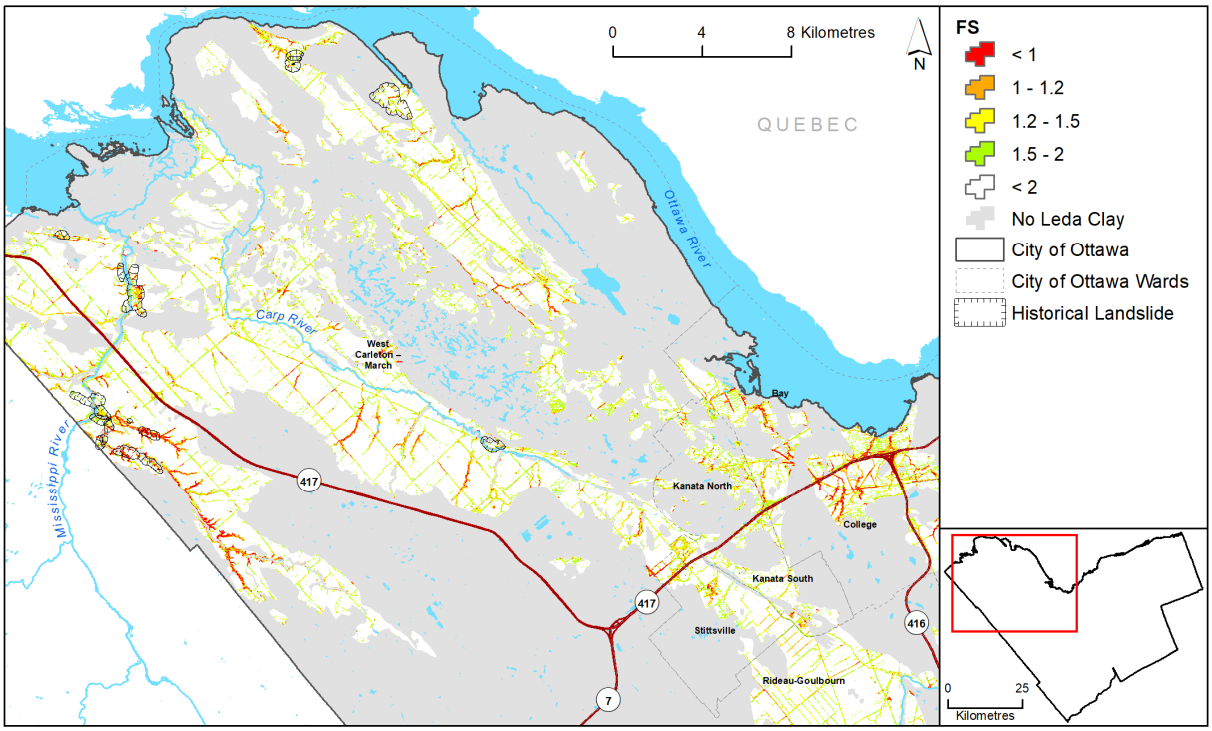

Figure 6-30 Projected factors of safety, under the worst case scenario, within the sensitive marine clay zones in the northwest sector of the study area at 48 hr of the simulation, compared with the study area's landslide land units (based on surficial geology). See Appendix C2 for larger scale.

As noted in Section 6.2.2.2.3 above, the final step in TRIGRS's hydrology model before proceeding to the computation of the factor of safety, is the estimation of changes in the pressure head below the rising water table. The output of this step, using the worst-case scenario is presented in Figure 6-31. The figure shows the evolution of the groundwater pressure head across four successive rainfall durations to a maximum of 48 hours, along with the corresponding changes in factor-of-safety patterns resulting from the pressure head variations. As noted in earlier sections, as positive porewater pressure increases at the top of the water table, the soil's cohesion above the water table decreases, and as a result, the soil's shear resistance also decreases, causing a corresponding reduction in the factor of safety and therefore in the slope's stability. This correspondence between the groundwater pressure head and the factor of safety can be seen in successive stages presented in Figure 6-33 ((b) and (c)). Note that as the simulation progresses, the slope instability spreads to new areas.

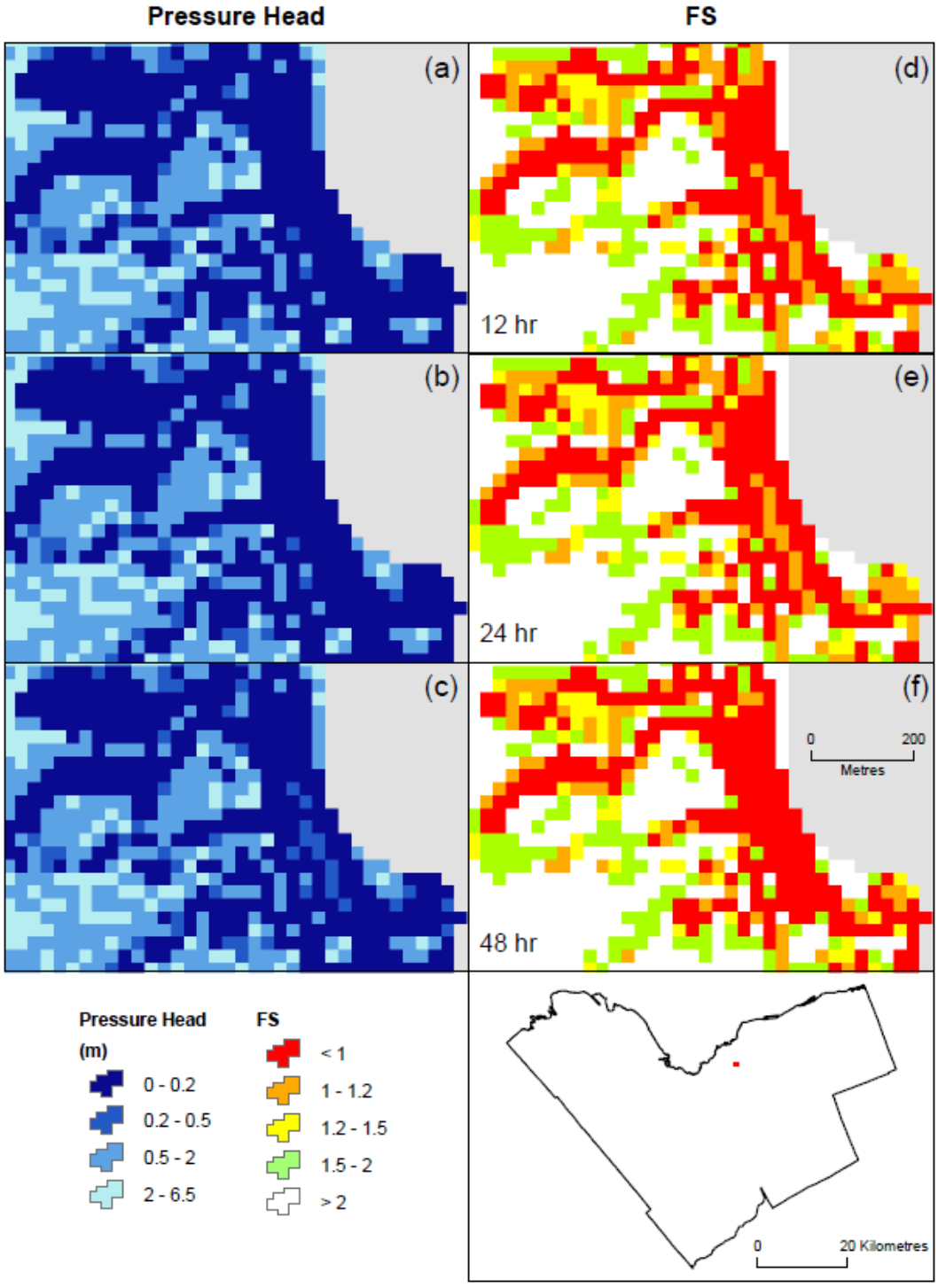

Figure 6-31 Evolution of groundwater pressure head and corresponding changes in factor of safety across three rainfall durations.

6.5 Effects on Future Rainfalls Probability of Slope Failure in Ottawa Sensitive Marine Clays

The TRIGRS model simulations from projected rainfall intensities RCP4.5 and RCP8.5 do not show any difference relative to factor of safety for each rainfall duration as described in section 6.4. Therefore, the future rainfalls have no impact on the probability of slope failure in sensitive marine clays in this area. The probability of slope failure plot is generated for each of the scenarios of simulation for rainfall duration of 48 hours as shown in Figure 6-32 below. The relative-frequency approach probability analysis was carried out to assess the TRIGRS model simulations. This probability analysis looks at a result of factor of safety for each pixel, then compares the value to the rest of the study areas. Values of factor of safety were extracted to a table from raster datasets simulated from the TRIGRS model. Data is sorted and calculates the frequency as a table in ArcMap. The probability of occurrence refers to the relative frequency when the frequency is plotted to a Cumulative Distribution Function (CDF). According to Figure 6-32, the probability of FS = 1 for the worst-case scenario is about 0.02 or 2%, that says, there is 2% chance of slope failure for rainfall duration of 48 hours under the worst-case scenario. It is unlikely for the slope failure to occur at 48 hours of rainfall duration under the normal scenario and ideal scenario. The slope failure may occur at longer rainfall durations which were not investigated here due to unavailability of longer rainfall intensity data.

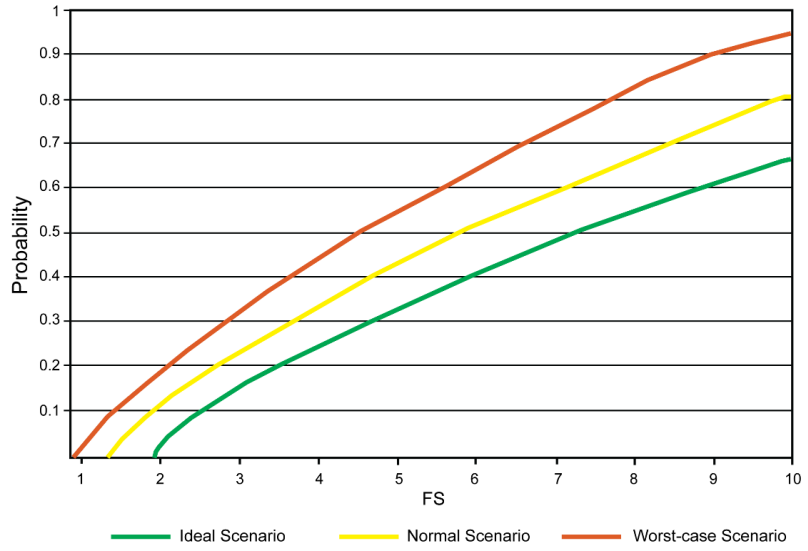

Figure 6-32 Cumulative Distribution Function (CDF) plot of factor of safety of model simulation of 48 hours rainfall duration under three scenarios.

6.6 Effects on Future Rainfalls on Groundwater Level Changes

Two locations of a single cells are picked to observe the change in groundwater level under the worst-case scenario simulation. The relationship of groundwater level, factor of safety and pressure head is illustrated in Figure 6-33. Figure 6-33 (a) shows the groundwater rises from 24 hours to 48 hours for both locations. The water level reaches the ground surface at the end of 48 hours of rainfall duration. Changes in groundwater levels from both RCP 4.8 and RCP 8.5 show identical results. This can be implied that the projected rainfall from RCP4.5 and RCP8.5 do not directly impact the groundwater level changes in sensitive marine clays. It is noted that the surface rainfall runoff is expected to be higher as shown in Figure 6-28 in section 6.4. The higher excess rainfall from the projected climate could contribute to the groundwater levels from other permeable surfaces or other types of soil. The higher excess runoff could also contribute to flooding in the area. Consequently, flooding along river meanders may trigger landslides. Snowfall and frozen groundwater storage during the freeze period would also influence the groundwater levels to rise faster in the early spring or an early thawing period, however, the impact of these factors to rainfall-induced landslides is not covered in this study.

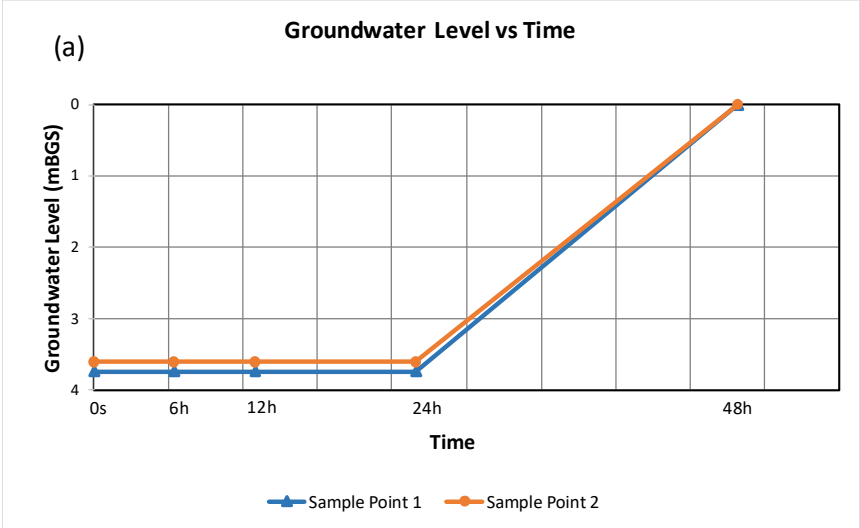

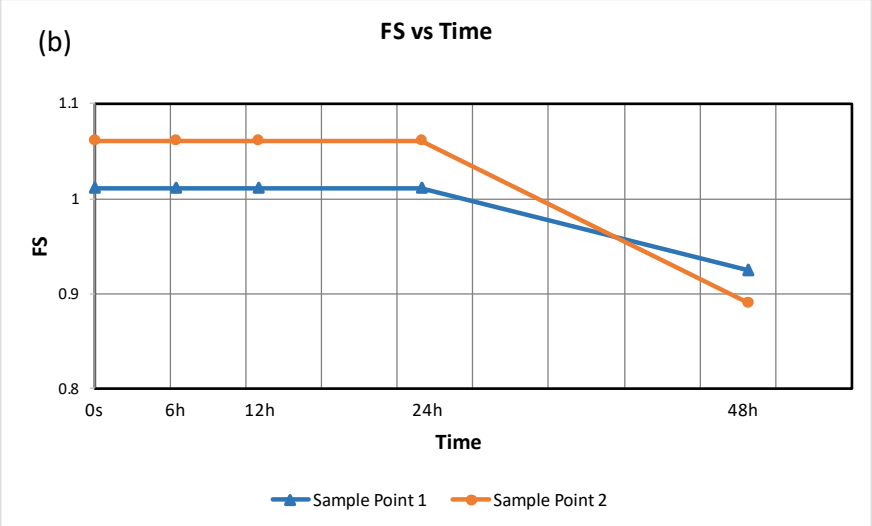

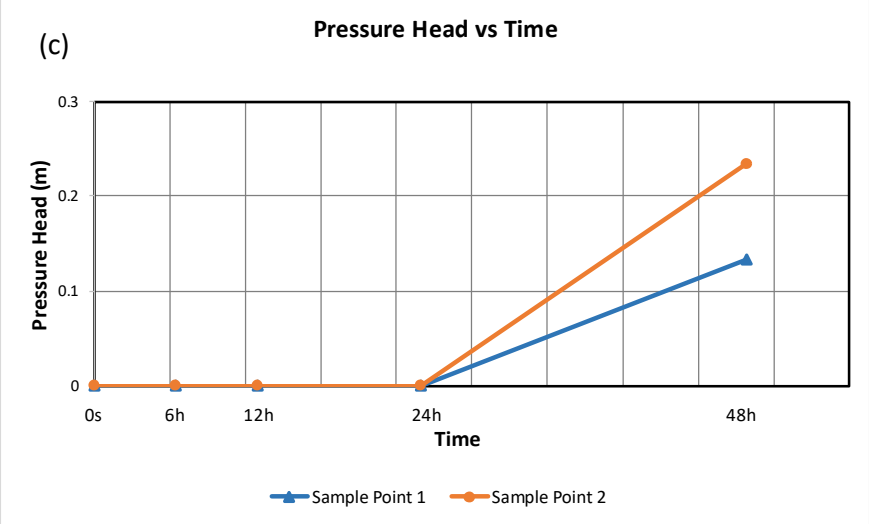

Figure 6-33 Relationship of Groundwater Level (a), Factor of Safety (b), and Pressure Head with rainfall durations from worst-case scenario model simulation for two sample locations

6.7 Conclusions

In assessing the impact of rainfall intensity under climate change to rainfall-induced landslides in sensitive marine clays in the Ottawa area, the TRIGRS model was selected as a tool to simulate the factor of safety from available geospatial data within the study area. Geospatial data included topography, geology, hydrology, climate data, and geotechnical data. The data was compiled from difference sources using the GIS platform to prepare and view results from TRIGRS including generating landslide susceptibility maps.

The model was calibrated using average geotechnical soil properties, then inspected the change of factor of safety results as the rainfall duration progressed. Sensitivity analysis was carried out to asses the change in factor of safety to a range of geotechnical properties. Three model scenarios were set based on the sensitivity analysis and the range of geotechnical properties found in samples of sensitive marine clays in Ottawa. The model simulations were carried out for projected IDF RCP4.5 and RCP8.5 under 10 years and 50 years returning period, with rainfall duration of 12 hr, 24 hr, and 48 hr.

The resulting rainfall-induced landslide susceptibility maps show a slow increase in the factor of safety value as the rainfall duration progressed. The worst-case scenario shows the more areas of unstable (FS < 1) with probability of slope failure of 2% for 48 hr rainfall duration. There are no changes in areas having FS < 1 from 24 hours to 48 hours of rainfall intensity, however, the value of factor of safety is steady decreasing. It is assumed that areas become susceptible to landslides with lower rainfall intensity and longer rainfall duration than a short duration and higher rainfall intensity. Groundwater level and infiltration rate are associated with the time it takes for the slope to become unstable (FS to become < 1).

The model results also show the distribution of areas susceptible to landslides, which are located in the east of the City of Ottawa along the Ottawa River and river valleys in the Orleans area, in the west of Ottawa along the Carp and Mississippi Rivers, also along the Rideau River valley in the central area. The model was validated using the historical landslides layer and a visual inspection of the areas with FS <1, the distribution of unstable areas aligns in the general area of the historical landslides.

It can be assumed that soil properties are an important factor to FS and slope stability. The main soil properties that contribute to lower FS are; lower soil cohesion, lower effective internal friction of the soil, and higher unit weight of the soil. The worst-case scenario simulations show some areas having FS < 1 at the initial start time (0s – at the beginning of rainfall), this may be the result of the worst-case scenario settings and the lack of accuracy of spatial distribution of geotechnical data.

According to the results of TRIGRS model simulations, it can be implied that rainfall intensity is not a significant factor in undermining the slope stability of sensitive marine clays in the Ottawa area. Despite the fact the projected rainfall presents overall higher precipitation and rainfall intensities in the City of Ottawa areas, they do not pose different results in factor of safety. There are also no changes in factor of safety comparison between RCP4.5 and RCP8.5 projected rainfall for each rainfall durations. The result shows a constant infiltration rate throughout the model simulations. This is due to the properties of sensitive marine clays of low saturated hydraulic conductivity, the soil will not allow higher infiltration larger than its saturated hydraulic conductivity, that leads to the excess rainwater leaving the area in the form of runoff. Consequently, there is more excess water runoff along the ground surface which can potentially cause floods. Flooding along river meanders can create erosion and a potentially higher probability of slope failure along the riverbank as well.

The hydraulic conductivity of sensitive marine clays is an important factor in controlling the infiltration rate of water through the ground. Infiltration reduces the shear strength of sensitive marine clays and that reduces the factor of safety. It is also noted from previous studies there may be changes in hydraulic conductivities due to thawing processes in a higher number, which allow higher infiltration rates and accelerates the time for groundwater to rise. Climate changes such as higher overall temperature can impact the freeze and thaw periods i.e. faster thawing periods or earlier spring melts. A more comprehensive data collection for sensitive marine clays in this area is highly recommended in order to improve the initial model results and accuracy.

The study may exclude other factors that may be at play in the triggering of rainfall-induced landslides in sensitive marine clays in the Ottawa area such as snowmelts or frozen water in ground as storage during wintertime. The model also accounted for only a single layer of the soil, in this case sensitive marine clays is based on available surficial geology in the area. It is also a one-dimensional model that considers rainfall from ground surface and does not consider water from adjacent tiles at other elevations than from ground surface.

The results from this study can be used as a preliminary planning in developing in sensitive marine clay areas as well as assisting in decision making for mitigation processes. For example, some engineering guidelines, the factor of safety of up to 1.5 is to be considered when building certain geotechnical infrastructure such as roads and bridges, etc. The landslide susceptibility map can help answering initial questions such as; Does the interest area overlay with sensitive marine clays? Is it susceptible for slope failure? Does the area require further geotechnical investigation?

6.8 General Conclusions and Recommendations

This study has incorporated GIS and the TRIGRS model to assess the impact of climate change on rainfall-induced landslides in sensitive marine clays in the City of Ottawa. Projected rainfall intensities from RCP4.5 and RCP8.5 IDF curves were used as input data. Other data input includes topography, hydrology, geology, and geotechnical data. Geotechnical properties of sensitive marine clays in Ottawa were derived from a previous study. ArcGIS software was used in the preparation of input data for the TRIGRS model, to display output, as well as to generate maps from the TRGIRS model simulations.

The TRIGRS model calculates the factor of safety value as an output based on rainfall intensities and the soil properties. The model was calibrated with ranges of geotechnical properties for different rainfall intensities and was visually and quantitatively validated. Sensitivity analysis were performed to identify the geotechnical properties that would yield the lowest FS value. The model was developed to predict ideal, normal, and worst-case scenarios for the projected climate IDF under RCP4.5 and RCP8.5. For the worst-case scenario, the model used lowest soil cohesion, lowest effective internal friction of soil, and highest soil weight from soil samples from historical engineering reports found in the City of Ottawa area. The normal scenario model is set to use the average soil cohesion, effective internal friction of soil, and soil weight. The ideal scenario model is set to use the highest soil cohesion, highest effective internal friction of soil, and lowest soil weight.

Even though the rainfall intensity from projected climate data RCP 8.5 is higher compared to the historical rainfall intensities, results of factor of safety simulations from the TRIGRS model for historical rainfall intensities, projected climate data between RCP4.5, and RCP8.5 are identical for the same rainfall durations. However, higher rainfall runoff values were produced from RCP8.5 than RCP4.5. It is assumed that the hydraulic conductivity of the sensitive marine clays limits the infiltration rate, as the rainfall intensities input from both historical and projected climate data are higher than the hydraulic conductivity. Historical study noted that the hydraulic conductivities may change due to thawing processes and can impact the infiltration rate (Gautier and Hitchinson, 2012). With more rainfall intensities from the projected climate data but the same infiltration rate that allows water to travel through soil, excess water from surface runoff is expected to be higher, this could contribute to flooding problems. The initial groundwater level is also an important factor to predict the time when the slope becomes unstable.

Longer duration of rainfall reduces slope stability as it reduces the factor of safety, resulting in areas becoming more susceptible to landslides (susceptible areas are areas with FS < 1). Some areas were shown to be unstable at the beginning of the rainfall (t = 0) for the worst-case scenario. It is

believed to be due to the worst-case scenario setting for the model and has proven the initial geotechnical properties for each location within the study area is very important to the model. Additional soil sampling for geotechnical properties in sensitive marine clays throughout the study are is highly recommended.

The worst-case scenario presents 2% probability of slope failure at 48 hours of rainfall. Under the normal and ideal scenario, it is unlikely for slope failure to occur for 48 hours of rainfall, however the longer rainfall may increase the probability of slope failure. The unstable areas prone to landslides are distributed in the east along the valleys and Ottawa River, the Carp and Mississippi River valleys in the west, and along the Rideau River in the central areas. Some of these areas are located within the historical landslide zone. When considering developing, engineering and constructing buildings and infrastructure in these areas, further investigations are highly recommended.

This study provides general areas prone to rainfall induced landslides within sensitive marine clays in the City of Ottawa area based on available data. There are a number of uncertainties that contributed to the model results. These are insufficient geotechnical data and their distribution, uncertainties from the downscaled climate models and the projected IDF curves, and uncertainty from surficial geology data. The geotechnical properties of sensitive marine clays are different between each location, the numbers were collected in ranges, therefore the sensitivities analysis for each geotechnical property can provide some guidance on the fluctuation of the factor of safety values. A single value of each geotechnical property was applied to the entire soil layer identified as sensitive marine clays. However, the surficial geology may not reflect detailed soil layers in the areas needed, some areas were classified as sensitive marine clays but the surface overlay layer might contain fill, sand or organic. There are other factors that may contribute to future rainfall-induced landslides that were not included in this study such as snowmelts, type of land-use, projected groundwater level, and projected rainfall intensity for longer than 48 hours duration, etc. In addition, considering higher resolution data set such as geotechnical properties, surficial geology of soil classification, groundwater elevation and higher resolution of DEM (10m or smaller grid size) could improve the model results.

There are limitations from the TRGIRS model itself. As it is a one dimensional model, it is limited to a single layer of property, for example, the limitation of allowing only one type of soil in one cell, only single value of hydraulic conductivity is allowed per cell, etc. It is also not suitable for long-term response because the model does not consider the lateral flow (Baum et al., 2008).

The resulting landslide susceptibility map can be useful to engineers and city planners in decision making to mitigate the damage of the future event of rainfall-induced landslides in the City of Ottawa areas.

6.9 References

Al-Umar, M. (2018). GIS based assessment of climate-induced landslide susceptibility of sensitive marine clays in the Ottawa region, Canada. Unpublished doctoral thesis. The University of Ottawa, Ottawa, Canada. Available at: http://dx.doi.org/10.20381/ruor-21490.

Alvioli, M. and Baum, R. L. (2016). Parallelization of the TRIGRS model for rainfall-induced landslides using the message passing interface. *Environmental Modelling & Software*, 81, pp. 122-135.

Baum, R. L., Savage, W. Z., and Godt, J. W. (2008). TRIGRS—A Fortran Program for Transient Rainfall Infiltration and Grid-Based Regional Slope-Stability Analysis, Version 2.0. U.S. Geological Survey, Reston, Virginia, U.S.A. Available at: https://pubs.usgs.gov/of/2008/1159/downloads /pdf/OF08-1159.pdf.

Baum, R. L., Godt, J. W., and Savage., W. Z. (2010). Estimating the timing and location of shallow rainfall-induced landslides using a model for transient, unsaturated infiltration, *Journal of Geophysical Research*, 115, F03013, doi:10.1029/2009JF001321.

Bhandary, N.P., Yatabe, R., Kumar Dahal, K., Hasegawa, S., Inagaki, H., (2013), Areal distribution of large-scale landslides along highway corridors in central Nepal. Georisk, 7 (1), pp. 1–20.

Brooks, G. R. (2019). Sensitive clay landside inventory map and database for Ottawa, Ontario. Geological Survey of Canada Open File 8600. Geological Survey of Canada, Ottawa, Canada. Available at: https://doi.org/10.4095/315024

Carrara, A., Cardinali, M., Detti, R., Guzzetti, F., Pasqui, V., Reichenbach, P., (1991), GIS techniques and statistical models in evaluating landslide hazard. Earth Surface Processes and Landforms, 6, pp. 427–445.

Carrara, A., Guzzetti, F. (Eds.), (1995), Geographical information systems in assessing natural hazards. Kluwer Academic Publisher, Dordrecht, The Netherlands, 353 pp.

Chen, H.X., Zhang L.M., GaoL., Zhu H., Zhang S., (2015), Presenting regional shallow landslide movement on three-dimensional digital terrain. Engineering Geology, 195, pp. 122-134.

Chung, C. F., Fabbri, A. G., (1999), Probabilistic prediction models for landslide hazard mapping. American Society for Photogrammetry and Remote Sensing. Vol. 65, No. 12, pp. 1389-1399.

Collins, B. D. and Znidarcic, D. (2004). Stability analyses of rainfall induced landslides. *Journal of Geotechnical and Geoenvironmental Engineering*, 130 (4), pp. 362-372. Available from: https://people.uwec.edu/jolhm/EH/Beaver/Adobe/Stability%20analyses%20of%20Rainfall %20Induced%20landslides.pdf.

Dai, F. C., and Lee, C. F. (2001). Terrain-based mapping of landslide susceptibility using a geographical information system: a case study. *Canadian Geotechnical Journal*, 38, pp. 911-923.

Digital Elevation Model (DEM), Ministry of Natural Resources, Land Information Ontario, version 2, published in 2008.

Eden, W. J. and Mitchell, R. J. (1970). The mechanics of landslides in Leda clay. *Canadian Geotechnical Journal*, 7 (3), pp. 285-296. Available at: http://web.mit.edu/parmstr/Public/ NRCan/rp441.pdf.

Fall, M., Azzam, R., Noubactep., C., (2006), A multidisciplinary study of the stability of natural slopes and landslide hazard mapping. Engineering Geology 82 (4), pp. 241-263.

Fall, M., Dia, A., Fall, Meï., Gbaguidi, I., Diop, I., (1996), Un cas d'instabilité de pente naturelle: le versant des madeleines: analyse, cartographie des risques et prévention. In Bulletin of Engineering Geology and Environment, 53, pp. 65-74.

Fredlund, D. G. and Xing, A., (1994). Equations for the soil-water characteristic curve. *Canadian Geotechnical Journal*, 31 (4), pp. 521-.532. Available at: https://doi.org/10.1139/t94-061.Freeze, R. A. and Cherry, John A. (1979). *Groundwater*, Prentice-Hall, Englewood Cliffs, New Jersey.

Gardner, W. R., (1958), Some steady-state solutions of the unsaturated moisture flow equation with application to evaporation from a water table. Soil Sci., 85, pp. 228–232.

Gauthier D. and Hutchinson D. J., (2012), Evaluation of potential meteorological triggers of large landslides in sensitive glaciomarine clay, eastern Canada. Natural Hazards and Earth System Sciences, 12, pp. 3359–3375.

Godt, J. W., Baum, R. L., Savage, W. Z., Salciarini, D., Schultz, W. H., and Harp, E. L. (2008). Transient deterministic shallow landslide modeling: Requirements for susceptibility and hazard assessments in a GIS framework. *Engineering Geology*, 102, (3-4), pp. 214-226. Doi: 10.1016/j.enggeo.2008.03.019

Kaur, H. Gupta, S., Parkash, S., and Thapa R. (2018). Knowledge-driven method: a tool for landslide susceptibility zonation (LSZ). *Geology, Ecology, and Landscapes*. Published online on 17 December 2018. Available at: https://doi.org/10.1080/24749508.2018.1558024

Klugman, M.A., and Chung, P. (1976). Slope Stability Study of the Regional Municipality of Ottawa-Carleton; Ontario Geological Survey, Miscellaneous Paper MP68, 13p. Accompanied by Geotechnical Series Maps, 2374, 2375, 2376, and 2377, scale 1:50,000 and Map 2378, scale 1:25,000.

Leoni, G., Campolo, D., Falconi, L., Gioê, C., Lumaca, S., Puglisi, C., and Torre, A. (2015). Heuristic Method for Landslide Susceptibility Assessment in the Messina Municipality. In: G. Lollino et al. (eds.), *Engineering Geology for Society and Territory*, Vol 2, pp. 501-504. Springer International Publishing, Switzerland.

LRL Associates Ltd., 2017, *Slope Stability Analysis, 6909 Notre Dame Street*, Ottawa.

Nader, A. (2014). Engineering Characteristics of Sensitive Marine Clays—Examples of Clays in Eastern Canada. Master's thesis. University of Ottawa, Ottawa, Canada. ProQuest Dissertations Publishing, MS26684.

Pardeshi, S. D., Autade, S. E. and Pardeshi, S. S. (2013). Landslide hazard assessment: recent trends and techniques. *SpringerPlus*, 2 (1), Article 523, pp. 1-11. Available at: https://link.springer.com/content/pdf/10.1186%2F2193-1801-2-523.pdf.

Qiu, C., Esaki, T., Mitani, Y., and Xie, M. (2008). A GIS-based method for predicting the location, magnitude and occurrence time of landslides using a three-dimensional deterministic model. In: Z. Chen, J. Zhang, Z. Li, F. Wu, and K. Ho, (eds.), *Landslides and Engineered Slopes: From the Past to the Future,* Vol. 1, pp. 893-900. CRC Press, The Netherlands.

Rahardjo, H., Kim, Y., and Satyanaga, A. (2019). Role of unsaturated soil mechanics in geotechnical engineering. *International Journal of Geo-Engineering*, 10 (Article a), pp. 1-23. Available at: https://doi.org/10.1186/s40703-019-0104-8.

Raia, S., Alvioli, M., Rossi, M., Baum, R. L., Godt, J. W., ad Guzzetti, F. (2014). Improving predictive power of physically based rainfall-induced shallow landslide models: a probabilistic approach. *Geoscientific Model Development*, 7, pp. 495-514.

Savage, W. Z., Godt, J. W., and Baum, R. L. (2004). Modeling time-dependent areal slope stability. In: W. Lacerda, M. Ehrlich, S. Fontoura, and A. Sayão, (eds.), *Landslides: Evaluation and Stabilization*, pp. 23-36. Taylor & Francis Group, London.

Stanley, T. and Kirschbaum, D. B. (2017). A heuristic approach to global landslide susceptibility mapping. *Natural Hazards*, 87, pp. 145-164. DOI 10.1007/sl 1069-017-2757-y.

Taha, A. M. (2010), Interface Shear Behavior of Sensitive Marine Clays—Leda Clay. Master's Thesis, Department of Civil Engineering, The University of Ottawa, Ottawa.

van Westen, C. J., van Asch, T. W. J., and Soeters, R. (2006). Landslide hazard and risk zonation—why is it still so difficult? *Bulletin of Engineering Geology and the Environment*, 65 (2), pp. 167-184.

Wahono, B. F. D. (2010). Applications of Statistical and Heuristic Methods for Landslide Susceptible Assessments. Master's Thesis. Gadjah Mada University, Yogyakarta, Indonesia. Available at: https://webapps.itc.utwente.nl/librarywww/papers_2010/msc/aes/wahono.pdf.

Wati, S. E., Hasturi, T., Widjojo, S., and Pinem, F. (2010). Landslide susceptibility mapping with

heuristic approach in mountainous area: a case study in Tawangmangu Subdistrict, Central Java, Indonesia. *International Archives of the Photogrammetry, Remote Sensing, and Spatial Information Sciences*, Vol. 38, Part 8, Kyoto, Japan. Available at: http://citeseerx.ist.psu.edu/viewdoc/download?doi=10.1.1.222.3152&rep=rep1&type=pdf.

Zhang, L. L, Zhang, J., Zhang, L. M., and Tang, W. H. (2011). Stability analysis of rainfall-induced slope failure: a review. *Geotechnical Engineering*, 164 (GES), pp. 299-315. Available at: http://dx.doi.org/10.1680/geng.2011.164.5.299.

Zhang, G.-R., Qian, Y.-J., Wang, ZZ.-C., and Zhao, B. (2014). Analysis of rainfall infiltration law in unsaturated soil slope. *The Scientific World Journal*, 2014, Article ID 567250, 7p. Available from: https://www.hindawi.com/journals/tswj/2014/567250/.

Appendix A - List of Symbols

α = inverted capillary fringe

β = physical limitation

c = cohesion

c' = soil cohesion for effective stress

γ_S = unit weight of soil

γ_W = unit weight of water

d = steady-state depth of the water table measured in the vertical direction

d_{LZ} = depth of failure

d_{LZw} = the vertical height or thickness of the saturated layer

D_0 = saturated hydraulic diffusivity

d_t = depth to the transient water table

d_u = the vertical depth to the top of the capillary fringe

D_ψ = the soil-water diffusivity

$D_\Psi t$ = the non-dimensional time

∂ = a change in the value of a variable

δ = slope angle

E_K = electrokinetic potential

θ = the volumetric water content

θ_r = residual water content

θ_s = volumetric soil-water content at saturation

I_{ZLT} = steady (initial) surface flux

I_{nZ} = rate of surface flux for the n^{th} time interval

K_s = saturated hydraulic conductivity

Λ = the root of equation

$q(d_u, t)$ = the flux exiting from the base of the unsaturated zone

q_{Zmax} = excess flux at the water table or the top of the capillary fringe

ρ = density

σ = normal stress

S_s = specific storage

S_t = sensitivity

S_u = shear strength

τ = shear strength

t = time

ϕ = angle of internal friction

φ' = soil friction angle for effective stress

ψ = groundwater pressure head

ψ_0 = pressure head at the top of the capillary fringe

V_A = volume of water arriving at the base of the water table

V_f = volume of fillable pore space

w_n = *in-situ* water content

w_l = liquid limit

Z = vertical coordinate direction (positive downward) and depth below the ground surface

z = slope-normal coordinate direction (positive downward)

Z_w = the vertical distance below the initial water table

Appendix B

Factors of safety for sensitive marine clay in the study area computed by TRIGRS for time (t) = 12 hr under 10 years IDF RCP 4.5 and 8.5 for the ideal scenario, normal scenario, and the worst-case scenario

Appendix B-1

Factors of safety for sensitive marine clay in the study area computed by TRIGRS for time (t) = 12 hr under 10 years IDF RCP 4.5 ideal scenario

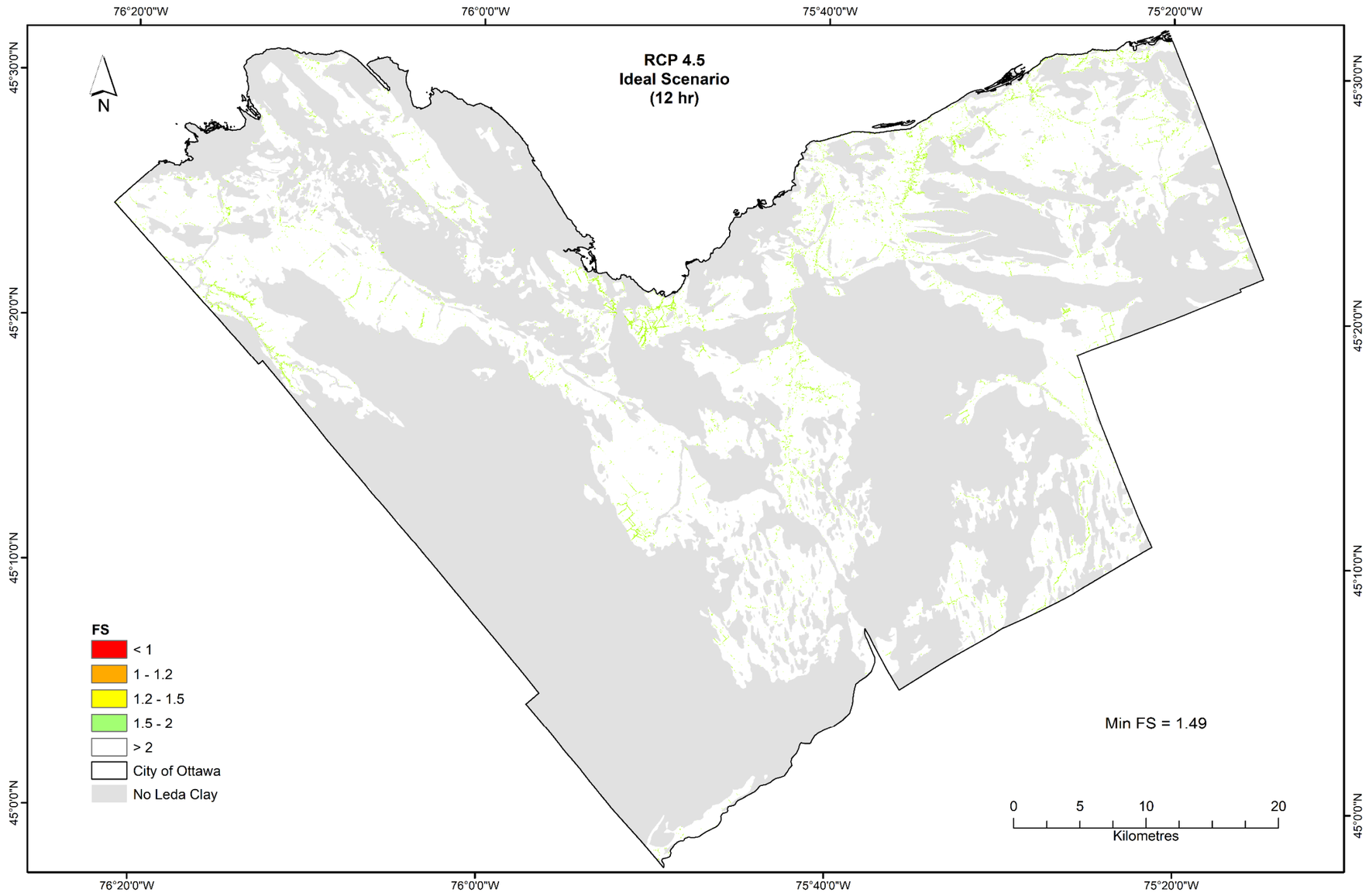

Appendix B-2

Factors of safety for sensitive marine clay in the study area computed by TRIGRS for time (t) = 12 hr under 10 years IDF RCP 8.5 ideal scenario

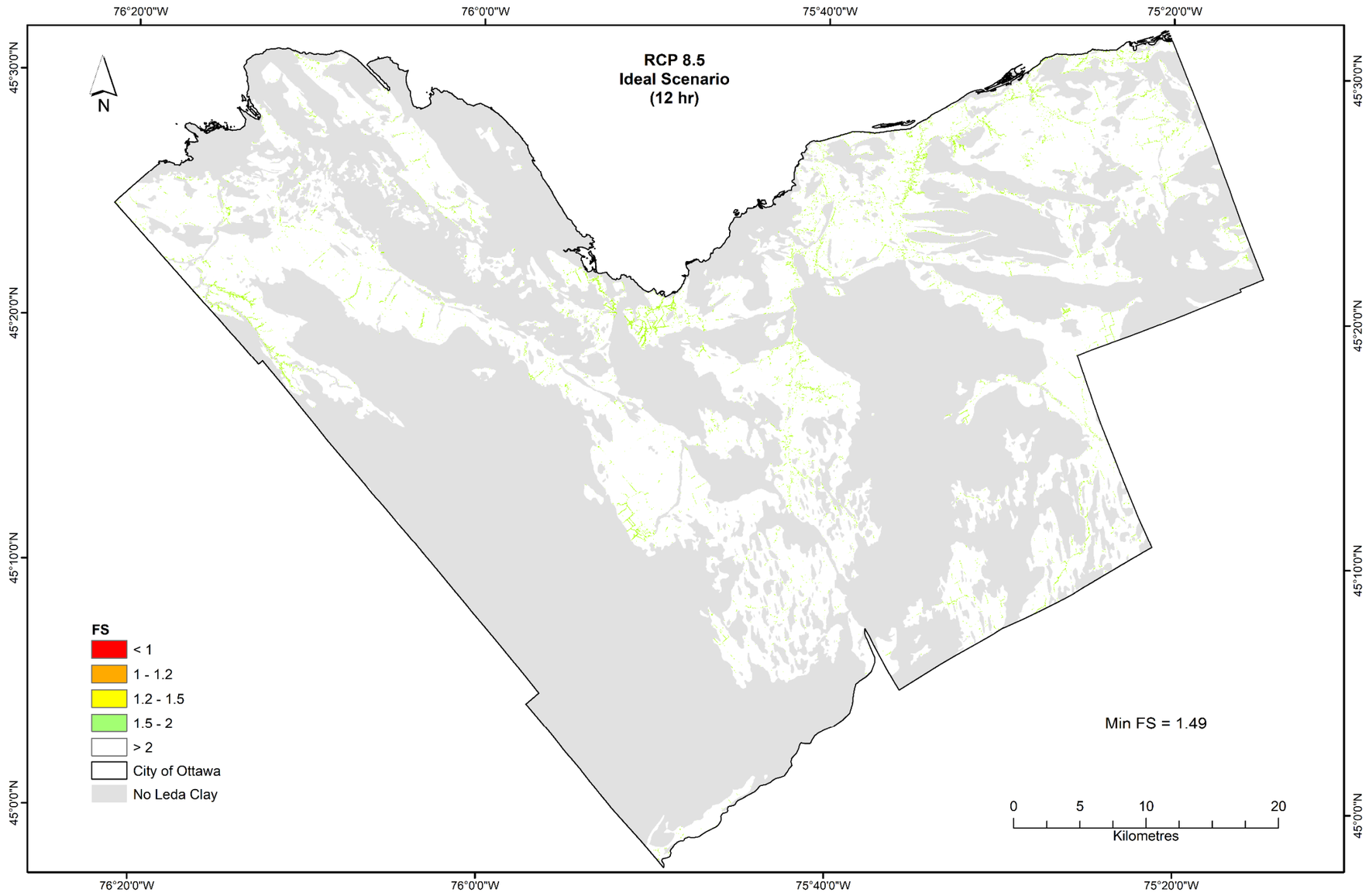

Appendix B-3

Factors of safety for sensitive marine clay in the study area computed by TRIGRS for time (t) = 12 hr under 10 years IDF RCP 4.5 normal scenario

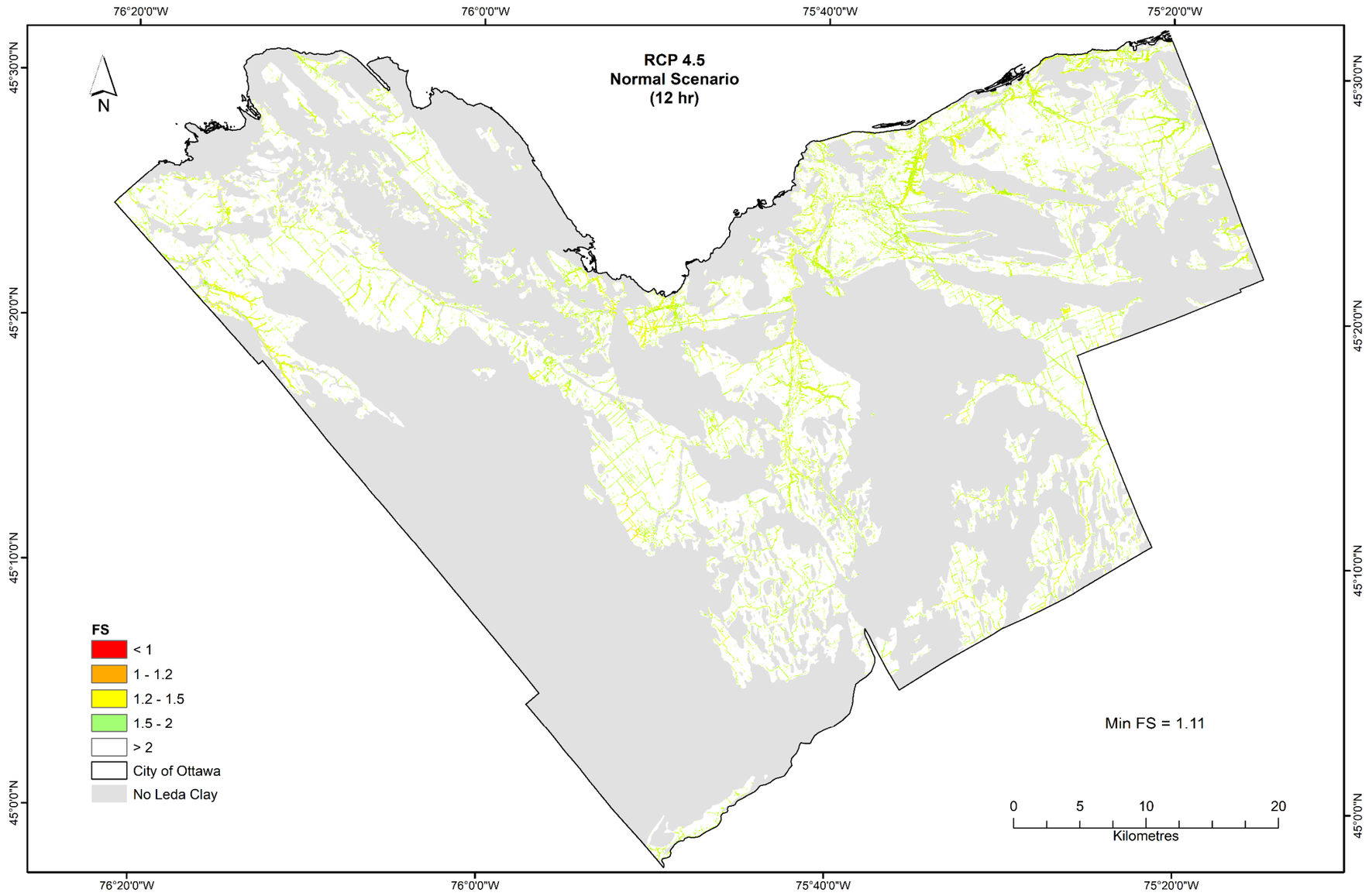

Appendix B-4

Factors of safety for sensitive marine clay in the study area computed by TRIGRS for time (t) = 12 hr under 10 years IDF RCP 8.5 normal scenario

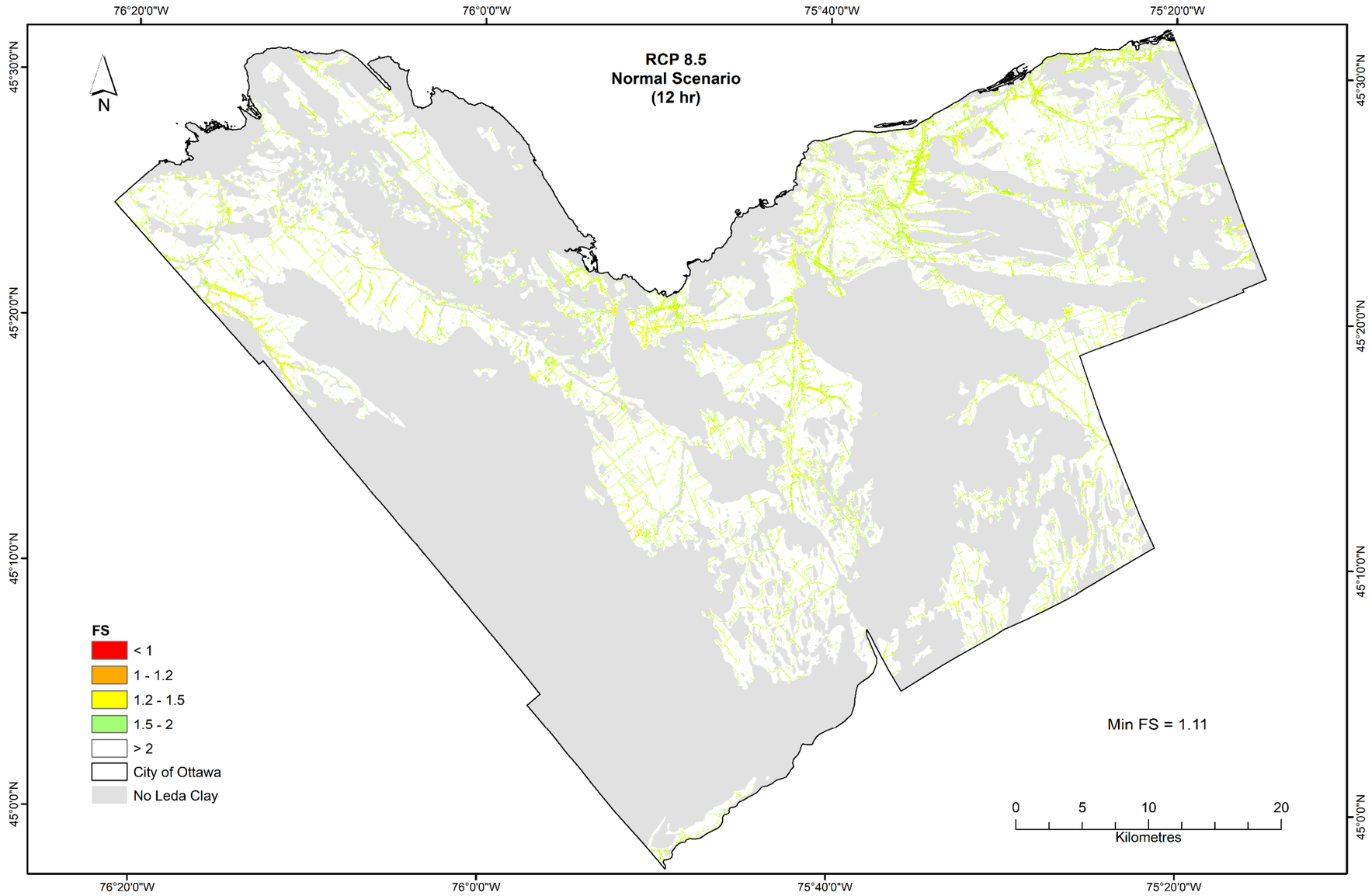

Appendix B-5

Factors of safety for sensitive marine clay in the study area computed by TRIGRS for time (t) = 12 hr under 10 years IDF RCP 4.5 worst-case scenario

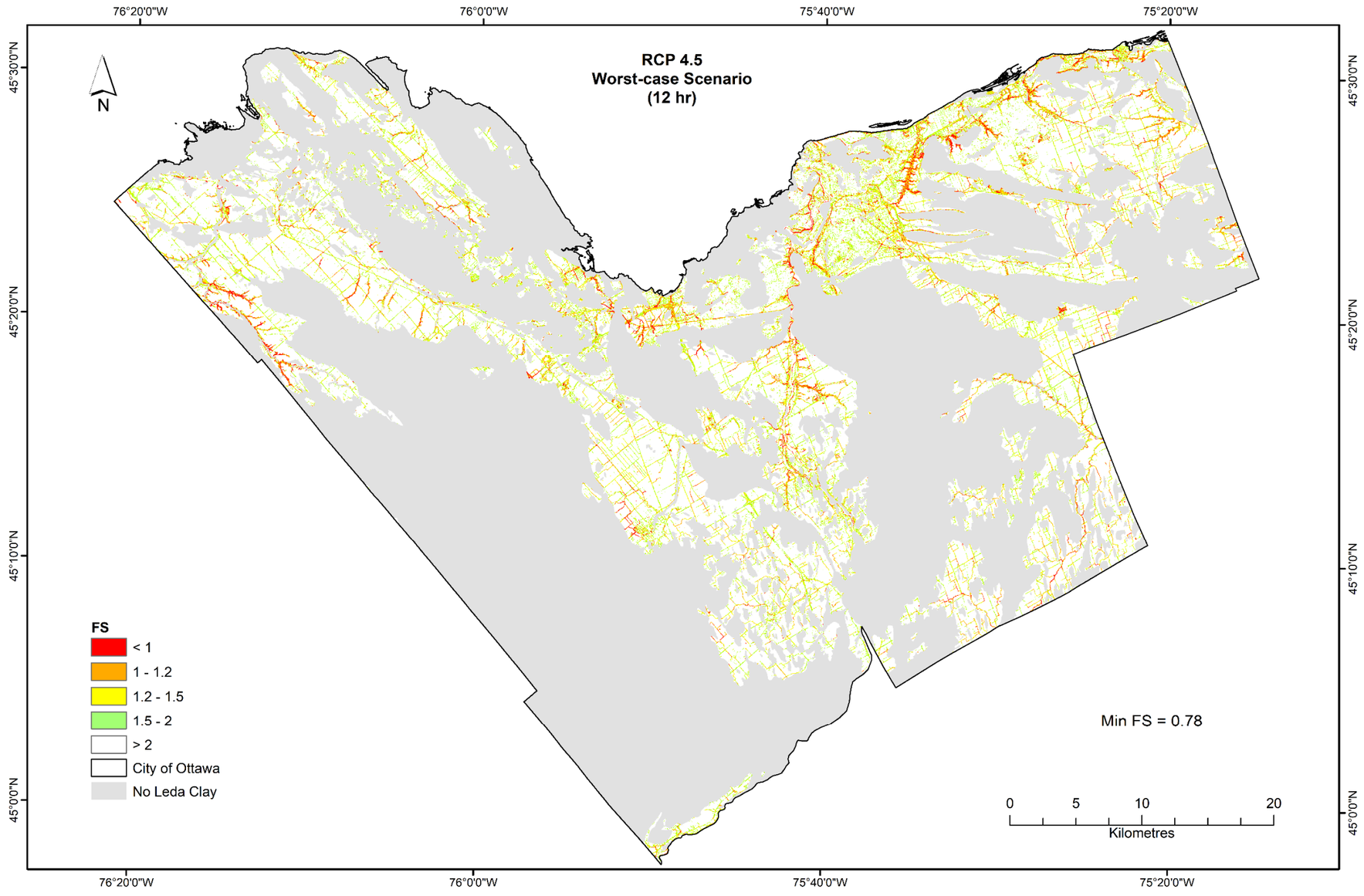

Appendix B-6

Factors of safety for sensitive marine clay in the study area computed by TRIGRS for time (t) = 12 hr under 10 years IDF RCP 8.5 worst-case scenario

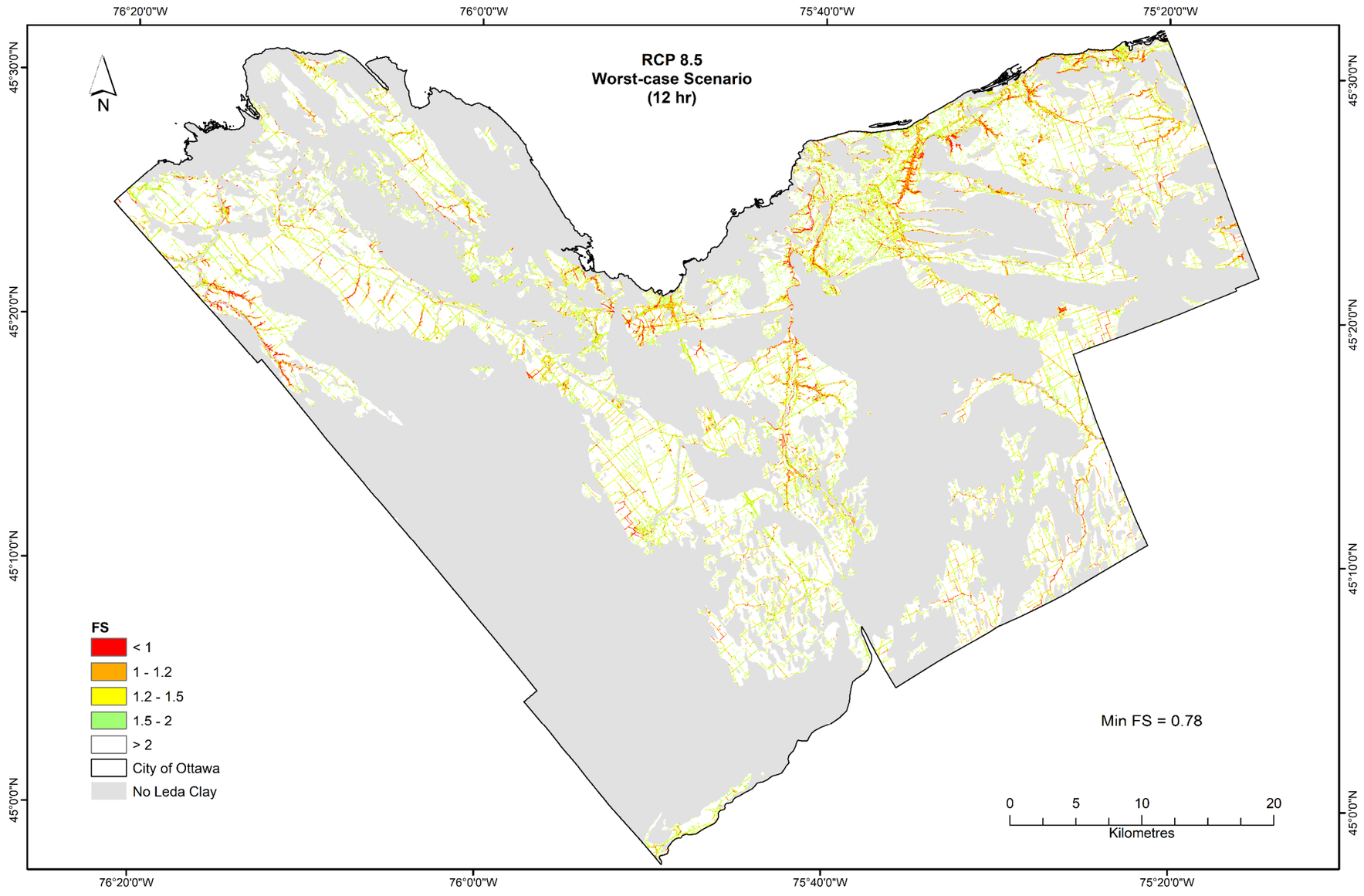

Appendix B-7

Factors of safety for sensitive marine clay in the study area computed by TRIGRS for time (t) = 24 hr under 10 years IDF RCP 4.5 ideal scenario

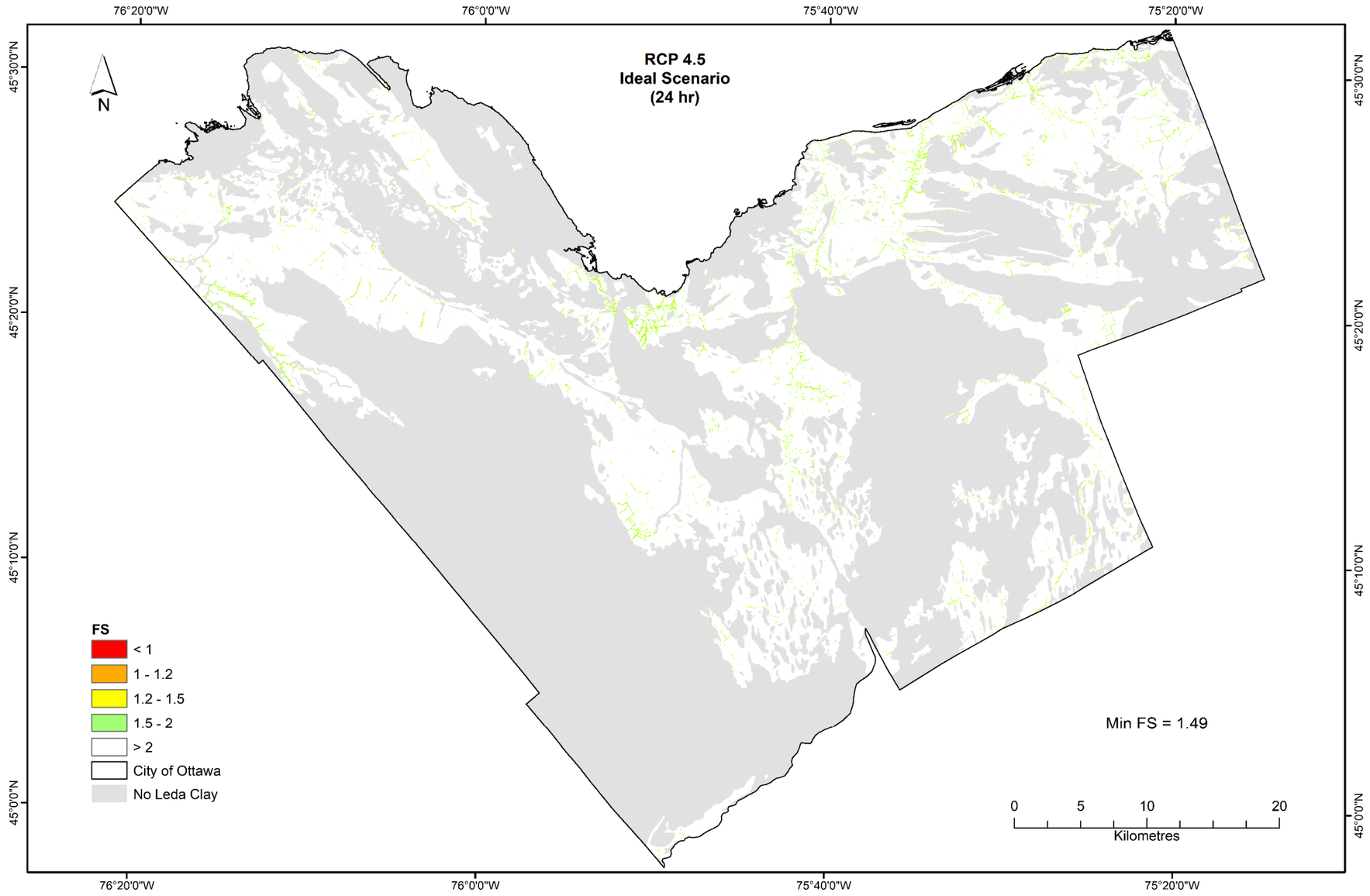

Appendix B-8

Factors of safety for sensitive marine clay in the study area computed by TRIGRS for time (t) = 24 hr under 10 years IDF RCP 8.5 ideal scenario

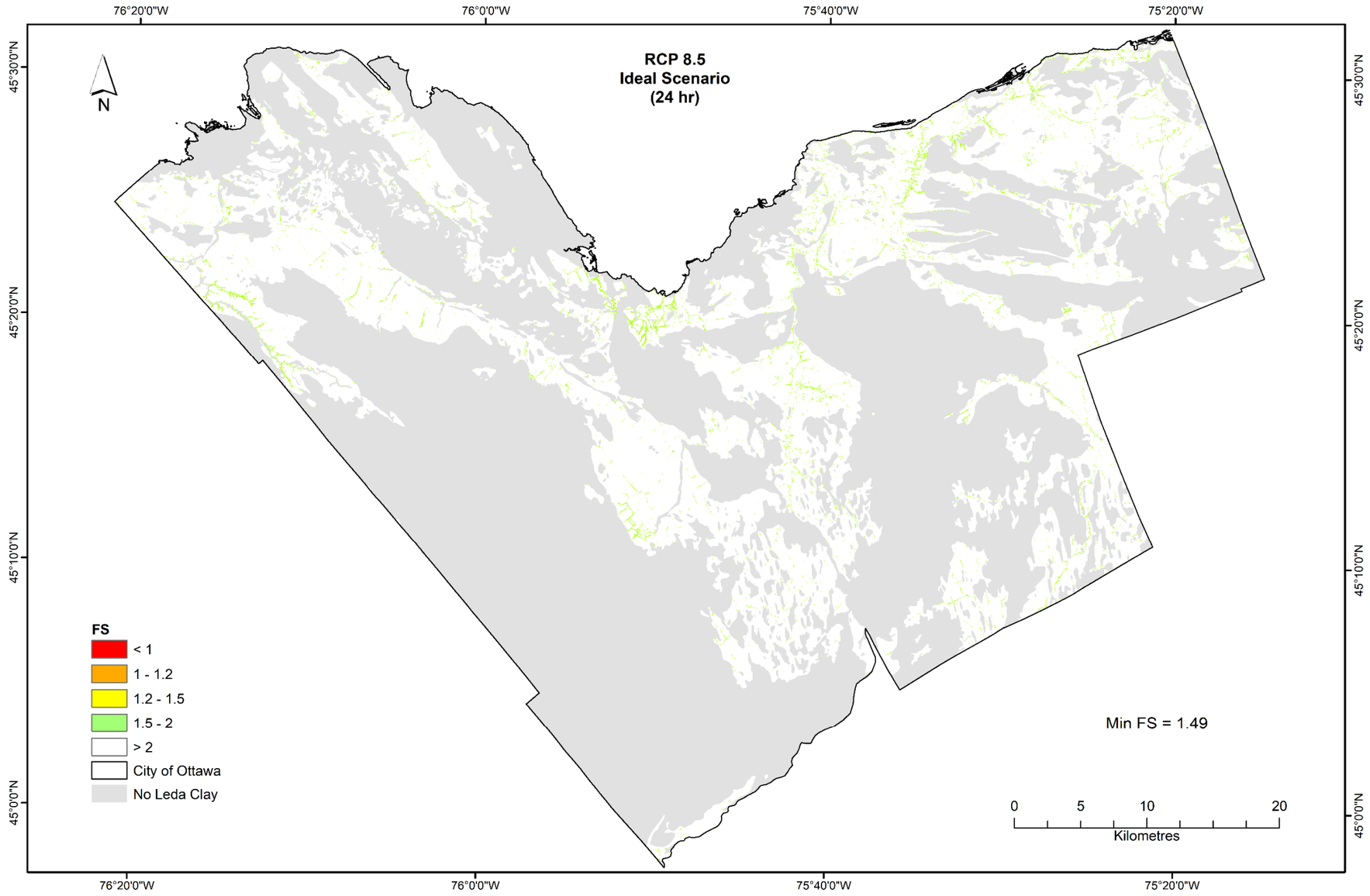

Appendix B-9

Factors of safety for sensitive marine clay in the study area computed by TRIGRS for time (t) = 24 hr under 10 years IDF RCP 4.5 normal scenario

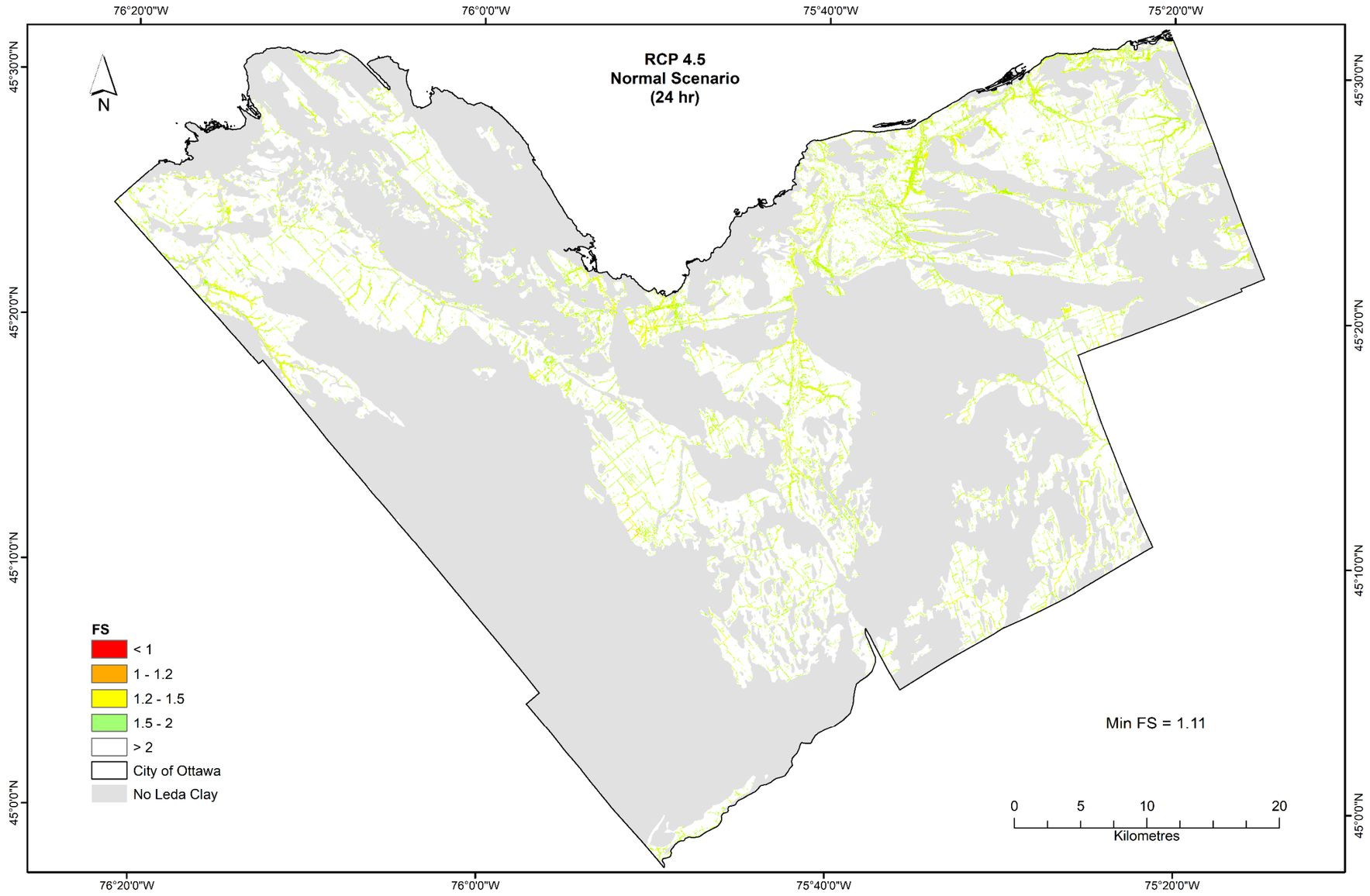

Appendix B-10

Factors of safety for sensitive marine clay in the study area computed by TRIGRS for time (t) = 24 hr under 10 years IDF RCP 8.5 normal scenario

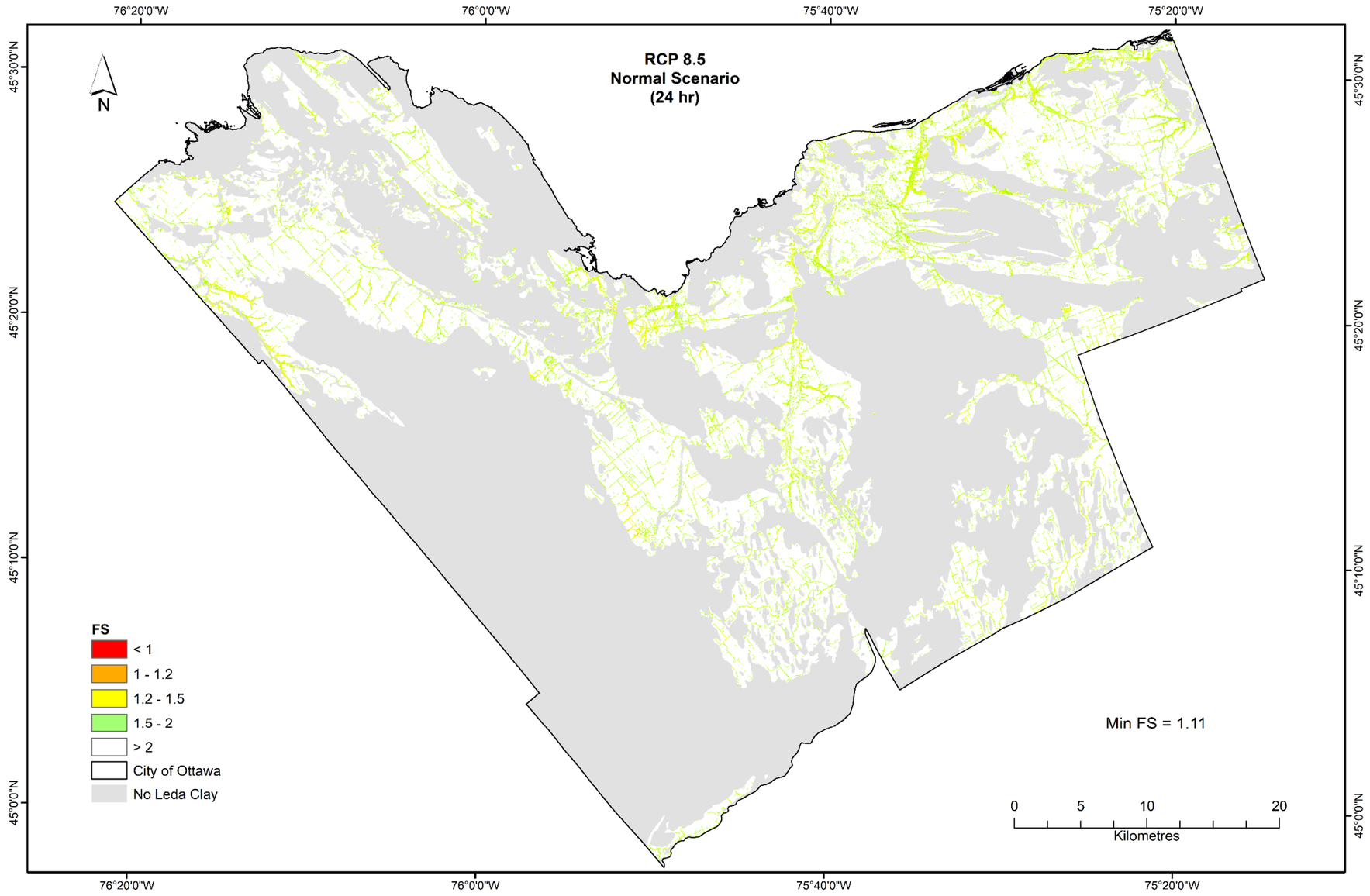

Appendix B-11

Factors of safety for sensitive marine clay in the study area computed by TRIGRS for time (t) = 24 hr under 10 years IDF RCP 4.5 worst-case scenario

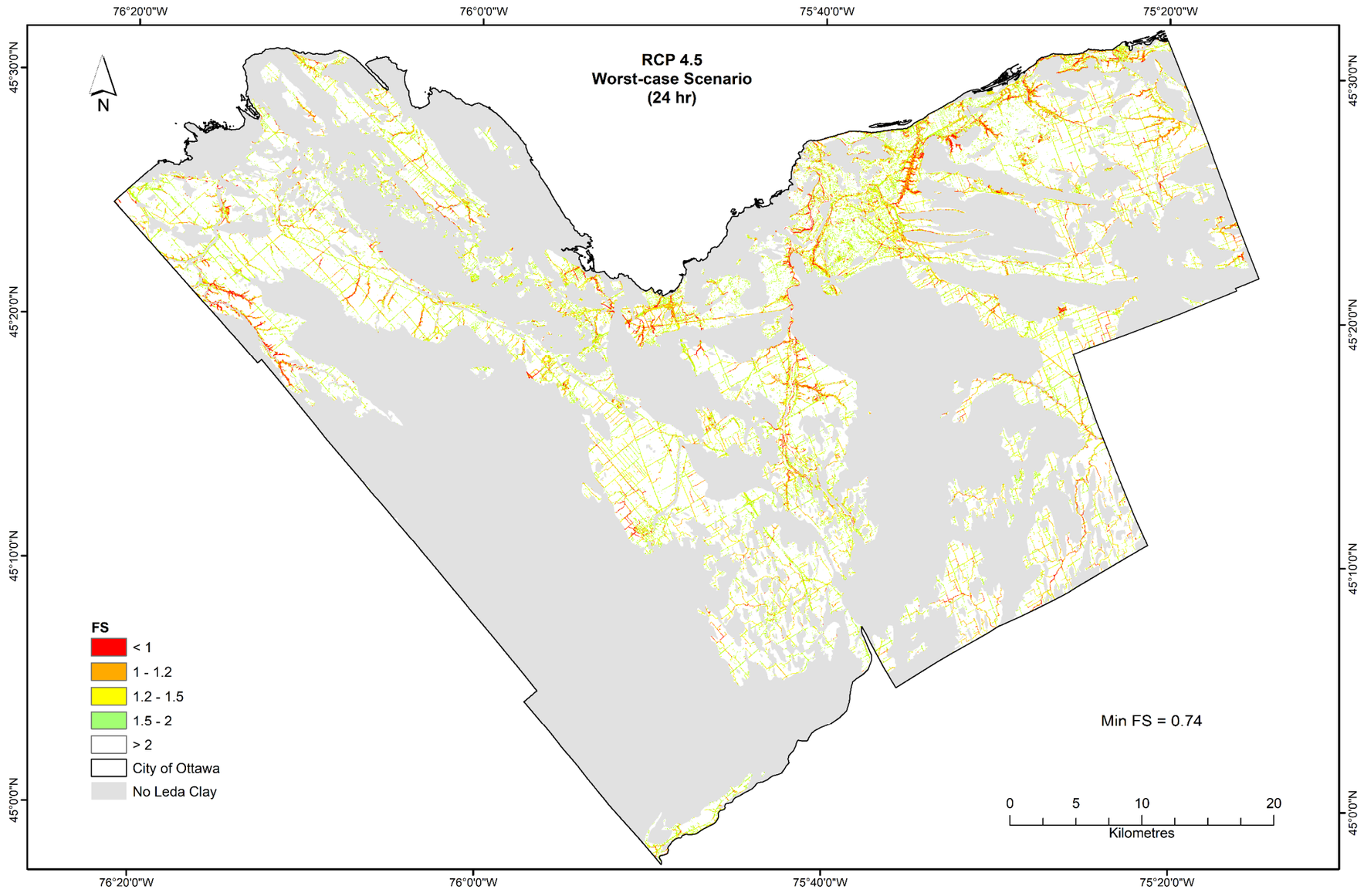

Appendix B-12

Factors of safety for sensitive marine clay in the study area computed by TRIGRS for time (t) = 24 hr under 10 years IDF RCP 8.5 worst-case scenario

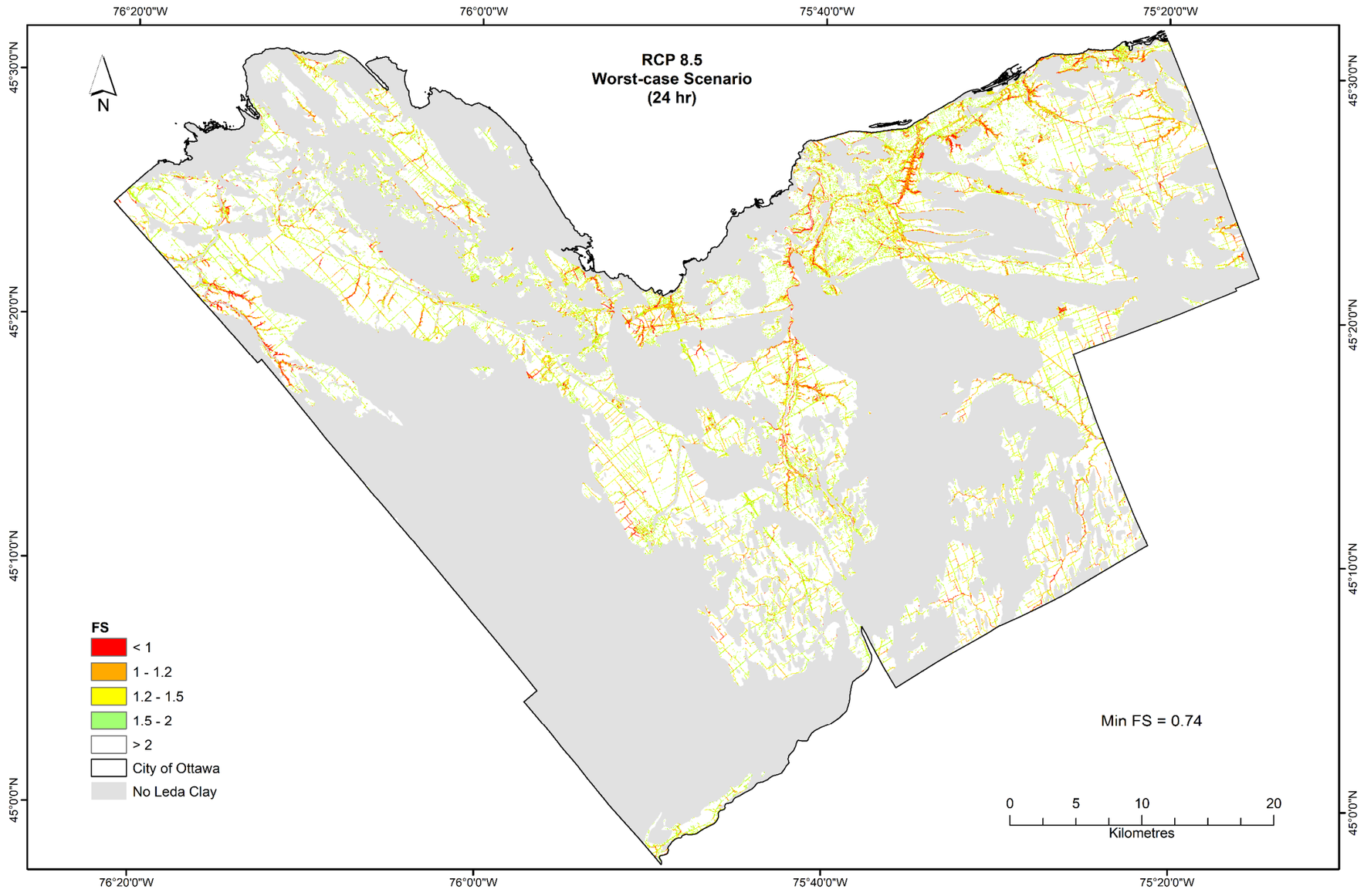

Appendix B-13

Factors of safety for sensitive marine clay in the study area computed by TRIGRS for time (t) = 48 hr under 10 years IDF RCP 4.5 ideal scenario

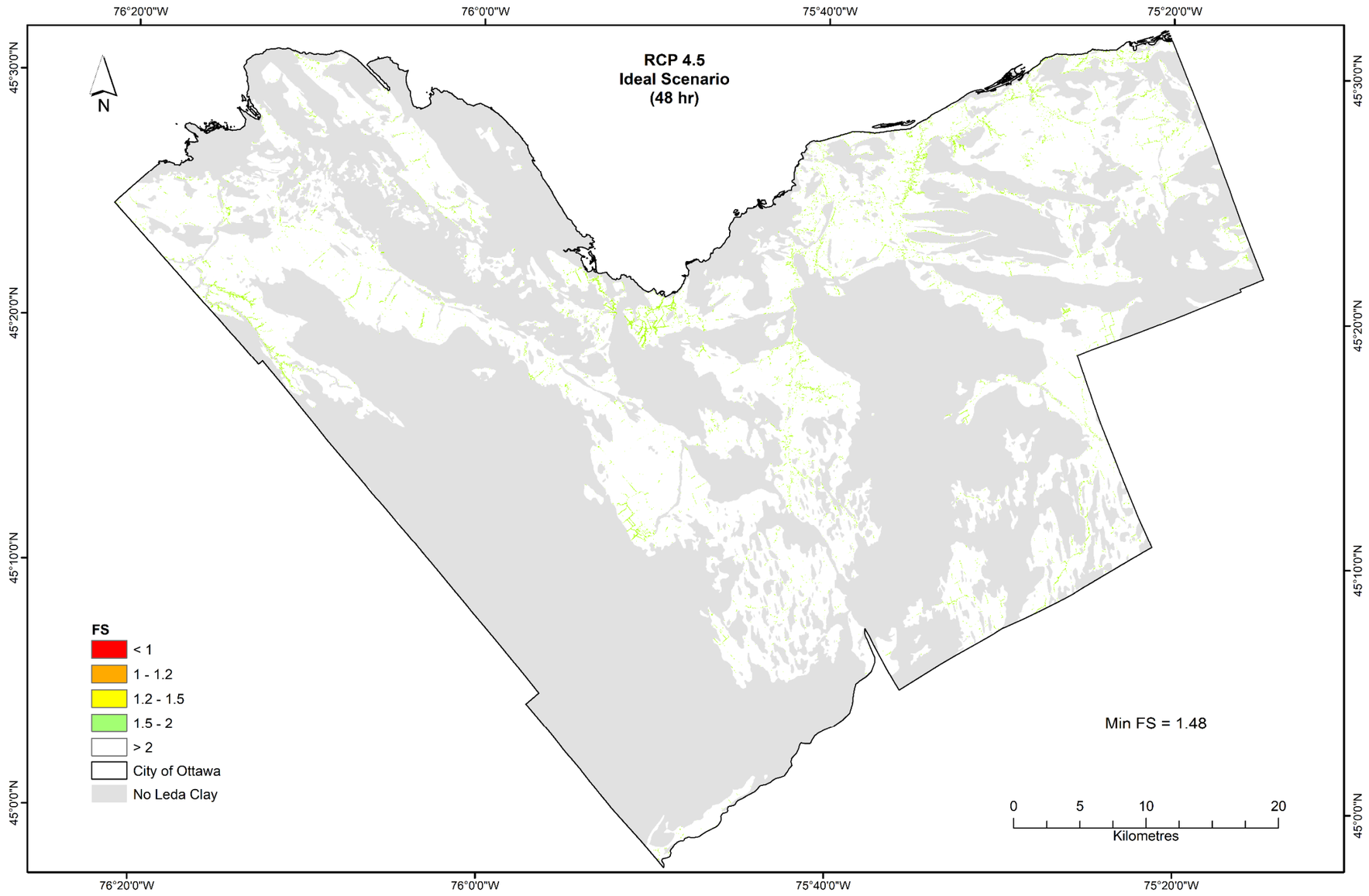

Appendix B-14

Factors of safety for sensitive marine clay in the study area computed by TRIGRS for time (t) = 48 hr under 10 years IDF RCP 8.5 ideal scenario

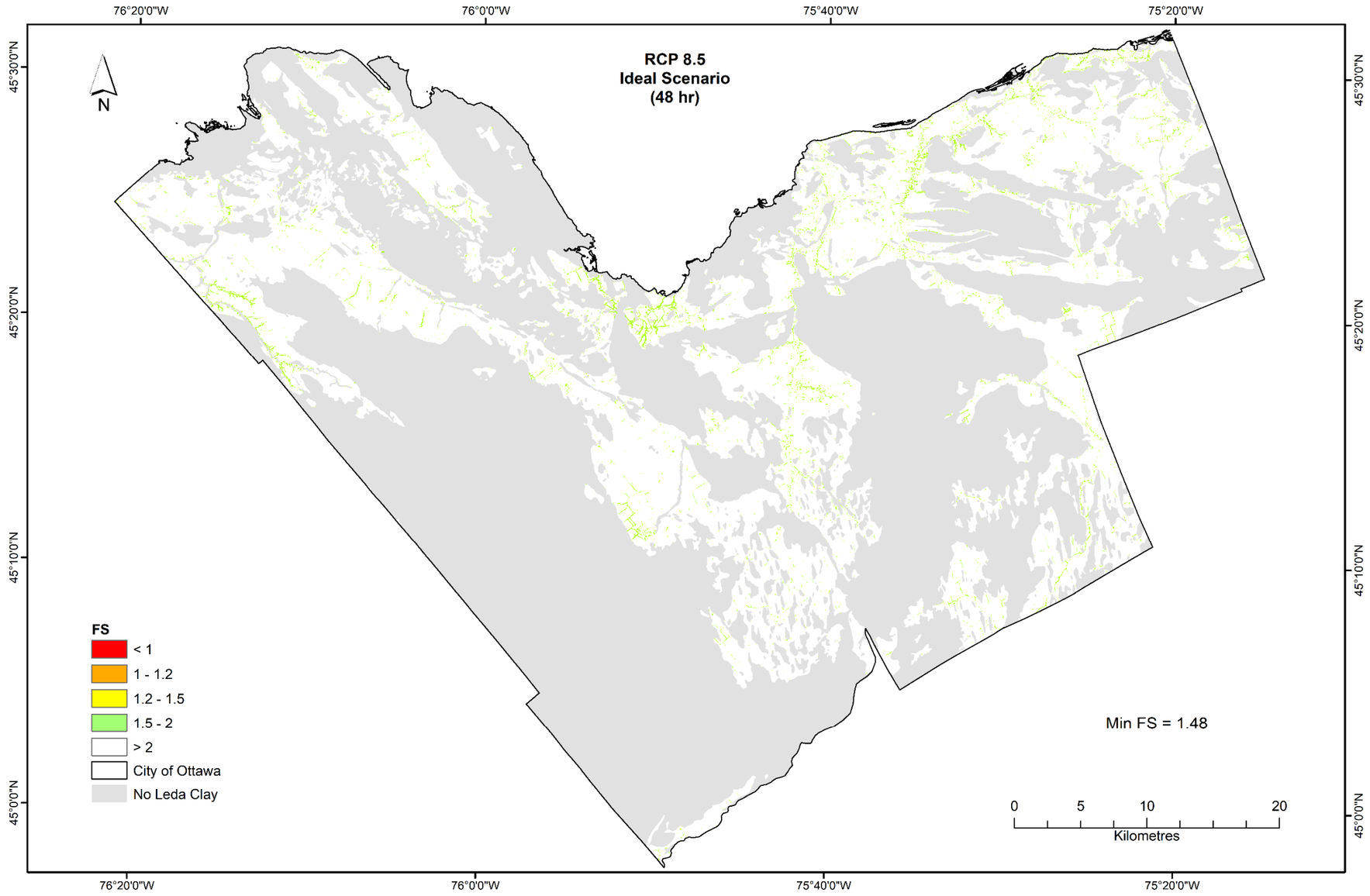

Appendix B-15

Factors of safety for sensitive marine clay in the study area computed by TRIGRS for time (t) = 48 hr under 10 years IDF RCP 4.5 normal scenario

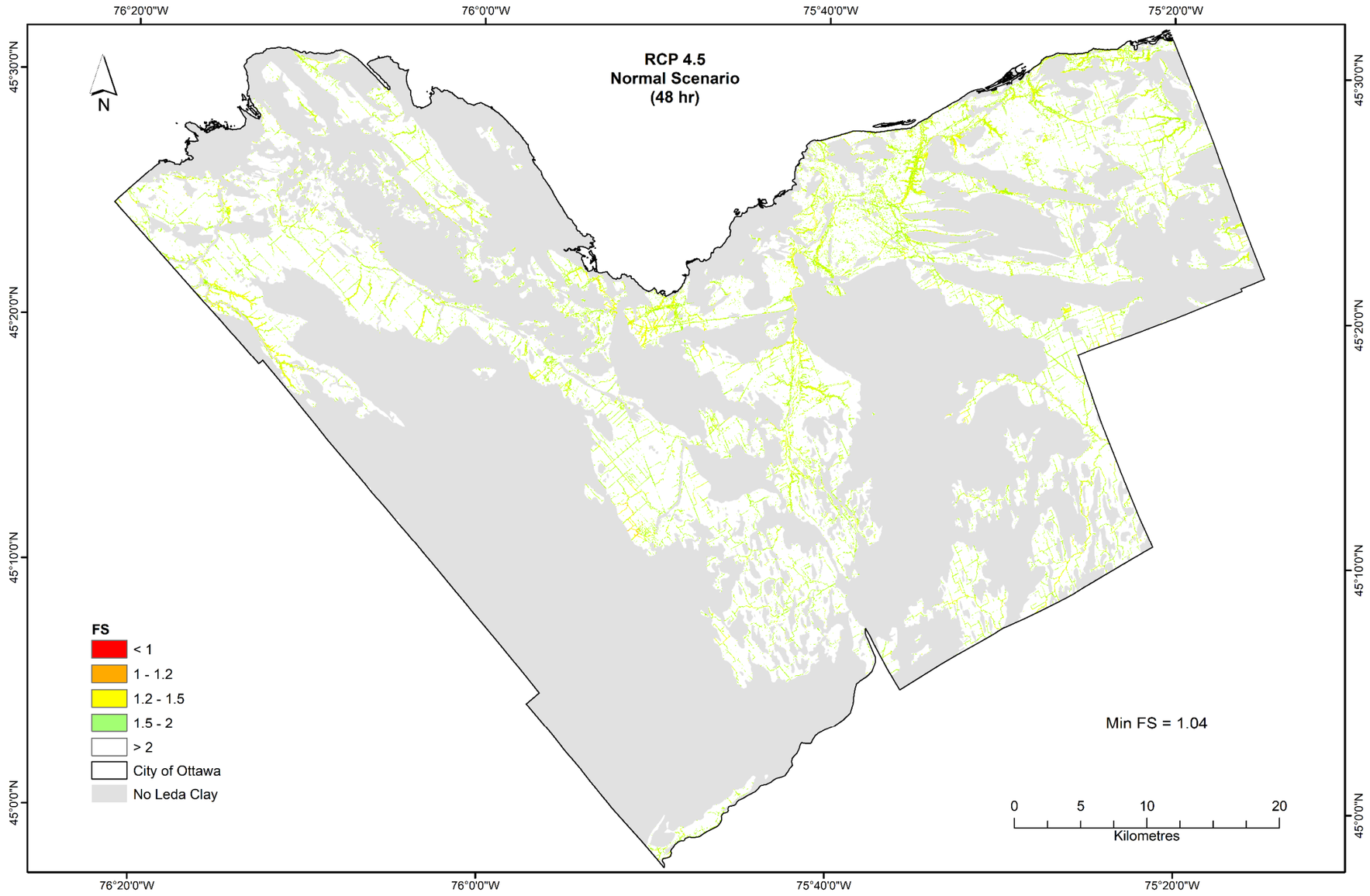

Appendix B-16

Factors of safety for sensitive marine clay in the study area computed by TRIGRS for time (t) = 48 hr under 10 years IDF RCP 8.5 normal scenario

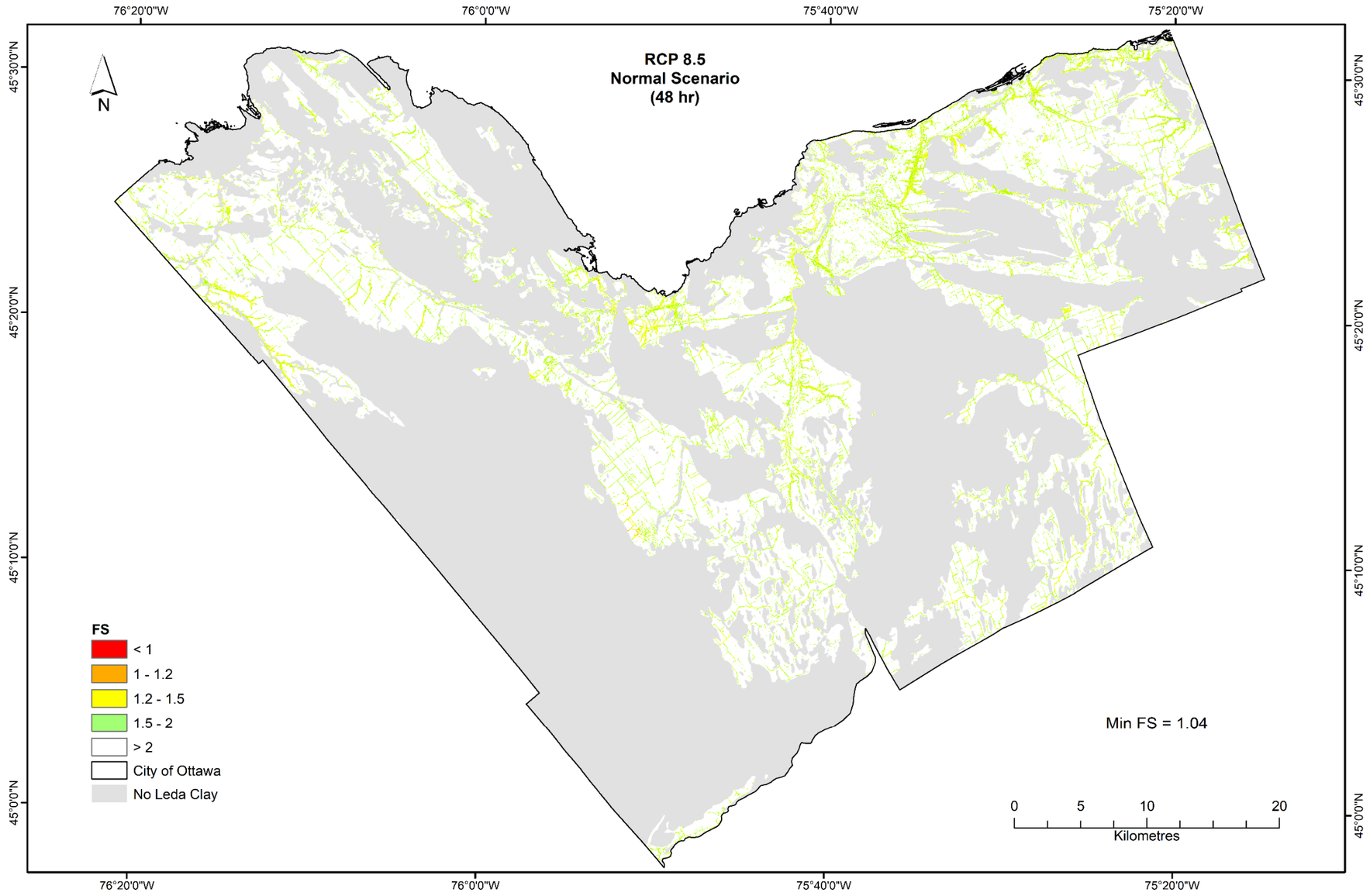

Appendix B-17

Factors of safety for sensitive marine clay in the study area computed by TRIGRS for time (t) = 48 hr under 10 years IDF RCP 4.5 worst-case scenario

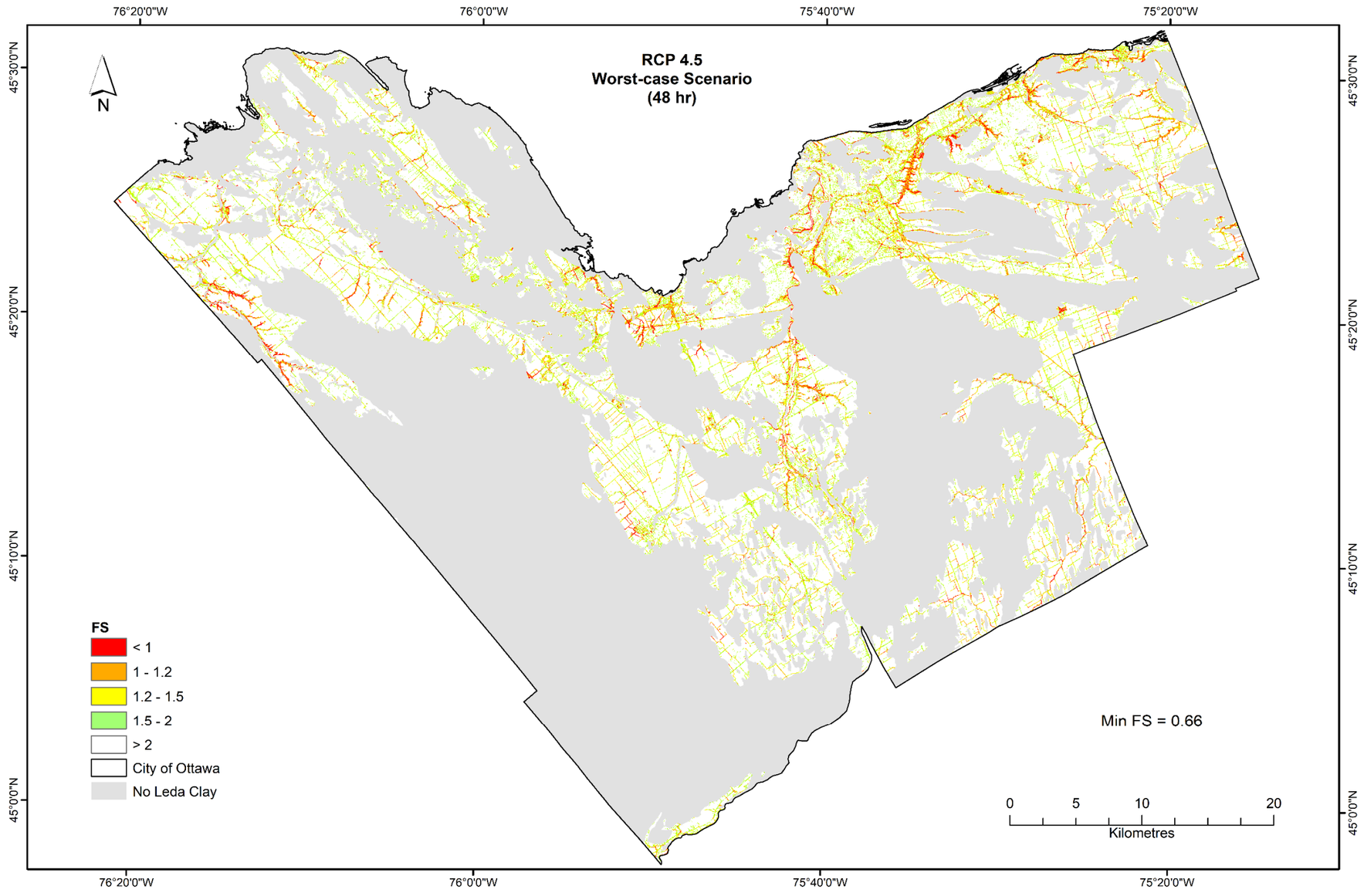

Appendix B-18

Factors of safety for sensitive marine clay in the study area computed by TRIGRS for time (t) = 48 hr under 10 years IDF RCP 8.5 worst-case scenario

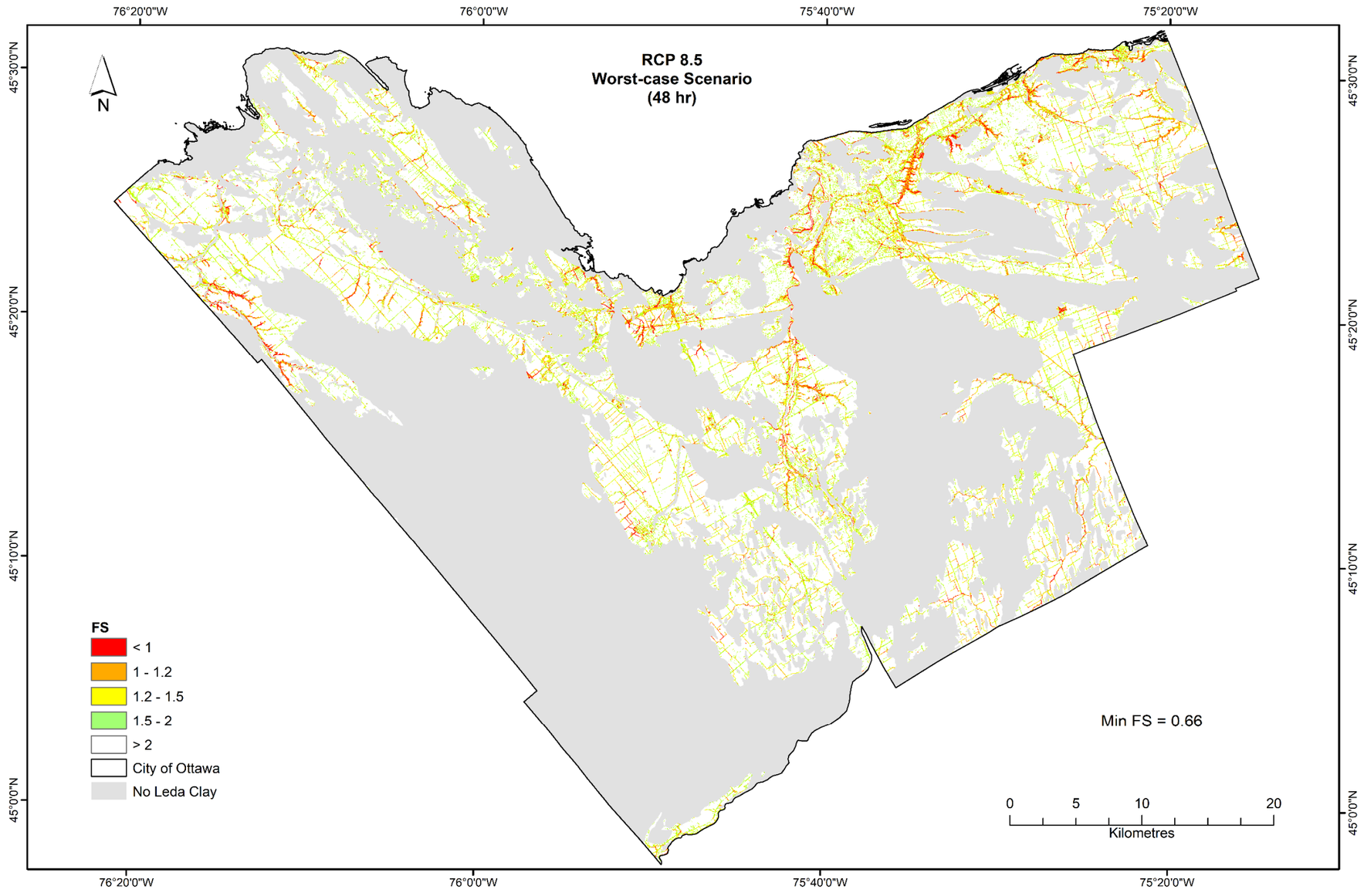

Appendix C

Projected factors of safety, under the worst case scenario, within the sensitive marine clay zones in the northeast sector of the study area at 48 hr of the simulation, compared with the study area's landslide land units

Appendix C-1

Projected factors of safety, under the worst case scenario, within the sensitive marine clay zones in the northeast sector of the study area at 48 hr of the simulation, compared with the study area's landslide land units (based on surficial geology).

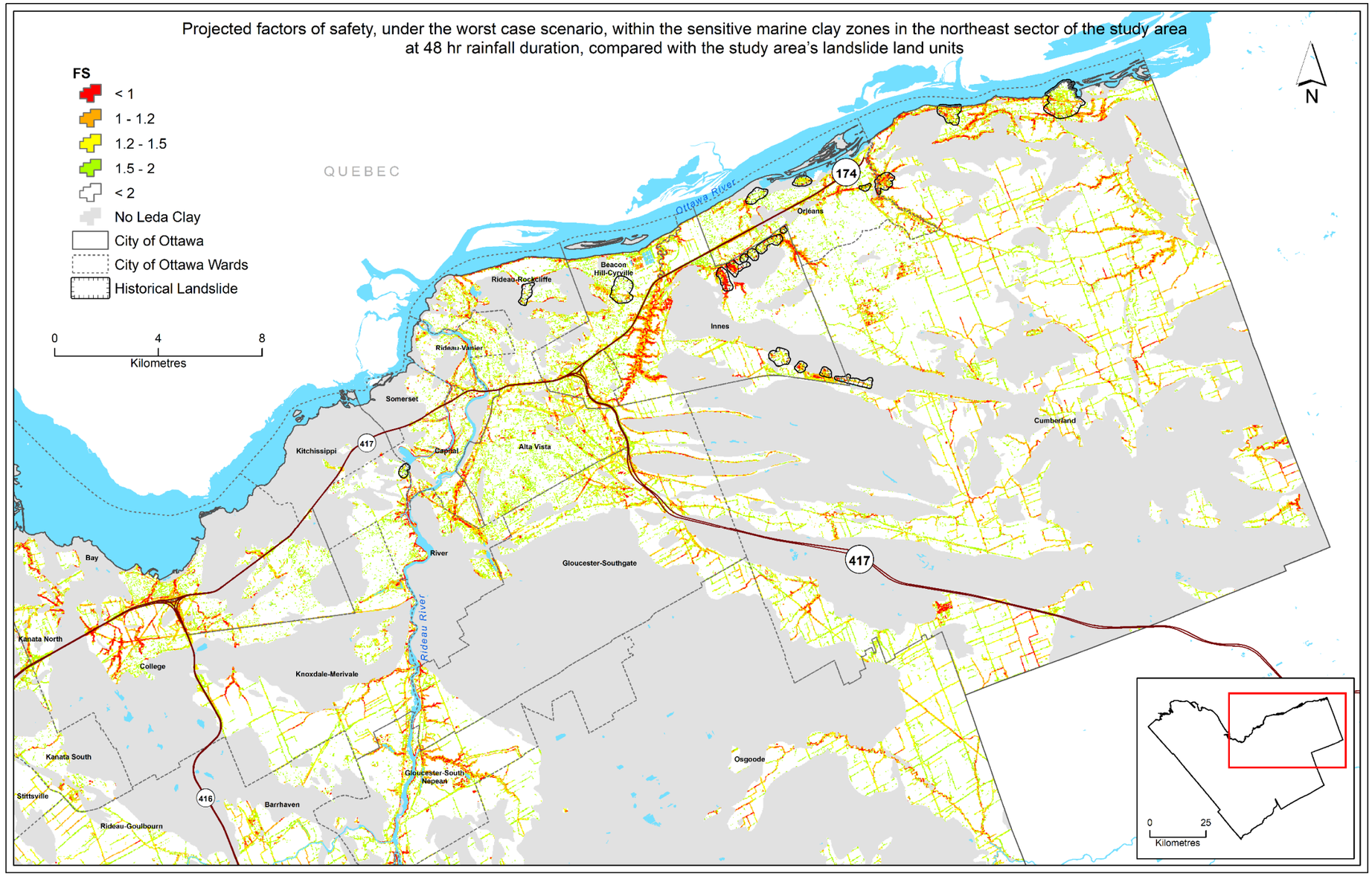

Appendix C-2

Projected factors of safety, under the worst case scenario, within the sensitive marine clay zones in the northwest sector of the study area at 48 hr of the simulation, compared with the study area's landslide land units (based on surficial geology).

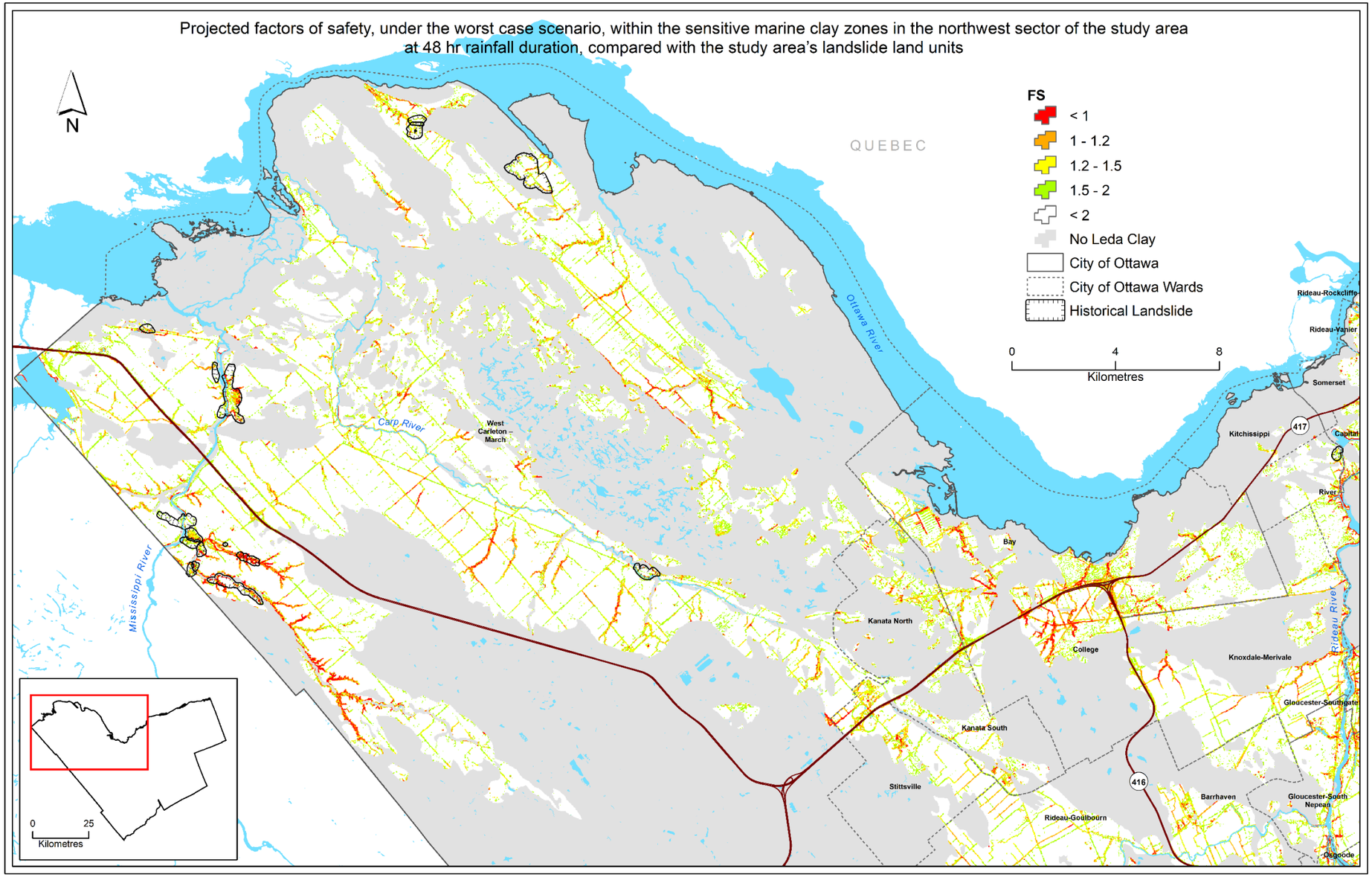

Appendix D
Example of rainfall induced landslide susceptibility map